UNIVERSITÀ
DEGLI STUDI
DI PADOVA

Sede Amministrativa: Università degli Studi di Padova

DIPARTIMENTO DI GEOSCIENZE

SCUOLA DI DOTTORATO DI RICERCA IN: SCIENZE DELLA TERRA

CICLO XXV

LATE BRONZE AGE METALLURGY IN THE ITALIAN EASTERN ALPS: COPPER SMELTING SLAGS AND MINE EXPLOITATION

Direttore della Scuola: Ch.mo Prof. Massimiliano Zattin

Supervisore: Ch.mo Prof. Gilberto Artioli

Co-supervisore: Dott.ssa Ivana Angelini

Dottorando: Anna Addis

Abstract

At the end of the second millennium B.C., the extractive metallurgy of copper in Trentino (Italy) achieved a peak of technological efficiency and mass production, as evidenced by the large number of metallurgical sites and the huge amount of slags resulting from the smelting activities.
Though different scholars proposed several smelting process models, so far an agreed interpretation of the whole process is lacking.
Over 70 slags from the Luserna, Transacqua and Segonzano sites (all located Trentino, Italy) were investigated in order to verify: 1) the technological development of the smelting processes performed, 2) the possible use of different working-steps in the metal production process and the copper extraction efficiency, 3) the ore source of the smelted minerals.
For these purposes a multi-analytical approach was applied, involving physical measurements and chemical-minero-petrographic analyses by means of OM, XRPD, XRF and SEM-EDS. Pb-isotope analyses were also performed on several slags in order to correlate mines, smelting sites and metal objects on the basis of the Alpine Archaeocopper database (AAcP).
Three different slag types were identified from the mineralogical and chemical points of view, each being the product of distinct metallurgical steps.
On the basis of these considerations, it is proposed a new Cu-smelting model in the Late Bronze Age.

Riassunto

Alla fine della secondo millennio a.C. in Trentino (Italia) la metallurgia estrattiva del rame ha raggiunto un alto livello di efficienza tecnologica e produttiva, evidenziato dal grande numero di siti metallurgici e dal grande quantitativo di scorie ottenute dalle attività fusorie.
Sebbene differenti studiosi abbiano proposto diversi modelli relativi al processo di fusione *(smelting)* ad oggi manca una interpretazione condivisa dell'intero processo.
A tal proposito sono state analizzate più di 70 scorie provenienti dai siti archeologici di Luserna, Transacqua e Segonzano (tutti situati in Trentino, Italia) al fine di comprendere: 1) lo sviluppo tecnologico dei processi di fusione, 2) la possibile presenza di differenti fasi operative durante la produzione del metallo e il grado di efficienza estrattiva del rame raggiunto, 3) la provenienza dei minerali utilizzati per l'estrazione del rame.
Per questi scopi è stato adottato un approccio multi analitico che ha riguardato misure fisiche e analisi di tipo chimico e minero-petrografico, attraverso l'utilizzo della microscopia ottica (OM), della diffrazione a raggi-X da polveri (XRPD), la spettrometria a fluorescenza di raggi X (XRF) e la microscopia elettronica a scansione abbinata a microanalisi EDS (SEM-EDS). Inoltre sono state condotte sulle scorie misure relative ai rapporti isotopici del piombo al fine di collegare le miniere da cui si è estratto il minerale, i siti di fusione del minerale e gli oggetti metallici attraverso il database delle mineralizzazione alpine e degli oggetti (AAcP).

Sulla base dei risultati ottenuti tre diversi tipi di scorie sono stati identificati ognuno dei quali connesso a diverse fasi del processo di fusione. Sulla base di queste considerazioni, è stato proposto un nuovo modello relativo al processo di fusione della Tarda Età del Bronzo.

INDEX

Chapter V – The Slags of Segonzano

Chapter VI – Technological Process

Chapter VII – Lead Isotope Analyses of the Slags

I - Introduction

1.1 Historical Context of the Late Bronze Age in the Italian Eastern Alps

The Italian Bronze Age is conventionally divided into four periods: the Early Bronze Age (EBA: 2300–1700 B.C.), the Middle Bronze Age (MBA: 1700–1350/1300 B.C.), the Recent Bronze Age (RBA: 1350/1300–1200 B.C.), and the Final Bronze Age (FBA: 1200–1000/975 B.C.), (Bietti Sestieri 1996, De Marinis 1999, Peroni 2000).
Contrary to the English speakers that refer to the RBA as the *Late*-BA, the Italian academics use the term *Late* in order to describe the RBA and the FBA (Pearce, 2004).
In this thesis, it will be used the Italian convention, i.e. the Late Bronze Age will indicate both the Recent and the Final Bronze Ages.

The RBA in northern Italy was a period of cultural continuity from the Middle Bronze Age (1700-1350/1300 B.C.), which was a period characterised by 1) the *Palafitticolo-Terramaricola* culture *(*settlements located to the north and to the south of the Po river and Alpine lake villages), and 2) the *Castellieri* (fortified hilltop sites) culture in Venezia Giulia province.
During the first half of the RBA, the craftwork acquired great specialization testified by the production of standardised objects and luxury goods. The metalwork and the pottery changed from the ones of the previous Middle Bronze Age, by introducing innovative technologies. Several metalwork hoards and weapons votive deposits were found in the rivers as part of water-associated cult that become increasingly important during the Recent Bronze Age.
In the first Recent Bronze Age, some terremare settlements were abandoned and others became quite large, indicating the presence of a significant organization of the territory and a political stable tribal organization lead by the military power (Cardelli, 1997, Cupitò and Leonardi 2005).
At around 1200 B.C., during the second half of the Recent Bronze Age an unstable situation occurred bringing to the system collapse, with a strong demographic reduction and depopulation of the whole central part of the Po Plain and wetland settlements around the Alpine lakes.
Several explanations were proposed in order to explain the Palafitticolo-Terramaricola culture collapse, such as those of Pigorini (emigration to the central Italy) and Saflund (climatic deterioration or epidemic).

In the Final Bronze Age (1150-950 B.C.), following the collapse of the Terramare culture in the area of the central Po plain and adjacent areas of the Apennines and Alpine margin, a new cultural phase begins as the Proto-Villanovian culture that shows many features related to the Urnfield culture of the central Europe (c. 1300 BC – 750 BC). This period was characterised by a general change regarding the settlement strategy, production technology, economy of sustenance and food procurement (Bagalon and Leonardi 2000, Leonardi 1979, Harari and Pearce 2000).

The Proto-Villanovian was a homogeneous culture in which it is possible identified regional variations, such as those of the western Lombardy and Veneto called proto-Golasecca and proto-Veneto, respectively.
The Proto-Villanovian culture did not arrive to the border upland regions of north-eastern Italy. On the contrary, the Luco/Laugen-Meluno/Melaun culture spread in the Italian South Tyrol and Trentino in Italy and in Austrian East Tyrol, Liechtenstein and Swiss Grisons in Europe (Marzatico et al. 2000, Leonardi 2010, Metzer Gleircher..).
In particular, the italian southern Alps where characterised by a massive expansion of copper production documented by smelting sites that are associated with the Luco–Laugen A culture group, the probably predecessor of the Iron Age Raeti (Pearce, 2004).

Fig. 1.1: Map of Italy where are highlighted (red rim) the Trentino and Alto Adige provinces.

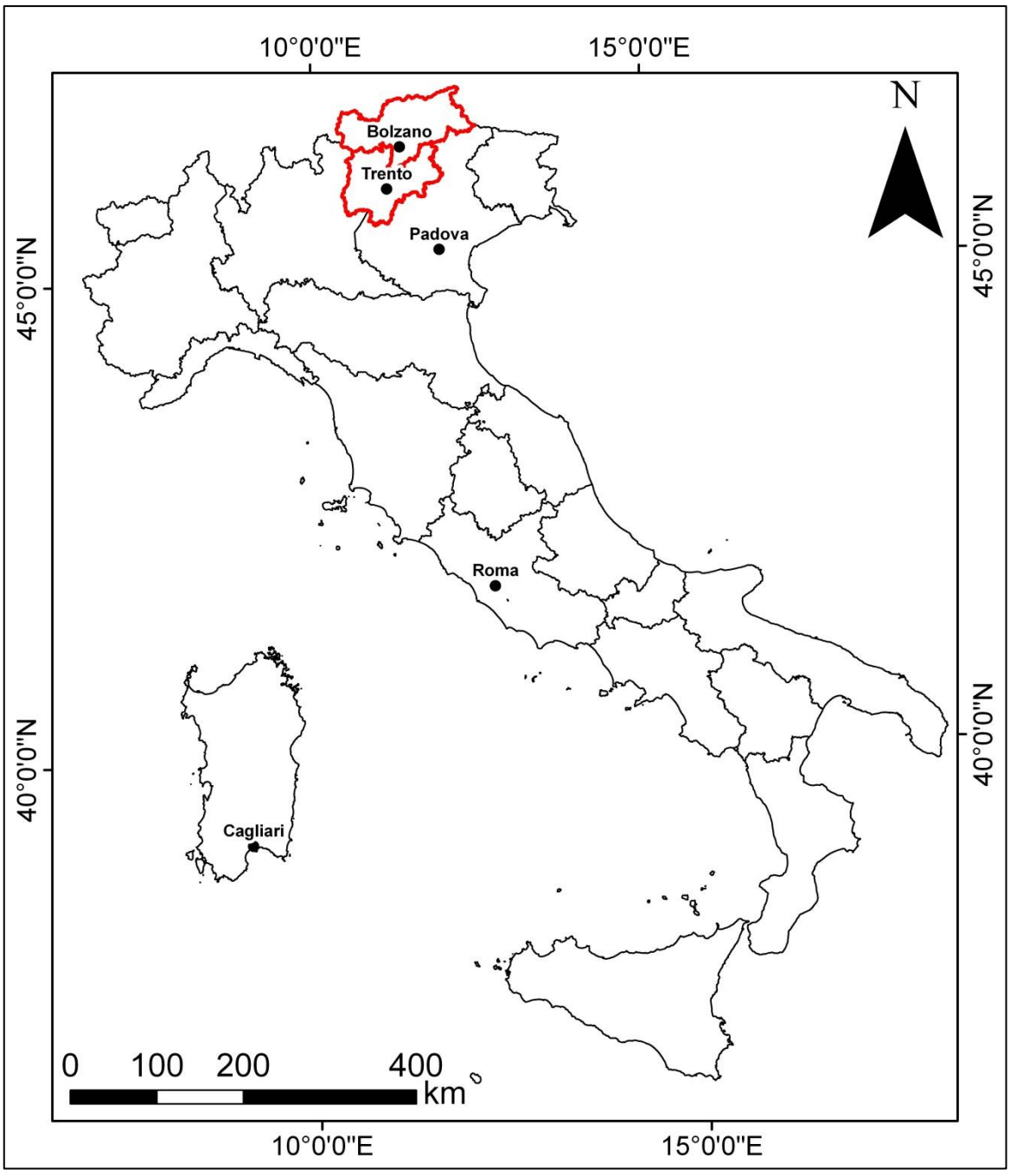

1.2 Copper slag production during the LBA in Trentino (Italy)

The metallurgical activities, which started with the ore extraction and enrichment, found fertile ground in the Cu-rich mines of the Trentino province, where the ore deposits occurs mainly in the Valsugana, in the Valle dei Mocheni, in the Val di Non and in the Valli Giudicarie (Preuscen, Sebesta, Pearce).
As Perini pointed out, the copious evidence of ancient Cu-metallurgy activity in Trentino during the Chalcolitic Period and Bronze Age are referred to two different Trentino areas.
In the central area, at the valley floor smelting sites located in Valdadige and Alta Valsugana are distributed the most ancient metallurgical sites. These sites - such as Romagnano Loc, Vela Valbusa, Acquaviva di Besenello and Montesei di Serso - can be dated between the Chalcolitic Period and the initial stages of the Early Bronze Age.
During the Recent and the Final Bronze Ages the most important smelting sites were found in Val dei Mocheni, Fiera di Primiero Area and in Valsugana, especially in the Lavarone/Vezzena Plateau area, where more than one hundred of smelting sites were identified. In these smelting sites, the extractive metallurgy of copper, based on the polymetallic Cu-Fe sulphides, achieved a peak of technological efficiency and mass production that is testified by the huge amount of slags found in the smelting sites. Since a smelting process from sulphides is always connected with production of the durable slags, they are often the only witnesses of the metallurgical processes (Bachmann, 1982). For this, the slag characterization constitute a relevant issue of archaeometallurgical researches. In fact, the analyses of the slags could provide substantial information about the process, such as their composition, the smelted charge materials, the reached temperatures, the viscosity of the slags and the red-ox condition. All of these parameters result in the identification of the global efficiency of smelting process as the grade of metal/slag separation, the velocity of the process and the use of different working-steps in metal production. Additionally, the analyses of the slags could be provide important information on geographic provenance of the charge component.
In order to defined the parameters that controlled the ancient metallurgical Cu-extraction, several petro-chemical analyses on the slags founded in different LBA Alpine smelting sites were carried out in the last 20 years (Cattoi et al., 1995; Anguilano et al., 2002; Herdits, 2003; Metten, 2003; Cierny et al., 2004; Burger et al., 2007).
Regarding the Trentino LBA smelting sites, an interesting case of study is the Acqua Fredda site on the Redebus Pass, where a the whole copper extraction process can be studied due to the founding of furnaces, metal objects and slags (Metten, 2004).
In Acqua Fredda, as in the other LBA sites of the Alps and of Central Europe, two types of slags were recognised: slags cake and flat slags, indicating a standardised process.
However - even if different studies on the LBA copper smelting sites based on the slag analyses were carried out - an agreed interpretation of the whole process is lacking. two big archaeological issues remain unresolved: 1) the level of metallurgical knowledge achieved at the LBA in this area, such as the smelting and the reached temperatures, 2) and the minerals supply.

1.3 Aim of the Work

The new current excavations at the smelting sites of Luserna (Pletz Von Mozze), Transacqua (Petze Alte) and Segonzano (Peciapian) carried out by the Archaeological Heritage Office of Trento have offered(give?) a great opportunity to find out what level of metallurgical knowledge was achieved at the end of the Bronze Age in the Trentino area.
In these coeval sites dated to the Late Bronze Age, a huge amount of slags were found showing different morphologies related to the extractive process performed.
The starting point of this research was to investigate whether these differences are linked to variation during a single stage process (Craddock) or are related to the presence of different working-steps, as a multi stage smelting process performed during the Late Bronze Age.
Moreover, the study was also addressed to understand the local production process in order to verify the presence of a standardised metallurgical process.
The smelting copper slags of Luserna, Transacqua and Segonzano were fully analysed by using a mineralogical, physical and chemical multi analytical approach in order to define homogenous minero-petrographical groups and therefore to reconstruct the extractive *chaîne opératoire* from the ore to the raw metal that involved the production of slags.
Since the archaeological remains did not provide so far specific evidences of furnaces or other information about the process as the roasting treatment, the model proposed in this work is entirely based on the analyses of the slags.
In addition, since the correlation between mine and smelting sites is often unclear, it was carried out lead isotopes analyses directly on the archaeological slags in order to identify the ore source using the geochemical database of Alpine copper deposits developed from Artioli et al. (2008).

Fig. 1.2: The Trentino province and the three smelting sites.

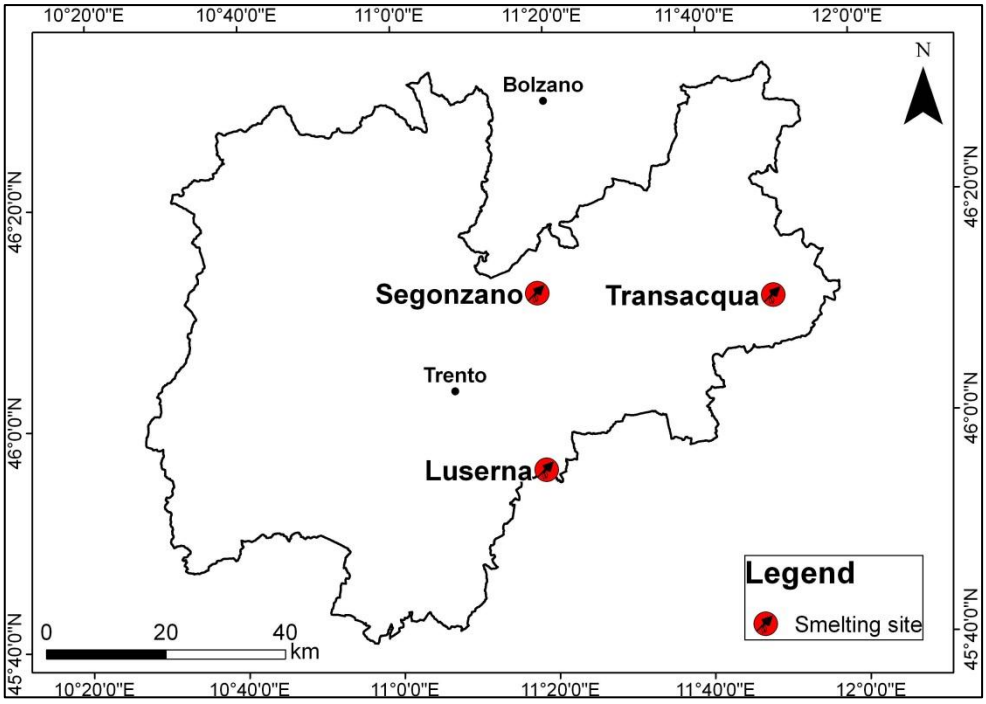

Chapter II – Analytical Methods

The various analytical methods and protocol applied to the characterisation of the slags are summarised in this chapter. Some of these methods overlap with regard to the results and information they can give, others are unique and have no alternative.
For example, microscopic investigation of thin sections gives detailed information about small fragments of the sample, while the overall mineralogical phase composition is adequately revealed by XRPD.
On the contrary, the mineralogical phases that compound the slags obtained by means of XRPD were supported by the bulk chemical composition using the XRF spectrometer.
The physical properties of slags that yield valuable information on the process were derived on the basis of the chemical and minero-petrographic analyses.

2.1 Density measurements

The density measurements and their subsequent statistical analysis were performed in order to: 1) obtain a first evaluation of the mineralogical phases in the slags; 2) to preliminary verify from the mineralogical point of view the validity of the morphological types of the slags based on the archaeological evidence; 3) to gain a helpful tool for choosing the most representative samples of each type of slags for the analyses.
The relative density (called density in the next paragraphs) was measured on the total numbers of slags by means of a hydrostatic weighing apparatus at the Department of Geoscience, University of Padua by comparing the weight of a slag in air (W_a) with that of the slags suspended in water (W_w), as the following expression: $G=[W_a/(W_a-W_w)] *T_w$ (°C). The density is measured in grams per cubic centimetre

2.2 Optical Microscopy

The optical microscopy observations were carried out on the most representative slag samples with the aim to obtained information about their production process on the basis of the type of minerals identified and their texture.
Standard petrographic thin sections (30 μm thick) were prepared at the Geoscience Department, Univeristy of Padova. They were cut with a diamond saw perpendicularly to the base and vacuum impregnated with epoxy to stabilize the sample enough for the following polishing process. At this point they were attached to a glass slide, grinded and polished with diamond abrasive powders until the achievement of a 30 μm thickness. They were then analysed under optical microscope (Nikon Eclipse ME600) that operates in reflected and transmitted light (OM-RL and OM-TL).
The interpretation of the sulphides were carried out on the basis of the comprehensive work of Ramdohr (1969), in which the systematic presentation of the ore minerals was treated.

2.3 X-ray powder diffraction (XRPD)

X-Ray powder diffraction (XRPD) is a technique that allows the determination of the mineral phases on bulk of a slag by their crystalline structure. Through the measure of the diffraction effects intensities, it can provide also semi-quantitative information about the minerals phases present in amount more than 2%.
XRPD analyses were carried out at the Geoscience Department, Univeristy of Padova, with a Philips X-Pert PRO diffractometer. The instrument is a PW3710 parafocusing geometry Bragg-Brentano diffractometer equipped with a copper anode, sample spinner, a goniometer PW3050/60 (Theta/Theta) with minimum step size 2Theta: 0,001, and a RTMS detector (X'Celerator). The analyses were conducted in the range 3–80° 2Theta using a step interval of 0.017° 2theta, with a counting time of 100 s.
The phase identification and semi-quantitative analysis were performed using the software package X'Pert HighScore Plus (3.0 version) with whom the integral profile width and shape of multiple peaks were closely examined. The phase identification was gained by the comparison with the reference pattern databases PDF2 (ICDD), Panalytical-ICSD and COD (Crystallography Open Database. It contains inorganic crystal structure data and includes structures from the American Mineralogist database) in order to find similar features.
The semi-quantitative data were calculated through the estimation of the accepted phases mass fraction with the RIR (Reference Intensity Ratio) values (Chung 1974).

2.4 X Ray Fluorescence spectroscopy (XRF)

The bulk chemistry of the samples were determined by X Ray Fluorescence spectroscopy at the Department of Geoscienze, University of Padova.
The samples analysis was carried out on a WDS sequential Philips PW2400 spectrometer, operating under vacuum conditions and equipped with a 3kW Rh tube, five analysing crystals (LiF220, LiF200, Ge, PE, TlAP), two detectors (flow counter and scintillator), three collimators (150 µm, 300 µm and 700 µm) and four filters (Al 200 µm, Brass 100 µm, Pb 1000 µm and Brass 300 µm). The quantitative analyses were performed using the software package SuperQ; the concentration of the major and minor elements is expressed in wt% of their oxides (SiO_2, TiO_2, Al_2O_3, Fe_2O_3, MnO, MgO, CaO, Na_2O, K_2O, P_2O_5), and for trace elements the concentration is expressed in ppm (Sc, V, Cr, Co, Ni, Cu, Zn, Ga, Rb, Sr, Y, Zr, Nb, Ba, La, Ce, Nd, Pb, Th, and U). Instrumental precision (defined by several measurements performed on the same sample) is within 0,6% relative for major and minor elements, and within 3% relative for trace elements.
The XRF accuracy was checked by reference standards (Govindaraju 1994) and was within 0,5 wt% for Si, lower than 3% for other major and minor elements, and lower than 5% for trace elements. The lowest detection limits of XRF were within 0,02 wt% for Al_2O_3, MgO and Na_2O, within 0,4 wt% for SiO_2, within 0,005 wt% for TiO_2, Fe_2O_3, MnO, CaO, K_2O and P_2O_5 and within a range between 3 and 10 ppm for trace elements. The calibration curves were calculated using 60 reference standards (Govindaraju 1994).

2.5 Scanning electron microscopy with energy dispersive X-ray spectrometry (SEM-EDS)

The SEM-EDS analyses were carried out at the Department of Geosciences (University of Padova) using a SEM CamScan MX 2500 microscope, coupled with an energy dispersive spectrometer, equipped with a LaB6 cathode, working in high vacuum mode (HV).. Samples were prepared as polished thin sections, coated with a thin layer of conductive material, carbon. Both back-scattered electrons images (BSI) and chemical analyses were acquired. SEM-BSE images were acquired with acquisition analytical parameters - such as working distance, spot size, luminosity and contrast - that changed time by time considering the distinctive features of each sample.

2.6 Multi-collector inductively coupled plasma mass spectrometry (MC-ICP-MS)

Lead isotope analyses were performed at the Institut für Geologie of the University of Bern. I chemically treated the selected slag samples at the ultra-clean laboratory of the Institut für Geologie, as explained by Villa (2009).
An amount of 4 mg of powder slags was weighted, dissolved in 1000 µl of hydrofluoric acid to degrade the silicate matrix and left to evaporate. Then the samples were dissolved in 1000 µl of nitrohydrochloric acid (aqua regia) at the temperature of 120°C for 12 hours and evaporated. The formed chlorides were converted to nitrates using 100 µl of nitric acid 14.4 M and evaporated. The nitrates were dissolved in 500 µl of nitric acid 1M at 70°C for five minutes. In order to separate the lead from all the other elements, a Sr Spec^{TM} resin (EIChroM Industries; Horwitz et al.,1992) was used. The resin, loaded into 3mm diameter hand-made PTFE columns, was conditioned with 500 µl of nitric acid 0.01 M (the eluting solution) and then 500 µl of nitric acid 1 M (the washing solution). Subsequently, the sample solutions were loaded onto the columns and washed with 1500 µl nitric acid 1M for removing all elements except the lead. At this point the lead was eluted from the matrix metals using 3000 µl of nitric acid 0.01 M and collected in miniature glass beakers. The chemical separation is a crucial part of the isotopic analysis, because the accuracy of the measurement depends on the purity degree of the lead separation achieved in the ultra-clean laboratory (Villa, 2009).
The mass spectrometer used for the analysis is a multiple-collector inductively coupled plasma mass spectrometer (MC-ICP-MS) produced by Nu Instruments^{TM} (see the Chapter III – Analytical Methods). In order to monitor the mass fractionation and eventually to correct it, a few nanograms of natural tallium were added in the solution samples before being ionized by the mass spectrometer.
Every five sample solutions measured, the isotopic ratios of the reference material (NIST SRM 981) were checked. The standard measured and its analytical precision (SE, the standard error referred to in-run precision) match very similarly with the reference data in the following table.

Tab. 7.2: Published MC-ICP-MS results for NIST SRM 981 modified after Rehkamper et al. (2000). Analytical errors are given in parenthesis and refer to the last significant digits; results shown in italics were calculated from the data given in the original publication.

Reference	Year	$^{208}Pb:^{206}Pb$	$^{207}Pb:^{206}Pb$	$^{206}Pb:^{204}Pb$	$^{207}Pb:^{204}Pb$	$^{208}Pb:^{204}Pb$
Hirata (Plasma 54)[a]	1996	2.16636 (82)	0.914623 (37)	16.9311 (90)	*15.4856*	36.6800 (210)
Rehkamper et al. (Plasma 54)[b]	1998	2.1667 (14)	0.91469 (5)	16.9364 (55)	15.4912 (51)	36.6969 (128)
Belshaw et al. (Nu Plasma)[c]	1998	2.1665 (2)	0.91463 (6)	16.932 (7)	*15.487*	*36.683*
White et al. (Plasma 54)[d]	2000	2.1646 (8)	*0.91404*	16.9467 (67)	15.4899 (39)	36.6825 (78)
Rehkamper et al.	2000	2.16691 (29)	0.91459 (13)	16.9366 (29)	15.4900 (17)	36.7000 (23)
This study (Nu Plasma)	2012	2.16711 (10)	0.91469 (4)	16.942 (2)	15.495 (1)	36.712 (3)

[a]= Modified power law normalization relative to $^{205}Tl/^{203}Tl$=2.3871. [b]=Exponential law normalization relative to $^{205}Tl/^{203}Tl$=2.388808. [c]=Exponential law normalization relative to $^{205}Tl/^{203}Tl$= 2.3875. [d]=Empirical external normalization technique relative to $^{205}Tl/^{203}Tl$=2.3871.

2.7 Experimental Features

Two seasons of copper smelting experiments were performed in the Summer of 2010 and 2011 in the collaboration with the ARCA group.
The first session of experiments principally aimed to explore the effect of different roasting cycles on the process. A number of twenty roasting experiments starting from three different types of commercial chalcopyrite were carried out using different strategies: charge roasting in crucibles heated in a furnace, and an open air roasting on piles of wood. X-Ray powder diffraction analyses on the starting materials and on the roasted products were performed at different stages during the process, which was repeated several times. These experiments allowed to select the most suitable charge to be used for subsequent smelting, to understand the efficiency of roasting strategies, and to assess the degree of transformation in the ores.
Several smelting experiments were performed using a charge of roasted/unroasted chalcopyrite plus quartz, inserted in crucibles within a furnace heated by artificial air source and coal. Thin sections were made on the crucibles and on the slags obtained in the experiments; on them OM and SEM-EDS analyses were performed.

III – The Slags of Luserna

3.1 Introduction

At the end of the second millennium B.C., the extractive metallurgy of copper in North-Eastern Italy, especially in the Trentino region, achieved a peak of technological efficiency and mass production. This was evidenced by the large number of metallurgical sites and the huge amount of slags derived from the smelting activities.
In fact, more than one hundred smelting sites of the Late Bronze Age (LBA) have been found in the Valsugana Valley, which is one of the most important valleys in the province of Trentino. These sites are located more than 1000 metres above sea level (a.s.l.), on dry or gravelly sites and close to the water, either ponds or streams (Perini, 1988).
The major concentration of the LBA smelting sites documented by slag heaps is on the Mesozoic limestone Lavarone-Vezzena-Luserna plateau, in which there was a density of one foundry every square kilometre (Perini, 1988). Unlike the other Late Bronze Age smelting sites, these foundries are not situated nearby sulphide ore outcrops (Preuschen, 1973, Perini, 1988, Pearce and De Guio, 1999, Pearce 2007).
As Pearce stated (2007), several hypotheses have been proposed in order to explain the high density of smelting sites in the plateau, from which the ore sources were distant.
Preuschen (1973) suggested that the ore was taken to the plateau because of the absence of wood fuel near the mine areas due to deforestation for the fire-setting (mining method well described by Weisgerber and Willies, 2000) and because of the request of new wood and water available in the Lavarone-Vezzena-Luserna plateau.
More recently, Pearce and De Guio (1999) proposed a similar but more elaborated model than the one just described. They agreed with the Preuschen interpretation, i.e. the need to obtain and maintain a good supply of fuel, and suggested new arguments.
The first argument was about the Alpine grazing practices during the Bronze Age.
As pointed out by Pearce (2007), this seasonal activity should be correlated to the hard cheese production, which must have been the most important source of food for the smelters and metal workers in terms of protein and fat (De Guio and Pearce, 1999).
The second argument concerned the closeness between the Lavarone-Vezzena-Luserna plateau and the Altopiano dei Sette Comuni located South-West to the Veneto Region.
As shown by De Guio (1994), during the Middle and Recent Bronze Age this area was exploited by the transhumant herders of the closely Po plain area for summer grazing. These cultural groups located in the alluvial areas lacking copper ores must have been dependent on the Trentino groups for metal supplies.
Therefore, De Guio and Pearce affirmed that the Lavarone-Vezzena-Luserna plateau was chosen by the inhabitants of the Trentino area for the smelting activities both due to the need of fuel supply and to the trading location.

This model is in contrast with what stated by Carancini (1997 and 1999). The author assumed that the Trentino metallurgists were part of a self-sufficient group, where the grazing was practised and milk and cheese were made as their primary food source.
As stated by Carancini, for this reason the trade between these two peoples (the Po inhabitants and the Trentino smelters) must not have been essential for the subsistence of the latter.
Additionally, Cierny et al. (2004) doubted that the lasting hard cheese was produced in this area as it was not found any evidence of structure built for shaping and ripening the hard cheese. The authors pointed out that the metal-cheese exchanges could not provide significant quantity of fresh cheese because of its low storability.
However, the model proposed by Pearce and De Guio has so far provided the most complete explanation about the high smelting site density in the Lavarone-Vezzena–Luserna plateau.

Fig. 3.1: CTP map of Luserna.

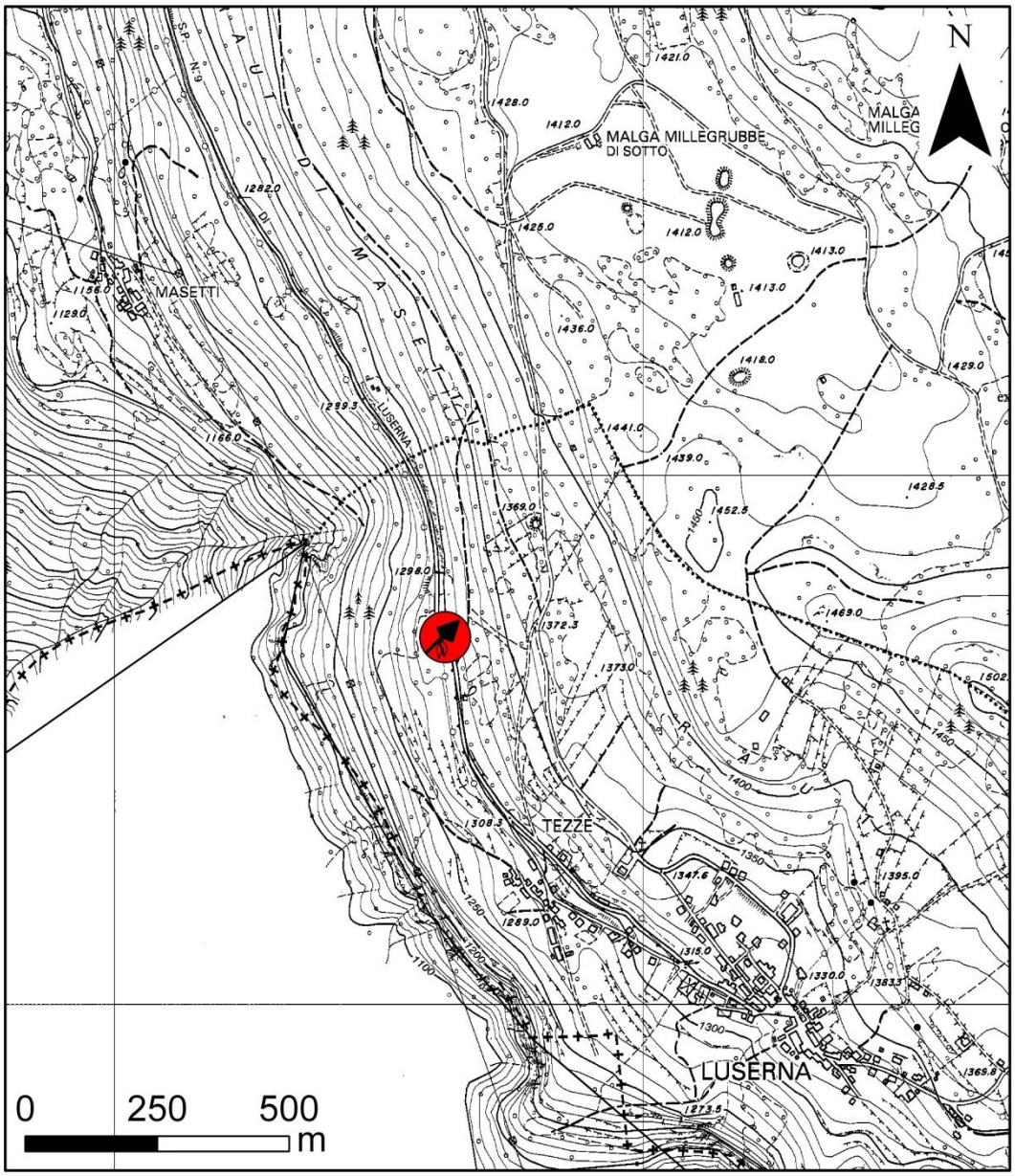

The Luserna slags studied in this work were found in the Plez von Mozze (or Platz von Mozze, later often abbreviated: PvM) site, located a few kilometres from the Luserna city centre and belonging to the type of LBA Lavarone-Vezzena-Luserna plateau smelting sites mentioned above.
The excavations on the site directed by F. Nicolis of the Archaeological Heritage Department of the Autonoma Province of Trento started in 2005. The site was already known in archaeology because of the preliminary excavation conducted by Preuschen in 1960 during which slag fragments and furnace remains were unearthed (Preuschen, 1973) and as a result of the accurate excavations performed by Cierny in 1992 and 1995 (Cierny, 2008).
Other excavations were conducted nearby the city of Luserna in sites such as Tezze and Millegrobbe, where a large quantity of copper smelting slags was found (Perini, 1988).
As described by Nicolis et al. (2007), the PvM site is situated in an altitude of around 1300 metres a.s.l., and it is characterised by a modest flat basin, bounded to the east by the western slopes of the Raut di Masetti and to the west by a long ridge that dominates the underlying Valle dell'Astico.

The excavation produced significant evidence of the smelting activity, such as fragments of pottery, remains of animal bones, fragments of bronze pins, remains of two probable smelting furnaces and several burnt clay structures, likely associated with roasting beds (Bellintani et al., 2009).
The pottery fragments appear to belong largely to the remains of vessels of the early phase of the Luco group. Therefore, they belong both to the last phase of the Recent Bronze Age and to the central and main phases of the Final Bronze Age (Nicolis et al., 2007).
Accordingly, the site is dated from the second half of the XIV century to the XI century B.C. and it is not situated nearby sulphide ore outcrops.
The nearest copper sulphide mines are Vetriolo and Calceranica both located in the Valsugana Valley, 10 km to the North of the smelting site.
Cierny produced the only published topographic map (Fig. 3.2) of the site (Cierny, 2008).

Fig. 3.2: Topographic map of the Plez von Mozze site, drawn by Cierny (2008).

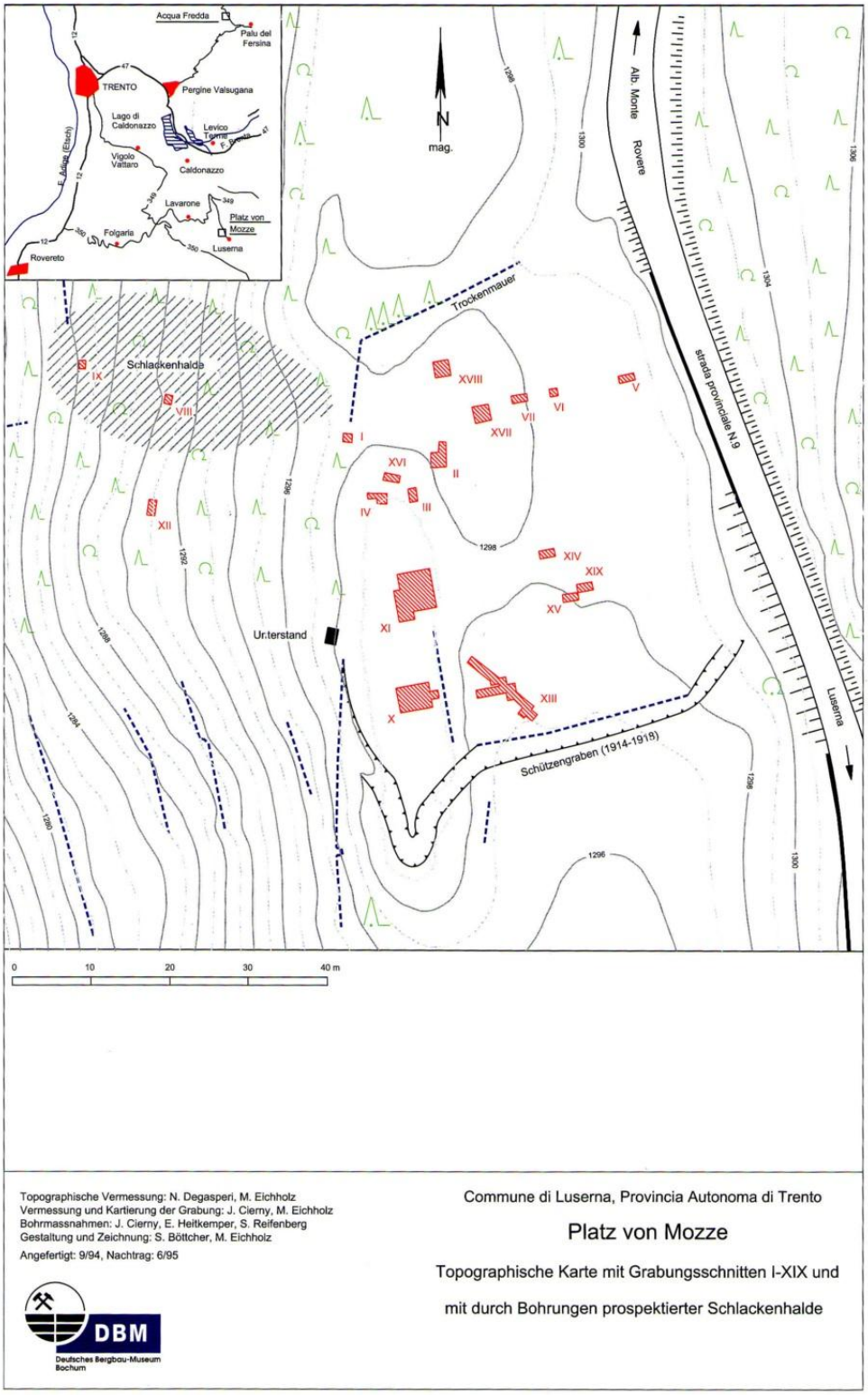

During the excavations started in 2005, a careful survey of the slags was carried out. Specifically, the archaeologists used several test pits with a size of 30x30 cm^2 and positioned in the site in order to investigate the whole smelting area. The content of each pit was recorded and the systematic sampling of the slags was performed in order to obtain representative samples of the whole metallurgical chaîne opératoire.
The archaeologists recorded each sample of slag in a database with the weight, the size and the stratigraphic unit they came from.
A number of eight categories of slags was identified on the basis of the macroscopic features and a significant number of each category of slags was selected for the analyses.
Several studies were already conducted on the slags of the Plez von Mozze site.
Cattoi et al. (1995) analysed 11 slags of PvM, 3 of which were macroscopically classified as flat slags and the remaining were classified 8 as *bollose*-coarse slags.
Flat and coarse slags together with the slag sand are the three types of slags systematically encountered in the Late Bronze age smelting sites.
The results of the chemical and petrographic analyses performed by Cattoi et al. supported the differentiation in two groups, the flat slags characterised by a higher amount of fayalite (ranging from 35% to 60%) and a lower amount of quartz (0-15%) than the second type of slags. The latter type of slags called bollose has a higher amount of quartz (20-60%) and a lower content of fayalite (10-25%) compared to the flat slags.
Cattoi et al. asserted that the quartz was intentionally added as a flux to the sulphide charge used, the chalcopyrite.
On the basis of the two types of slags identified, they assumed two different smelting processes. The first process is composed of two different steps: the first step is related to the formation of the coarse slags and the second is connected to the production of the flat slags.
The second process hypothesis regards only one step in the pyrometallurgical process from which two types of slags were produced depending on the different position of formation that the slags had into the furnace.
Anguilano et al. (2002) published the summary analytical results of several slags produced in 12 smelting LBA Eastern alpine sites located in Trentino and Alto Adige, including the Luserna site (the effective number of PvM slags analysed was not specified).
They distinguished two groups of slags on the basis of mineralogical, chemical and texture features. These two types, called platy and coarse, were considered to derive from two different steps of the smelting process.
In 2003, Metten analysed 21 slags of the LBA Acqua Fredda site and 22 slags from other Trentino sites, among which 4 were from the Luserna site. The author identified three types of slags called *Plattenschlacke* (flat slags), *Schlackenkuchen* (coarse slags) and *Schlackensand* (sand of slags). The slags of Luserna studied were two of the coarse type and two of the flat type.
Metten assumed that only one metallurgical step can be proved for the smelting site of Acqua Fredda and for the other Late Bronze Age smelting sites in the Trentino region. The two types of slags, both coarse and flat, were assumed to be produced by this

single step process. The author also believed that the sand of slags (800-1000 tons found in the Acqua Fredda site) is the by-product of the beneficiation of slags containing copper and matte inclusions.
As shown by the concise summary on the literature, only a few samples of the Plez von Mozze-Luserna site were already investigated and an agreed interpretation of the whole process is lacking.
For this reason, I investigated about one hundred of PvM slag samples using a multi-analytical approach. Specifically, the slags were analysed in order to understand: 1) what minerals were used as charge, 2) the possible presence of different working-steps in the metal production process and their extraction efficiency, 3) the ore source of the charge minerals (chapter 7).

3.2 Analytical Protocol and Materials

A number of 93 slag samples was preliminary analysed for macroscopic features (colour, texture, shape, thickness, weight, presence/absence of visible quartz, charcoal, voids) and subsequently the relative density was measured by water pycnometer and hydrostatic balance.
The measured densities were statistically treated using descriptive methods and inferential procedures (Box and Whiskers plots, one-way ANOVA, etc.) by the Statgraphics Centurion software.
In agreement with the macroscopic observations and the statistical analysis the slags were reclassified into morphological types.
On the basis of the results of the statistical analysis, the most representative slags of each type were firstly analysed by means of the optical microscopy operating in reflected and transmitted light (OM-RL and OM-TL). Later they were analysed by X-ray powder diffraction (XRPD). The results of the XRPD analyses were treated by the Reference Intensity Ratio method for semi-quantitative phase evaluation.
On the basis of the minero-petrographic analyses, the most representative samples of each group were selected for chemical analysis using XRF spectrometer and the scanning electron microscope coupled with X-ray energy dispersive spectrometer (SEM-EDS).
The investigated slag samples were classified by the archaeologists into 8 morphologic types (archaeo-types of slags). A number of 6 new typological classes was identified in addition to the two common Late Bronze Age types: coarse/cake slags and flat (Plattenschlacke) slags.

We called this type: massive, flat-thick, flat-coarse, flat-thick-coarse, coarse-massive and fluid.
The sand of slags, found in other LBA smelting sites, such as the Acqua Fredda site, was not found in Luserna (Cierny, 2008).

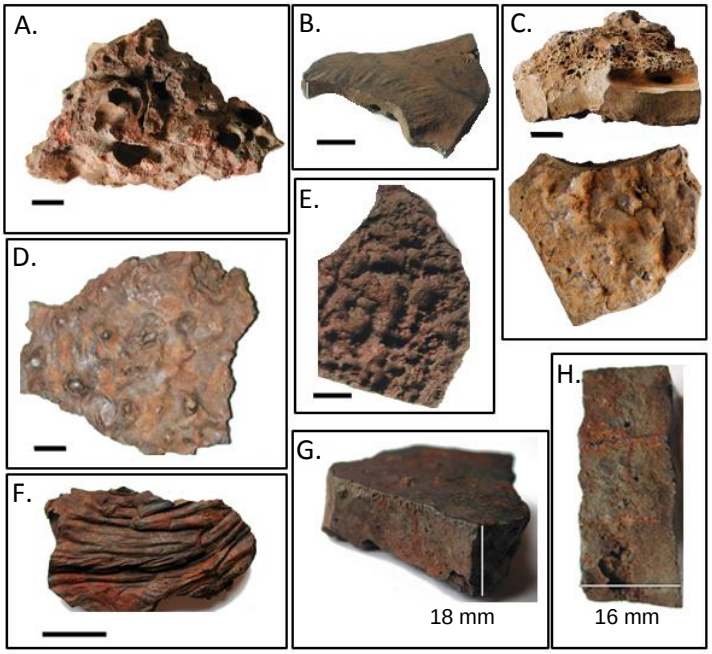

Fig. 3.3. Macroscopic archaeo-types of slags. The black line is 1 centimetre.

A. Coarse

B. Flat

C. Massive

D. Coarse Massive

E. Flat Coarse

F. Fluid

G. Flat Thick Coarse

H. Flat Thick

The three types of slags that show the most significant differences from the point of view of the macroscopic features are the coarse, the flat and the massive types.
The coarse type is constituted by slags with irregular shapes, high porosity and the diffuse presence of unreacted quartz relics and other minerals of the charge. This type of slags is similar to the LBA slag cakes described by Herdits (2003). It has an inhomogeneous texture with rough surface and no sign of flow features.
The flat type has the typical features of the Plattenschlacke slags (Cierny et al., 2004; Herdits, 2003; Burger et al., 2007). These features are limited thickness from a few millimetres to one centimetre, lack of porosity, homogeneous texture and very smooth sides, sometimes with clear cooling marks. A particular feature of the flat slags is their edges, which are curved and thicker than the middle part.
The massive slag type was not distinct in the previous studies of the LBA Eastern Alpine slags, although sometimes it seems to be included in the coarse type (Anguilano et al., 2002) and in the flat type (Metten, 2003).
The macroscopic features of the massive slags are a mixture of the other two groups: they have a smooth surface – as in the flat slags - and an irregular surface –as in the coarse type. They also display a visible homogeneous core like the flat slags and a diffuse superficial porosity like the coarse slags.
The other five types of slags can be considered as a mix of the coarse, the flat and the massive slags. The flat thick are similar to the flat slags but thicker (the maximum thickness measured is 20 mm). The flat-coarse type displays the same macroscopic feature of the flat but with one irregular and unsmooth side. The flat-thick-coarse type has a thickness similar to the flat-thick type and an irregular surface like the flat-coarse slags.

The coarse-massive type shows a compact core like the massive slags and an irregular surface similar to the coarse type.
The fluid type is composed by a slag with a morphologic flow texture.

3.3 Results

3.3.1 Density

The slags sampled from the Plez von Mozze site are 93.
The statistical analysis of the densities measured was performed in order to: 1) obtain a first evaluation of the mineralogical phases in the slags; 2) to preliminary verify the validity of the eight morphological types of slags from the mineralogical point of view; 3) to gain a helpful tool for choosing the most representative samples of each type of slags for the following analyses.
A useful graphical display for summarizing data, invented by John Tukey in 1977, is the box and whiskers plot (STATGRAPHICS® Centurion XVI User Manual, 2009).

This procedure summarizes a data distribution through six statistic information (Fig. 3.4): 1) minimum, 2) lower quartile, 3) median, 4) upper quartile, 5) maximum and 6) outlier

Fig. 3.4: The box and whisker plot with its components.

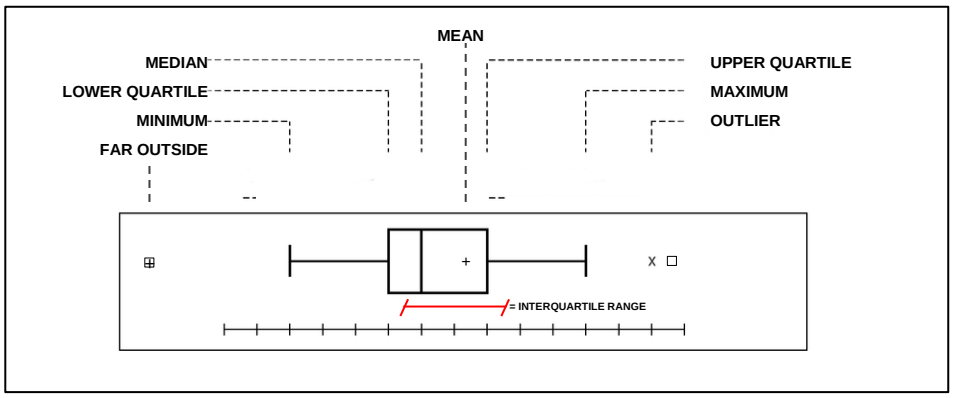

As it can be observed in the Fig.3.4, two types of outliers could be detected: 1) the data located at more than 1.5 times the interquartile range beyond the limit of the box are called outsides and denoted by a point symbol (small square).
2) The so-called far-outsides are points located at more than 3 times the interquartile range beyond the limit of the box. These outsides are indicated by a point symbol with a plus sign overlying on it.
Far outside points are usually indicative of true outliers or belonging to a non-normal distribution.
The box and whisker plots of the eight types of slags and the summary statistic referred to the density are shown in the Figure 3.5 and in the Table 3.1.
These two descriptive statistic outputs (Tab. 3.1 and Fig. 3.1) show that 4 groups of slags are composed by only 1 sample: flat-coarse, flat-thick-coarse, fluid, coarse-massive. For this reason they do not form a statistically representative groups.
The massive, the coarse and the flat-thick types are composed by 9, 10 and 13 samples respectively and do not show a normal distribution of data.
The flat type with 57 samples is the largest group and its data can be adequately modelled by a normal distribution with 95% confidence level (P-value>0,05 verified

using several tests for Normality: Chi-Square, Shapiro-Wilk W, Skewness Z-score and Kurtosis Z-score).

Tab. 3.1: Summary Statistics for the density values measured on the slag samples. Archaeo-Type: typology identified by the archaeologists. Count: total number of slags for each group. SD: standard deviation. Min.: Minimum. Max.: Maximum. LQ: Lower Quartile. UQ: Upper Quartile. IQR: Range Interquartile.

Archeo-Type	Count	Average	Median	SD	Min.	Max.	Range	LQ	UQ	IQ range
Coarse	9	2,59	2,63	0,17	2,34	2,79	0,44	2,44	2,70	0,26
Coarse Massive	1	2,89								
Flat	57	3,57	3,56	0,11	3,37	4,15	0,79	3,51	3,60	0,10
Flat Coarse	1	3,67								
Flat Thick	13	3,60	3,66	0,19	3,32	3,98	0,65	3,45	3,73	0,28
Flat Thick Coarse	1	3,76								
Fluid	1	3,12								
Massive	10	3,61	3,73	0,40	2,54	3,89	1,34	3,67	3,77	0,09
Total	93									

Fig. 3.5: Box an whiskers plots of the slags formed the 8 archaeo-type.

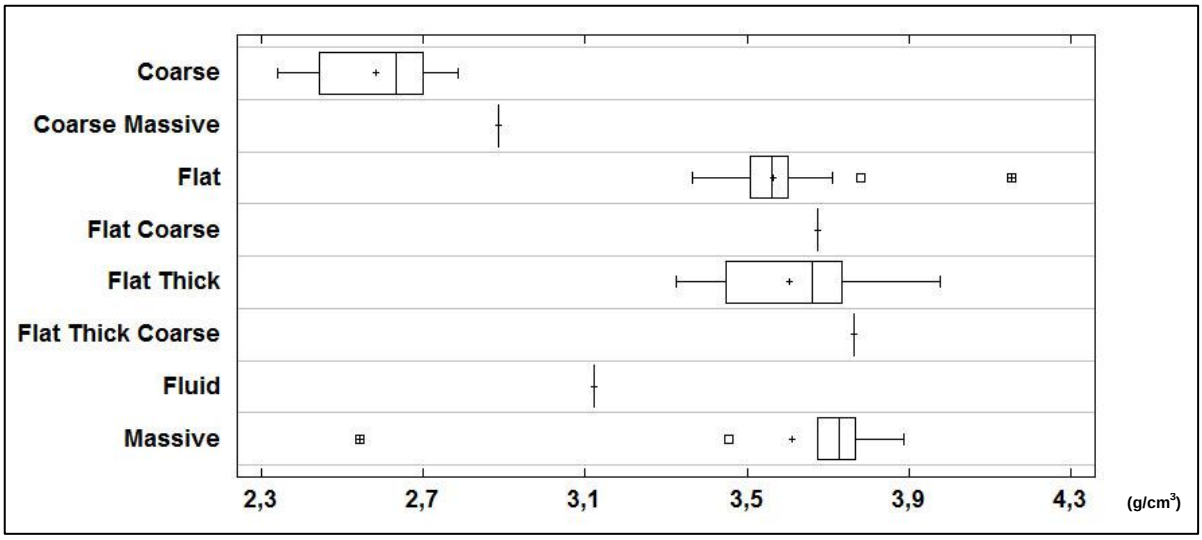

As shown in the Fig 3.5, two far-outsides are identified: one in the flat group and the other in the massive group of slags. The outlier identification procedure (Grubbs' Test), designed to determine if a sample of numeric observations contains outliers, assumes normality. Therefore this test was used only in the flat group. The most extreme density value in the flat group is 4,17 g/cm^3, which is 5,17 standard deviations away from the mean.

Considering that the P-value for Grubbs' test is less than 0,05 that value is a significant outlier at the 5,0% significance level.

The following box plots were drawn after the elimination of the two obvious outsides (far-outlier sample of the flat group: 4,17 g/cm^3, far-outlier sample of the massive group: 2,54 g/cm^3).

Fig. 3.6: Box an whiskers plots of the slags formed the 8 archaeo-type without far-outliers.

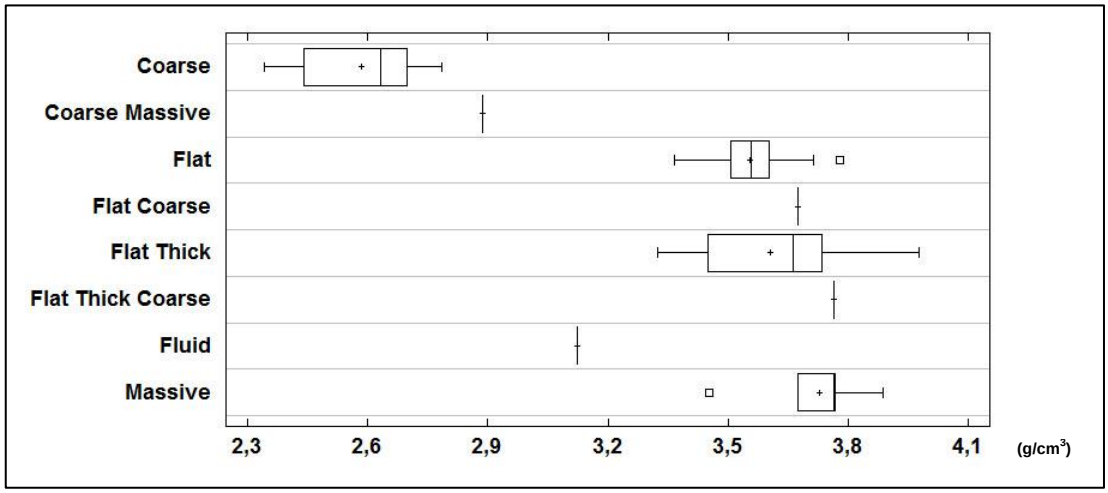

At this point the one-way analysis of variance (ANOVA) was used in order to test the hypothesis of equal population means. After identifying the statistically significant differences between the density means (parametric F-test: P-value<0,05) and the density medians (not parametric Kruskal Wallis test <0,05) of the 8 archaeo-types of slags at a 95% confidence level, the Multiple Range Test was used in order to determine which means are significantly different.

The table 3.2 shows the estimated difference between the means of each pair of slags types. The *Difference* column displays the mean of the first group minus the one of the second group. For each difference the software calculated an uncertainty interval, shown in the *+/- Limits* column. Any pair for which the absolute value of the difference exceeds the uncertainty interval has statistically significant differences and it is indicated by an asterisk symbol in the *Sig*. column. A number of 17 pairs show statistically significant differences at the 95,0% confidence level.

Tab 3.2: Table of the contrast. The symbol * denotes a statistically significant difference.

Contrast	Sig.	Difference	+/- Limits
Coarse - Coarse Massive		-0,30	0,40
Coarse - Flat	*	-0,97	0,14
Coarse - Flat Coarse	*	-1,09	0,40
Coarse - Flat Thick	*	-1,02	0,16
Coarse - Flat Thick Coarse	*	-1,18	0,40
Coarse - Fluid	*	-0,54	0,40
Coarse - Massive	*	-1,14	0,18
Coarse Massive - Flat	*	-0,67	0,38
Coarse Massive - Flat Coarse	*	-0,79	0,54
Coarse Massive - Flat Thick	*	-0,72	0,39
Coarse Massive - Flat Thick Coarse	*	-0,88	0,54
Coarse Massive - Fluid	*	-0,24	0,54
Coarse Massive - Massive	*	-0,84	0,40
Flat - Flat Coarse		-0,12	0,38

Contrast	Sig.	Difference	+/- Limits
Flat - Flat Thick		-0,05	0,12
Flat - Flat Thick Coarse		-0,21	0,38
Flat - Fluid	*	0,43	0,38
Flat - Massive	*	-0,17	0,14
Flat Coarse - Flat Thick		0,07	0,39
Flat Coarse - Flat Thick Coarse		-0,09	0,54
Flat Coarse - Fluid	*	0,55	0,54
Flat Coarse - Massive		-0,06	0,40
Flat Thick - Flat Thick Coarse		-0,16	0,39
Flat Thick - Fluid	*	0,48	0,39
Flat Thick - Massive		-0,12	0,16
Flat Thick Coarse - Fluid	*	0,64	0,54
Flat Thick Coarse - Massive		0,03	0,40
Fluid - Massive	*	-0,61	0,40

The second output of the Multiple Test Range is the homogeneous group table.

Tab 3.3: The homogeneous group table.

Archaeo-Type	Count	Mean	Homogeneous Groups			
Coarse	9	2,59	X			
Coarse Massive	1	2,89	X			
Fluid	1	3,12		X		
Flat	56	3,55			X	
Flat Thick	13	3,60			X	X
Flat Coarse	1	3,67			X	X
Massive	9	3,73				X
Flat Thick Coarse	1	3,76			X	X

In the table above, the types of slags were arranged into homogeneous groups, that is to say those groups within which there are no significant differences. The method used to discriminate among the means is Bonferroni's multiple comparison procedure. With this method, there is a 5,0% risk of calling one or more pairs significantly different when their actual difference equals 0.

The density analysis of the means shows two homogeneous groups (X symbol in the same column) of means: 1) the coarse and the coarse-massive slags and 2) the flat-thick, the flat-coarse and the flat-thick-coarse. This three types of slags are related with both the flat and the massive types of slags, showing an intermediate mean behaviour.

A close observation of the contrast and homogenous group tables display that there are three actual different types of slags: coarse, flat and massive.

On the contrary, the other types of slags could be incorporated into the three types just mentioned. Specifically, the coarse-massive slag belongs undoubtedly to the coarse type. On the other hand, the flat-thick, the flat-coarse and the flat-thick-coarse needed a macroscopic re-observation in order to verify their real affinity with the flat type rather than the massive type.

The fluid type, composed by only one sample shows a density value and morphological features not comparable with the other types of slags. Therefore, this sample was not considered as a type of slag and it was not included in the subsequent exposition of the result.

However, several analyses were performed on this sample, such as OM-RL/TL and XRPD.

On the basis of these considerations, a second morphological examination of the slags was performed as well as a new division into morpho-physical types (Fig 3.7, Tab.3.4).

Tab 3.4: Summary statistics for the density values measured on the slag samples of Luserna.
Count: total number of slags for each group. SD: standard deviation. Min.: Minimum. Max.: Maximum. LQ: Lower Quartile. UQ: Upper Quartile. IQR: Interquartile Range.

Type	Count	Average	Median	SD	Min.	Max.	Range	LQ	UQ	IQR
COARSE	10	2,62	2,64	0,19	2,34	2,89	0,55	2,44	2,74	0,30
MASSIVE	19	3,68	3,73	0,17	3,32	3,98	0,66	3,60	3,77	0,17
FLAT	61	3,56	3,56	0,09	3,37	3,78	0,41	3,51	3,61	0,10
Total	90									

Fig.3.7 Box an whiskers plots of the 3 type of slags: coarse, massive and flat.

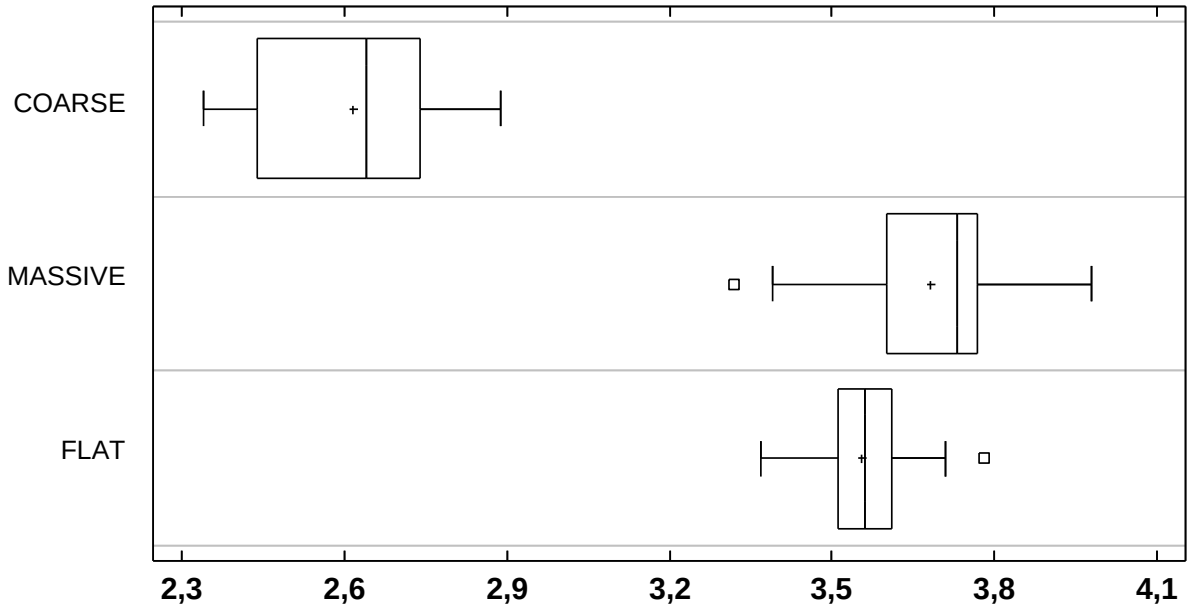

In conclusion, it has been verified that the measured densities of the slags show systematic differences between the coarse group, the flat type and the massive slags.
The coarse group formed by 9 samples has the lowest density range (ρ = 2.34 - 2.89 g/cm^3) with the mean value around 2.62 g/cm^3, which is close to the theoretical density of quartz.
The massive slags with 16 samples (ρ = 3.32 - 3.98 g/cm^3) and the flat type composed by 57 slags (ρ = 3.36 – 3.78 g/cm^3) are in the range expected for slags composed primarily by fayalite 50% and quartz 50% ($\rho_{Fa50\%-Qz50\%}$ = 3.50 g/cm^3).
However, the difference between the density values measured and the theoretical values expected – as far as concerned the flat slags essentially composed by fayalite (ρ_{Fa} = 4.39 g/cm^3) and magnetite (ρ_{Ma} = 5.15 g/cm^3) – is considered to be caused by the polycrystalline and the heterogeneous nature of the material, on one hand.
On the other hand, it is thought to be caused by the presence of microporosity.

The following chemical and minero-petrographic analyses were performed on the samples selected on the basis of the statistical distribution of the density data.
In particular, the samples of each type were chosen in order to cover the whole density range of variability.
Additionally, several samples with density values similar to the mean and to the median were selected in order to have the most representative data of each group.
The Figure 3.8 shows the box and whiskers plots of the three types with the samples analysed (dots). The table 3.5 displays the total number of slags analysed and the kind of analytical investigation performed.

Fig 3.8: Box an whiskers plots of the coarse, massive and flat types. The dots were located at the density values of the samples analysed.

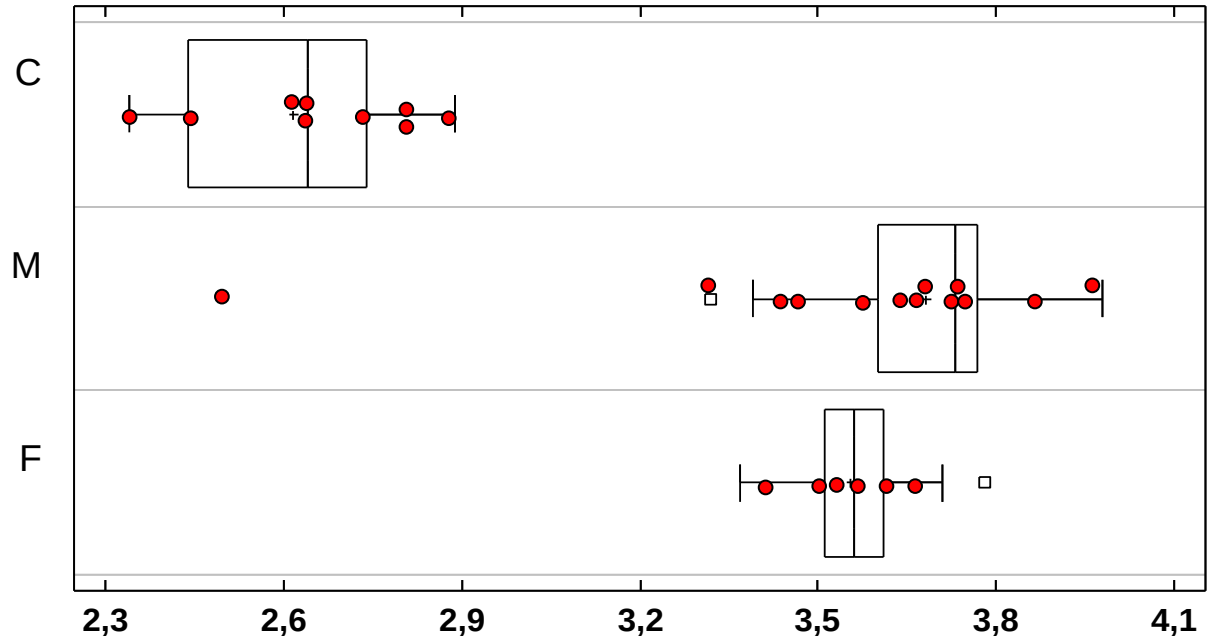

Tab. 3.5: List of the Luserna slags fully investigated and the types of measurements carried out.

Type	N.	Density (g/cm^3)	Analytical Name	OM	XRPD	XRF	SEM-EDS	MC-ICP-MS.
Fluid	1	3,12	LU-F52	√	√			
COARSE	9	2,34	LU-G74	√	√	√	√	
		2,44	LU-G72	√	√	√		
		2,63	LU-G70	√	√	√	√	√
		2,63	LU-G71	√				√
		2,65	LU-G69	√	√			√
		2,76	LU-G56	√	√	√	√	√
		2,79	LU-G58	√	√	√	√	√
		2,79	LU-G59	√	√			√
		2,89	LU-GM57	√	√	√	√	√
MASSIVE	13	2,54	LU-M48	√	√			
		3,32	LU-PS63	√				
		3,45	LU-M4	√	√		√	√
		3,45	LU-PS64	√	√	√		
		3,60	LU-PS65	√	√	√		√
		3,67	LU-PS66	√				
		3,68	LU-M50	√			√	
		3,69	LU-M47	√	√	√	√	√
		3,76	LU-PS38	√	√	√		
		3,75	LU-PS45	√	√			√
		3,77	LU-M5	√	√	√		
		3,89	LU-M60	√	√		√	
		3,98	LU-PS67	√				
FLAT	6	3,43	LU-P68	√	√	√	√	√
		3,52	LU-P9	√	√	√	√	√
		3,55	LU-P61	√	√	√	√	√
		3,56	LU-P62	√				
		3,62	LU-P6	√	√	√	√	√
		3,67	LU-P34	√	√	√	√	√
TOT	28							

3.3.3 Minero-petrographic and Chemical Analyses

Slags are almost totally composed of silicate minerals. As Bachmann pointed out (1982), the term mineral in its strict sense is only valid for naturally formed compounds, while the slags are artificial materials. When the term “mineral” is used to refer to the slag components, it indicates the naturally occurring equivalents to which the slag components nearly resemble.

Coarse Slags

The semi-quantitative phase evaluation (XRPD-RIR method) performed on 8 coarse slags shows that quartz is the most abundant mineral in the coarse slags with a mean value of 74,9 wt%.
A such high amount of quartz would be anomalous in the modern slags. In fact, its occurrence may indicate a problem occurring during the smelting process, such as a lack of temperature or an interruption of the process.
The presence of cristobalite (3wt%), the high temperature polymorph of silica, indicates the achievement of high temperature.

Tab 3.6: Mineralogical phases expressed in weight percentages (%wt) calculated by XRPD-Rir Method.

	Sample	Quartz	Olivine	Cristobalite	Magnetite	Pyroxene
COARSE	LU-G56	71	14	3	3	0
	LU-G57	66	17	3	5	0
	LU-G58	81	15	2	1	0
	LU-G59	80	18	2	0	0
	LU-G69	76	15	3	1	5
	LU-G70	70	11	4	0	0
	LU-G72	82	10	2	1	4
	LU-G74	72	14	3	0	0
	Mean	**74,8**	**14,3**	**2,8**	**1,4**	**1,1**
	SD	5,9	2,7	0,7	1,8	2,1

The second most abundant mineral is the newly formed phase olivine (14,3 wt%), mainly composed by fayalite (Fe_2SiO_4) with several percentages of forsterite (Mg_2SiO_4), the magnesium rich end-member of the olivine solid solution serie.
The semi-quantitative evaluation of the mineralogical phases reveals also few percentages of magnetite (Fe_3O_4) and pyroxenes, mostly formed by diopside ($MgCaSi_2O_6$).
The optical microscopy observations carried out on 9 coarse slags display large grains of quartz as a relict phase (restitic quartz, see Fig. 3.9 A).
The presence of residual carbonised wood (Fig. 3.9 B), probably used as fuel during the smelting, was observed in 2 coarse slags (LU-G72 and LU-G74).
The olivines are present with different morphologies ranging from polyhedral texture (euhedral –subhedral outlines, no internal structure, solid core) to hopper texture (skeletal crystals, with hollow cores and/or embayed edges).

Fig.3.9 : A) Large grain of fracture quartz. B) Reflected and transmitted light image of carbonised wood.

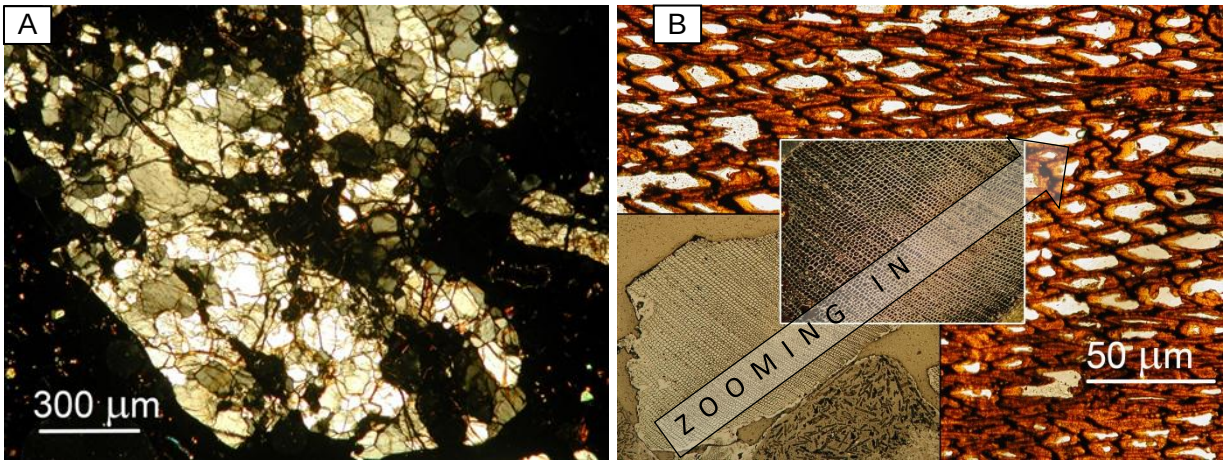

Fig 3.10: A) Prismatic olivine in transmitted light observation. B) Hopper olivine crystal in cross polarized light.

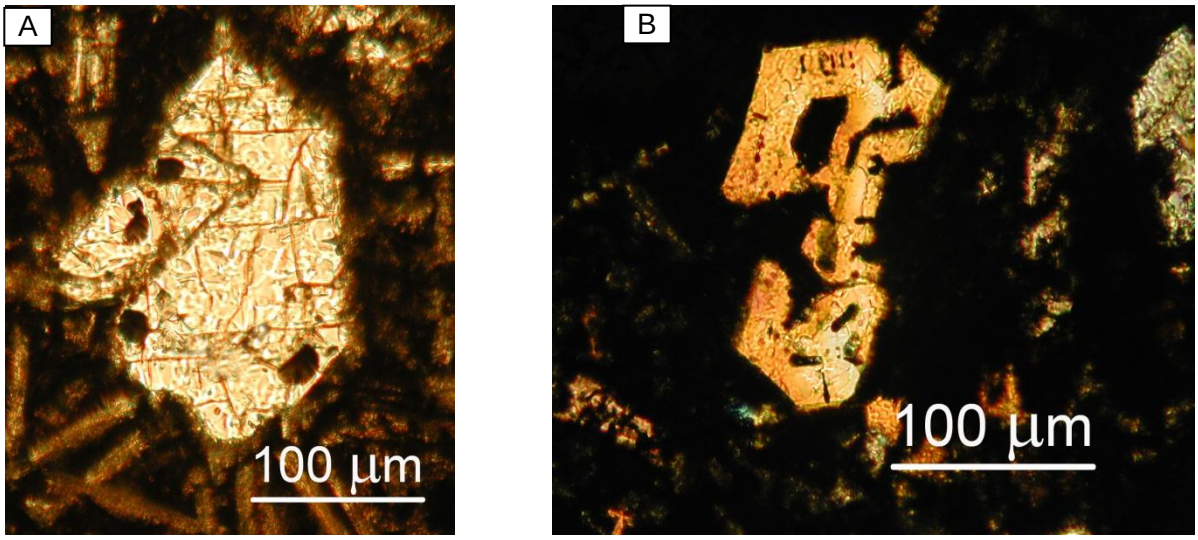

Fig. 3.11: Backscattered scanning electron photomicrographs image of hopper (A) and prismatic (B) olivines (Ol). Magnetite (Ma: light grey) dendritic (A) and sub-euhedral (B).

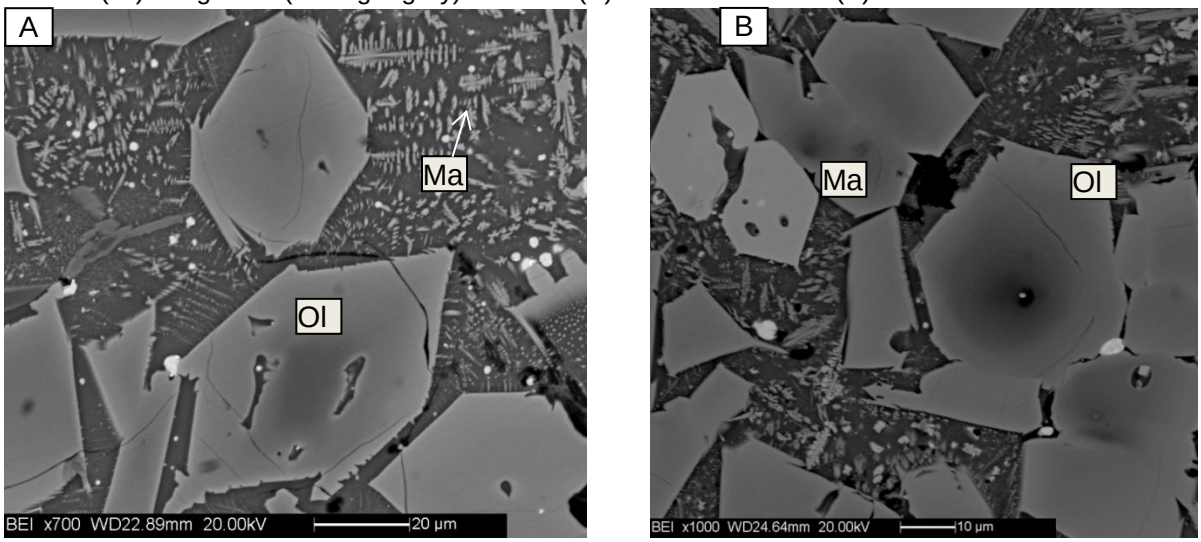

As evaluated by the experimental studies of Donaldson (1974), the olivine morphologies observed in the coarse slags suggest low cooling rates. The polyhedral one has grown at 0,5°C/hr whereas the skeletal with hollow cores and/or embayed edges has grown at 2,5°C/hr.

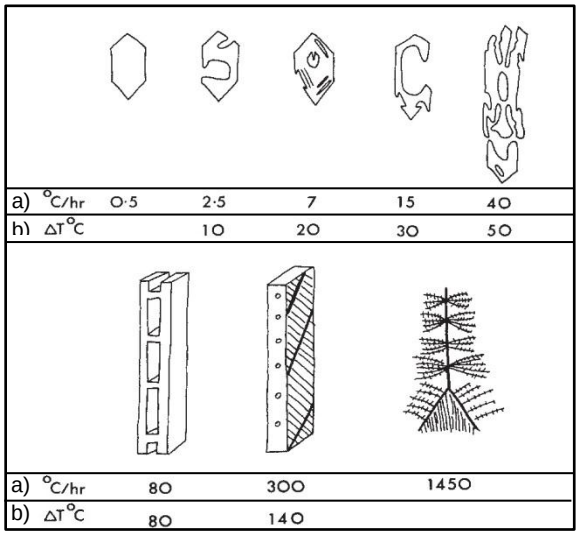

Fig. 3.12: Donaldon's summary of the change in shape of olivine crystals during different cooling rates on anhydrous rock compositions.
a) cooling rates; b) supercooling.
0.5°C/hr: polyhedral crystal;
2.5°C/hr: hopper crystals with round indentations;
7°C/hr: externally subhedral to euhedral hoppers, with marked internal skeletal;
15°C/hr: externally euhedral, but internally hollow, hoppers, with perceptible edge growth;
40°C/hr: more elongate hoppers, with marked edge growth;
80°C/hr: acicular chains, lacking dendritic structure in the (010) plane
350°C/hr: chain olivines with bladed parallel to (010) and develop internal dendritic structure (lattice olivine); 1450°C/hr: parallel growth of chain and lattice olivine.

The observations on backscattered electron image (BEI) reveals an olivine compositional zoning. In particular, it was observed a concentric zoning, in which the zones are parallel to the advancing crystal faces.
The binary equilibrium phase diagram fayalite (Fa) – forsterite (Fo) displays a complete miscibility both in the solid and in the liquid states. This kind of diagram requires that the compositions of the solid and the liquid phases are in equilibrium during cooling. The equilibrium can only be maintained if cooling is very slow in order to have sufficient time for the atomic diffusion.

Fig. 3.13: Olivine binary phase diagram.

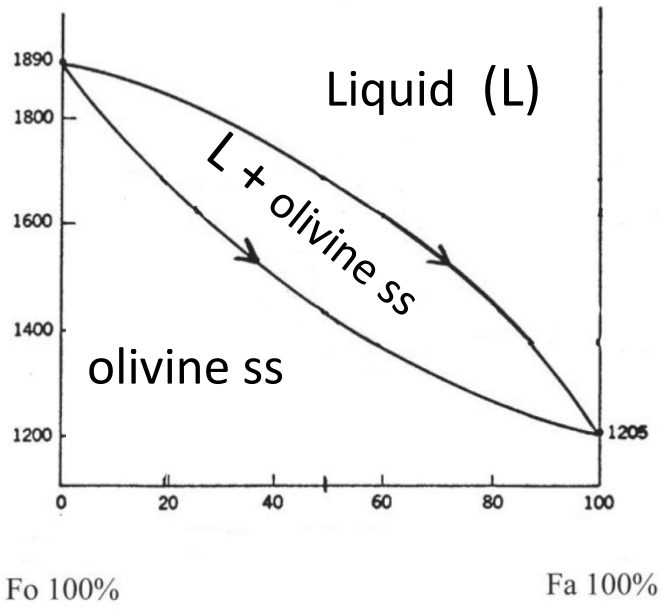

However, during the smelting processes, the equilibrium condition were not satisfied, forming non-equilibrium microstructural features such as zoning.
This type of segregation results in the formation of a core of the crystal, which was firstly formed, with different chemical composition to the outer rim, lastly formed.
Two plots of the same generic binary diagram with different equilibrium conditions are presented above.
In the plot 1, the slow cooling allowed the formation of a crystal with a homogeneous chemical composition. The plot 2 shows a non-equilibrium behaviour due to the faster cooling rates, resulting in a heterogeneous composition of the crystals.
In fact, the rim of the crystals are enriched with the low melting component. On the other hand, the core of the crystal has an higher amount of the high-melting component.
Fig. 3.14: 1) Equilibrium freezing. 2) Non-equilibrium freezing.

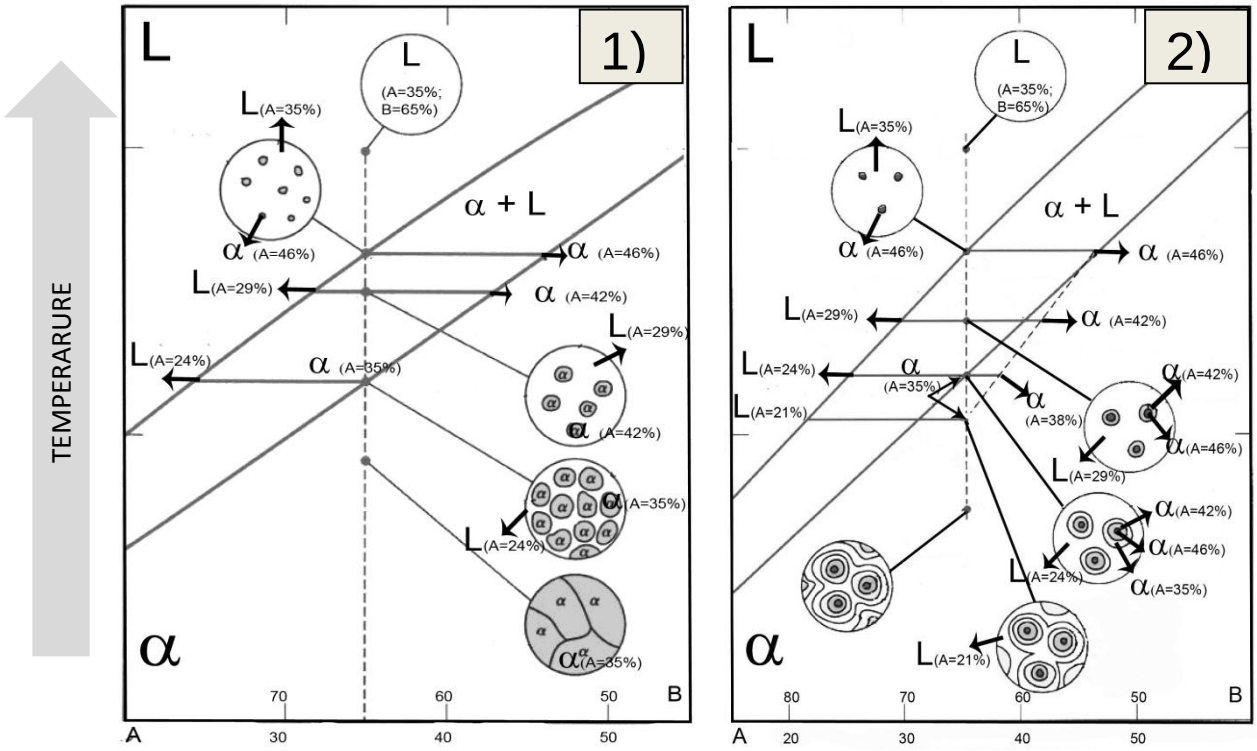

The micro chemical analyses (EDS) showed that the cores of the olivine are relatively rich in forsterite reflecting crystallization at higher temperatures than the rim. In response to falling temperatures, the successive outer zones (ending with the rim) are progressively richer in fayalite.
The analyses of the opaque minerals in reflected light microscopy display several crystals of partially reacted sulphides.
Two different types of sulphides were detected: 1) small grain of fractured and partially reacted chalcopyrite (maximum diameter measured 0,50 mm) and 2) large prills (maximum diameter measured 2 mm) of sulphides with more complex chemical compositions.
In addition to these two main types of sulphides, a few small droplets of Cu-sulphides mostly formed by covellite (CuS) were observed.
The first type of sulphides (Fig. 3.18 A, Pag. 31) is mostly composed by chalcopyrite (Cp: $CuFeS_2$), indicating that it was the ore used as the charge, confirming what previously suggested by Cattoi et al (1995). These primary copper-bearing minerals are

often associated with pyrite and partially transformed in bornite (Bo: Cu_5FeS_4), a newly formed mineral with an higher content of copper than the chalcopyrite charge.
The second type of sulphides (Fig. 3.18 C, pag. 31) shows spheroidal crystals of symplectitic intergrowth (later often abbreviated: *sym*) of bornite and pyrrhotite (Po: $Fe_{(1-x)}S$, where x ranges from 0 to 0,17) formed from chalcopyrite, often associated to exsolution and decomposition textures.
Symplectites are distinctive penetration textures, formed by vermicular intergrowths of two and occasionally three minerals, which are present in variable and almost comparable, amounts. This kind of texture is variously named: eutectic, cotectic, eutectoid, pseudo-eutectic, myrmekitic, symplectitic, granophyric, graphic, subgraphic, micrographic (Ramdohr, 1969).
The vermicular shape presumably results from the inability of either mineral to impose a crystal form against the other, coupled with growth outwards from a single nucleus (Vernon, 2006).
Ramdohr (1969) listed the known minerals that occur in *sym*, some of them are: chalcocite – bornite, chalcocite - covellite, bornite - covellite, chalcopyrite - chalcocite, chalcopyrite - bornite, pyrite - chalcopyrite. The author proposed a classification of the processes that generate the symplectitic textures. He classified the pyrite – chalcopyrite intergrowth as simultaneous formation at low temperature. The *sym* of chalcopyrite – bornite and of chalcopyrite-chalcocite were classified as eutectoid and exsolution intergrowths, respectively. The chalcocite-covellite symplectitic intergrowth occurs as a result of the decomposition of the solid solution, whereas the chalcocite-bornite *sym* is the product of a replacement process.
The other type of intergrowth found in the slags sulphides are exsolution (unmixing), defined by Ramdohr as a kind of transformation texture that could occurs as a result of both simple and complex processes. The simple case occurs when the initially high-temperature homogeneous solid solution separates during cooling into different crystalline minerals without the addition or the removal of any materials. On the other hand, the complex exsolutions involve a disturbance of the stoichiometric relationship, for example the formation of high-temperature crystals without precisely stoichiometric called anomalous solid solution as the chalcopyrite – pyrrhotite exsolution. It should be noted that the addition or the removal of material is frequent in systems and events, in which large mobility is involved. In addition, the high temperature solid solution could form products with different crystallography or chemical composition (the bulk composition do not change), producing a exsolution texture strictly linked to a decomposition structure. The chalcopyrite can exsolve bornite and pyrrhotite (Ineson, 1989).

In order to verified their Cu-Fe-S compositions, a meticulous study on the sulphides was carried out by means of SEM-EDS and plotted in the Cu-Fe-S system isothermal diagram at 700°C.
An isothermal plot shows the phases formed at a particular temperature and it is useful for predicting the phases and their amounts at that temperature (Campbell, 2012).
The ternary Cu-Fe-S referential diagram at 700°C was drawn after 200 experiments summarized by Yund and Kullerud (1966) in their paper and it is shown in Fig. 3.15.

Fig 3.15: Ternary Cu-Fe-S diagram in wt% at 700°C modified after Yund and Kullerud (1966). Bo: bornite, Cp: chalcopyrite, Py: pyrite, Po: pyrrhotite, L: liquid, ss: solid solution.

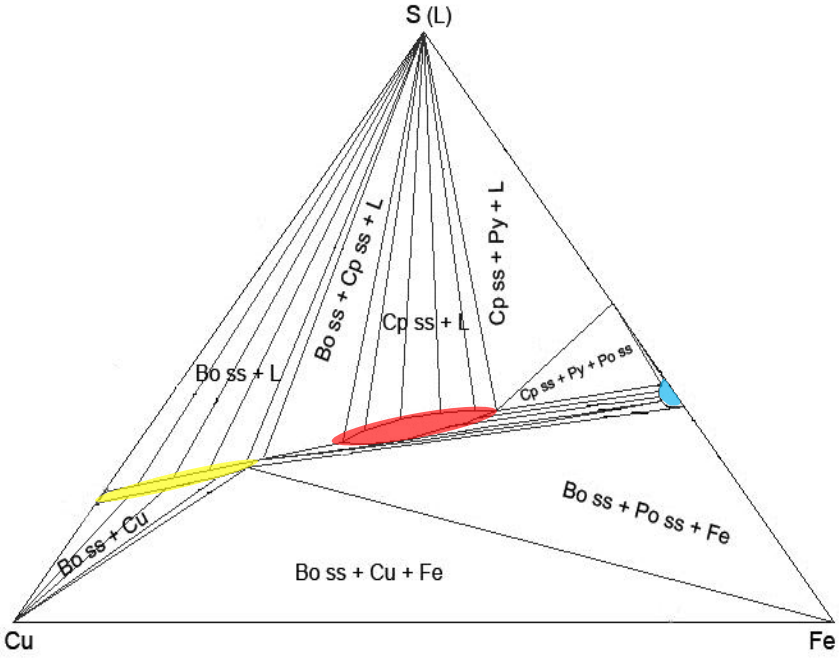

Considering the central area of the Cu-Fe-S diagram (Fig. 3.15), it is notable that three extensive solid solutions are stable: bornite (shaded yellow area), chalcopyrite (shaded red area) pyrrhotite (shaded blue area). The compositional variability field of bornite includes the following compositions: Cu_2S (chalcocite), $Cu_{1,8}S$ (digenite) and Cu_5FeS_4 (stoichiometric bornite). The chalcopyrite field is positioned in the central part of the plot, just below its stoichiometric composition.

The extension of the pyrrhotite field into the ternary, is quite limited; containing a maximum of 3 atom % copper at 700°C (Yund and Kullerud, 1966).

The following binary diagram of the temperature- sulfur-rich phase compositions of the Cu-Fe-S system could be useful to summarize many of the aspects of the ternary diagram.

Fig. 3.16: Speculative diagram drawn by Barton and Skinner (1967). ccp: chalcopyrite, cb: cubanite, py: pyrite, id: idaite, po: pyrrhotite, dg: digenite, cv: covellite, su: sulphur, iss: intermediate solid solution. The authors omitted details associated with the numerous low-temperature phases on the copper-sulfur and iron-sulfur joins.

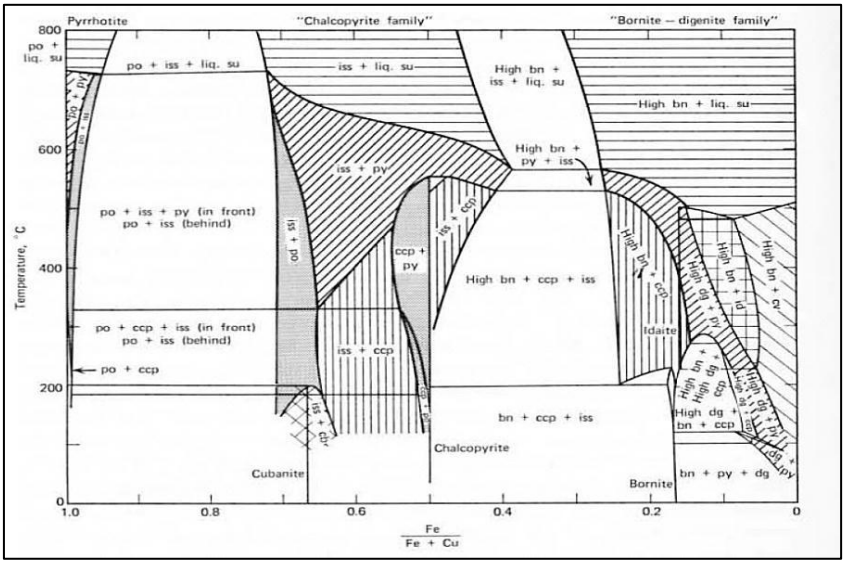

This phase diagram displays that extensive solid miscibility remains possible among the sulphides even to low temperatures (bornite-chalcopyrite-intermediate solid solution; bornite-pyrite-digenite, pyrrhotite chalcopyrite, etc.). This results in the formation of intricate intergrowth of sulphides (symplectites, exsolutions, decompositions), like those observed in the second type of sulphide showed in the Fig.3.18C (pag. 31).

The sulphides of the coarse slags were plotted in the Cu-Fe-S diagram at 700°C. They are mostly Cu-Fe sulphides and are located between the chalcopyrite and bornite fields of stability and in the field of stability of bornite .This indicates a partial transformation from the chalcopyritic-charge to the copper enriched bornite-like sulphides. A few Cu-sulphides were observed in small droplets with a composition ranging from CuS to Cu_2S.
The Fe-sulphides in the coarse slags have a pyrrhotite-like composition, that derived from the transformation of the sulphide charge, mostly composed by chalcopyrite and secondly by pyrite.
However, it cannot be excluded that several quantities of pyrrhotite were present in the sulphide charge (before the smelting), together with chalcopyrite and pyrite.

Fig. 3.17: Compositions of the sulphides in the coarse slags plotted in the ternary Cu-Fe-S diagram at 700°C.

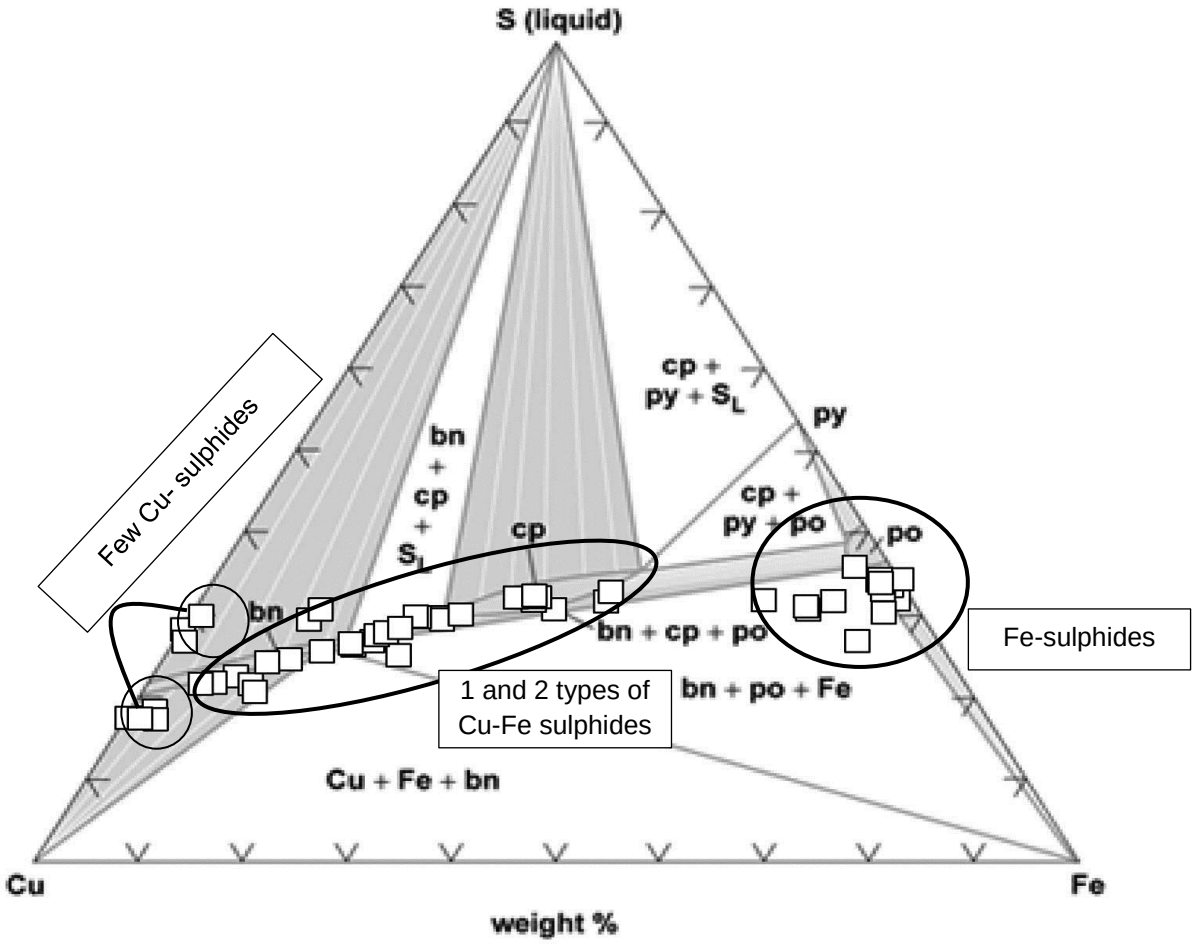

Fig. 3.18: A) Micrograph of a chalcopyrite (Cp: light yellow) with enriched bornite-like composition areas (Bo:pinkish-brown coloured). B) Small grain of chalcopyrite (core) with incipient transformation in bornite (rim). C) symplectite texture (central) of pyrrhotite (Po: light yellow-white) and bornite (sky-blue oxidised colour) and chalcopyrite surrounded by bornite. D) Relitic sulphide association of chalcopyrite and pyrite with blue areas of partially oxidised bornite. E) Pyrrhotite-dominant area with exsolution and symplectitic-like intergrowth of bornite (blue) and chalcopyrite (yellow). The latter is also in small areas rounded by bornite. F) Grain of covellite (cv: bluish white).

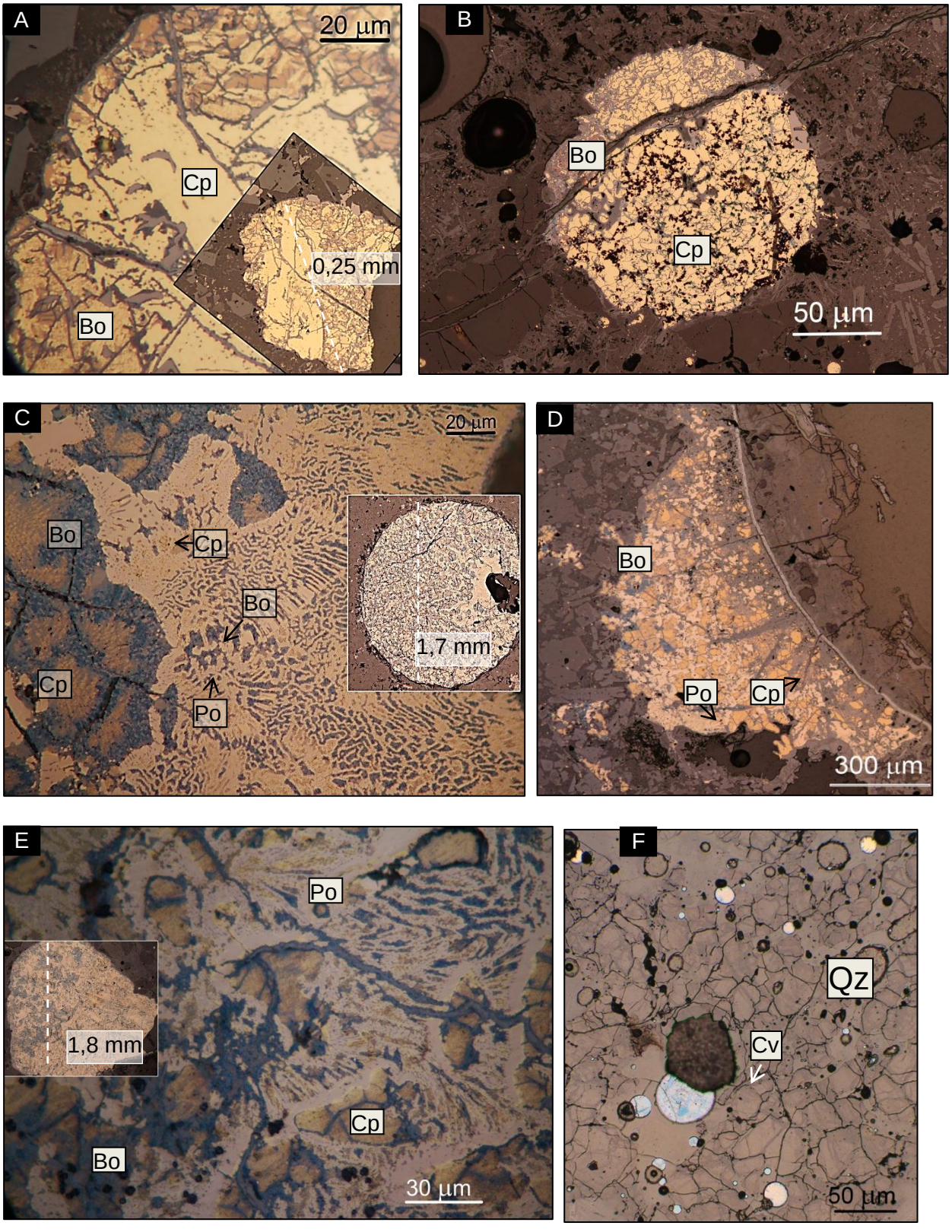

The chemical bulk analyses (XRF) of the most representative coarse slags detected by the minero-petrographic analyses were performed using the same powders analysed by XRPD.

Tab. 3.7: Chemical bulk compositions of the coarse slags of Luserna

	Sample	SiO_2	TiO_2	Al_2O_3	Fe_2O_3	MnO	MgO	CaO	Na_2O	K_2O	P_2O_5
COARSE	LU-G74	47,15	0,18	5,46	38,34	0,09	1,09	3,19	0,17	1,28	0,18
	LU-G72	54,54	0,30	8,03	27,39	0,20	2,95	2,34	0,11	0,97	0,21
	LU-G70	56,85	0,16	4,75	27,57	0,12	1,66	3,01	0,11	0,95	0,12
	LU-G56	54,89	0,22	6,38	29,07	0,19	2,19	3,92	0,19	1,45	0,16
	LU-G58	60,26	0,15	3,91	26,96	0,12	1,72	1,84	0,05	0,67	0,10
	LU-GM57	47,95	0,18	5,25	36,62	0,14	2,14	2,98	0,10	1,02	0,15
	Mean	**53,61**	**0,20**	**5,63**	**30,99**	**0,14**	**1,96**	**2,88**	**0,11**	**1,06**	**0,15**
	SD	5,12	0,06	1,43	5,10	0,04	0,63	0,72	0,08	0,27	0,04

As Bachmann (1982) suggested, it is necessary to use a liquid plot for a ternary phase diagram in order to study the relationship between chemical composition and compound formation during and after the solidification of the slags. In a liquid plot, the temperatures at which freezing begins for each composition are transferred onto a triangular diagram in which the liquidus temperatures are plotted as isothermal contours (Camppell, 2012).

The chemical composition of the slags may be interpreted in terms of their major oxide components. For this reason, several ternary systems have been proposed.

In particular, I used the one suggested by Morton and Wingrove (1969b; 1972), which involved the anorthite (CaAl2Si2O8) - FeO – SiO_2 system.

Fig:3.19: Ternary anorthite-FeO-SiO_2 diagram.

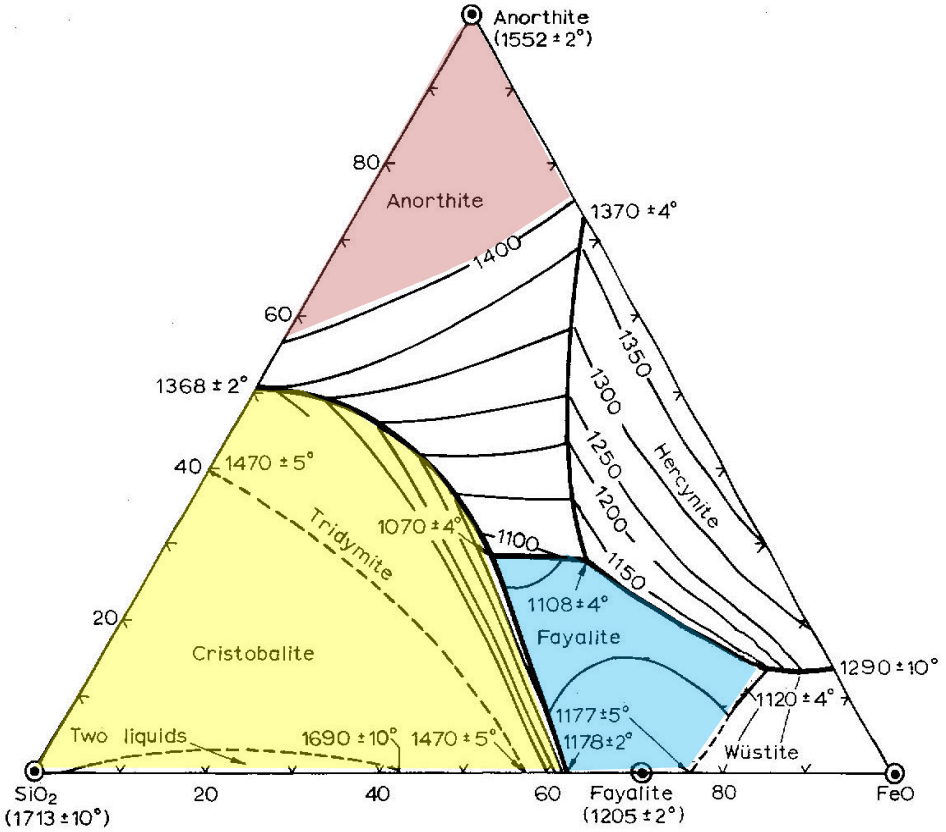

An examination of the system on anorthite – FeO (+MgO) – SiO_2 join plain reveals three wide ranges of stability: 1) the lowest-melting composition range around the fayalite area (shaded blue colour), at a temperature lower than 1250°C, culminating with low-melting reactions at 1120°C, 1108°C and 1070°C. 2) The area coloured in red indicates the anorthite field of stability (1552-1400°C) and 3) the area coloured in yellow indicates the field of stability of quartz with its high-temperature polymorphs (cristobalite and tridimite).

It should be possible to verify the melting temperature of each slag by plotting the slag chemical compositions on this diagram.

As suggested by Morton and Wingrove (1969), in order to correctly plot the data on the diagram it is necessary to assume that: 1) any possible presence of Fe_2O_3 derives from FeO by oxidation. Actually, the Fe-oxides present in the Luserna slags is magnetite, as the XRPD analyses shown. However, in order to use the ternary diagram we assumed that all the Fe-oxides of the bulk analyses are FeO. 2) The maximum amount of anorthite will be calculated from the CaO and Al_2O_3 oxides measured by the bulk chemical analyses. No more anorthite can be formed after each of these oxides has been exhausted. The excess of SiO_2 can then be calculated and used as the third component of the ternary diagram together with FeO and anorthite.

All the bulk chemical compositions of the five coarse slags are gathered together into the SiO_2 region. SiO_2 is in fact the major component of these type of slags, in accordance with the mineralogical phase analyses (XRPD tab).

If all the components had undergone a total melting and the system had been in equilibrium, the ternary diagram would have indicated that these slags were produced in a high-temperature process, ranging from 1470°C to 1690°C.

On the basis of the optical observations, it was observed that the high amount of SiO_2 in the coarse slags is a “restitic” or residual material that did not take part in the melting. On the contrary, the newly formed phases like fayalite and Fe-oxides are the result of a partial melting.

Fig 3.20: Bulk chemical compositions of the coarse slags plotted in the ternary SiO2-FeO(+MgO)-Anorthite diagram.

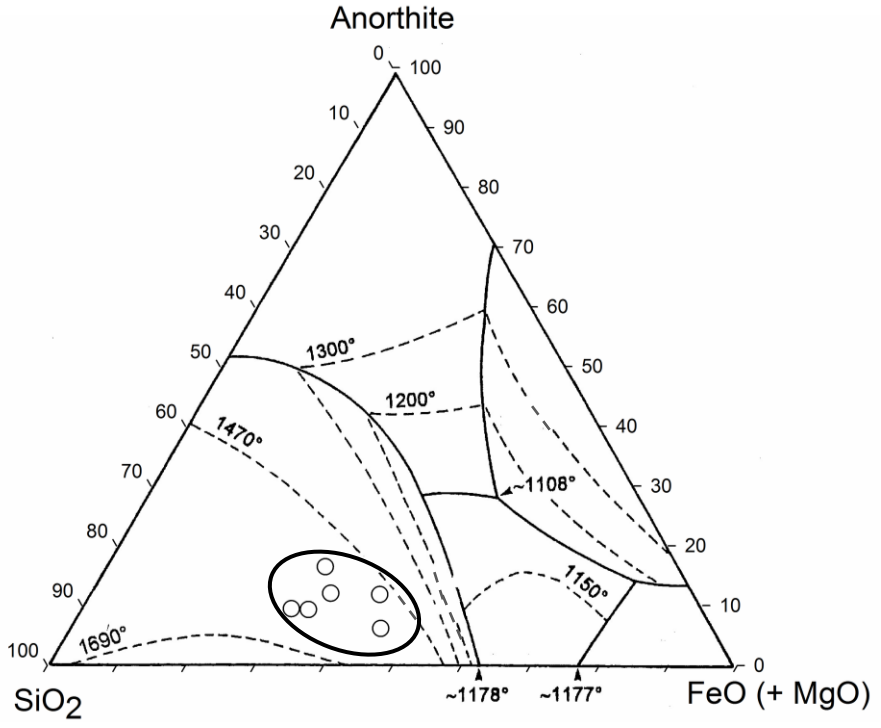

Massive Slags

The Massive slags are characterised by a higher amount of olivine and magnetite (71,25 wt% and 17,75 wt% respectively), whereas quartz was detected only in one of the 8 samples analysed by X-ray powder diffraction. In this type of slags, the sum of the olivine and magnetite is more than 80wt%, as shown in the table below.

Tab 3.8: Mineralogical phases of the massive slags expressed in weight percentages (%wt) and calculated by the XRPD-Rir Method.

	Sample	Quartz	Olivine	Cristobalite	Magnetite	Pyroxene
MASSIVE	LU-M4	-	71	-	17	12
	LU-M5	-	54	-	32	14
	LU-M47	-	68	-	17	15
	LU-M60	-	68	-	25	7
	LU-PS38	-	64	-	18	18
	LU-PS45	-	84	-	12	4
	LU-PS65	-	86	-	14	0
	LU-PS64	4	79	-	7	14
	Mean	**0,5**	**71,25**	-	**17,75**	**10,5**
	SD	1,4	10,5	-	7,7	6,2

The 12 massive thin sections analysed by the optical microscopy revealed that the most abundant phase is olivine with different low-cooling rate habits ranging from prismatic to elongate hoppers (cooling rates from 0,5°C/hr to 40°C/hr) and showing a Forsterite-rich core zoning (Fo-zoning). Only in two samples (LU-PS65 and LU-PS66) a few acicular chain olivines were found (cooling rate: 80°C/hr).

Fig.3.21: A) Backscattered scanning electron photomicrographs image (BSI) of the Fo-zoning in a prismatic olivine. B) and C): Elongate hoppers olivine.

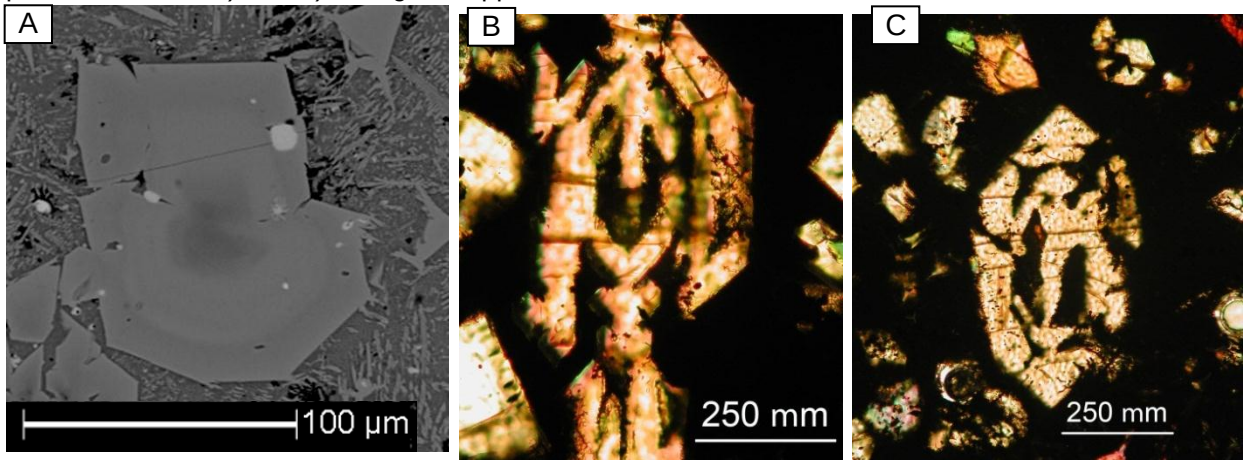

Magnetite was observed in aggregate and it is often associated with copper droplets widespread in the slags (Fig.3.22). The copper droplets have a maximum diameter of 350 µm.

Two types of sulphides were found: the first is characterised by a large grain of an intermediate chalcopyrite-pyrrothite composition with alteration to covellite (CuS) and chalcocite (Cu_2S) as well as bornite (Cu_5FeS_4). The sizes of these sulphide grains range from 1 to 2 mm.

The second and most common type consists of covellite-chalcocite-like compositions. Here, the matte reached the highest copper enrichment, showing only copper sulphides.

Fig. 3.22: A) Aggregates of magnetite (Ma: light grey). B) Copper prills associated with magnetite. C) copper droplet surrounded by chalcocite (Ch: grey)

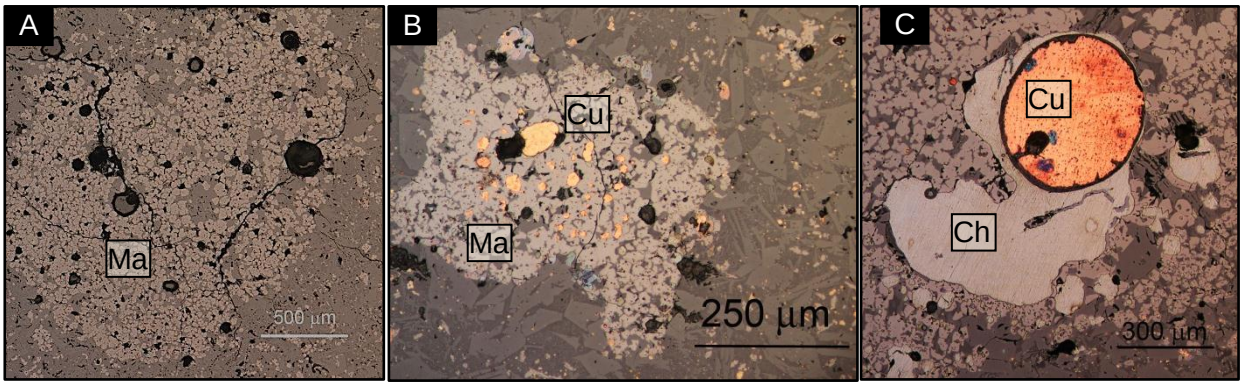

Fig. 3.23: Secondary pyrrhotite (light yellow) grain with exsolution net of chalcopyrite (Cp:yellow) partially decomposed in bornite (Bo) - covellite (Cv: blue in the chalcopyrite rims).

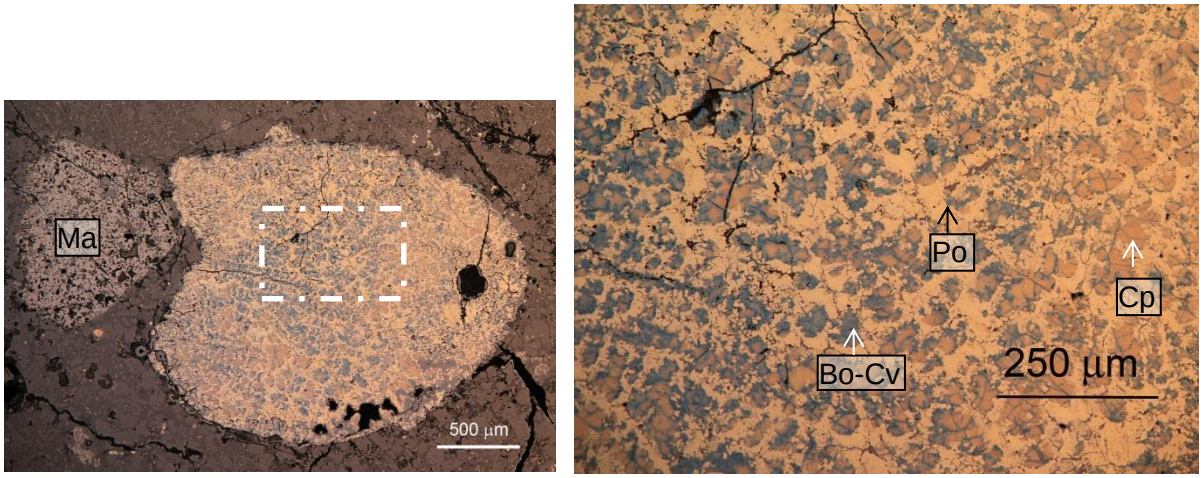

Fig. 3.24 A) Large crystal of covellite (cv: indigo.blue). B) Small grain of chalcocite-digenite (grey) with exsolution lamellae of bornite (brown-red).

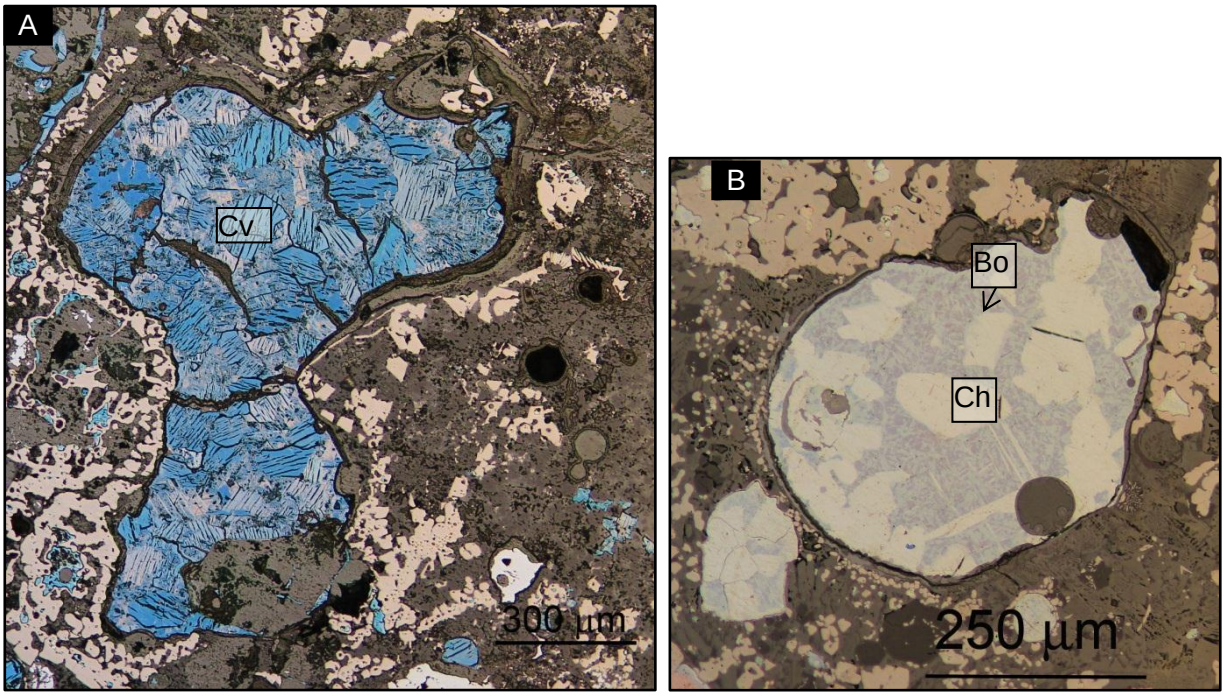

The iron, mostly involved in the formation of olivines and in the formation of magnetite, has been observed in the first group of sulphides as pyrrhotite.
Plotting the compositions of the sulphides analysed by means of SEM-EDS, a correspondence with the micro-chemical analyses and the optical microscopy observations was identified.

Fig. 3.25: Compositions of the sulphides in the massive slags plotted in the ternary Cu-Fe-S diagram at 700°C.

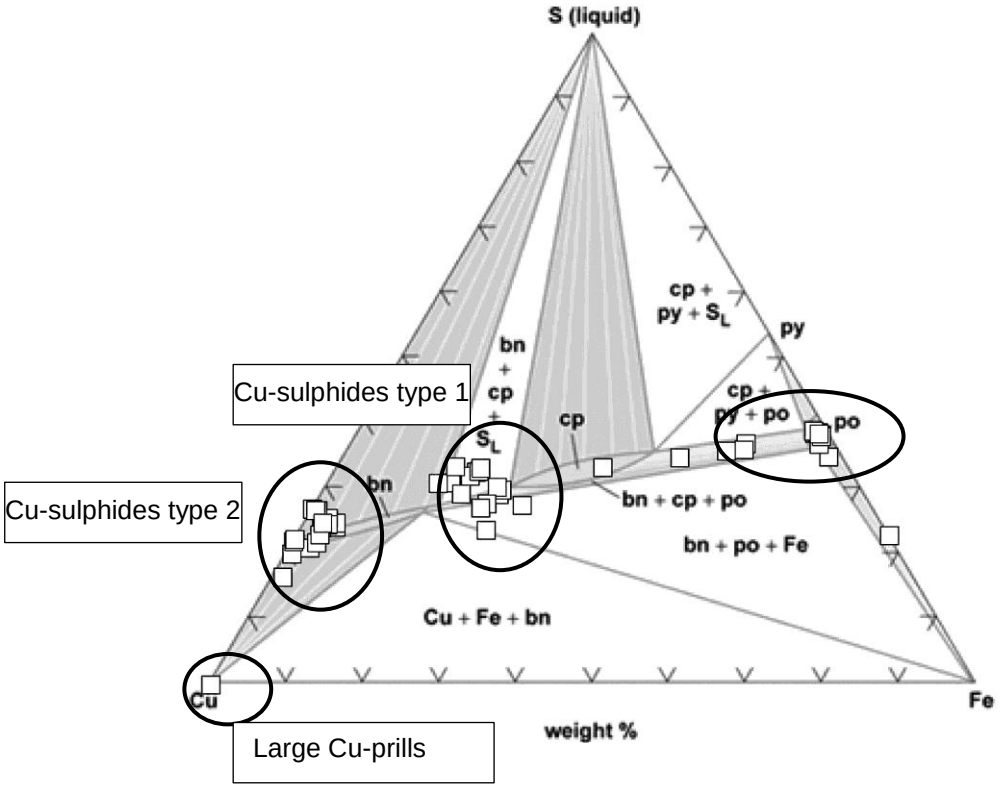

Unlike the mean sulphide composition of the coarse slags, the majority of the massive sulphides are a high copper-enriched matte with a chalcocite-covellite like composition.
Other sulphides have an intermediate bornite-chalcopyrite composition.

The chemical bulk analyses performed on 5 representative massive samples are consistent with the mineralogical phases evaluation.
They show a lower mean content of SiO_2 and a higher mean content of iron oxide compared to the coarse slags.

Tab. 3.9: XRF chemical bulk compositions of the massive slags of Luserna.

	Sample	SiO_2	TiO_2	Al_2O_3	Fe_2O_3	MnO	MgO	CaO	Na_2O	K_2O	P_2O_5
MASSIVE	LU-PS64	34,52	0,24	6,55	44,34	0,24	3,24	6,77	0,16	1,36	0,17
	LU-PS65	28,41	0,19	5,41	55,55	0,20	2,76	3,23	0,07	0,95	0,14
	LU-M47	25,45	0,18	4,96	57,54	0,19	2,52	3,56	0,04	0,76	0,16
	LU-PS38	26,04	0,19	5,03	56,97	0,23	3,18	3,73	0,05	0,7	0,13
	LU-M5	25,77	0,18	4,64	56,43	0,26	2,33	3,73	0,10	0,87	0,14
	Mean	**28,04**	**0,20**	**5,32**	**54,17**	**0,22**	**2,81**	**4,20**	**0,08**	**0,93**	**0,15**
	SD	3,81	0,03	0,74	5,54	0,03	0,40	1,45	0,05	0,26	0,02

The chemical bulk data, plotted in the ternary diagram FeO (+MgO) – Anorthite – SiO_2, display a slag composition that overlapped with the field of stability of the olivine.
The data show a low variability, except for one sample: LU-PS64, which has a higher amount of SiO_2 (confirmed by the XRPD-RIR analyses), Al_2O_3 and CaO.
Through this diagram, the temperatures achieved during the process of massive slags formation were estimated and ranged from 1100 to 1200°C.
It is possible to assume that 1100-1200°C is the range of the temperatures achieved also during the formation of the coarse slag, characterised by such a high amount of restitic quartz that did not allow the evaluation of the process temperatures.

Fig 3.26: Bulk chemical compositions of the massive slags plotted in the ternary SiO_2-FeO(+MgO)-Anorthite diagram.

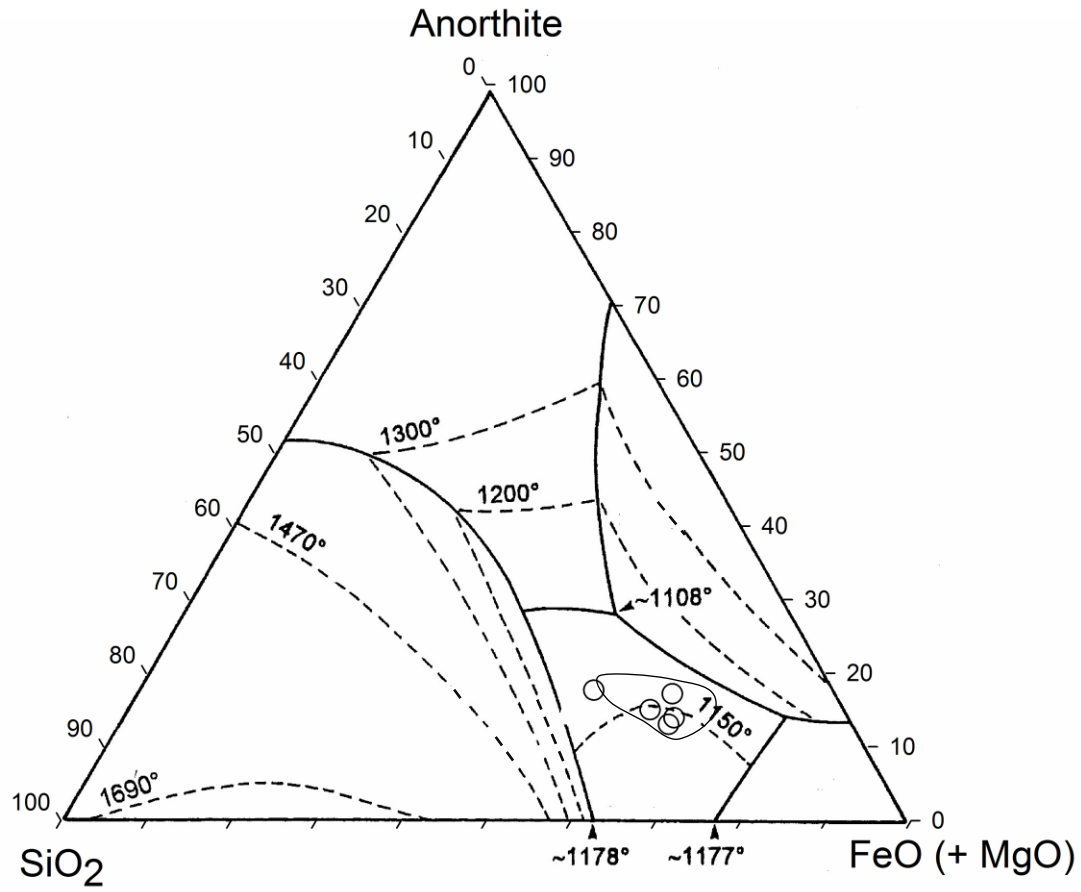

Flat Slags

The flat slags are characterized by the highest amount of fayalite (70 wt%) and the lowest amount of quartz (≈ 1 wt%). The amount of magnetite and pyroxene are 12 wt% and 9,5 wt% respectively.

Tab 3.10: Mineralogical phases of the flat slags expressed in weight percentages (%wt) and calculated by the XRPD-Rir Method.

	Sample	Quartz	Olivine	Cristobalite	Magnetite	Pyroxene
FLAT	LU-P68	7	74	-	19	0
	LU-P6a	0	81	-	12	7
	LU-P6b	0	82	-	13	5
	LU-P9	0	72	-	6	22
	LU-P34	0	75	-	18	7
	LU-P61	0	79	-	5	16
	Mean	**1,2**	**77,2**	**-**	**12,2**	**9,5**
	SD	2,9	4,1	-	5,8	8,0

Optical and electron microscopy investigations reveal olivines in the typical chain morphology, (80°C/hr -350°C/hr). In a few central parts of the slags, the olivines display also a prismatic habit, showing Forsterite-zoning in the core.

Fig. 3.27: A) BSI micrographs of chain olivines with dendritic magnetite (white) and B) prismatic olivine showing a core Fo-zoning.

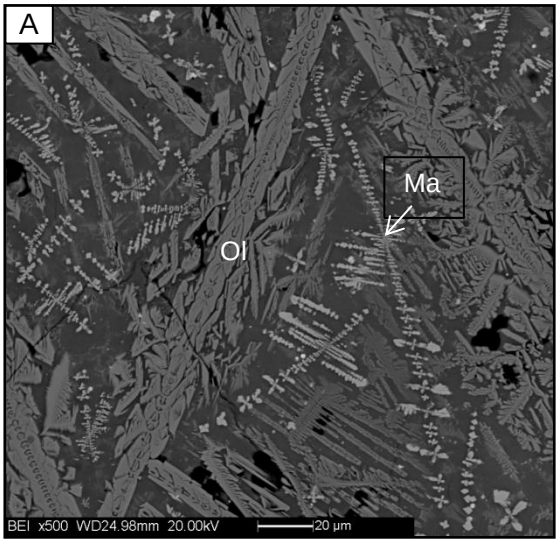

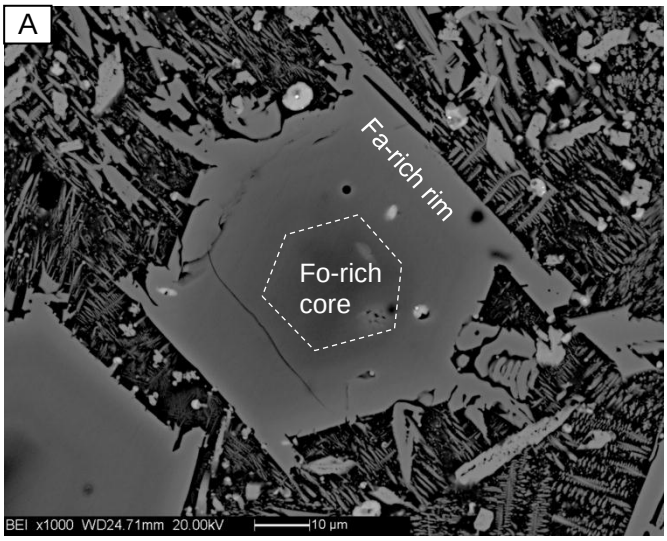

Magnetite and matte are both finely dispersed within the olivine matrix. The copper prills, in association with high Cu-enriched sulphides (matte), are smaller than the one present within the massive slags (the maximum diameter encountered is about 10 µm).

Fig. 3.28:) BSI micrographs of small copper droplets (white) associate with Cu-Fe sulphides (light grey).

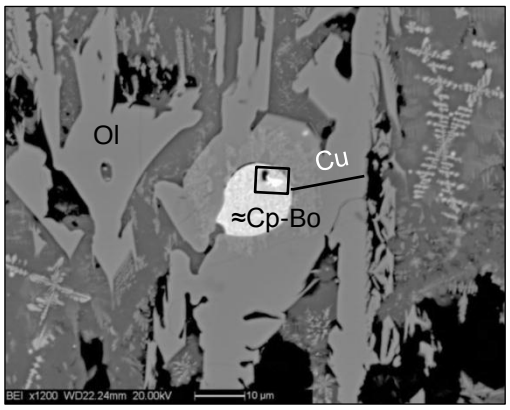

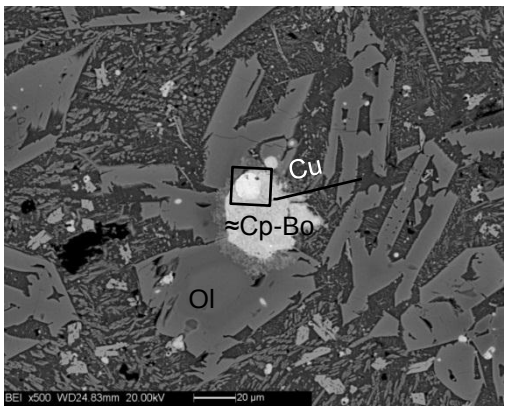

The total number of sulphides encountered in this type of slags is lower than the quantity observed in the coarse and the massive types. As shown in the ternary Cu-S-Fe diagram, these small sulphides are mostly characterized by a composition ranging from chalcopyritic to bornitic, with a numerous intermediate non-equilibrium phases. A few Fe-sulphides were observed and are always associated with the Cu-Fe-sulphides.

In contradiction to what the optical observation of the massive slags showed, no covellite, digenite or chalcocite were identified.

Fig. 3.29: Compositions of the sulphides in the flat slags plotted in the ternary Cu-Fe-S diagram at 700°C.

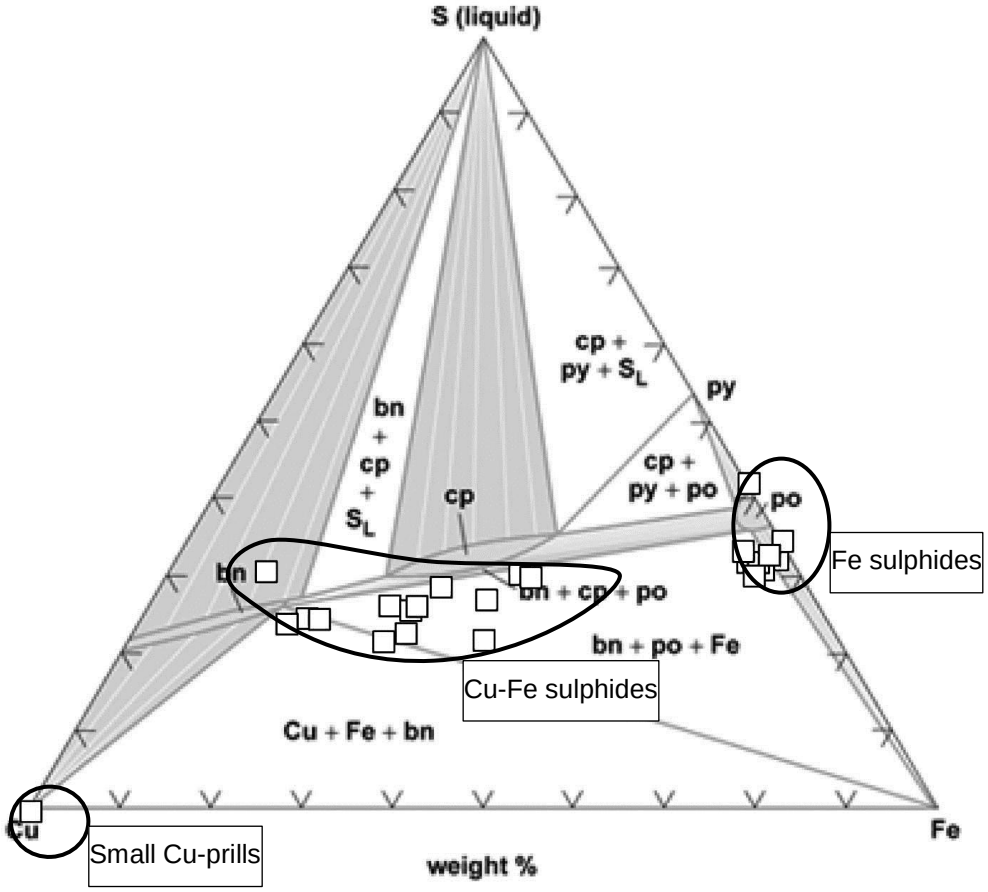

The bulk chemical analyses were performed on the most representative flat slag samples (tab. 3.11) using the powders prepared for the XRPD analyses.
The data were plotted in the ternary SiO_2- FeO (+MgO)-Anorthite diagram.

Tab. 3.11: XRF chemical bulk compositions of the flat slags of Luserna.

	Sample	SiO_2	TiO_2	Al_2O_3	Fe_2O_3	MnO	MgO	CaO	Na_2O	K_2O	P_2O_5
FLAT	**LU-P68**	35,09	0,25	7,33	45,22	0,23	3,86	4,05	0,1	1,13	0,15
	LU-P9	35,61	0,17	4,83	47,48	0,24	2,52	6,14	0,12	1,38	0,16
	LU-P61	33,87	0,21	5,86	47,31	0,22	2,92	5,39	0,12	1,29	0,16
	LU-P6	31,23	0,22	5,34	52,45	0,24	2,85	4,22	0,08	1,07	0,14
	LU-PR34	28,55	0,23	5,61	53,47	0,26	2,59	4,45	0,04	1,35	0,26
	Mean	**32,87**	**0,22**	**5,79**	**49,19**	**0,24**	**2,95**	**4,85**	**0,09**	**1,24**	**0,17**
	SD	2,95	0,03	0,94	3,58	0,01	0,54	0,89	0,03	0,14	0,05

As shown in Figure 3.30, all the slags analysed are in the field of fayalite stability, similar to the massive slags. However, these two types of slags are in two different areas of the field, due to the slightly higher amount of the total Si, Ca and Al oxides in the flat slags compared to the massive slags. On the contrary, the massive slags showed a higher amount of Fe-oxide.
Nevertheless, on the basis of the ternary diagram the flat slags were produced during a pyrometallurgical process characterised by temperatures ranging from 1100 and 1200°C, like the temperatures involved in the formation process of the massive slags.

Fig 3.30: Bulk chemical compositions of the flat slags plotted in the ternary SiO_2-FeO(+MgO)-Anorthite diagram.

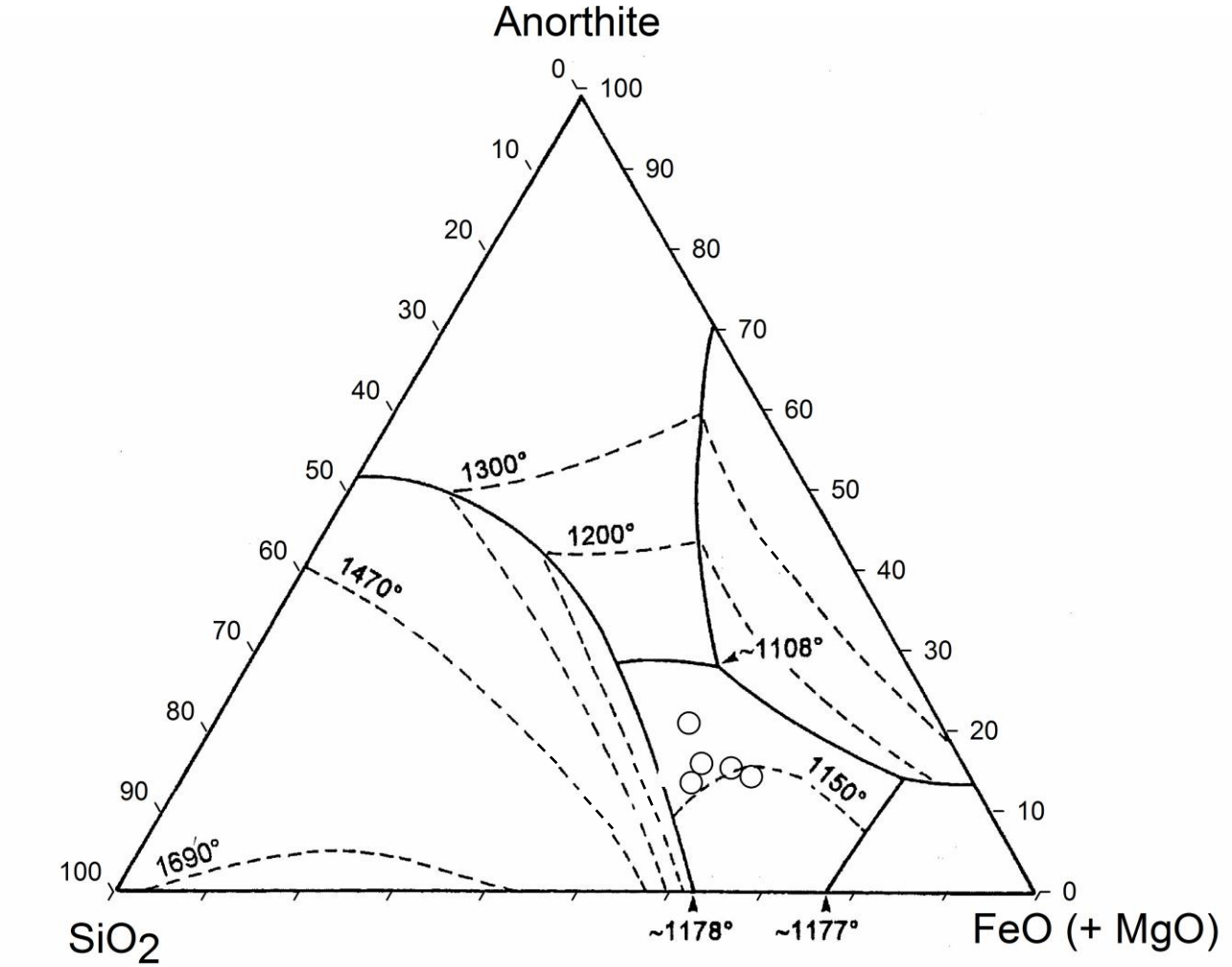

3.4 Discussion and Conclusion

On the basis of the macroscopic observations and the statistical analyses of the densities, three types of slags have been verified: coarse, flat and massive.
The minero-petrographic analyses confirmed the classification of the Luserna slags into the three types and lead to affirm that each type of slags is the by-product of distinct pyro-metallurgical operations with working-temperatures ranging from 1100 to 1200°C.
The coarse type of slags with the highest amount of quartz and the lowest amount of olivine as well as the presence of sulphides unreacted and partially transformed, may be the by-product of the first smelting process.
During the first smelting, the chalcopyrite dominant charge and a large amount of quartz were used in order to produce a Cu-enriched matte.
However, this first matte must have a chalcopyrite-bornite composition as evidenced by the coarse slag sulphides. Due to the low Cu-content, this matte has to be reprocessed probably without adding quartz-flux.

From the minero-petrographic point of view, the massive slags display a substantially lower amount of quartz, a higher amount of fayalite and magnetite compared to the coarse slags.
In addition, the sulphide relicts are almost completely transformed into the most abundant Cu-enriched sulphides (mostly with bornite and covellite-chalcocite compositions) and into large copper prills.
On the basis of all these differences, it is evident that the massive slags belong to a different process in comparison to that of the coarse slag formation. The latter slags were produced during the smelting of the natural sulphides (the chalcopyrite charge) plus the flux (quartz). On the contrary, the massive slags are related to a re-smelting of the low-grade Cu-enriched matte (first matte) formed during the smelting of the natural charge.
The products of the second smelting process are a high-grade Cu-enriched matte (second matte) and the massive slags in which this second matte is partially entrapped.

The amount of the mineralogical phases of the flat slags are comparable to those measured in the massive slag. In fact, they are mainly formed by olivines and magnetite whereas the quartz is almost absent.
However, the petrographic observations of the flat slags revealed a completely different textures. They are formed by long chain olivine, the aggregate of magnetite are in small dendrites widespread in the silicate matrix. The sulphides and the copper prills are less and smaller compared to the ones in the massive slags. In particular, the main composition of the sulphides has a lower copper enrichment degree. All these differences lead to exclude that the massive and the flat slags are the products of the same process.
In fact, the flat slags must be related to the last process of the metallurgical chain in which the optimal extraction efficiency was achieved, producing raw copper.

Differently from the sulphides observed in the coarse and massive slags, the ones encountered in the flat slags are not the witnesses of the main product of the process – in this case raw copper - but they must be derived from the matte of the earlier process.
More specifically, the flat slag sulphides may be the low Cu-enriched sulphides present in the second matte, which were partially transformed in raw copper as a result of the third process and partially entrapped in the flat slags.
It cannot be excluded that during the smelting of the second matte some charges were added.

Tab 3.12: List of the 93 slags of Luserna Platz Von Mozze site.

	Sample Name	Archeo-Type	Density (g/cm3)	Analytical name
1	US 111, B8 61	Coarse	2,34	LU-G74
2	US 111, B8 61	Coarse	2,34	LU-G73
3	US 111, B8 61	Coarse	2,44	LU-G72
4	No US	Massive	2,54	LU-M48
5	US 111, B8 61	Coarse	2,63	LU-G70
6	US 111, B8 61	Coarse	2,63	LU-G71
7	US 111,B8 61	Coarse	2,65	LU-G69
8	US1 Campione 31	Coarse	2,70	LU-G59
9	No US	Coarse	2,74	LU-G56
10	US111, Campione 61	Coarse	2,79	LU-G58
11	No US	Coarse Massive	2,89	LU-G57
12	No US	Fluid	3,12	LU-F52
13	PVM sacch. 17, n. 4	Flat Thick	3,32	LU-PS63
14	PVM sacch. 8, n. 7	Flat	3,37	
15	PVM sacch. 17, n. 10	Flat Thick	3,39	
16	PVM sacch. 8, n. 32	Flat	3,40	
17	PVM sacch. 8, n. 21	Flat	3,40	
18	PVM sacch. 17, n. 16	Flat	3,41	
19	PVM sacch. 17, n. 1	Flat Thick	3,42	
20	PVM sacch. 8, n. 30	Flat	3,43	LU-P68
21	PVM sacch. 8, n. 1	Flat	3,44	
22	PVM sacch. 17, n. 8	Flat Thick	3,45	LU-PS64
23	PVM sacch. 17, n. 7	Flat	3,45	
24	PVM sacch. 17, n. 18	Flat Thick	3,45	
25	PVM sacch. 17, n. 5	Massive	3,45	LU-M4
26	PVM sacch. 8, n. 2	Flat	3,46	
27	PVM sacch. 17, n. 17	Flat	3,47	
28	PVM sacch. 8, n. 23	Flat	3,49	
29	PVM sacch. 8, n. 19	Flat	3,49	
30	PVM sacch. 8, n. 20	Flat	3,49	
31	PVM sacch. 8, n. 18	Flat	3,50	
32	PVM sacch. 8, n. 28	Flat	3,51	

	Sample Name	Archeo-Type	Density (g/cm3)	Analytical name
33	PVM sacch. 2, n. 5	Flat	3,51	
34	PVM sacch. 17, n. 20	Flat	3,52	
35	US x	Flat	3,52	LU-P9
36	PVM sacch. 8, n. 27	Flat	3,52	
37	PVM sacch. 8, n. 34	Flat	3,52	
38	PVM sacch. 8, n. 37	Flat	3,52	
39	PVM sacch. 17, n. 15	Flat	3,53	
40	PVM sacch. 2, n. 2	Flat	3,53	
41	PVM sacch. 17, n. 13	Flat	3,53	
42	PVM sacch. 2, n. 18	Flat	3,54	
43	PVM sacch. 8, n. 6	Flat	3,54	
44	PVM sacch. 8, n. 15	Flat	3,55	LU-P61
45	PVM sacch. 2, n. 14	Flat	3,55	
46	PVM sacch. 8, n. 10	Flat	3,56	
47	PVM sacch. 8, n. 4	Flat	3,56	LU-P62
48	PVM sacch. 2, n. 4	Flat	3,56	
49	PVM sacch. 8, n. 33	Flat	3,57	
50	PVM sacch. 2, n. 9	Flat	3,57	
51	PVM sacch. 2, n. 1	Flat	3,57	
52	PVM sacch. 8, n. 24	Flat	3,58	
53	PVM sacch. 8, n. 11	Flat	3,58	
54	PVM sacch. 17, n. 19	Flat	3,58	
55	PVM sacch. 17, n. 14	Flat	3,58	
56	PVM sacch. 2, n. 12	Flat	3,59	
57	PVM sacch. 8, n. 35	Flat	3,59	
58	PVM sacch. 8, n. 14	Flat	3,59	
59	PVM sacch. 8, n. 12	Flat	3,60	
60	PVM sacch. 2, n. 13	Flat	3,60	
61	PVM sacch. 2, n. 3	Flat	3,60	
62	PVM sacch. 8, n. 17	Flat Thick	3,60	
63	PVM sacch. 8, n. 25	Flat	3,61	
64	PVM sacch. 8, n. 16	Flat	3,62	LU-P6
65	PVM sacch. 2, n. 11	Flat	3,62	
66	PVM sacch. 8, n. 29	Flat	3,62	

	Sample Name	Archeo-Type	Density (g/cm3)	Analytical name
67	PVM sacch. 2, n. 8	Flat	3,63	
68	PVM sacch. 8, n. 9	Flat	3,64	
69	PVM sacch. 8, n. 22	Flat	3,65	
70	PVM sacch. 2, n. 6	Flat Thick	3,66	
71	PVM sacch. 2, n. 17	Flat	3,66	
72	PVM sacch. 8, n. 13	Flat Thick	3,67	
73	No US	Flat Coarse	3,67	LU-PR34
74	PVM sacch. 8, n. 36	Flat	3,67	
75	PVM sacch. 2, n. 16	Massive	3,67	
76	No US	Massive	3,68	LU-M50
77	PVM sacch. 8, n. 26	Flat	3,68	
78	PVM sacch. 2, n. 10	Flat	3,68	
79	PVM sacch. 17, n. 2	Flat Thick	3,68	
80	LU-M47	Massive	3,69	LU-M47
81	PVM sacch. 17, n. 9	Flat	3,71	
82	PVM sacch. 8, n. 3	Flat Thick	3,73	
83	PVM sacch. 2, n. 7	Flat Thick	3,75	
84	No US	Flat Thick	3,75	LU-PS45
85	PVM sacch. 17, n. 6	Massive	3,76	
86	LU-PSR38	Flat Thick Coarse	3,76	LU-PSR38
87	PVM sacch. 17, n. 12	Massive	3,77	
88	PVM sacch. 8, n. 5	Massive	3,77	LU-M5
89	PVM sacch. 8, n. 8	Flat	3,78	
90	PVM sacch. 17, n. 11	Massive	3,89	LU-M60
91	PVM sacch. 2, n. 15	Massive	3,89	
92	PVM sacch. 8, n. 31	Flat Thick	3,98	LU-PS67
93	PVM sacch. 17, n. 3	Flat	4,15	

IV – The Slags of Transacqua

4.1 Introduction

At Pezhe Alte (or Pezze Alte), near the village of Transacqua and the city of Fiera di Primiero, the Archaeological Heritage Office of Trento has started a new extensive excavation in the smelting site called *Transacqua* (Bellintani et al. 2009).
In the area of Fiera di Primiero Area, several smelting sites were already known in archaeology, such as the sites named *Pezze Alte 1* and *Pezze Alte 2* (Preuschen, 1973).
The excavation carried out at *Transacqua* allowed to discover slag heaps with a dispersion area of 1150 m^2, remains of fire structures and ore-dressing tools (Silvestri et al. 2011).
The site is located at 1080 m a.s.l. and it is dated to the Late Bronze Age (Bellintani, personal communication).

Fig. 4.1: Map of the smelting site of Transacqua (dot with an arrow) drawn using the *Carta Tecnica Regionale del Trentino-Alto Adige* (CTR) on ArchGis.

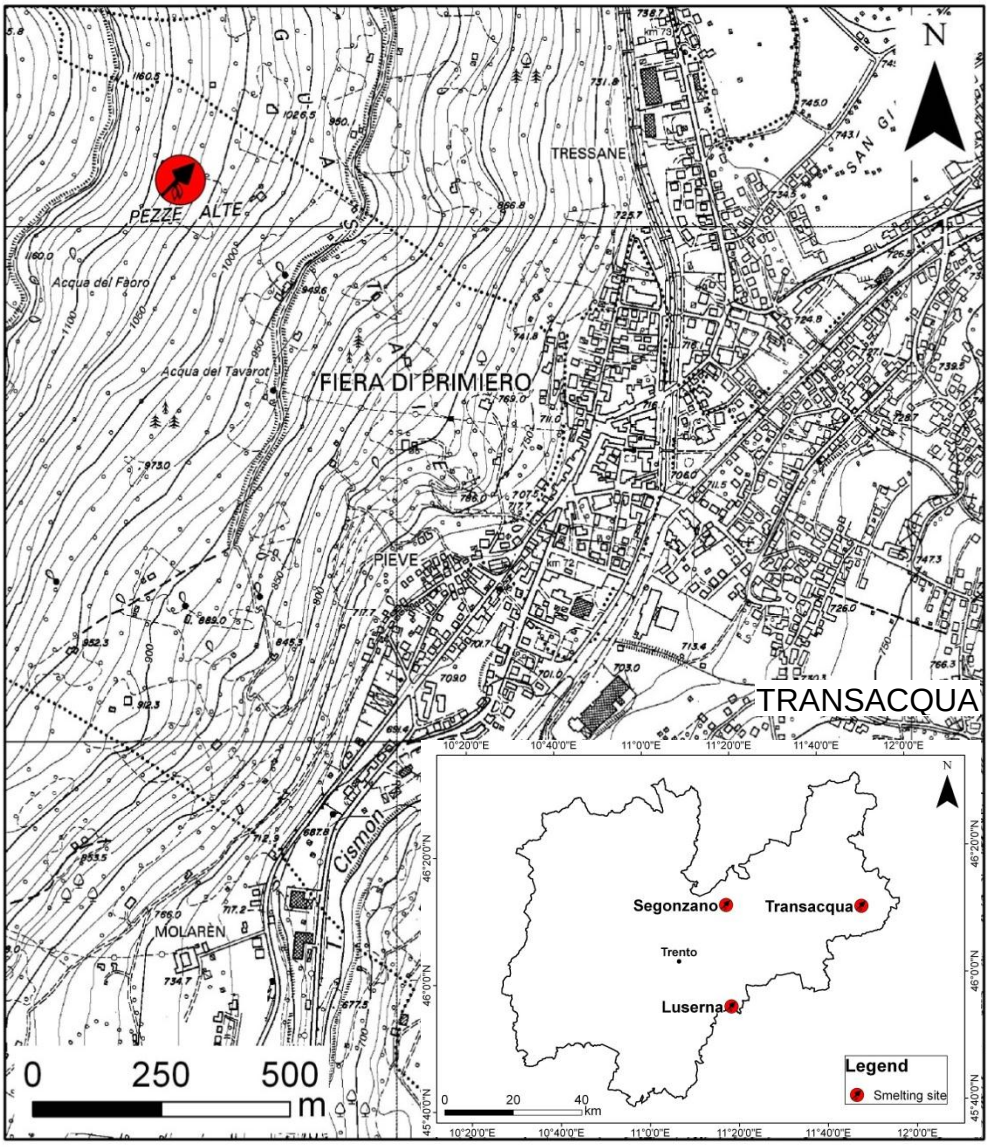

4.2 Analytical Protocol and Materials

As it was done with the Luserna slags, the slag samples of the Transacqua site were preliminary analysed for macroscopic features (colour, texture, shape, thickness, weight, presence/absence of visible quartz, charcoal, voids). Subsequently, the relative density was measured by water pycnometer and hydrostatic balance.
The measured densities were statistically treated using descriptive methods and inferential procedures (Box and Whiskers plots, one-way ANOVA, etc.) by the Statgraphics Centurion software. On the basis of the results of the statistical analysis, the most representative slags of each type were firstly analysed by means of the optical microscopy operating in reflected and transmitted light (OM-RL and OM-TL). Later they were analysed by X-ray powder diffraction (XRPD). The results of the XRPD analyses were treated by the Reference Intensity Ratio method for semi-quantitative phase evaluation.
On the basis of the minero-petrographic analyses, the most representative samples of each group were selected for the chemical analysis using the XRF spectrometer and the scanning electron microscope coupled with the X-ray energy dispersive spectrometer (SEM-EDS).

The slags of Transacqua were preliminary classified by the archaeologist in 4 macro-typological groups (archaeo-types): coarse slags, flat slags, massive slags and flat-thick slags. As it was fully described in the chapter 3 on the Luserna slags, the macroscopic characteristics of these groups are: a) irregular shapes and high porosity for the coarse slags (Fig. 4.2, C: coarse), b) limited thickness and homogenous texture for the flat slags (Fig. 4.2, F: flat), c) one smooth side - one irregular surface (Fig. 4.3, M: massive) or two smooth sides (Fig. 4.3, M bis) and a homogeneous core for the massive slags, d) homogenous texture, smooth sides and thick core for the flat-thick slags (Fig. 4.3, FT: flat-thick).

Fig. 4.2: Images of the two common types of slags founded in the LBA Alpine smelting sites (coarse slag: C, and flat slag: F)

Fig 4.3: Images of two representative massive slags (M: one rough side and one smooth side, M bis: two smooth sides) and of a flat-thick slag.

4.3 Results

4.3.1 Density

The Transacqua slag samples provided to us by the archaeologists are 107.
The descriptive statistical analysis of the density measured was performed on the total number of slags and the box and whisker plots of the 4 types of slags were drawn.

Tab. 4.1: Summary statistics for the density values measured on the slag samples of Transacqua. Archaeo-Type: typology identified by the archaeologists. Count: total number of slags for each group. SD: standard deviation. Min.: Minimum. Max.: Maximum. LQ: Lower Quartile. UQ: Upper Quartile. IQR: Range Interquartile.

Archeo-Type	Count	Average	Median	SD	Min.	Max.	Range	LQ	UQ	IQR
Coarse (C)	30	2,73	2,66	0,32	2,26	3,51	1,25	2,50	2,78	0,28
Massive (M)	18	3,75	3,80	0,22	3,28	4,11	0,83	3,65	3,90	0,25
Flat (F)	41	3,65	3,67	0,17	3,31	3,98	0,67	3,54	3,77	0,22
Flat Thick (FT)	18	3,59	3,64	0,25	2,81	3,82	1,02	3,54	3,72	0,19

Fig. 4.4: Box an whiskers plots of the Transacqua slag types identified by the archaeologists. C: coarse, M: massive, F: flat, FT: flat-thick.

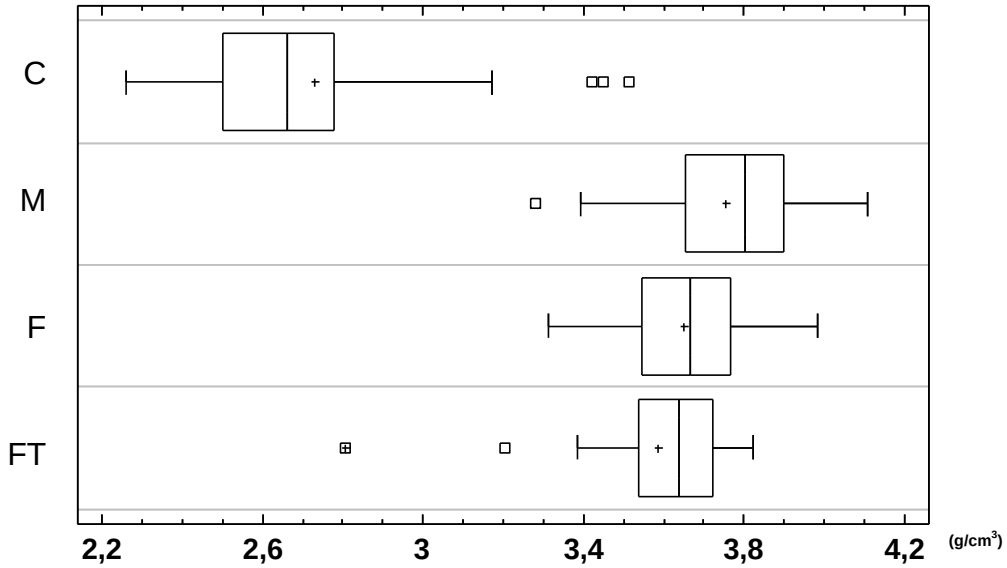

The summary statistic table (Tab. 4.1) and the box plots (Fig. 4.4) show that: a) the coarse type is composed by 30 slag samples with 3 outliers, b) the massive type is constituted by 18 slags with 1 outlier, c) the flat slags are 41 and no outlier was detected and d) the flat-thick type consists of 18 slag samples with 1 outlier and 1 far-outside.
Using the one-way analysis of variance (ANOVA), significant differences between the density means (parametric F-test: P-value<0,05) and the density medians (not parametric Kruskal Wallis test <0,05) were identified on the 4 archaeo-types of slags at a 95% confidence level. The Multiple Range test was used in order to determine the means that are significantly different at the 95,0% confidence level (Table 4.2) and the density homogeneous groups of means (Table 4.3).

The first output of the Multiple Range test is the table of the contrast, in which the groups of slags with statistically different means are indicated.

Tab 4.2: Table of the contrast. The *Difference* column displays the mean of the first group minus the one of the second group. For each difference the software calculated an uncertainty interval, shown in the *+/- Limits* column. Any pair for which the absolute value of the difference exceeds the uncertainty interval has statistically significant differences and it is indicated by an asterisk symbol in the *Sig*. column.

Contrast	Sig.	Difference	+/- Limits
Coarse - Massive	*	-1,02	0,19
Coarse - Flat	*	-0,92	0,16
Coarse - Flat-Thick	*	-0,86	0,19
Massive - Flat		0,11	0,18
Massive - Flat-Thick		0,17	0,21
Flat - Flat-Thick		0,06	0,18

The coarse and the massive types, the coarse and the flat types and the coarse and the flat-thick types have statistically different mean values.
The second output of the Multiple Range test is the homogeneous groups table (Tab. 4.3), in which the slags were arranged into homogeneous groups on the basis of the density measurements. The types of slags that do not have significant differences in terms of means are the flat-thick, the flat and the massive types.

Tab 4.3: The homogeneous groups table (H.G.: homogeneous groups)

Archaeo-Type	Count	Mean	H.G.	
Coarse	30	2,73	X	
Flat-Thick	18	3,59		X
Flat	41	3,65		X
Massive	18	3,75		X

However, the subsequent minero-petrographic analyses have indicated significant differences between the flat and the massive types of slags.
On the contrary, it was confirmed that the flat-thick type is not a distinct type of slags but it is partially related both to the flat slags and the massive slags.
On the basis of these remarks as well as the minero-petrographic analyses, the slags were divided into the following three types: coarse, massive and flat slags.

Fig.4.5 Box an whiskers plots of the densities measured on the Transacqua slags of the three type (C: coarse, M: massive, F: flat).

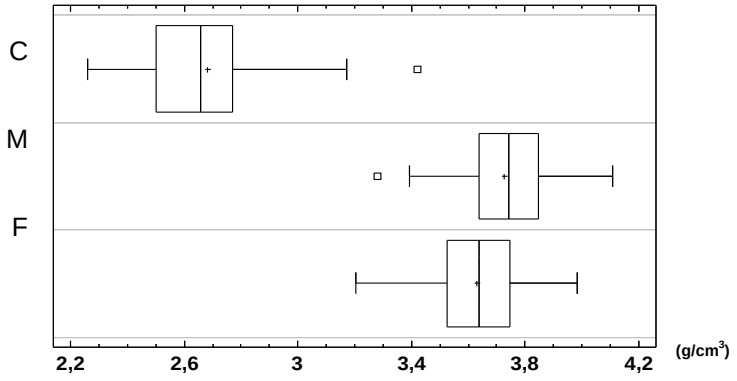

Tab 4.4: Summary statistics for the density values measured on the slag samples of Transacqua. Count: total number of slags for each group. SD: standard deviation. Min.: Minimum. Max.: Maximum. LQ: Lower Quartile. UQ: Upper Quartile. IQR: Interquartile Range.

Type	Count	Average	Median	SD	Min.	Max.	Range	LQ	UQ	IQR
COARSE	29	2,68	2,66	0,25	2,26	3,42	1,16	2,50	2,77	0,27
MASSIVE	30	3,72	3,74	0,18	3,28	4,11	0,83	3,64	3,85	0,21
FLAT	48	3,63	3,64	0,18	3,20	3,98	0,78	3,52	3,75	0,22

The densities measured on the 107 Transacqua slags show the same trend of the Luserna slags.
The coarse type (29 samples) has the lowest densities with a mean value of 2.68 g/cm^3 and a range of 2.26 – 3.42 g/cm^3.
The massive (30 slags) and the flat slags (48 samples) have higher density values than the coarse slags. In particular the massive type shows the highest densities with a ranges of $\rho_{massive}$ = 3.28 – 4.11 g/cm^3. The flat slags have a range of densities ρ_{flat}= 3.20 – 3.98 g/cm^3 with a mean value of 3.63 g/cm^3.

The Figure 4.6 shows the box and whiskers plots of the three types with the samples analysed (dots). The table 4.5 displays the total number of slags analysed and the kind of analytical investigation performed.

Fig 4.6: Box an whiskers plots of the coarse, massive and flat types of Transacqua with the samples selected for the analyses (dots).

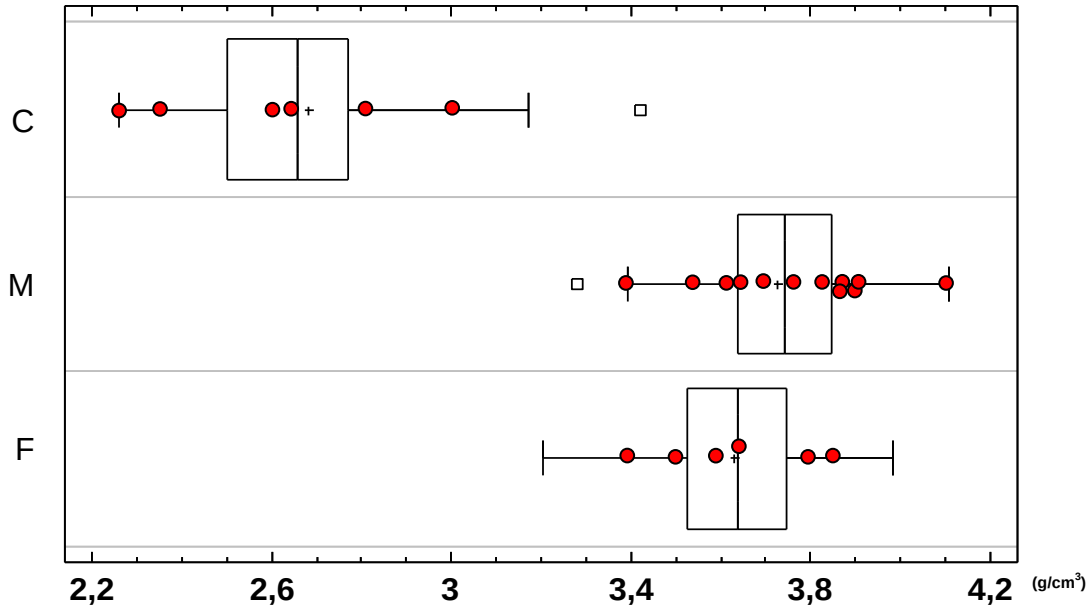

Tab. 4.5: List of the Transacqua slags fully investigated and the types of measurements carried out.

Type	N.	Density (g/cm^3)	Analytical Name	OM	XRPD	XRF	SEM-EDS	LIA
COARSE	6	2.26	**TR-G10**	√				
		2.38	**TR-G9**	√	√		√	√
		2.62	**TR-G8**	√	√	√	√	√
		2.62	**TR-G7**	√	√	√		√
		2.78	**TR-G3**	√	√	√	√	√
		3.03	**TR-G1**	√	√		√	√
MASSIVE	12	3.40	**TR-M5**	√	√	√		
		3.69	**TR-PS17**	√	√	√		√
		3.65	**TR-M20**	√	√	√	√	
		3.80	**TR-M6**	√	√	√		
		3.56	**TR-M21**	√	√	√		
		3.63	**TR-M25**	√	√	√		
		3.89	**TR-M12**	√	√	√	√	
		3.90	**TR-M2**	√	√	√	√	√
		4.11	**TR-M13**	√	√	√		
		3.86	**TR-M23**	√	√	√		
		3.85	**TR-M24**	√	√	√		
		3.77	**TR-M11**	√	√	√	√	√
FLAT	6	3.41	**TR-P15**	√	√	√	√	
		3.52	**TR-PS16**	√	√	√	√	
		3.65	**TR-P14**	√	√	√		√
		3.58	**TR-P22**	√	√	√		
		3.82	**TR-PS18**	√	√	√	√	√
		3.86	**TR-P4**	√	√	√	√	
TOT	24							

4.3.2 Minero-petrographic and Chemical Analyses

Coarse Slags

The semi-quantitative phase evaluation (XRPD-RIR method) performed on 5 coarse slags shows that quartz is the most abundant mineral with a mean value of ≈ 62wt%.
The olivine $(Mg,Fe)_2[SiO_4]$, mostly composed by fayalite (Fe_2SiO_4), is the second most abundant mineral with ≈ 27 wt%.

Tab 4.6: Mineralogical phases of the coarse slags of Transacqua expressed in weight percentages (%wt) calculated by XRPD-Rir Method.

	Sample	Quartz	Olivine	Cristobalite	Magnetite	Pyroxene
COARSE	TR-G1	56	30	1	6	7
	TR-G3	64	29	3	4	0
	TR-G7	71	24	3	2	0
	TR-G8	63	25	6	2	4
	TR-G9	58	25	6	5	6
	Mean	**62,4**	**26,6**	**3,8**	**3,8**	**3,4**
	SD	5,9	2,7	2,2	1,8	3,3

The semi-quantitative evaluation of the mineralogical phases reveals few percentages of cristobalite (3,8 wt%), of magnetite (3,8 wt%) and pyroxenes, mostly diopside, (3,4 wt%).
The optical microscopy observations were carried out on 6 coarse slag samples, showing large grains of quartz as a relict phase and different olivine morphologies ranging from polyhedral (euhedral –subhedral outlines, no internal structure, solid core) to acicular chains.
On the basis of the work of Donaldson (1974), these different olivine morphologies indicate different cooling rates, ranging from 0,5°C/hr (polyhedral) to 80°C/hr -300°C/hr (chain).
The observations on backscattered electron image (BEI) do not reveals olivine compositional zoning.

Fig 4.7. A) Chain olivine, B) Prismatic and hopper olivine.

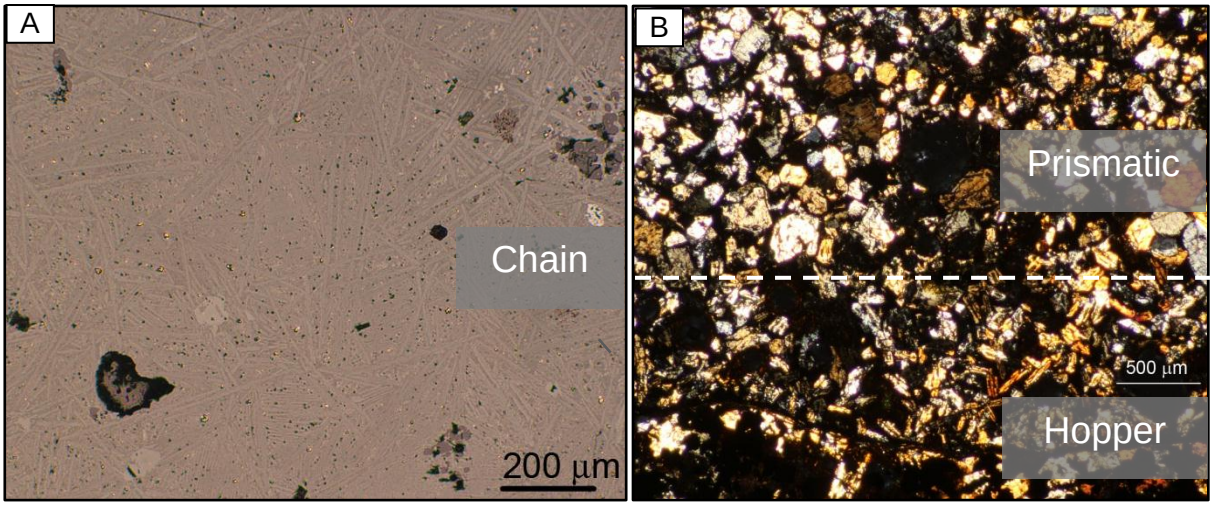

The analyses of the opaque minerals in reflected light microscopy display crystals of partially reacted sulphides. The ore charge was chalcopyrite and it is observed in a few small and fractured grains, often associated to pyrrhotite.

Fig: 4.8. Two characteristic sulphides observed in the coarse slags of Transacqua. They are mostly composed by Cp: chalcopyrite (A) and chalcopyrite-Po:pyrrhotite (B).

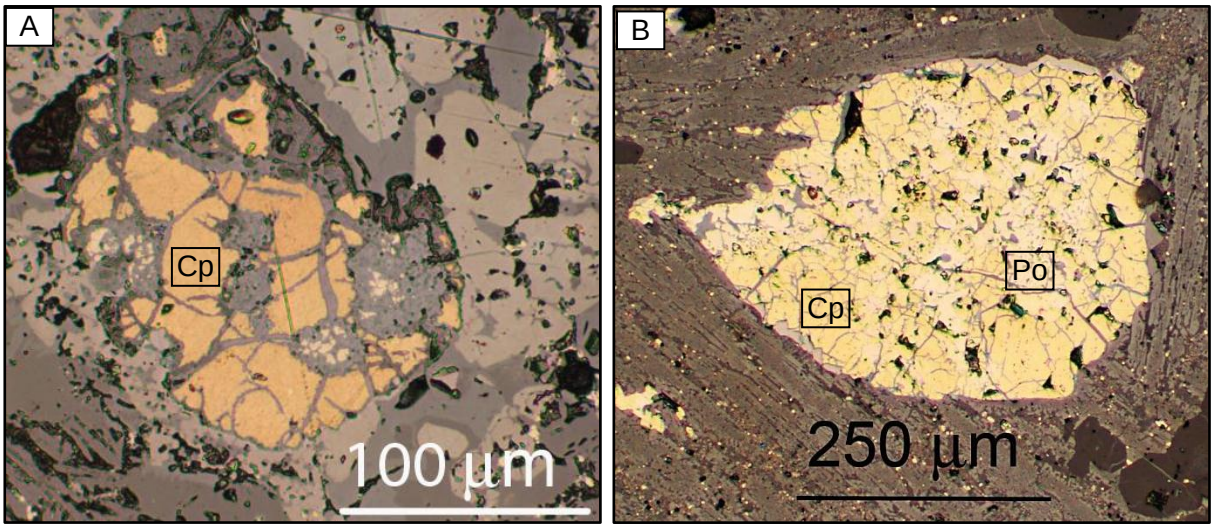

Large grains of Cu-Fe-sulphides were also observed, they show more complex chemical compositions, in which chalcopyrite and pyrrhotite are associated to bornite, especially identified in the grain fracture. No copper prills were observed.

Fig. 4.9: Large Cu-Fe sulphide. Cp: chalcopyrite, Po: pyrrothite. Bo: bornite. FeOx: Fe-oxide.

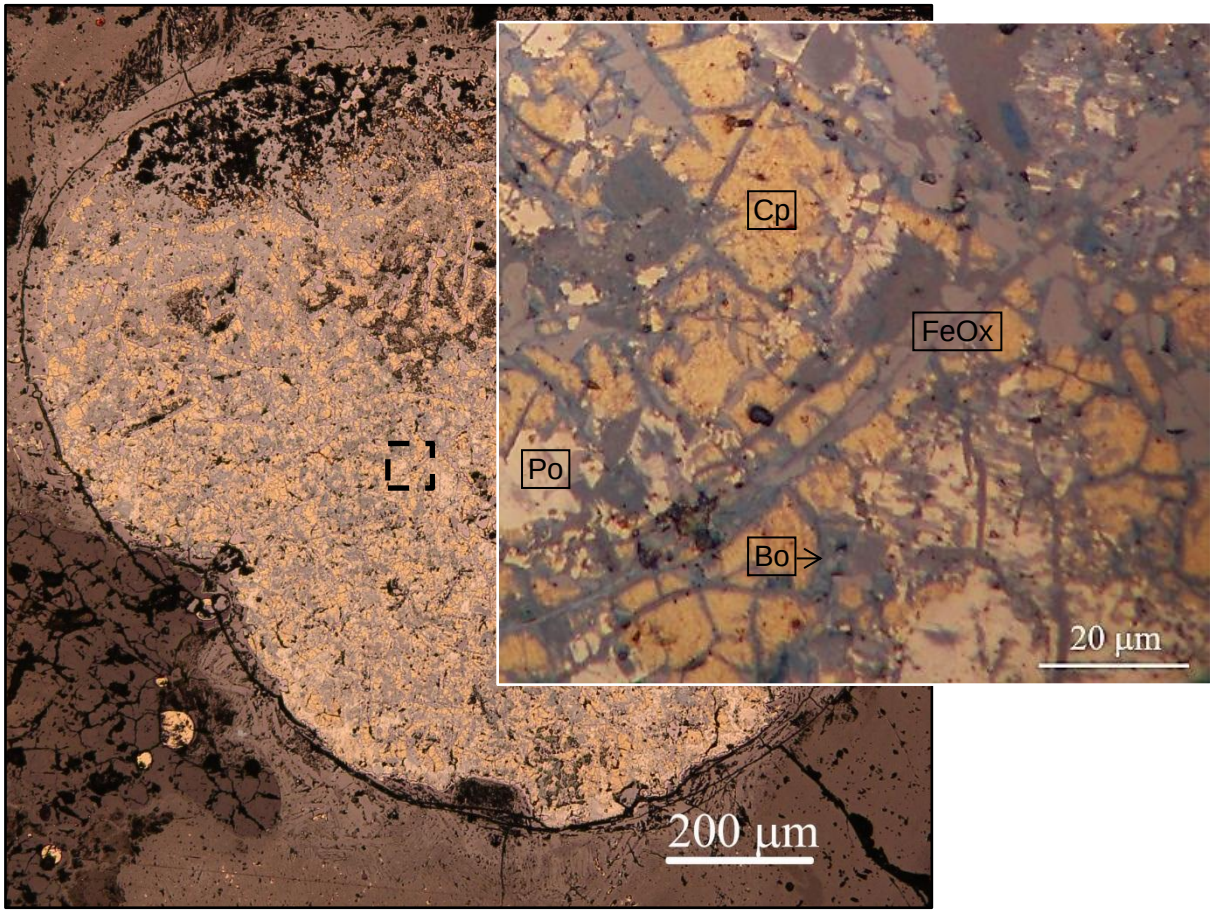

The chemical compositions of the sulphides were studied by means of the the SEM-EDS microscope and they were plotted into the Cu-Fe-S isothermal diagram at 700°C. Confirming the optical microscope observations, the main type of sulphides has an intermediate Cp-Bo chemical composition.

Fig. 4.10: Chemical compositions of the sulphides in the Transacqua coarse slags plotted in the ternary Cu-Fe-S diagram in wt% at 700°C modified after Yund and Kullerud (1966).
Bo: bornite, Cp: chalcopyrite, Py: pyrite, Po: pyrrhotite.

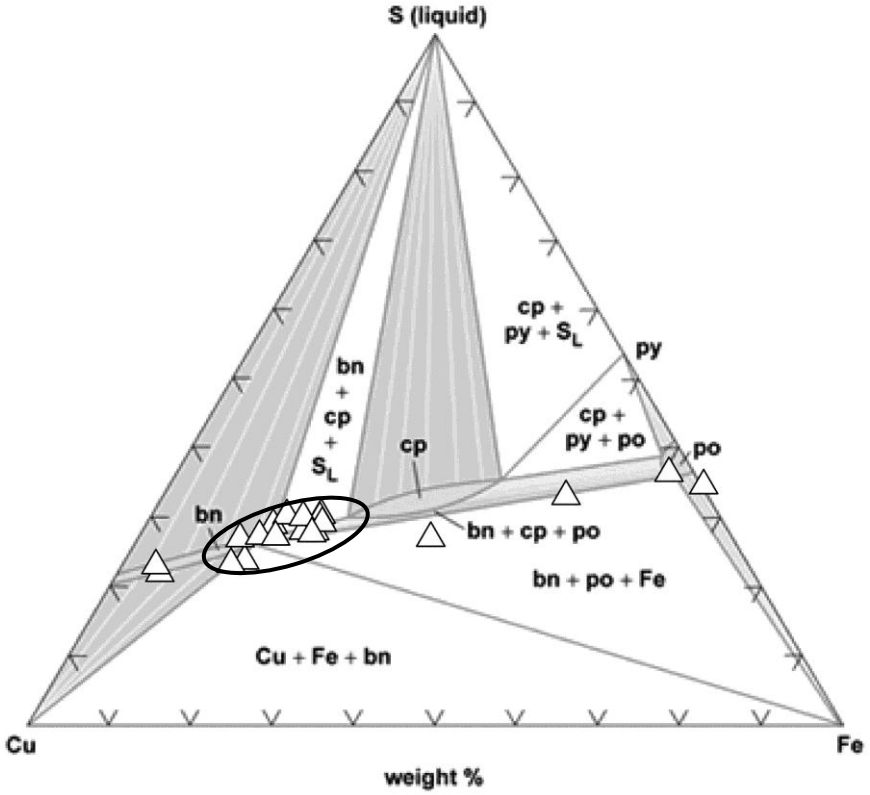

The chemical bulk analyses (XRF) of the most representative coarse slags detected by the minero-petrographic analyses were performed using the same powders analysed by XRPD.

Tab. 4.7: Chemical bulk compositions of the coarse slags of Transacqua

	Sample	SiO_2	TiO_2	Al_2O_3	Fe_2O_3	MnO	MgO	CaO	Na_2O	K_2O	P_2O_5
COARSE	TR-G1	27,67	0,16	4,45	61,4	0,24	0,94	1,91	0,31	0,94	0,14
	TR-G3	54,11	0,19	7,1	31,1	0,21	1,27	2,27	0,55	1,68	0,16
	TR-G7	61,19	0,15	6,05	26,72	0,2	0,74	1,54	0,3	1,79	0,15
	TR-G8	53,55	0,13	5,95	34,58	0,21	0,57	0,68	0,26	1,81	0,09
	TR-G9	47,41	0,22	7,86	35,18	0,57	1,99	2,46	0,63	1,77	0,11
	Mean	**48,79**	**0,17**	**6,28**	**37,80**	**0,29**	**1,10**	**1,77**	**0,41**	**1,60**	**0,13**
	SD	12,77	0,04	1,29	13,62	0,16	0,56	0,70	0,17	0,37	0,03

Except for the sample TR-G1, SiO_2 is the highest oxide detected followed by Fe_2O_3.
The chemical compositions of the slags were plotted in the ternary diagram anorthite ($CaAl_2Si_2O_8$) - FeO – SiO_2 system, using the procedure suggested by Morton and Wingrove (1969b) and described in the chapter 3 (Luserna Slags).

Similar to the coarse slags of Luserna, the coarse slags of Transacqua (except TR-G1 which is in the fayalite stability field) have a bulk chemical composition in the field of SiO_2 because of their high amount of restitic quartz that did not take part in the melting.

Fig. 4.11: Ternary anorthite-FeO-SiO_2 diagram, modified after Morton and Wingrove (1969b; 1972).

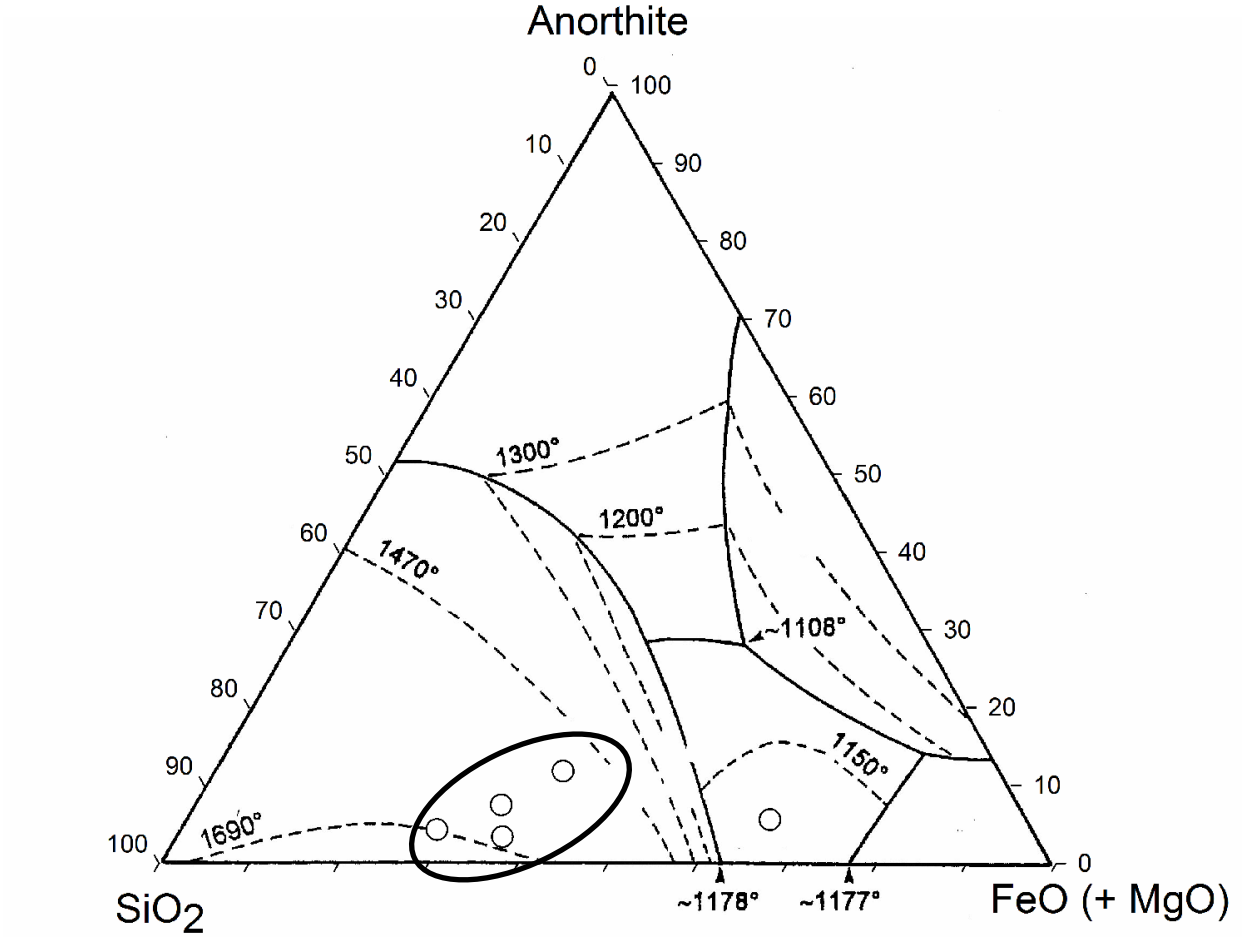

Massive Slags

The Massive slags of Transacqua analysed are 12. As shown by the XRPD-RIR table (Tab. 4.8), a number of 2 slag samples (TR-M6 and TR-PS17) have a different mineralogical composition compared to the other massive slags. Usually, the massive type is characterized by a higher amount of olivine and magnetite and a lower content of quartz than the coarse slags. Unlike the general trend of the massive slags, these two samples have a higher amount of quartz and a lower amount of fayalite and magnetite, similar to the coarse slags.

Tab. 4.8: Mineralogical phases of the Transacqua massive slags expressed in weight percentages (%wt) and calculated by the XRPD-Rir Method.

	Sample	Quartz	Olivine	Cristobalite	Magnetite	Pyroxene	Leucite
MASSIVE	TR-M6	61	17	2	10	9	1
	TR-PS17	53	39	3	5	0	0
	TR-M2	5	70	0	25	0	0
	TR-M5	22	52	0	10	0	16
	TR-M11	5	68	0	27	0	0
	TR-M12	0	62	0	27	11	0
	TR-M13	0	61	0	31	8	0
	TR-M20	2	63	0	23	12	0
	TR-M21	5	56	0	28	0	11
	TR-M23	0	74	0	19	0	7
	TR-M24	0	76	0	15	0	9
	TR-M25	3	77	0	11	0	9
	Mean	13	59,6	0,4	19,3	3,3	4,4
	SD	21,5	17,3	1	8,8	5	5,7

The Table 4.9 shows the mean and the standard deviation values calculated without considering the TR-M6 and TR-PS17 coarse-like slags.

The most abundant mineral is olivine (≈ 67 wt%), followed by magnetite (ranging from 10 to 31 wt%). Several percentages of pyroxene (as diopside: $CaMgSi_2O_6$) and leucite ($KAlSi_2O_6$) were detected.

Tab. 4.9: Mineralogical phases of the Transacqua massive slags with mean and standard deviation values calculated without considering the samples TR-M6 and TR-PS17.

	Sample	Quartz	Olivine	Cristobalite	Magnetite	Pyroxene	Leucite
	TR-M6	61	17	2	10	9	1
	TR-PS17	53	39	3	5	0	0
MASSIVE	TR-M2	5	70	0	25	0	0
	TR-M5	22	52	0	10	0	16
	TR-M11	5	68	0	27	0	0
	TR-M12	0	62	0	27	11	0
	TR-M13	0	61	0	31	8	0
	TR-M20	2	63	0	23	12	0
	TR-M21	5	56	0	28	0	11
	TR-M23	0	74	0	19	0	7
	TR-M24	0	76	0	15	0	9
	TR-M25	3	77	0	11	0	9
	Mean	**4,2**	**65,9**	**0**	**21,6**	**3,1**	**5,2**
	SD	6,6	8,5	0	7,4	5,1	5,9

The thin sections observed using the optical microscopy revealed the presence of different olivine habits, ranging from prismatic to hoppers with marked edges.

Fig. 4.12: A) Prismatic olivine (Ol: 0.5°C/hr cooling rate) in a silicate matrix (Si-matrix), with small magnetite (Ma) and sulphides (Su) grains. B) Hopper olivine (40°C/hr cooling rate).

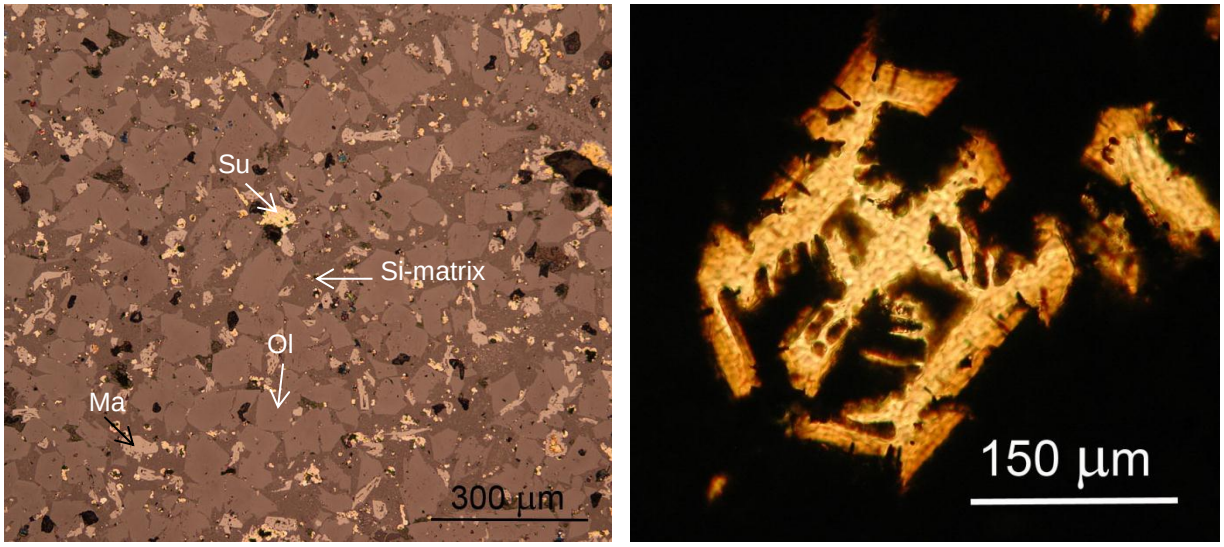

Fig. 4.13: Fo- olivine-zoning with the Fo-Fa phase diagram modified after Bowen and Schairer (1935).

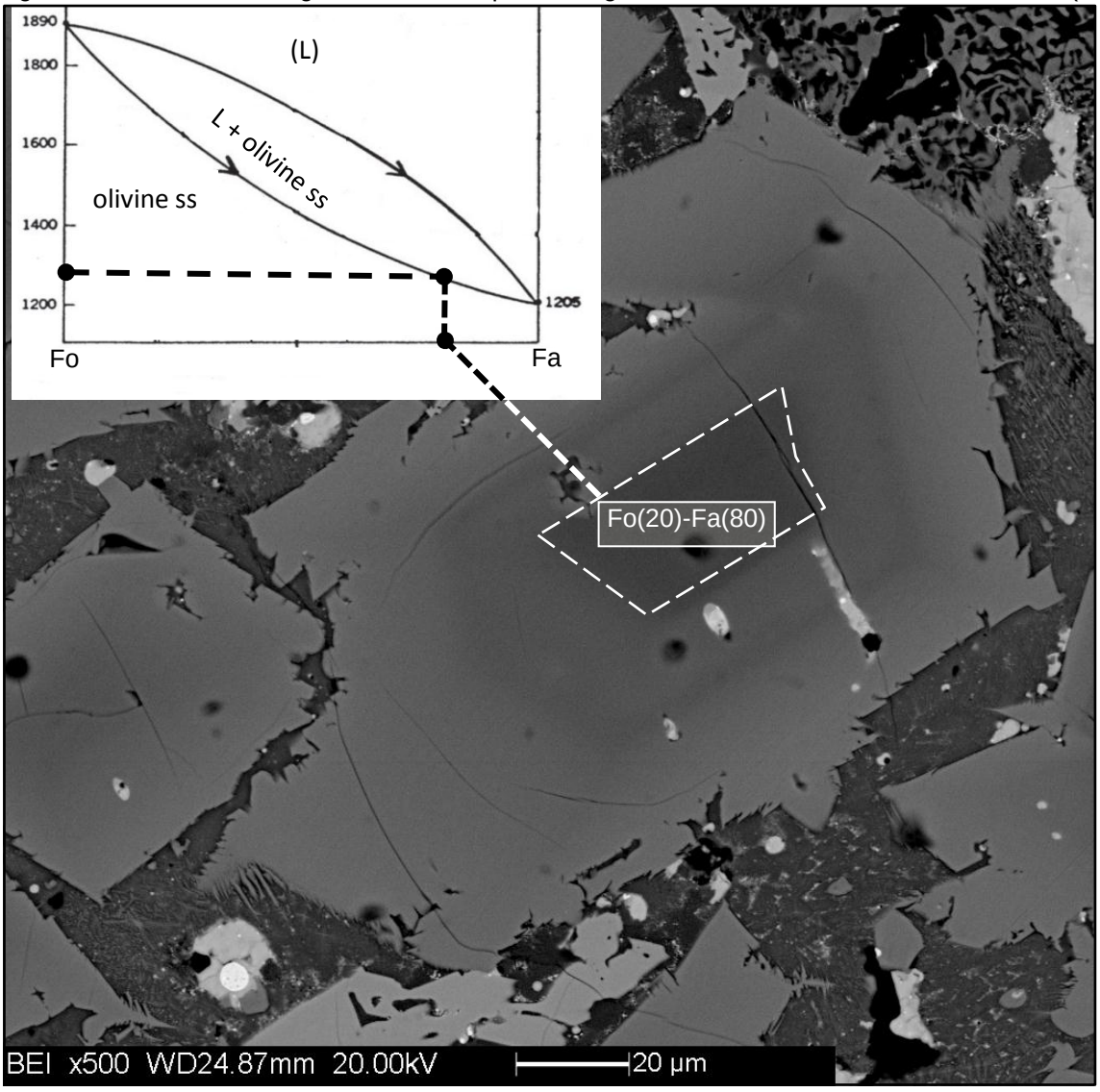

SEM-EDS analyses of olivine revealed a Forsterite-rich core zoning (Fo≈20%, Fig. 4.13). Using the forsterite-fayalite (Fo-Fa) phase equilibrium diagram (Bowen and Schairer, 1935), the core temperature of crystallization was estimated (≈1280°C).
As shown in Fig. 4.14, small copper droplets in association with large magnetite aggregate were observed.

Fig. 4.14: Reflected light micrograph of magnetite (Ma: grey with brown tint) and small copper droplets (Cu).

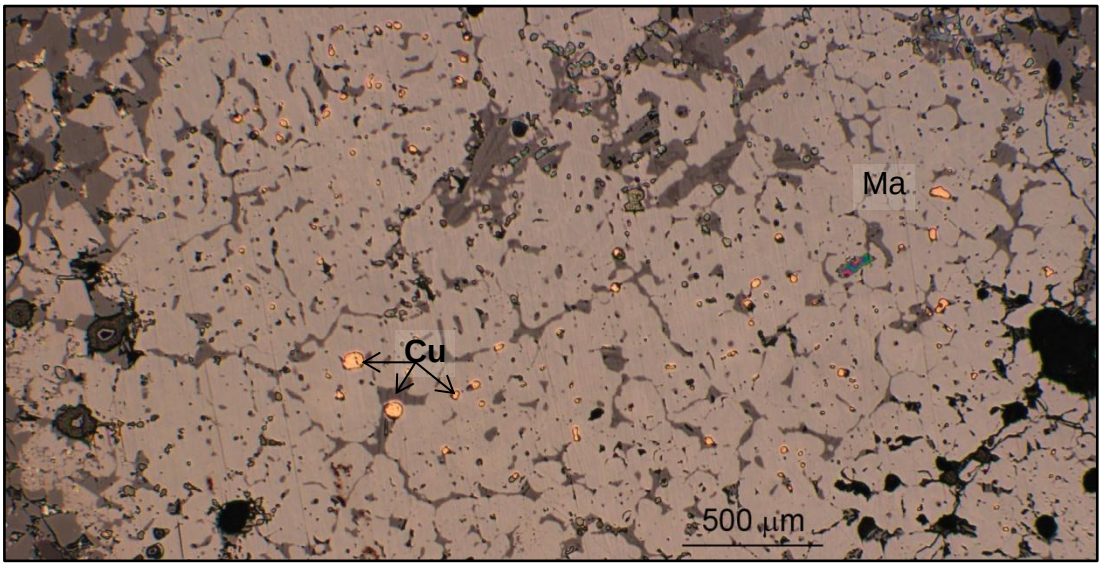

Similar to the sulphides observed in the massive slags of Luserna, the sulphide composition analyses (SEM-EDS) and the optical microscopy observations of the massive slags of Transacqua displayed two main types of sulphides. The first is composed by grain of intermediate bornite-chalcopyrite composition areas and areas of pyrrhotite (Fig. 4.16 A).
The second type is mostly composed by covellite (CuS) crystals, indicating the high Cu-enrichment grade of the sulphide ore during the smelting (Fig. 4.16 B).

Fig. 4.15: Chemical compositions of the sulphides in the Transacqua massive slags plotted in the ternary Cu-Fe-S diagram in wt% at 700°C modified after Yund and Kullerud (1966).

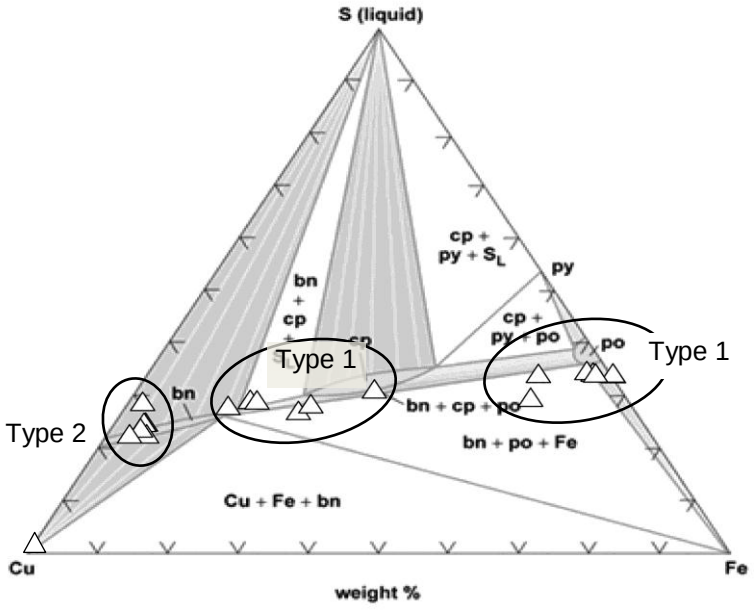

Fig. 4.16: A) Secondary sulphide grain composed by pyrrhotite (light yellow) and chalcopyrite (Cp: yellow) converted in bornite (Bo) and chalcocite (Ch: tarnished in fractures).
B) Covellite (cv: indigo.blue) in magnetite (Ma).

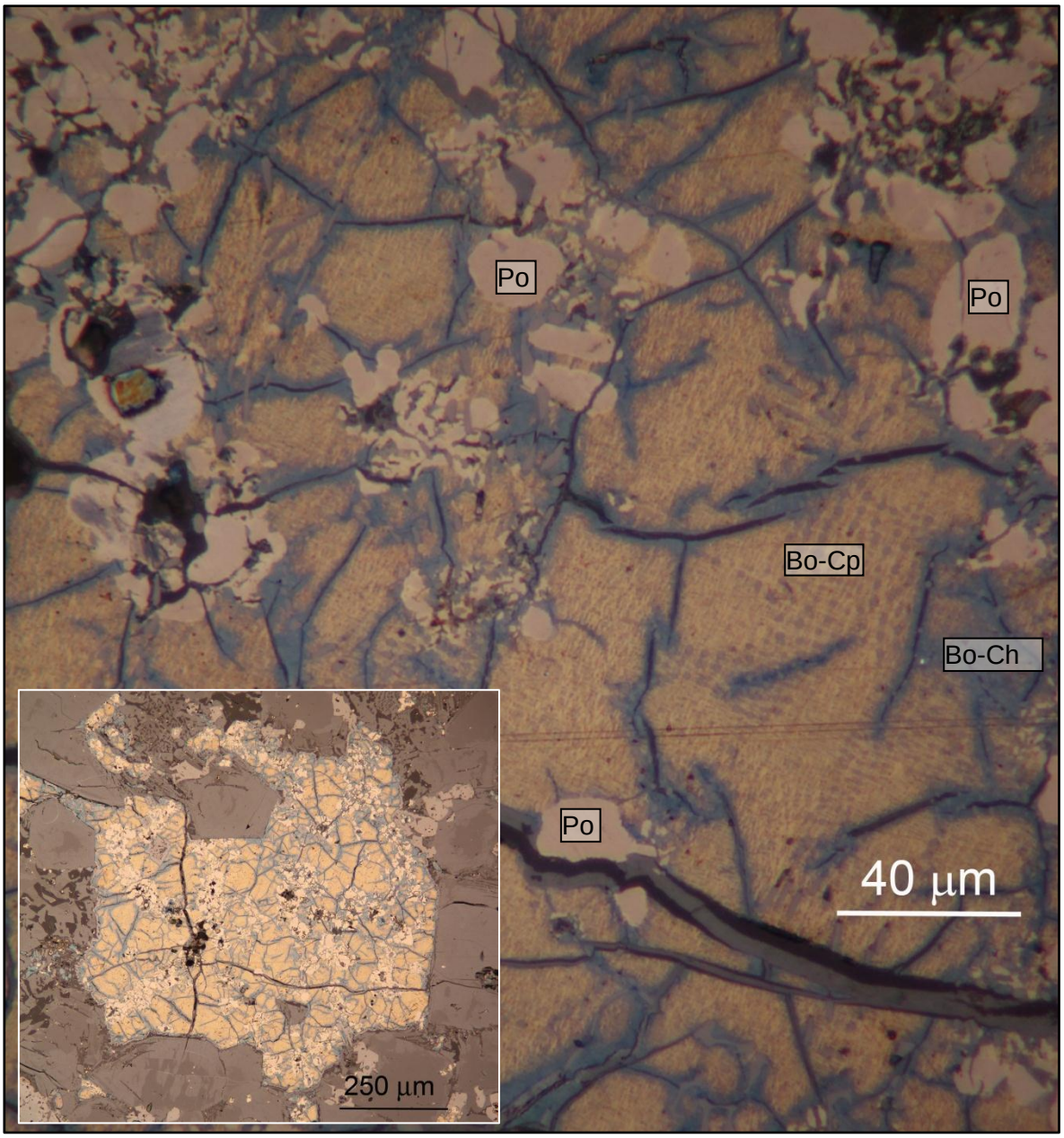

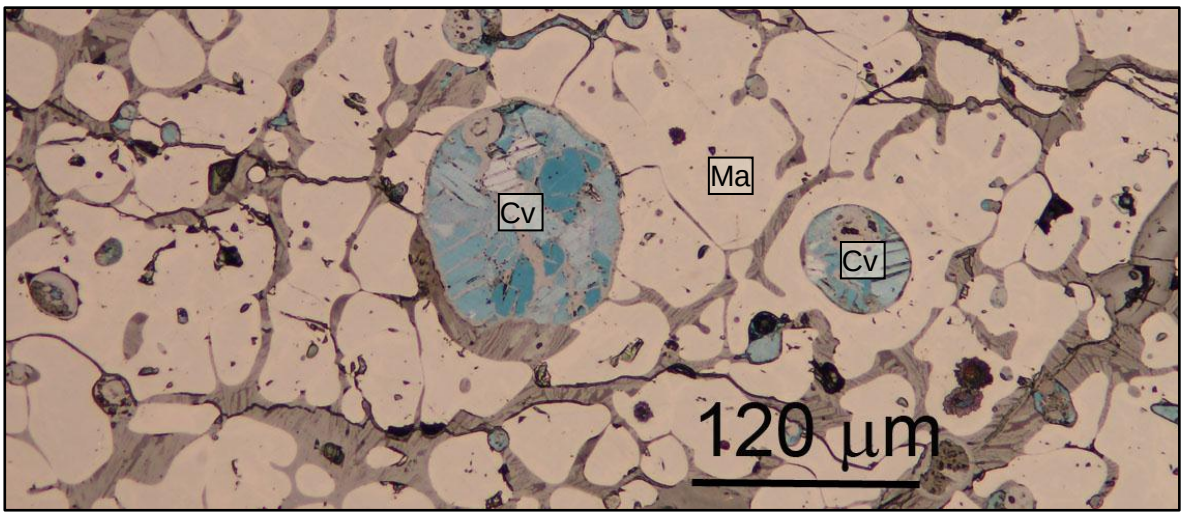

The chemical bulk analyses were performed on 12 representative massive slag samples.

Tab. 4.10: XRF chemical bulk compositions of the massive slags of Transacqua.

	Sample	SiO_2	TiO_2	Al_2O_3	Fe_2O_3	MnO	MgO	CaO	Na_2O	K_2O	P_2O_5
MASSIVE	TR-M6	42,01	0,09	4,67	45,49	0,35	1,37	2,35	0,12	1,20	0,12
	TR-PS17	47,71	0,14	6,78	38,76	0,21	0,79	1,57	0,18	1,97	0,11
	TR-M2	23,61	0,10	3,61	65,24	0,3	1,03	1,07	0,15	0,92	0,13
	TR-M5	30,05	0,11	5,77	54,17	0,55	1,90	2,10	0,12	1,43	0,16
	TR-M11	22,79	0,13	3,70	66,93	0,32	1,36	1,76	0,16	0,60	0,12
	TR-M13	18,01	0,05	1,68	73,67	0,16	0,49	1,05	0,06	0,21	0,05
	TR-M12	23,51	0,07	3,21	62,19	0,54	2,10	3,66	0,13	0,83	0,10
	TR-M20	26,79	0,13	4,94	58,32	0,36	1,65	3,15	0,23	1,14	0,14
	TR-M21	23,86	0,12	4,25	60,83	1,00	2,40	2,14	0,26	1,07	0,14
	TR-M23	25,01	0,10	3,19	64,86	0,26	1,18	1,20	0,15	0,91	0,13
	TR-M24	23,06	0,11	4,12	64,21	0,33	1,41	1,10	0,15	0,87	0,11
	TR-M25	26,79	0,12	4,96	59,78	0,36	1,46	1,82	0,19	1,27	0,14
	Mean	**27,77**	**0,11**	**4,24**	**59,54**	**0,40**	**1,43**	**1,91**	**0,16**	**1,04**	**0,12**
	SD	8,57	0,03	1,33	9,56	0,22	0,54	0,83	0,05	0,44	0,03

According to the mineralogical phase evaluation, the samples TR-M6 and TR-PS17 have a different chemical composition compared to the other massive slags, which is similar to the coarse sags, as shown in the ternary anorthite-FeO (+MgO)-SiO_2 diagram. They show a lower mean content of SiO_2 and a higher mean content of iron oxide compared to the one of the coarse slags.

Fig. 4.17: Bulk chemical compositions of the massive slags plotted in the ternary anorthite-FeO-SiO2 diagram.

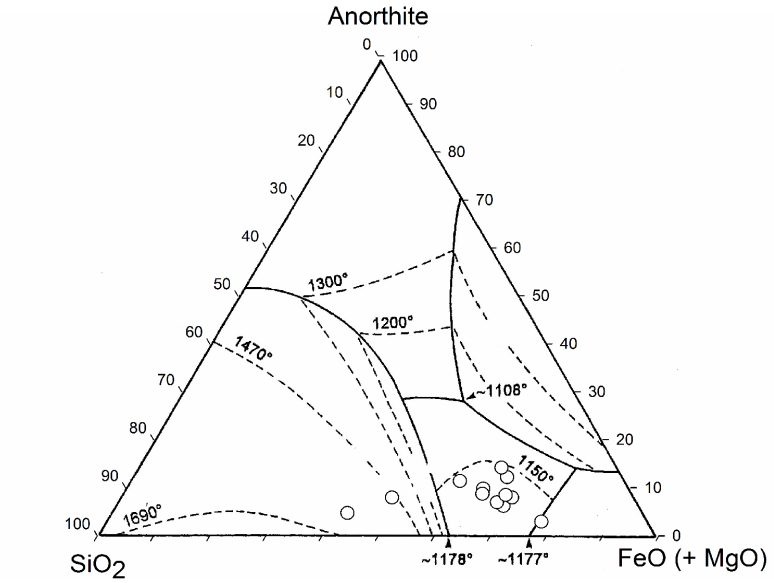

The chemical composition of the other massive slags is in the field of stability of the olivine, except for the sample TR-M13 located in the boundary between the field of fayalite and wustite (FeO).

The working-temperatures indicated by the ternary diagram are underestimated, as shown by the Fo-zoning temperature of the olivine (Fig. 4.13) and well-documented in literature (Freestone, 1988; Stot-Gale and Gale, 2006).

Flat Slags

The flat slags of Transacqua are characterised by the highest amount of fayalite (83 wt%). A few percentages of quartz were detected in two flat samples (TR-P4 and TR-P22).
The amount of magnetite is 13 wt% and no cristobalite or pyroxene was detected.

Tab. 4.11: Mineralogical phases of the flat slags of Transacqua expressed in weight percentages (%wt) and calculated by the XRPD-Rir Method.

	Sample	Quartz	Olivine	Cristobalite	Magnetite	Pyroxene
FLAT	TR-P4	3	84	0	13	0
	TR-P14	0	87	0	13	0
	TR-P15	0	88	0	12	0
	TR-PS16	0	80	0	20	0
	TR-PS18	0	86	0	14	0
	TR-P22	6	73	0	10	0
	Mean	**1,5**	**83**	**0**	**13,7**	**0**
	SD	2,5	5,7	0	3,4	0

Optical and electron microscopy observations have revealed different olivine habits: prismatic, hopper, elongate hopper and chain, indicating variable cooling rates (0,5°C/hr -350°C/hr).

Fig. 4.18: A) Prismatic and hopper olivine. B) Hopper olivine. C) Elongate hopper olivine D) BSI micrographs of chain olivines with dendritic magnetite (grey) and sulphides (white).

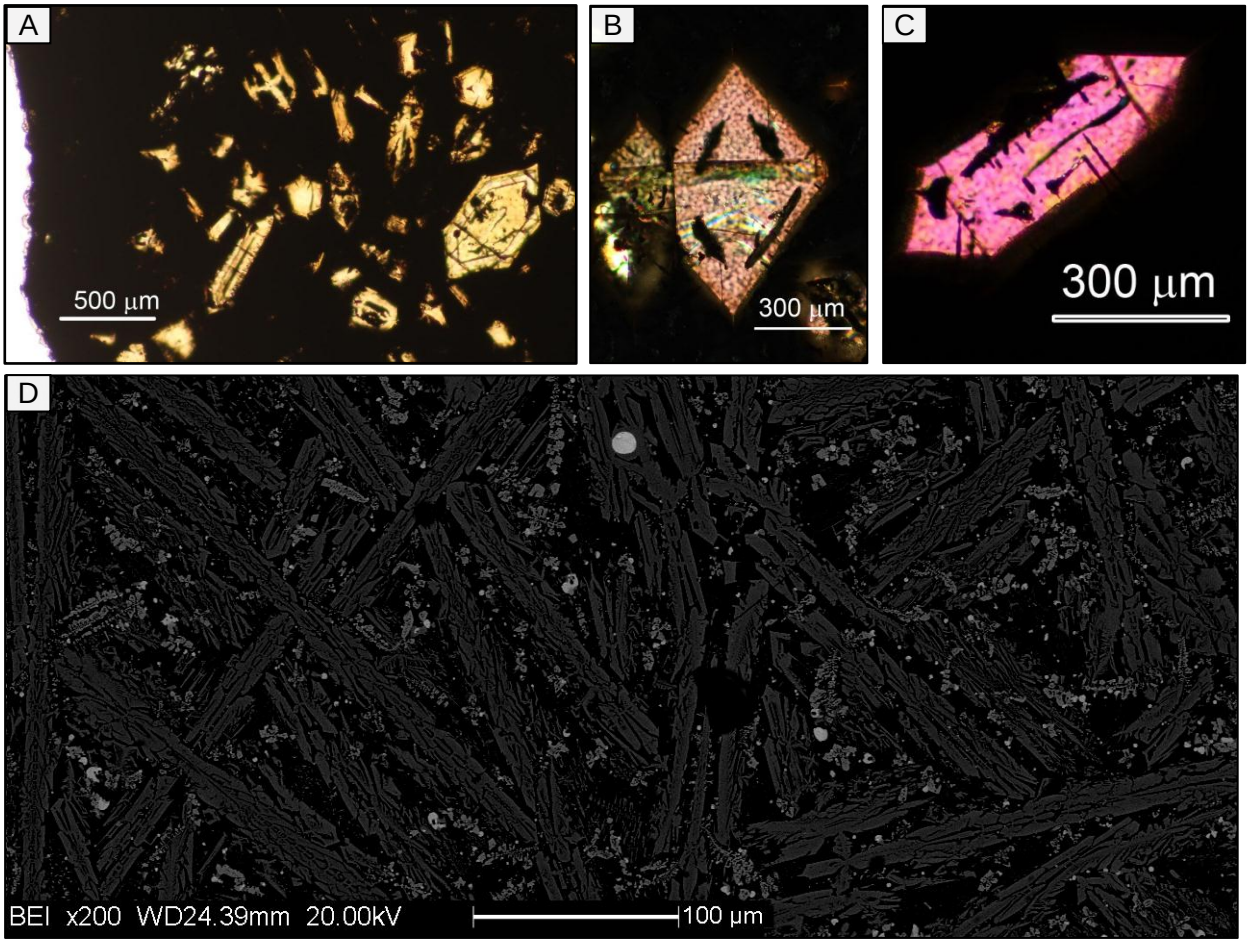

The prismatic olivines are zoned, with a Mg-enriched core (Fo≈20%) and a Fe-enriched rim (Fa ≈100%). The crystallization of the core occurred at 1280°C, indicating the minimum temperature enriched during the process.

Fig. 4.19: Prismatic olivines with a Fo-zoning core.

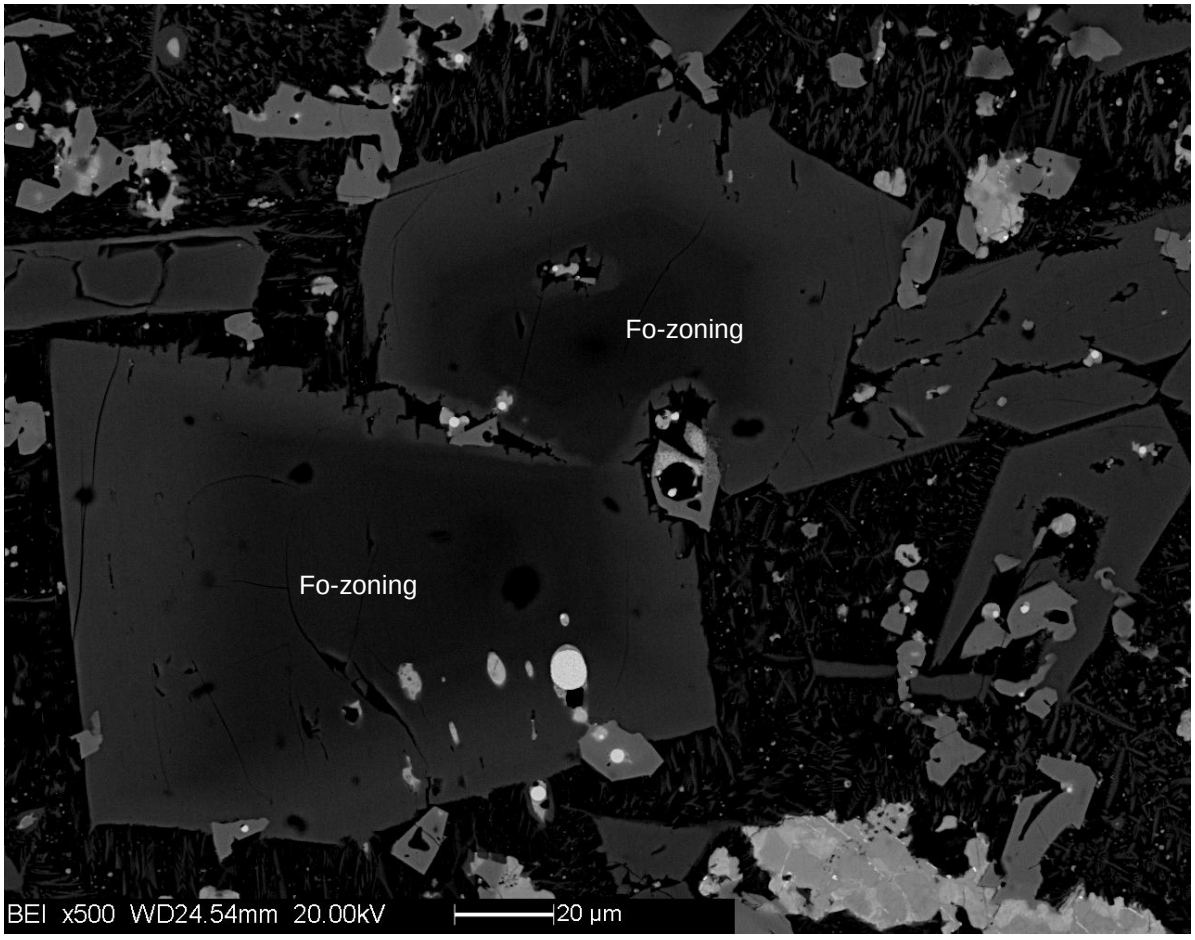

The small sulphides have a pyrrhotite-like composition with bornite-like and chalcopyrite-like area. No copper prills were observed.

Fig. 4.20: BSI micrographs of typical Cu-Fe sulphide observed in the flat slags of Transacqua and the ternary Cu-Fe-S diagram at 700°C with the compositions of the sulphides analysed.

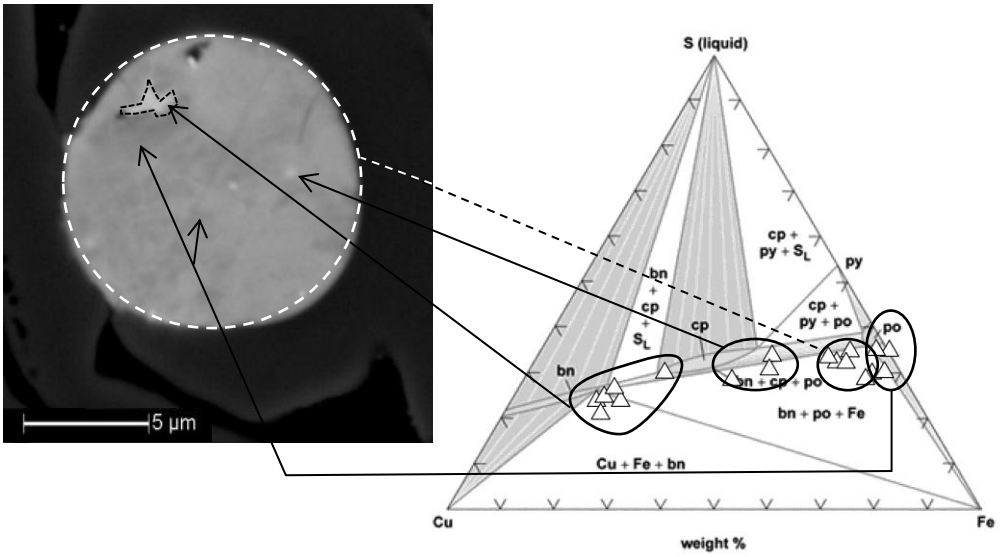

The bulk chemical analyses were performed on the most representative flat slag samples (Tab. 4.12) using the powders prepared for the XRPD analyses.

Tab. 4.12: XRF chemical bulk compositions of the flat slags of Transacqua.

	Sample	SiO_2	TiO_2	Al_2O_3	Fe_2O_3	MnO	MgO	CaO	Na_2O	K_2O	P_2O_5
FLAT	**TR-P4**	27,49	0,08	2,98	63,31	0,23	0,62	1,17	0,14	1,17	0,12
	TR-PS16	26,43	0,08	3,10	59,26	0,52	1,95	5,01	0,14	0,95	0,12
	TR-PS18	25,37	0,12	4,70	62,54	0,29	1,21	1,52	0,19	1,03	0,12
	TR-P22	32,20	0,10	3,90	56,12	0,42	1,81	2,55	0,17	0,81	0,06
	TR-P15	34,11	0,18	6,33	49,46	0,38	1,50	3,39	0,40	1,99	0,16
	Mean	**29,12**	**0,11**	**4,20**	**58,14**	**0,37**	**1,42**	**2,73**	**0,21**	**1,19**	**0,12**
	SD	3,82	0,04	1,38	5,63	0,11	0,53	1,55	0,11	0,47	0,04

Plotting the data in the ternary anorthite-FeO(+MgO)-SiO_2 diagram allowed to observe that all the flat slags are in the field of stability of fayalite, except for one sample (TR-P15) in the boundary between the field of stability of SiO_2 and fayalite.

Fig 4.21: Bulk chemical compositions of the Transacqua flat slags plotted in the ternary anorthite-FeO(+MgO)-SiO_2 diagram.

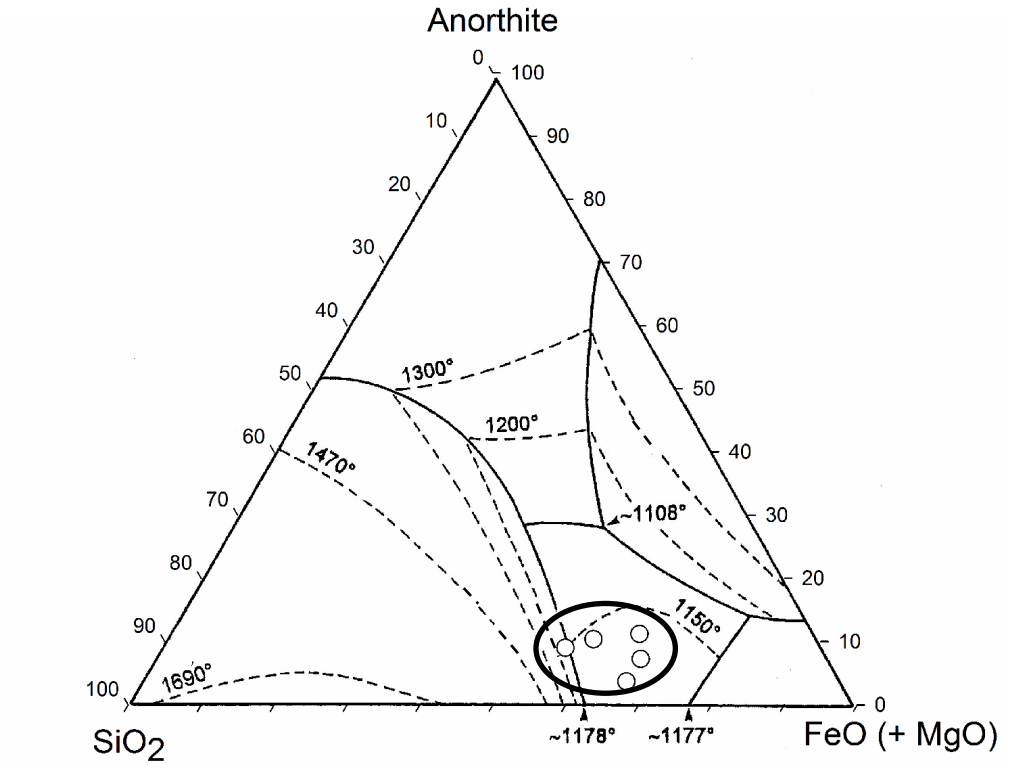

4.4 Discussion and Conclusion

The results of the mineralogical, petrographic and chemical analyses on the slags of Transacqua indicate the presence of three different smelting by-products: coarse slags, massive slags and flat slags.

The coarse slags with the highest amount of unreacted quartz, the lowest content of olivine and the presence of the sulphide-charge partially transformed, may be associated with the first steps of the smelting process. During this first step a low-copper enriched matte must be produced and reprocessed.

The analysis on the massive slags display a substantially lower amount of quartz and an increasing amount in fayalite and magnetite. In these slags the sulphide-charge is almost completely transformed, most of the sulphides are re-crystallised, and often copper prills are evident. The hypothesis for the formation of the massive slags is that they are related to a re-smelting of the first matte obtained during the formation process of the coarse slags.

In the flat slags, mainly formed by pure fayalite, the few remaining secondary sulphides are entrapped among the fayalite crystal matrix.
The morphological features and the textural analyses performed on this type of slags entail that they were produced during a final refining step of the enriched matte obtained during the massive process formation.

Tab 4.13: List of the 107 slags of Transacqua Pezze Alte site.

	Sample Name	Archeo-Type	Density (g/cm^3)	Analytical name
1	129/1	Flat	3,81	
2	129/2	Flat	3,31	
3	129/3	Coarse	2,47	
4	129/4	Massive	3,90	
5	129/5	Flat	3,32	
6	129/6	Flat-Thick	3,59	
7	129/7	Flat-Thick	3,64	
8	129/8	Coarse	3,42	
9	129/9	Coarse	2,48	
10	129/10	Coarse	3,45	
11	61/1	Massive	3,72	
12	61/2	Flat-Thick	3,54	
13	61/3	Coarse	2,58	
14	61/4	Flat	3,68	
15	61/5	Coarse	2,74	
16	61/6	Flat	3,65	TR-P14
17	61/7	Coarse	2,74	
18	61/8	Massive	3,90	TR-M2
19	61/9	Coarse	2,43	
20	Pezhe Alte Campione100/ 1	Flat	3,93	
21	Pezhe Alte Campione100/ 2	Flat	3,98	
22	Pezhe Alte Campione100/ 3	Flat	3,64	
23	Pezhe Alte Campione100/ 4	Flat	3,69	
24	Pezhe Alte Campione100/ 5	Flat	3,60	
25	Pezhe Alte Campione100/ 6	Flat	3,58	TR-P22
26	Pezhe Alte Campione100/ 7	Flat	3,59	
27	Pezhe Alte Campione100/ 8	Flat	3,76	
28	Pezhe Alte Campione100/ 9	Massive	3,81	
29	Pezhe Alte Campione100/ 10	Massive	3,89	TR-M12
30	Pezhe Alte Campione100/ 11	Flat	3,67	
31	Pezhe Alte Campione100/ 12	Flat-Thick	3,39	
32	Pezhe Alte Campione100/ 13	Flat	3,95	

	Sample Name	Archeo-Type	Density (g/cm^3)	Analytical name
33	Pezhe Alte Campione100/ 14	Flat	3,52	
34	Pezhe Alte Campione100/ 15	Flat	3,83	
35	Pezhe Alte Campione100/ 16	Flat	3,53	
36	Pezhe Alte Campione100/ 17	Flat-Thick	3,72	
37	Pezhe Alte Campione100/ 18	Flat	3,63	
38	Pezhe Alte Campione100/ 19	Flat	3,47	
39	Pezhe Alte Campione100/ 20	Flat	3,84	
40	Pezhe Alte Campione100/ 21	Flat	3,72	
41	Pezhe Alte Campione100/ 22	Flat-Thick	3,70	
42	Pezhe Alte Campione100/ 23	Massive	4,08	
43	Pezhe Alte Campione100/ 24	Flat	3,60	
44	Pezhe Alte Campione100/ 25	Flat	3,54	
45	Pezhe Alte Campione100/ 26	Flat	3,71	
46	Pezhe Alte Campione100/ 27	Flat-Thick	2,81	
47	Pezhe Alte Campione100/ 28	Flat-Thick	3,64	
48	Pezhe Alte Campione100/ 29	Flat	3,40	
49	Pezhe Alte Campione100/ 30	Coarse	3,51	
50	Pezhe Alte Campione100/ 31	Coarse	2,71	
51	Pezhe Alte Campione100/ 32	Flat-Thick	3,20	
52	Pezhe Alte Campione100/ 33	Coarse	3,12	
53	Pezhe Alte Campione100/ 34	Coarse	2,50	
54	Pezhe Alte Campione100/ 35	Coarse	2,62	TR-G8
55	Pezhe Alte Campione100/ 36	Coarse	2,76	
56	Pezhe Alte Campione100/ 37	Coarse	2,77	
57	Pezhe Alte Campione100/ 38	Coarse	2,59	
58	Pezhe Alte Campione100/ 39	Massive	3,74	
59	Pezhe Alte Campione100/ 40	Coarse	2,38	TR-G9
60	Pezhe Alte Campione100/ 41	Coarse	2,50	
61	Pezhe Alte Campione100/ 42	Coarse	2,36	
62	Pezhe Alte Campione100/ 43	Coarse	2,67	
63	Pezhe Alte Campione100/ 44	Coarse	2,62	TR-G7
64	Pezhe Alte Campione100/ 45	Coarse	3,17	
65	Pezhe Alte Campione100/ 46	Massive	3,70	
66	Pezhe Alte Campione100/ 47	Flat-Thick	3,72	

	Sample Name	Archeo-Type	Density (g/cm^3)	Analytical name
67	Pezhe Alte Campione100/ 48	Flat-Thick	3,82	TR-PS18
68	Pezhe Alte Campione100/ 49	Flat-Thick	3,64	
69	Pezhe Alte Campione100/ 50	Flat	3,41	
70	Pezhe Alte Campione100/ 51	Flat-Thick	3,81	
71	Pezhe Alte Campione100/ 52	Flat	3,77	
72	Pezhe Alte Campione100/ 53	Massive	4,11	TR-M13
73	Pezhe Alte Campione100/ 54	Flat	3,36	
74	Pezhe Alte Campione100/ 55	Flat-Thick	3,76	
75	Pezhe Alte Campione100/ 56	Flat	3,55	
76	Pezhe Alte Campione100/ 57	Massive	3,39	
77	Pezhe Alte Campione100/ 58	Massive	3,65	TR-M20
78	Pezhe Alte Campione100/ 59	Flat	3,67	
79	Pezhe Alte Campione100/ 60	Flat-Thick	3,63	
80	Pezhe Alte Campione100/ 61	Flat	3,69	
81	Pezhe Alte Campione100/ 62	Flat	3,52	
82	TPA 105/1	Massive	3,86	TR-M23
83	TPA 105/2	Coarse	2,80	TR-G3
84	TPA 105/3	Flat	3,86	TR-P4
85	TPA 105/4	Flat	3,90	
86	TPA 105/5	Flat-Thick	3,69	TR-PS17
87	TPA 105/6	Flat	3,69	
88	TPA 105/7	Massive	3,56	
89	TPA 105/8	Coarse	2,78	
90	TPA 105/9	Coarse	2,66	
91	TPA 105/10	Massive	3,40	TR-M5
92	TPA 105/11	Flat	3,80	
93	TPA 105/12	Massive	3,85	TR-M24
94	TPA 105/13	Flat-Thick	3,52	TR-PS16
95	TPA 105/14	Flat	3,80	
96	TPA 105/15	Massive	3,80	TR-M6
97	TPA 23/1	Coarse	2,68	
98	TPA 23/2	Flat	3,56	
99	TPA 23/3	Massive	3,77	TR-M11
100	TPA 23/4	Coarse	2,26	TR-G10

	Sample Name	Archeo-Type	Density (g/cm^3)	Analytical name
101	TPA 23/5	Flat-Thick	3,76	
102	TPA 23/6	Flat	3,36	
103	TPA 23/7	Flat	3,73	
104	TPA 23/8	Coarse	2,47	
105	TPA 23/9	Coarse	2,60	
106	TPA 23/10	Coarse	3,03	TR-G1
107	US 303	Massive	3,28	

V – The Slags of Segonzano

5.1 Introduction

The smelting site near Segonzano in the Peciapian Area is the third site, together with Luserna and Transacqua, excavated by the Archaeological Heritage Office of Trento since 2005. The smelting site of Segonzano is located at 1350 m a.s.l near a peat bog whose environment conditions allowed the conservation of organic materials and the subsequent radiocarbon datings (Bellintani et al. 2009, Silvestri et al. 2011).

Fig. 5.1: Map of the smelting site of Segonzano (dot with an arrow) drawn using the *Carta Tecnica Regionale del Trentino-Alto Adige* (CTR) on ArchGis software.

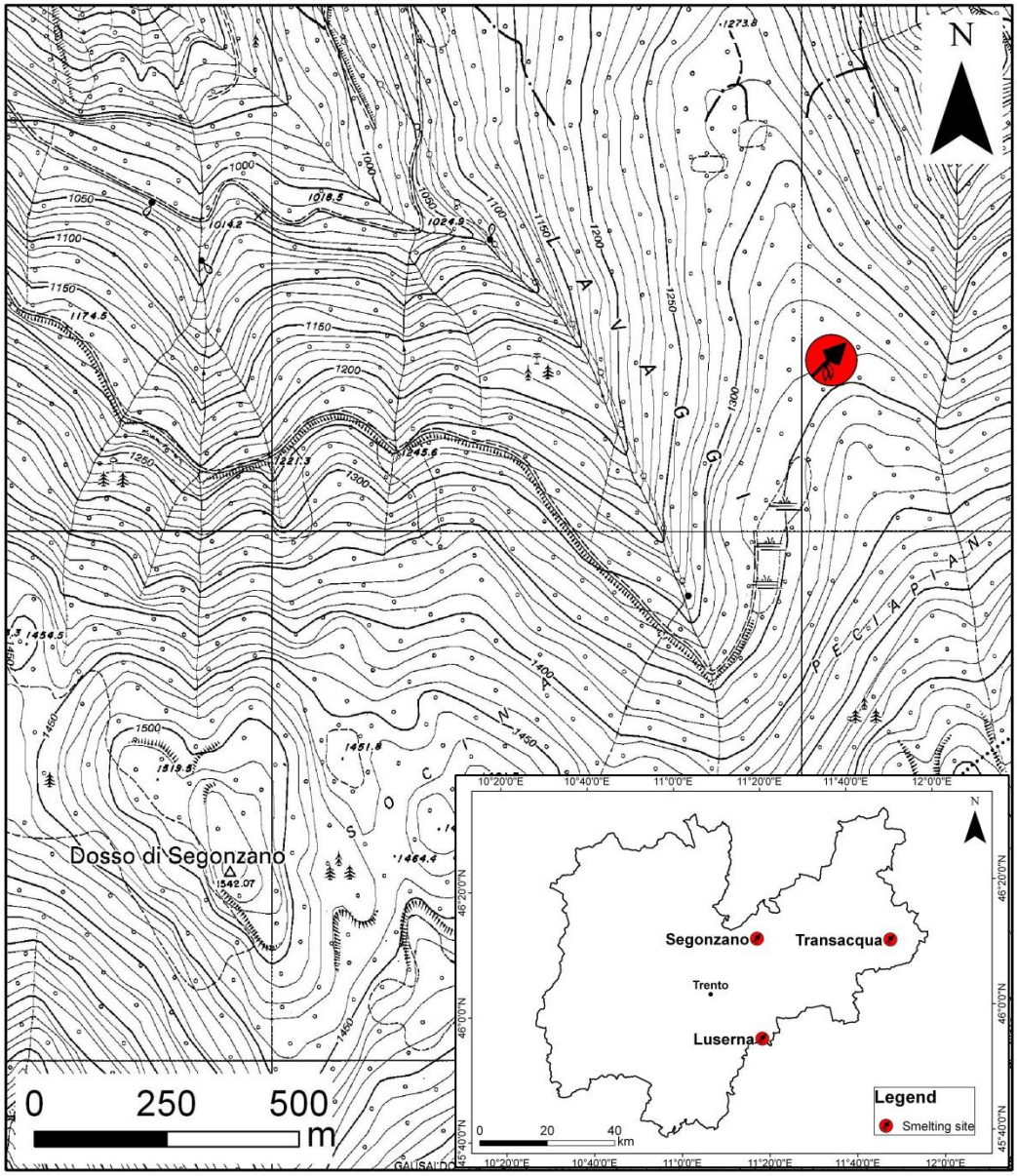

This site, already known for the extensive survey on the Late Bronze Age smelting sites carried out by Cierny (2008), was dated between 1400 and 1000 cal. BC (Bellintani et al. 2009, Silvestri et al. 2011).

During the excavation, a large heap of slag sand, different type of slags and horizontal wooden poles were found (Bellitani et al., 2009). The wooden poles have been

interpreted by the archaeologists as functional structures, likely associated to drainage or as containers for waste materials.
The total dispersion area of slags is about 1050 m^2 in Segonzano.

Fig. 5.2: Cross section of the Segonzano deposit, modified after Bellitani et al. (2009).

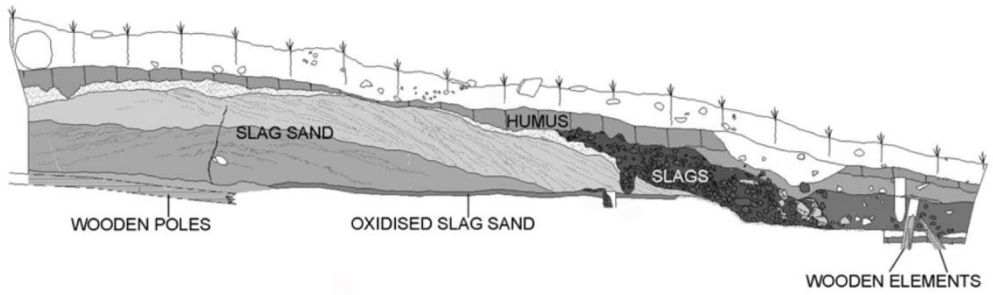

5.2 Analytical Protocol and Materials

A number of 30 slag samples was preliminary analysed for macroscopic features (colour, texture, shape, thickness, weight, presence/absence of visible quartz, charcoal, voids) and subsequently the relative density was measured by water pycnometer and hydrostatic balance.
The measured densities were statistically treated using descriptive methods and inferential procedures (Box and Whiskers plots, one-way ANOVA, etc.) by the Statgraphics Centurion software.
In agreement with the macroscopic observations and the statistical analysis the slags were reclassified into morphological types.
On the basis of the statistical analysis results, the most representative slags of each type were firstly analysed by means of the optical microscopy operating in reflected and transmitted light (OM-RL and OM-TL). Later they were analysed by X-ray powder diffraction (XRPD). The results of the XRPD analyses were treated by the Reference Intensity Ratio method for semi-quantitative phase evaluation.
On the basis of the minero-petrographic analyses, the most representative samples of each type were selected for chemical analysis using the XRF spectrometer and the scanning electron microscope coupled with the X-ray energy dispersive spectrometer (SEM-EDS).
The archaeologists identified 5 morphological types of slags (archaeo-types), the two common Late Bronze Age types: coarse slags and flat slags (Cierny et al., 2004; Herdits, 2003; Burger et al., 2007) and three new typological types called flat-thick, massive and fluid.
As described in the previous chapters, the coarse type is formed by slags with irregular shapes, high porosity and the diffuse presence of unreacted quartz relics.
The flat type has a limited thickness from a few millimetres to one centimetre. It also present a lack of porosity, a homogeneous texture and very smooth sides, sometimes with clear cooling marks. The macroscopic features of the massive are: one smooth

surface and one irregular surface, visible homogeneous core and diffuse superficial porosity.
The flat thick are similar to the flat slags but thicker.
The fluid type is composed by a slag with a morphologic flow texture.

Fig. 5.3: Macroscopic features of the 5 archaeo-types of slags.

5.3 Results

5.3.1 Density

The density was measured on the slags provided by the archaeologists (30 slag samples).
As shown in the summary statistic table (Tab. 5.1), the coarse slags (3 samples) have the lowest density values, ranging from 2.53 g/cm^3 to 2.95 g/cm^3.
The massive type (11 samples) has a means value of 3.12 g/cm^3. Unlike the massive slags of Luserna and Transacqua, the massive type of Segonzano has not the highest density values, but has a wide range of density starting with the minimum of the coarse and finishing with the maximum of the flat slags.
The flat slags (highest density range ρ = 3.33 - 3.87 g/cm^3) are composed by 14 samples and present a narrow interquartile range (0,17) and a mean value of 3,5 g/cm^3.
The fluid type (1 sample) and the flat-thick type (1 sample) have density values of 3,73 g/cm^3 and 3,21 g/cm^3, respectively.

Tab. 5.1: Summary statistics for the density values measured on the Segonzano slag samples.
Archaeo-Type: typology identified by the archaeologists.
Count: total number of slags for each group. SD: standard deviation. Min.: Minimum. Max.: Maximum. LQ: Lower Quartile. UQ: Upper Quartile. IQR: Range Interquartile.

Archeo-Type	Count	Average	Median	SD	Min.	Max.	Range	LQ	UQ	IQ range
Fluid	1	3,73								
Coarse	3	2,69	2,57	0,23	2,53	2,95	0,42	2,53	2,95	0,42
Massive	11	3,12	3,08	0,30	2,68	3,66	0,99	2,93	3,25	0,32
Flat	14	3,50	3,44	0,15	3,33	3,87	0,54	3,39	3,56	0,17
Flat-Thick	1	3,21								
Total	30									

Fig. 5.4: Box an whiskers plots of the slags formed the 5 Segonzano archaeo-type.

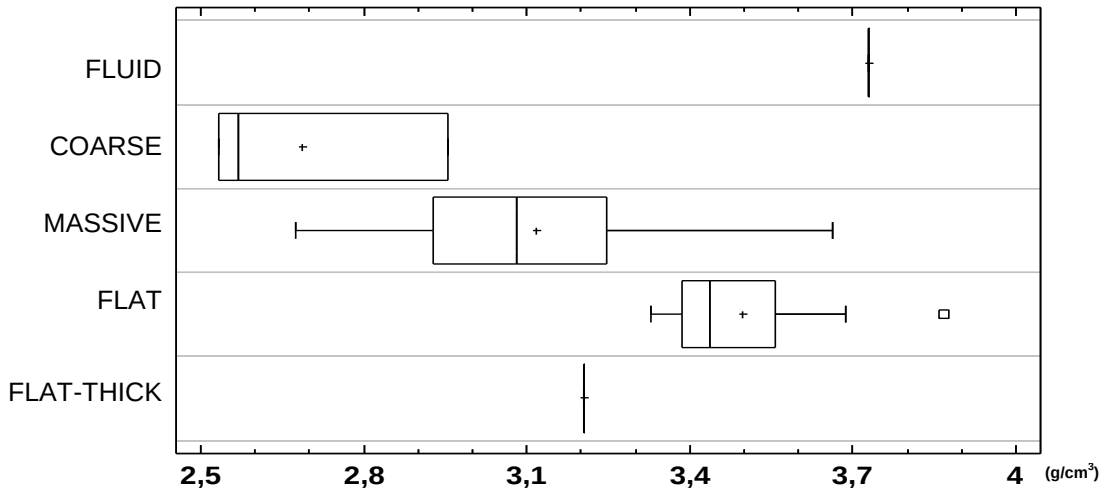

Using the one-way analysis of variance, it was verified that there are statistically significant differences between the mean and the medians of the density measured on the 5 types of slags (both the Fisher's Least Significance Different test and Kruskal Wallis test have P-value< 0,05).
The Multiple Range test (Duncan, 1955) was used to determine which types of slags differ significantly on the basis of their means.
The table of contrast shows the estimated difference between the means of each pair of slags types. The *Difference* column displays the mean of the first group minus the one of the second group. For each difference the software has calculated an uncertainty interval, shown in the *+/- Limits* column. Any pair for which the absolute value of the difference exceeds the uncertainty interval has statistically significant differences and it is indicated by an asterisk symbol in the *Sig*. column.

Tab. 5.2: Table of the contrast. The symbol * denotes a statistically significant difference at the 95,0% confidence level.

Contrast	Sig.	Difference	+/- Limits
Fluid - Coarse	*	1,04	0,55
Fluid - Massive	*	0,61	0,49
Fluid - Flat		0,23	0,49
Fluid - Flat-Thick		0,52	0,67
Coarse - Massive	*	-0,43	0,31
Coarse - Flat	*	-0,81	0,30
Coarse - Flat-Thick		-0,52	0,55
Massive - Flat	*	-0,38	0,19
Massive - Flat-Thick		-0,09	0,49
Flat - Flat-Thick		0,29	0,49

The homogeneous group table is a graphical illustration based on the contrast table and it indicates the archaeo-types of slags that form homogeneous groups of means.

Tab. 5.3: The homogeneous group (H.M.) table.

Archaeo-Type	Count	Mean	H.M.		
Coarse	3	2,69	X		
Massive	11	3,12		X	
Flat-Thick	1	3,21	X	X	X
Flat	14	3,50			X
Fluid	1	3,73			X

The Multiple Range test outputs showed significant differences mostly between the coarse, the massive and the flat types of slags, confirmed by the minero-petrographic and chemical analyses (Paragraph 5.3.2).

On the contrary, it was verified that the flat-thick type (1 sample) is not a distinct type of slag but minero-petrographically it could be included in the massive type.
The fluid type formed by 1 sample has a density value and morphological features that are not comparable with the other types of slags. However, the fluid type was not recognised as a distinct type of slags because it is an under-represented group of slags. However, several analyses were performed on this sample, such as optical microscopy and X-ray powder diffraction.

On the basis of these considerations, a second morphological examination of the slags was performed together with a new division into morpho-physical types (Tab. 5.4, Fig. 5.5).

Tab. 5.4: Summary statistics for the density values measured on the slag samples of Segonzano. Count: total number of slags for each group. SD: standard deviation. Min.: Minimum. Max.: Maximum. LQ: Lower Quartile. UQ: Upper Quartile. IQR: Interquartile Range.

Type	Count	Average	Median	SD	Min.	Max.	Range	LQ	UQ	IQR
COARSE	3	2,68	2,57	0,23	2,53	2,95	0,42	2,53	2,95	0,42
MASSIVE	12	3,13	3,14	0,29	2,68	3,66	0,98	2,95	3,24	0,29
FLAT	14	3,50	3,44	0,15	3,33	3,87	0,54	3,39	3,56	0,17

Fig. 5.5: Box an whiskers plots of the 3 type of slags: coarse, massive and flat.

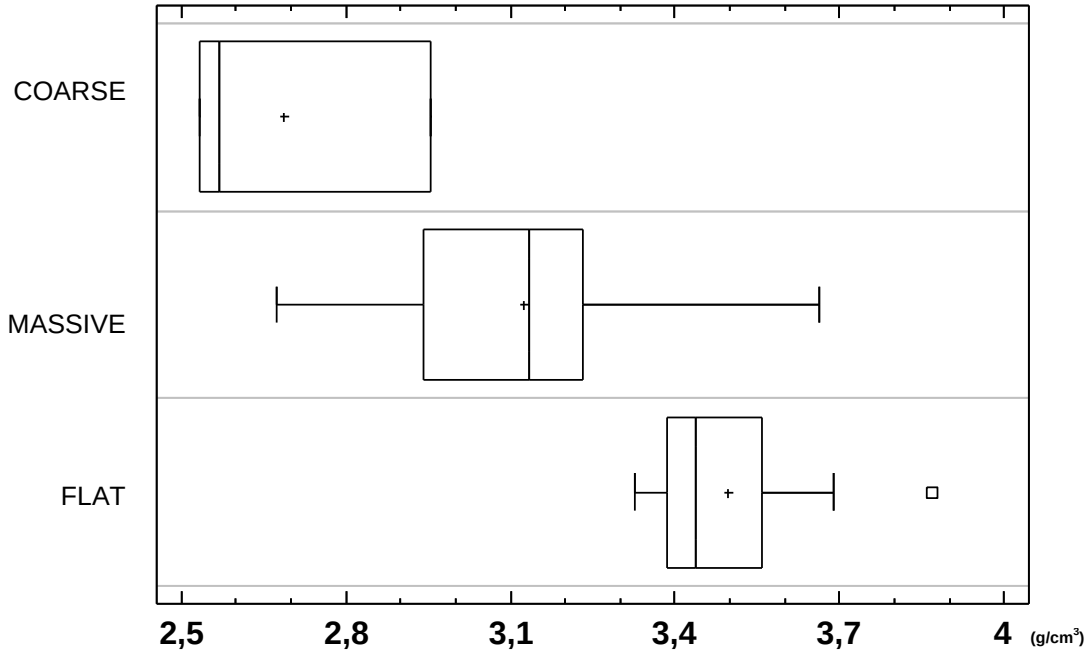

The following chemical and minero-petrographic analyses were performed on the total number of coarse and massive slags provided by the archaeologists and on the most representative flat slags chosen on the basis of the density measurements.
Figure 5.6 shows the box and whiskers plots of the three types with the samples analysed (dots). Table 5.5 displays the total number of slags analysed and the kind of analytical investigation performed.

Fig 5.6: Box an whiskers plots of the coarse, massive and flat types. The dots were located at the density values of the samples analysed.

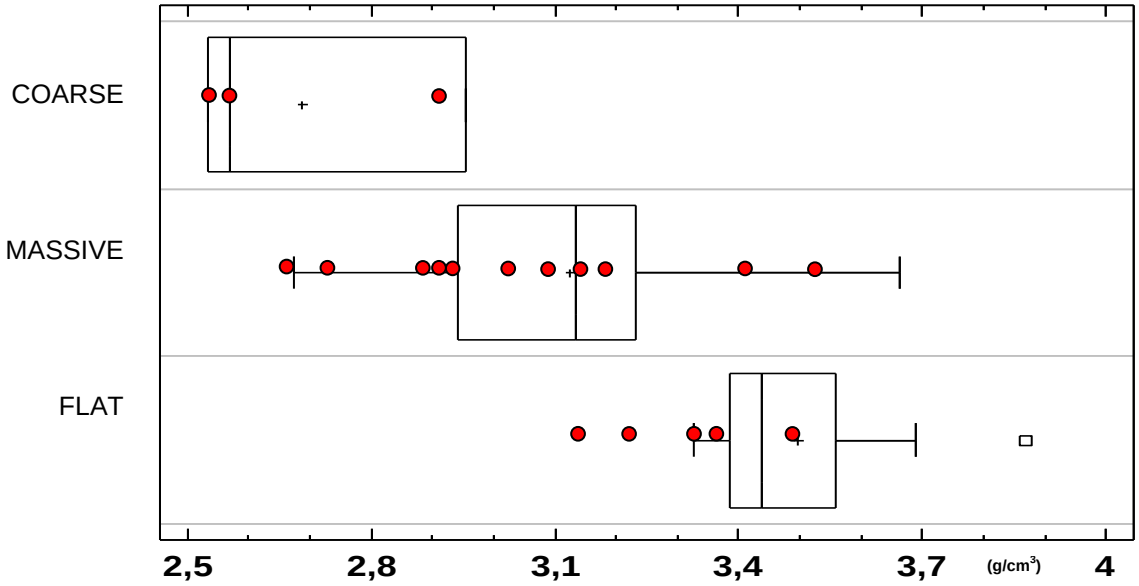

Tab. 5.5: List of the Segonzano slags fully investigated and the types of measurements carried out.

Type	N.	Density (g/cm^3)	Analytical Name	OM	XRPD	XRF	SEM-EDS	LIA
Fluid	1	3,73	SEG-F7	√	√			
COARSE	3	2,95	SEG-G4	√	√	√	√	√
		2,53	SEG-G8	√	√	√	√	
		2,57	SEG-G9	√	√	√		√
MASSIVE	12	2.93	SEG-M17	√	√	√	√	
		2.96	SEG-M2	√	√	√		√
		3.22	SEG-M3	√	√	√		
		2.68	SEG-M10	√	√	√		√
		3.19	SEG-M11	√	√	√	√	
		3.66	SEG-M12	√	√	√	√	
		3.25	SEG-M16	√	√	√	√	
		2.78	SEG-M21	√	√	√		
		3.00	SEG-M18	√	√	√	√	
		3.08	SEG-M20	√	√	√	√	
		3.54	SEG-M19	√	√	√		
		3.21	SEG-PS7	√	√	√		
FLAT	4	3.46	SEG-P5	√	√			√
		3.33	SEG-P13	√	√	√	√	√
		3.42	SEG-P14	√	√	√	√	√
		3.69	SEG-P15	√	√	√	√	
TOT	20							

5.3.2 Minero-petrographic and Chemical Analyses

Coarse Slags

The semi-quantitative phase evaluation (XRPD-RIR method) performed on the 3 coarse slags of Segonzano shows that two coarse slags (SEG-G4 and SEG-G8) have high quartz and low fayalite contents, as expected for this type of slags. On the contrary, the sample SEG-G9 has high content of fayalite and no quartz was detected.

Tab. 5.6: Mineralogical phases expressed in weight percentages (%wt) calculated by XRPD-Rir Method.

	Sample	Quartz	Olivine	Cristobalite	Magnetite
COARSE	SEG-G4	76	23	1	0
	SEG-G8	83	15	2	0
	SEG-G9	0	94	0	6
	Mean	**53**	**44**	**1**	**2**
	SD	46	43,5	1	3,5

Therefore, the mean content of the mineralogical phase of the coarse slags was calculated without taking into account the sample SEG-G9, whose low density compared to its mineralogical content is likely due to its high-porosity.

Fig. 5.7: Image of SEG-G9.

Tab. 5.6: Mineralogical phases expressed in weight percentages (%wt) calculated by XRPD-Rir Method.

	Sample	Quartz	Olivine	Cristobalite	Magnetite
COARSE	SEG-G4	76	23	1	0
	SEG-G8	83	15	2	0
	SEG-G9	0	94	0	6
	Mean	**79,5**	**19**	**1,5**	**0**
	SD	5	5,7	0,7	0

The coarse slags are composed by the highest amount of quartz and the lowest of fayalite in comparison to the massive and the flat types.
The optical microscopy observations of the two coarse samples revealed the presence of large grain of restitic quartz and prismatic olivine (low cooling rate ≈0,5°C/hr).

Fig. 5.8: Prismatic olivine in transmitted light observation.

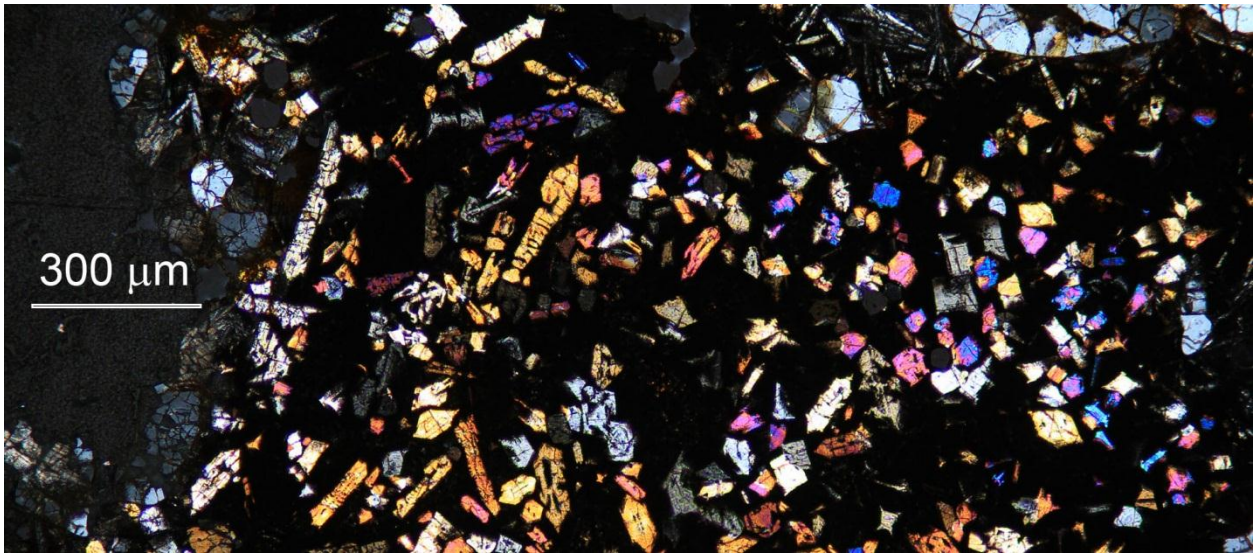

SEM-EDS analyses on the prismatic olivine displayed a Forsterite zoning core with a crystallization temperature of T(°C) ≈ 1380.

Fig. 5.9: Backscattered scanning electron photomicrographs of a zoned olivine with the Fo-Fa phase diagram modified after Bowen and Schairer(1935).

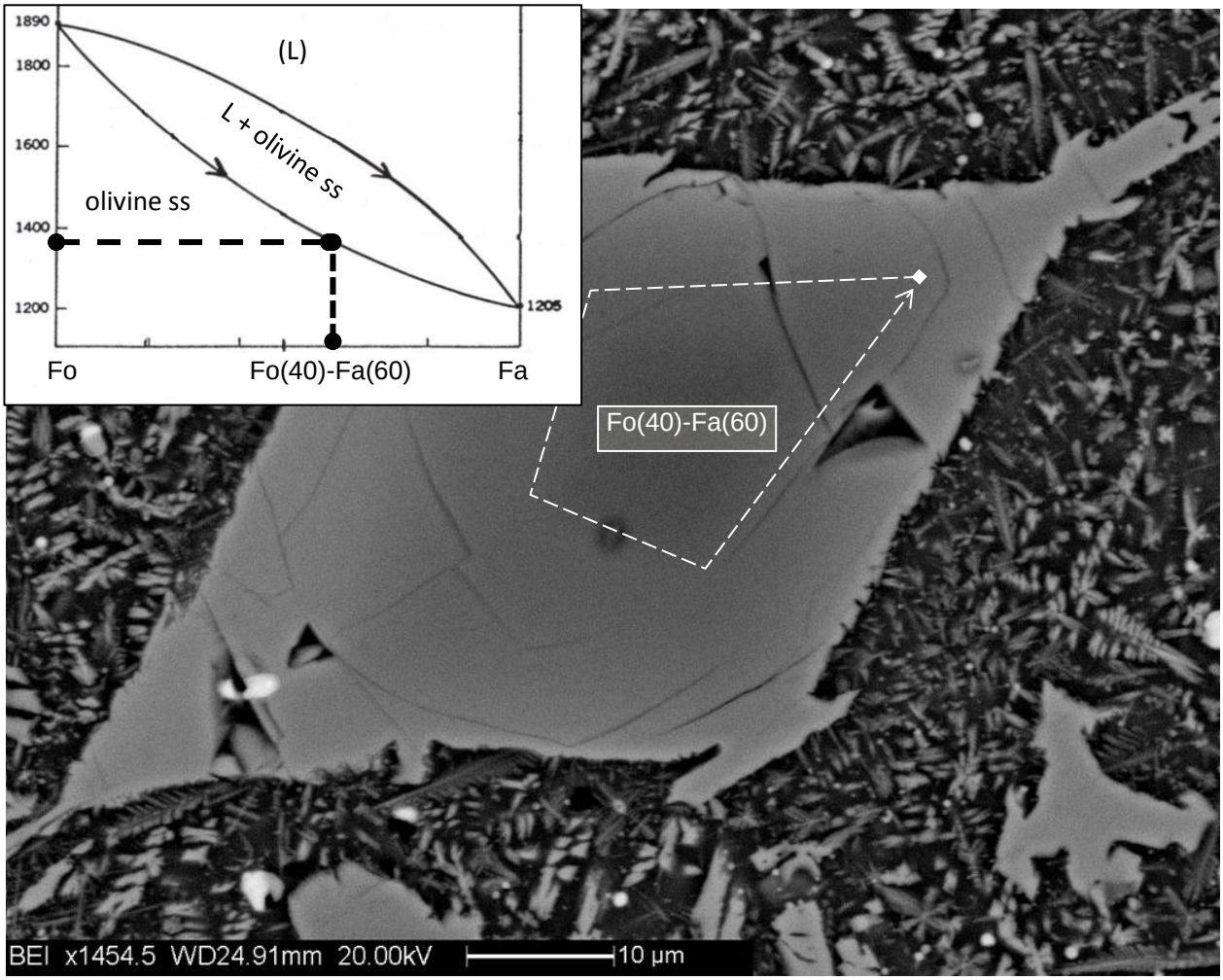

The analyses of the opaque minerals in reflected light microscopy display several crystals of partially reacted sulphides.
Two different types of sulphides were detected: 1) grain of chalcopyrite ($CuFeS_2$) as the charge sulphide and 2) small spheroidal crystals of sulphides with more complex chemical compositions mostly formed by bornite (Cu_5FeS_4).
The compositions of the coarse slag sulphides were analysed by means of SEM-EDS and plotted in the Cu-Fe-S system isothermal diagram at 700°C (Yund and Kullerud, 1966), confirming the two main sulphide types. The Fe-sulphides are often in association with the Cu-Fe-sulphides.

Fig. 5.10: Ternary Cu-Fe-S diagram in wt% at 700°C modified after Yund and Kullerud (1966). Bo: bornite, Cp: chalcopyrite, Py: pyrite, Po: pyrrhotite, L: liquid, ss: solid solution.

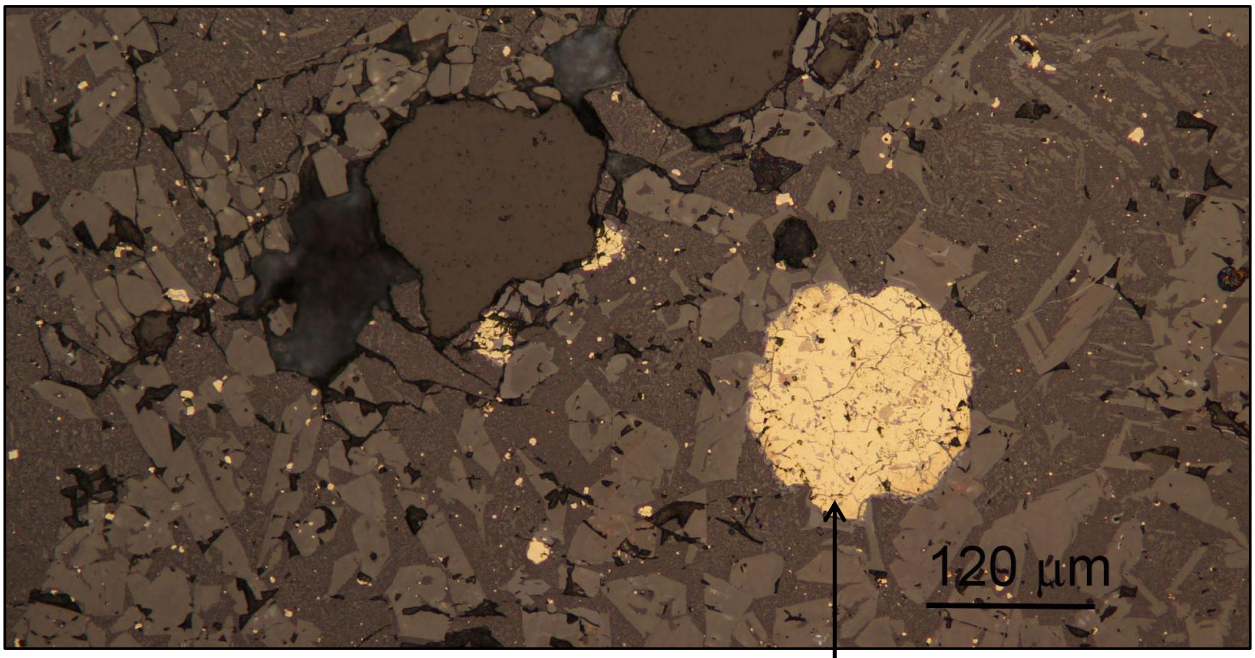

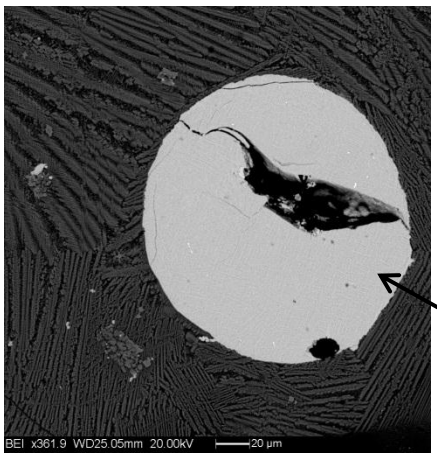

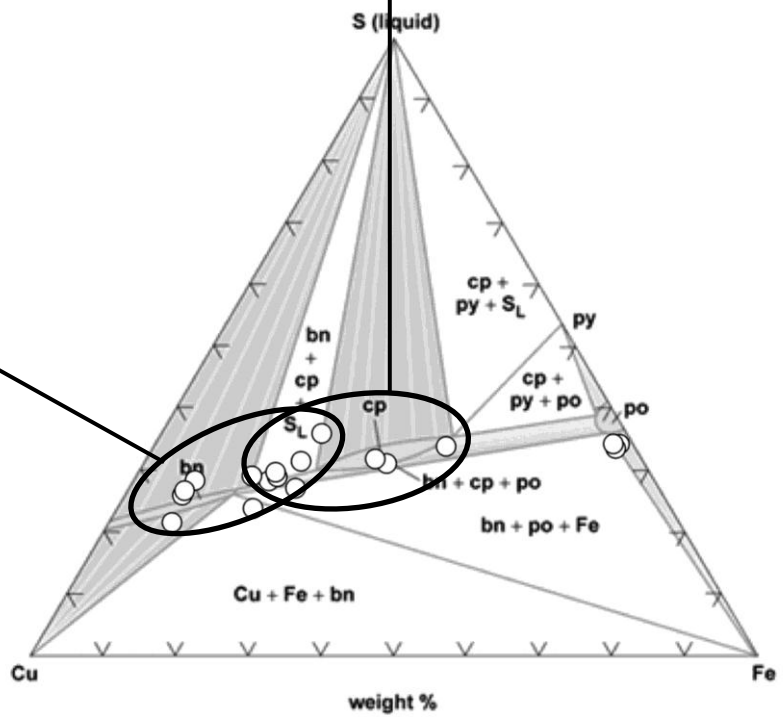

The chemical bulk analyses (XRF) of the two coarse slags were performed using the same powders analysed by XRPD.

Tab. 5.7: Chemical bulk compositions of the coarse slags (C) of Segonzano

	Sample	SiO_2	TiO_2	Al_2O_3	Fe_2O_3	MnO	MgO	CaO	Na_2O	K_2O	P_2O_5
C	SEG-G4	51,87	0,25	8,14	30,48	0,24	3,94	1,17	0,14	0,72	0,17
	SEG-G8	58,99	0,35	9,57	24,11	0,21	2,55	1,09	0,13	1,79	0,15
	Mean	**55,43**	**0,30**	**8,86**	**27,30**	**0,23**	**3,25**	**1,13**	**0,14**	**1,26**	**0,16**
	SD	5,03	0,07	1,01	4,50	0,02	0,98	0,06	0,01	0,76	0,01

The chemical compositions of the slags interpreted in terms of their major oxide components were plotted in the ternary anorthite ($CaAl_2Si_2O_8$)-FeO(+MgO)–SiO_2 system (Morton and Wingrove, 1969b; 1972).

Fig 5.11: Bulk chemical compositions of the coarse slags of Segonzano plotted in the ternary anorthite-FeO(+MgO)- SiO_2 diagram.

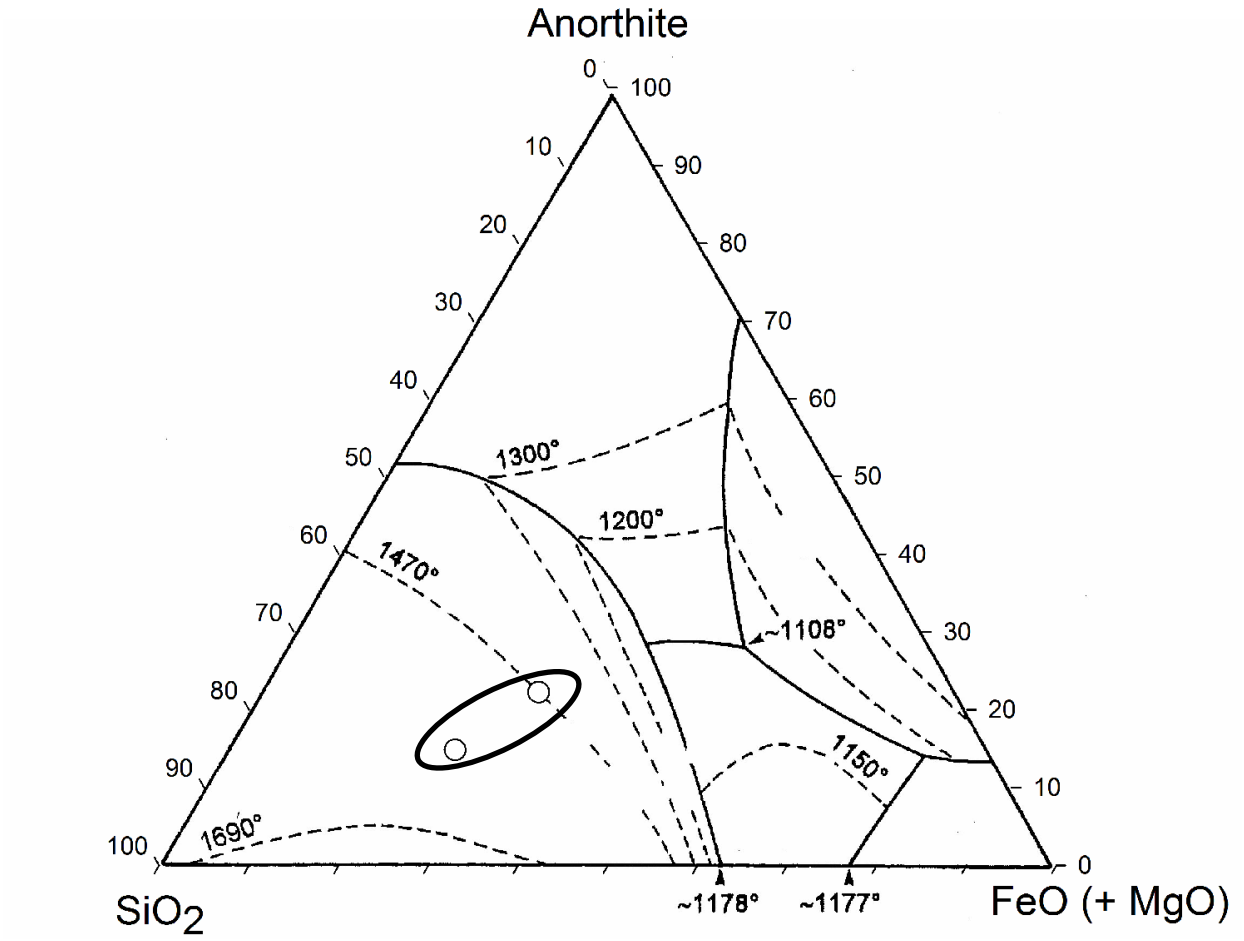

The bulk chemical compositions of the two coarse slags of Segonzano are into the SiO_2 field of stability. SiO_2 is in fact the major component of these types of slags, in accordance with the mineralogical phase analyses (Tab. 5.6). The optical observation has indicated that the SiO_2 present as quartz is a restitic phase that did not took part in the melting process.

The temperature reached during the production process of the coarse slags has to be referred to the temperature formation of the newly phases, as the olivine (Fig. 5.9).

Massive Slags

The X-ray powder diffraction analyses were performed on the total number of massive slags of Segonzano provided by the archaeologists. On the basis of the mineralogical phases analyses, the massive slags could be divided into two sub-groups: massive 1 (M1) and massive 2 (M2). The M1 subgroup is characterised by a higher amount of quartz (>20wt%) than the M2 group slags, which are essentially composed by fayalite (≈88 wt%).

Tab. 5.8: Mineralogical phases of the massive slags expressed in weight percentages (%wt) and calculated by the XRPD-Rir Method.

	Sample	Quartz	Olivine	Cristobalite	Magnetite	Pyroxene	Leucite
MASSIVE 1	SEG-M2	24	70	3	3	0	0
	SEG-M3	20	66	6	8	0	0
	SEG-M11	17	73	2	8	0	0
	SEG-M20	22	56	12	10	0	0
	SEG-M21	19	56	2	11	12	0
	SEG-M18	20	70	3	7	0	0
	Mean	**20,3**	**65,2**	**4,7**	**7,8**	**2**	**0**
	SD	2,4	7,4	3,9	2,8	4,9	0
MASSIVE 2	SEG-M10	0	83	0	6	11	0
	SEG-M12	1	93	0	6	0	0
	SEG-M16	4	88	0	8	0	0
	SEG-M17	2	89	0	9	0	0
	SEG-M19	0	86	0	9	0	5
	SEG-PS7	6	85	0	9	0	0
	Mean	**2,2**	**87,3**	**0**	**7,8**	**1,8**	**0,8**
	SD	2,4	3,5	0	1,5	4,5	2

The division into two sub-groups was also checked through the density measurements, as shown by the box and whiskers plots in Fig. 5.12.

Fig. 5.12: Box and whiskers plots of the M1 and M2 sub-groups.

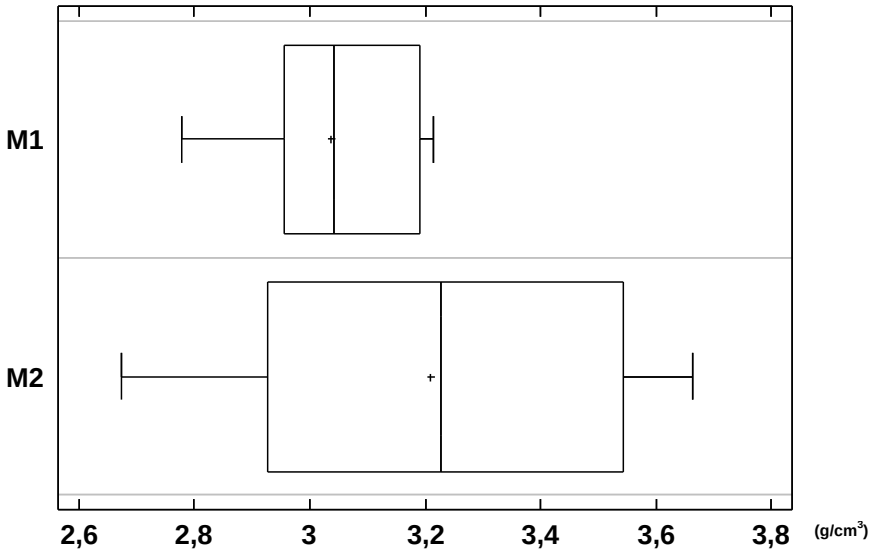

Confirming the density measurements and the XRPD analyses, the M1 thin sections observed by the optical microscopy revealed large grain of restitic and fractured quartz.

Fig. 5.13: Restitic quartz observed in a M1 slag sample.

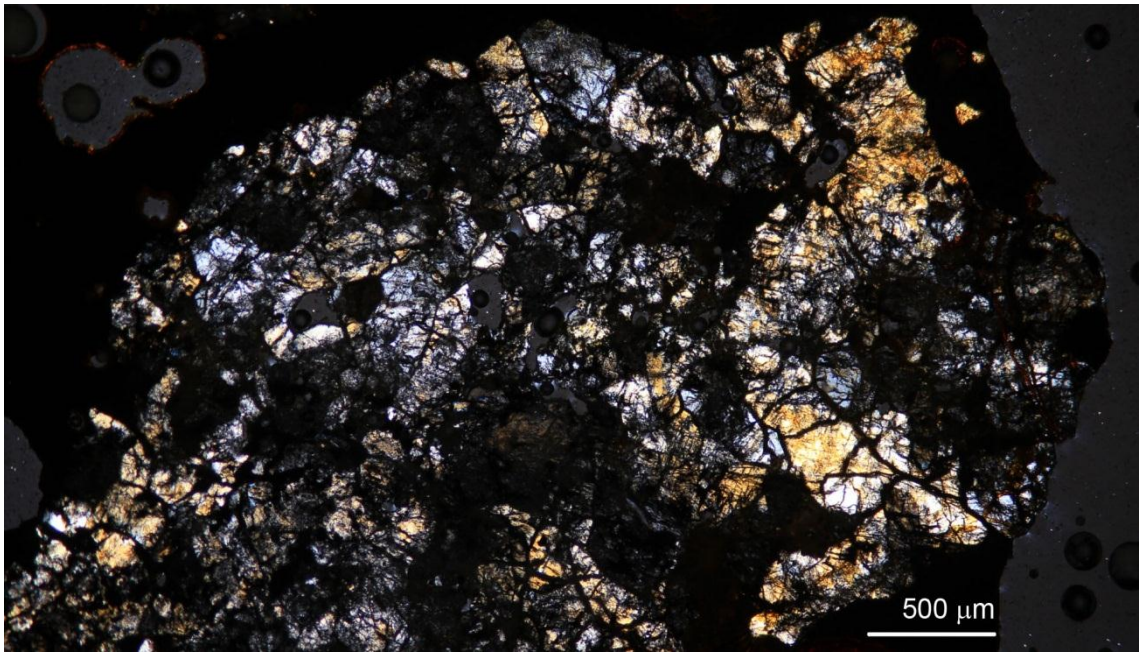

Both the M1 and M2 sub-groups are characterised by the presence of different olivine habits, mostly prismatic and chain, disseminated randomly in the slag matrix.

Fig.5.14: Backscattered scanning electron photomicrographs image (BSI) of the prismatic and chain olivines.

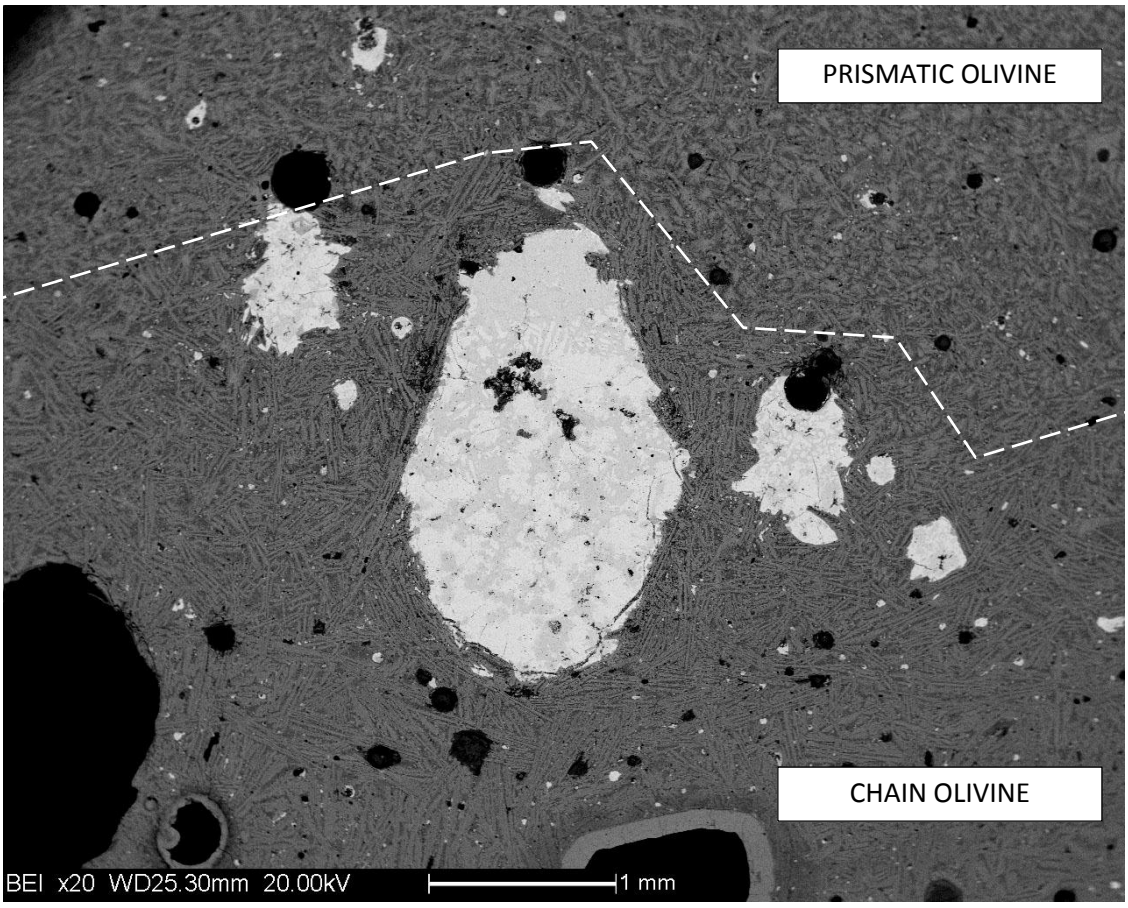

Several small copper droplets associated to magnetite were observed in M1 and M2 slags.

Fig. 5.15: Aggregates of magnetite (Ma: light grey), copper prills (Cu) surrounded by chalcocite (Ch: grey)

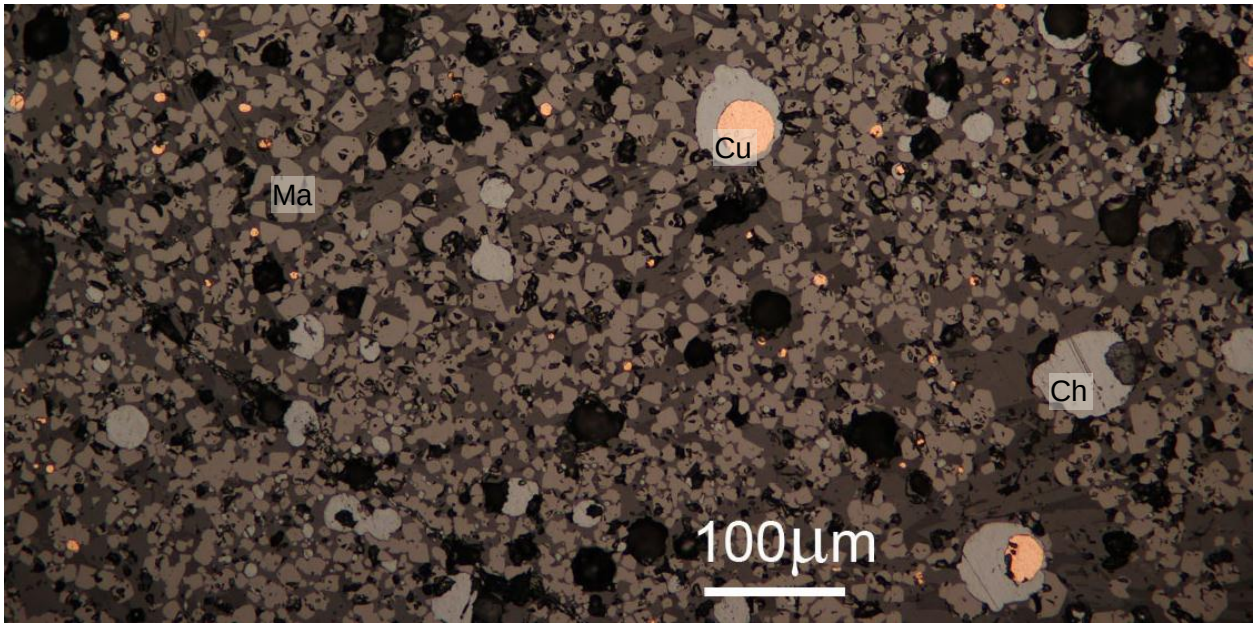

Apart from the different quartz contents, the M1 and M2 slags also differ in the types of sulphides that were observed in optical microscopy and analysed by means of SEM-EDS.

Fig. 5.15: Compositions of the sulphides in the M1 and M2 slags plotted in the ternary Cu-Fe-S diagram at 700°C.

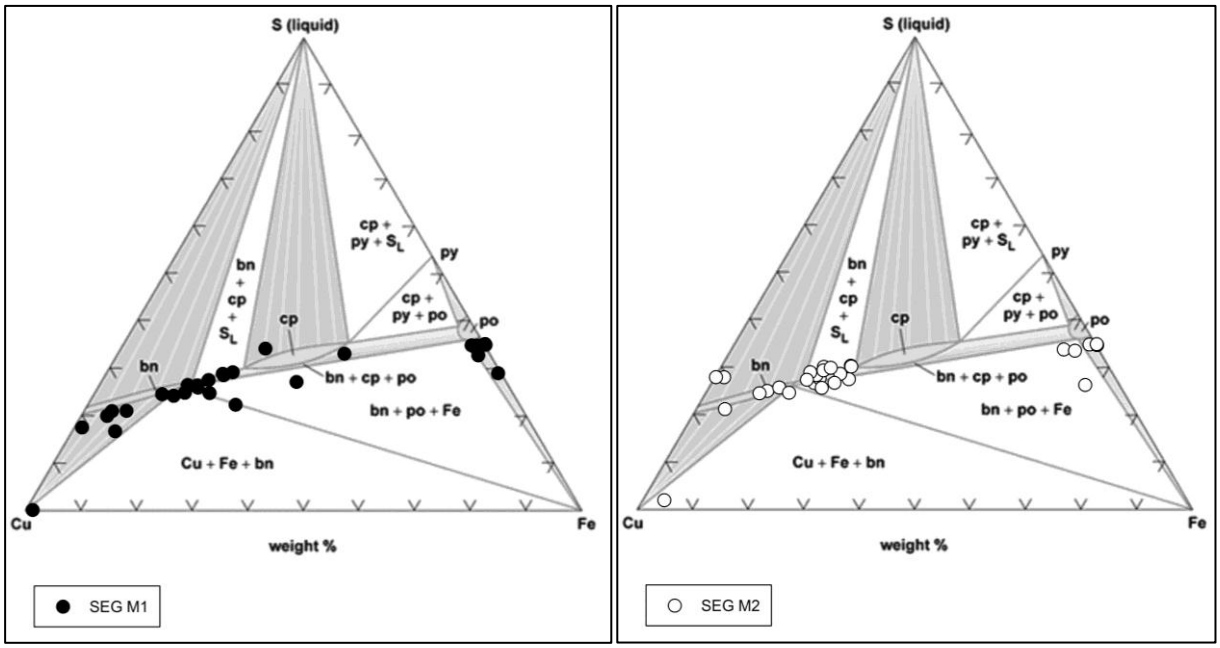

The M1 sulphides are characterised by an intermediate chalcopyrite-bornite-pyrrhotite composition. In addition, several small grains of chalcopyrite were observed. The Cu-sulphides are mostly chalcocite (Cu_2S) often associated to Cu-prills.

In the M2 slags no grain of chalcopyrite were observed and their large sulphides have essentially a bornite-chalcopyrite intermediate composition. Many covellite (CuS) crystals were observed (Fig. 5.18).

Fig. 5.16: M1 sulphide: symplectitic intergrowth of bornite (Bo) and chalcopyrite (Cp) in pyrrhotite (Po).

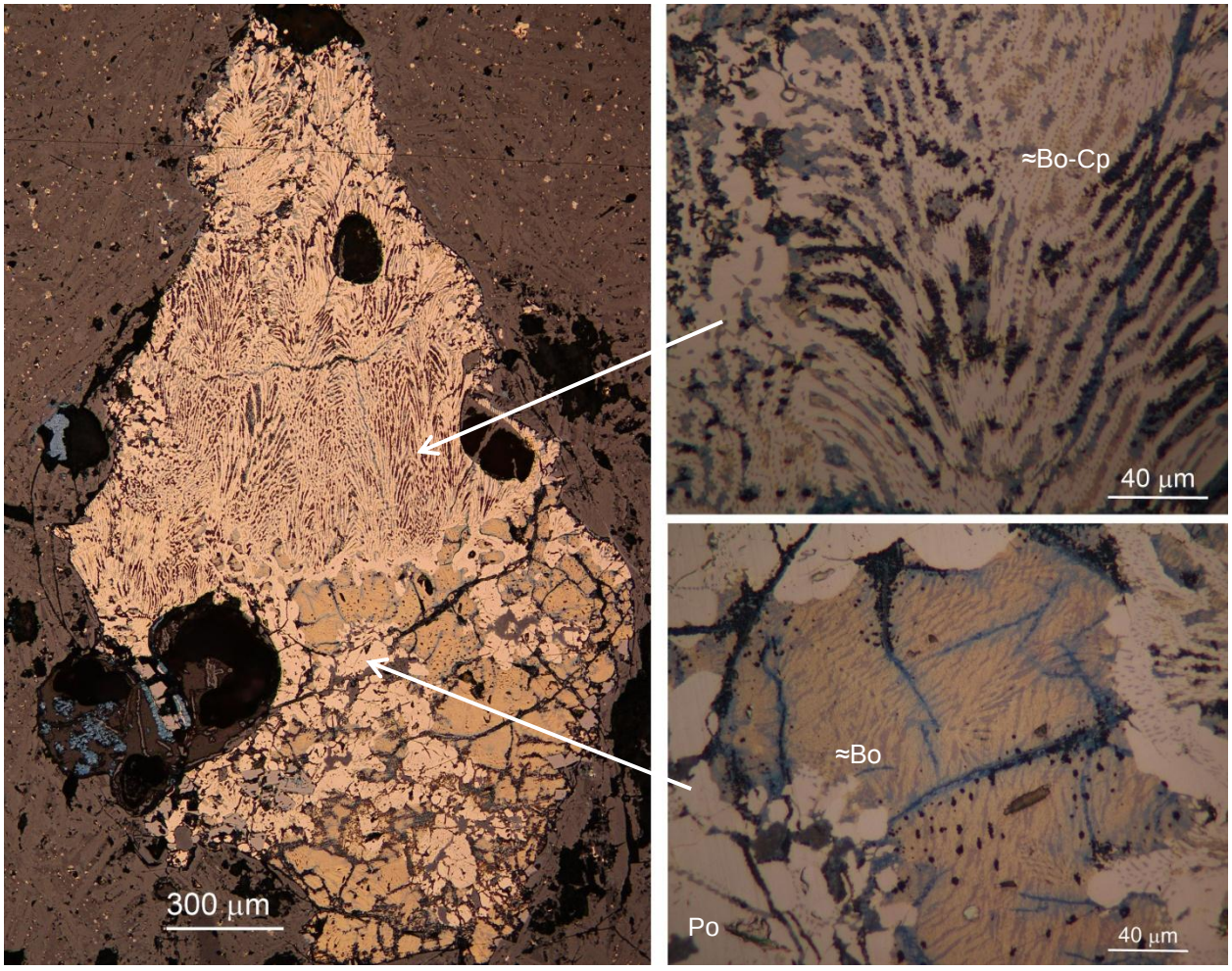

Fig. 5.17: M2 sulphide mostly composed by fine intergrowth of bornite-like composition.

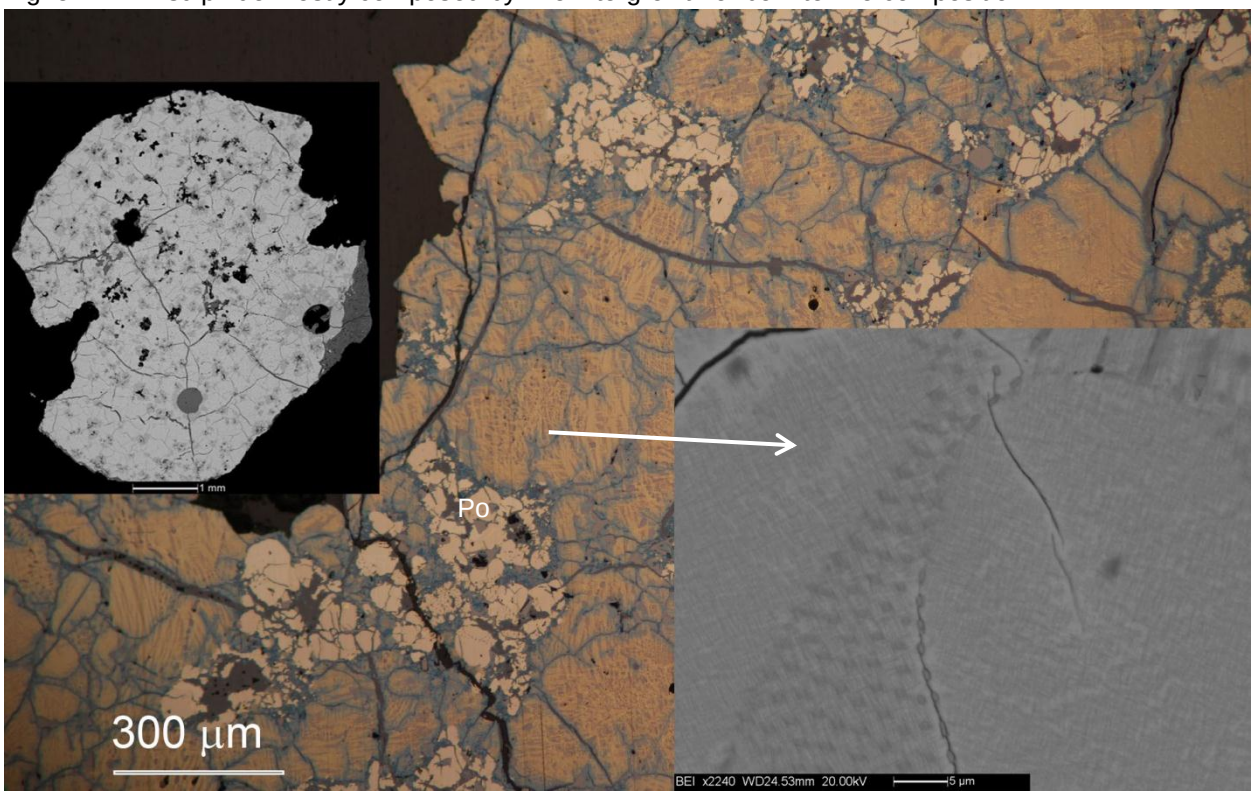

Fig. 5.18: Several crystals of covellite (deep-blue, light-blue) in M2 slags.

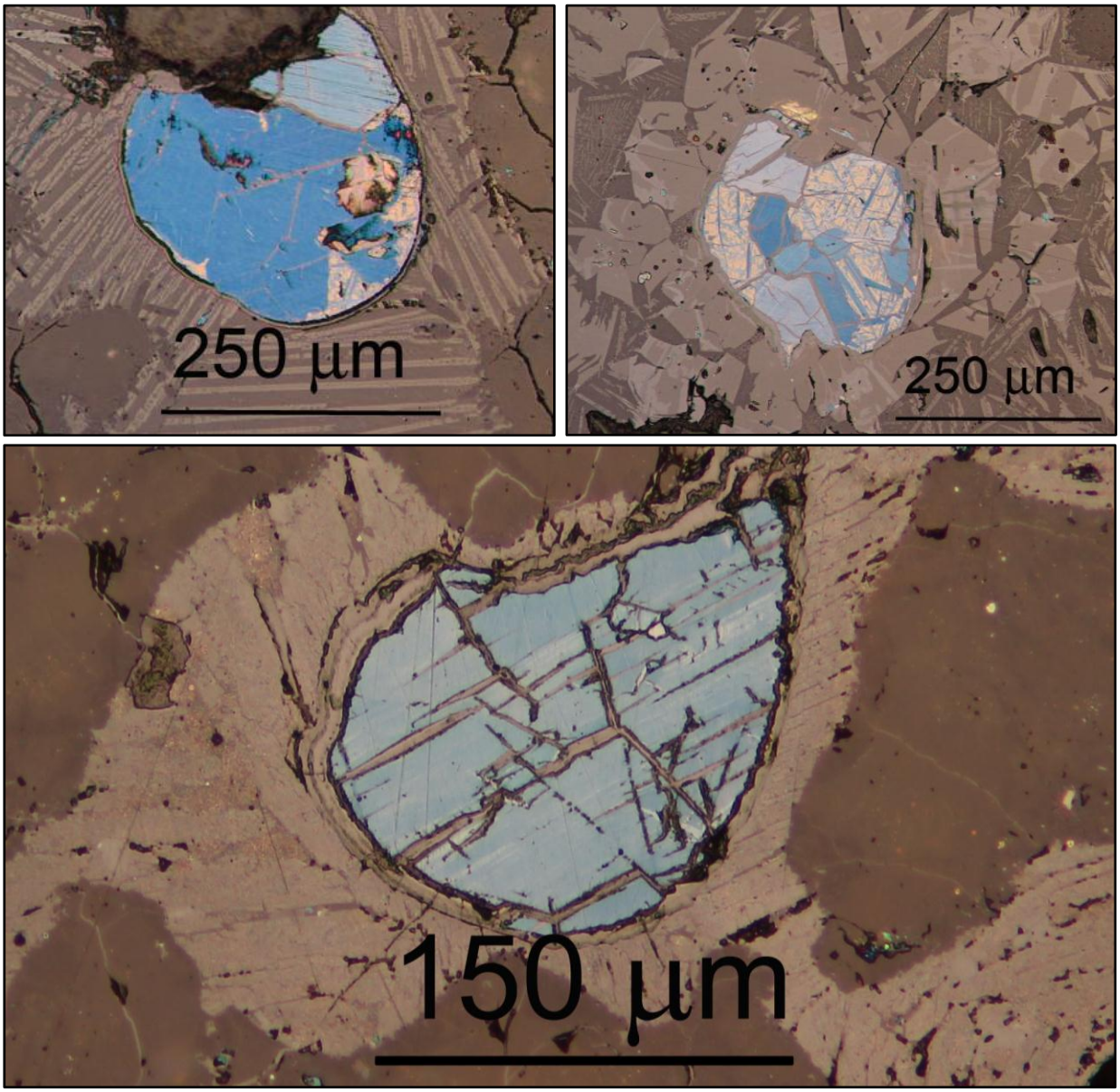

The chemical bulk analyses performed on the M1 and M2 slags are displayed in the Tab. 5.13 and Tab. 5.14 and plotted in the ternary anorthite-FeO (+MgO)–SiO_2 diagram (Fig. 5.19).

Tab. 5.13: XRF chemical bulk compositions of the M1 slags of Segonzano.

	Sample	SiO_2	TiO_2	Al_2O_3	Fe_2O_3	MnO	MgO	CaO	Na_2O	K_2O	P_2O_5
M1	SEG-M2	43,7	0,09	3,88	47,16	0,1	0,52	1,43	0,17	1,03	0,12
	SEG-M3	39,36	0,09	4,11	51,59	0,14	0,56	1,45	0,22	0,81	0,1
	SEG-M11	36,27	0,09	3,73	54,95	0,1	0,5	1,19	0,18	0,8	0,09
	SEG-M20	38,08	0,08	4,44	52,17	0,17	0,53	1,29	0,15	0,59	0,1
	SEG-M18	34,27	0,07	3,29	56,33	0,14	0,51	1,86	0,15	0,81	0,17
	SEG-M21	32,03	0,07	3,54	57,36	0,23	0,46	2,38	0,2	0,83	0,11
	Mean	**37,29**	**0,08**	**3,83**	**53,26**	**0,15**	**0,51**	**1,60**	**0,18**	**0,81**	**0,12**
	SD	4,09	0,01	0,41	3,75	0,05	0,03	0,45	0,03	0,14	0,03

Tab. 5.14: XRF chemical bulk compositions of the M2 slags of Segonzano.

	Sample	SiO_2	TiO_2	Al_2O_3	Fe_2O_3	MnO	MgO	CaO	Na_2O	K_2O	P_2O_5
M2	SEG-M10	39,42	0,15	5,91	45,97	0,18	1,1	3,01	0,51	1,94	0,25
	SEG-M12	30,54	0,08	6,07	57,86	0,21	0,77	1,31	0,21	0,76	0,11
	SEG-M16	33,3	0,09	4,89	54,64	0,16	0,7	1,47	0,24	1,13	0,16
	SEG-M17	30,47	0,11	5,21	57,86	0,2	0,74	2,09	0,3	1,07	0,18
	SEG-M19	27,39	0,09	3,46	63,59	0,13	0,7	1,66	0,25	0,66	0,17
	SEG-PS7	39,16	0,15	5,48	47,66	0,19	1,11	2,63	0,36	1,91	0,21
	Mean	**33,38**	**0,11**	**5,17**	**54,60**	**0,18**	**0,85**	**2,03**	**0,31**	**1,25**	**0,18**
	SD	4,95	0,03	0,94	6,70	0,03	0,20	0,68	0,11	0,56	0,05

Due to their high amount of restitic quartz, almost all the slag samples belonging to the M1 group are in the field of stability of SiO_2, while the M2 slags are in the fayalite area, except for the samples SEG-M10 and SEG-PS7.

Fig. 5.19: Bulk chemical compositions of the massive slags (M1 and M2) plotted in the ternary anorthite-FeO(+MgO)- SiO_2 diagram.

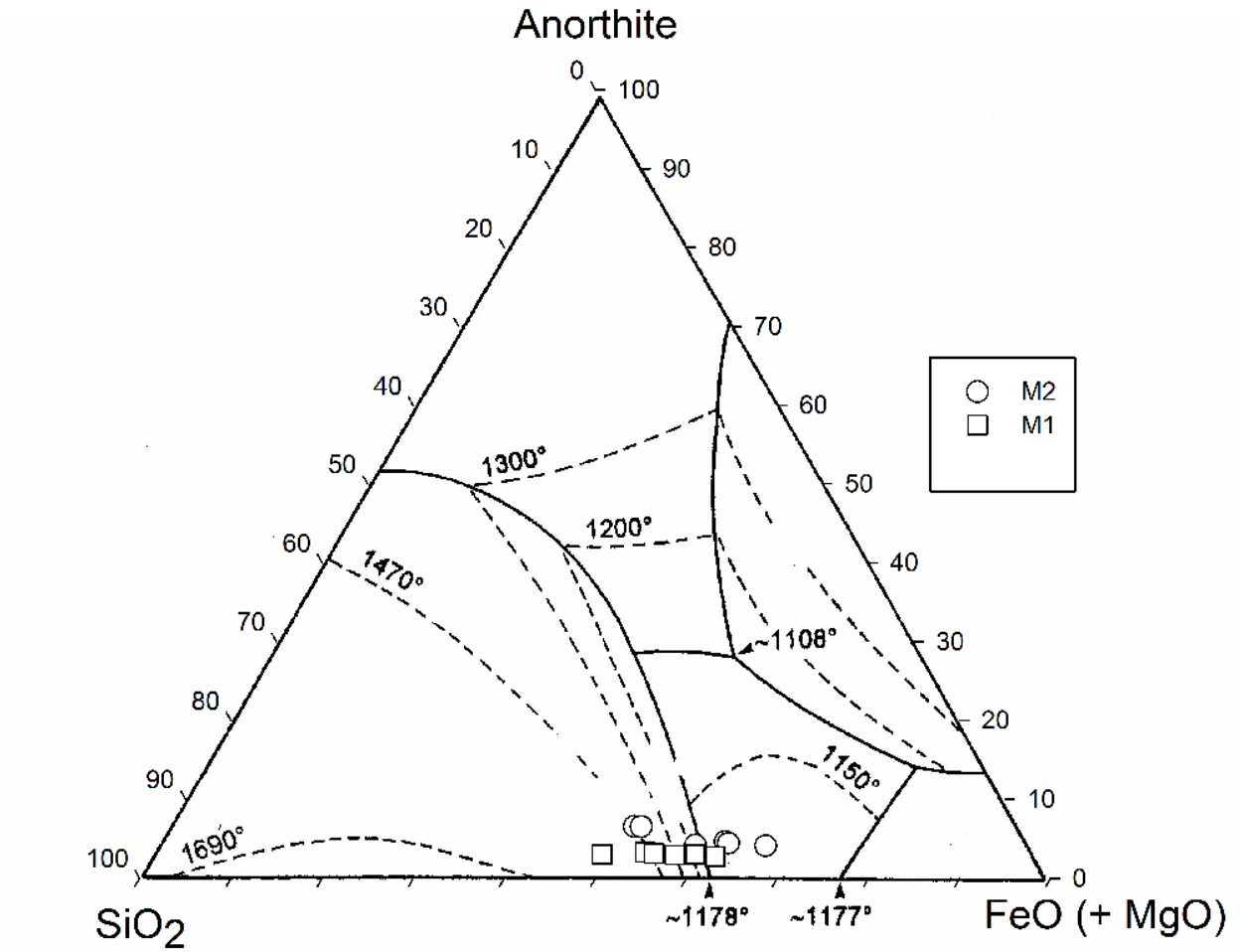

Flat Slags

The flat slags are characterised by the highest amount of fayalite (≈91 wt%). A low amount of quartz was detected in one flat samples (SEG-P14 = 3 wt%). The amount of magnetite ranged from 4 wt% to 9 wt%.

Tab. 5.15: Mineralogical phases of the flat slags expressed in weight percentages (%wt) and calculated by the XRPD-Rir Method.

	Sample	Quartz	Olivine	Cristobalite	Magnetite	Pyroxene
FLAT	SEG-P5	0	95	0	5	0
	SEG-P13	0	96	0	4	0
	SEG-P14	3	89	0	8	0
	Mean	**1,0**	**93,3**	**0**	**5,7**	**0**
	SD	1,7	3,8	0	2,1	0

Optical and electron microscopy investigations revealed different olivine habits, such as the typical chain morphology (cooling rate: 80°C/hr -350°C/hr) and the prismatic habit (0.5°C/hr) that often are zoned in the core (T≈1240°C).

Fig. 5.20: A) BSI micrographs of prismatic olivine showing a Fo-zoned core.
B) Prismatic and chain olivines.

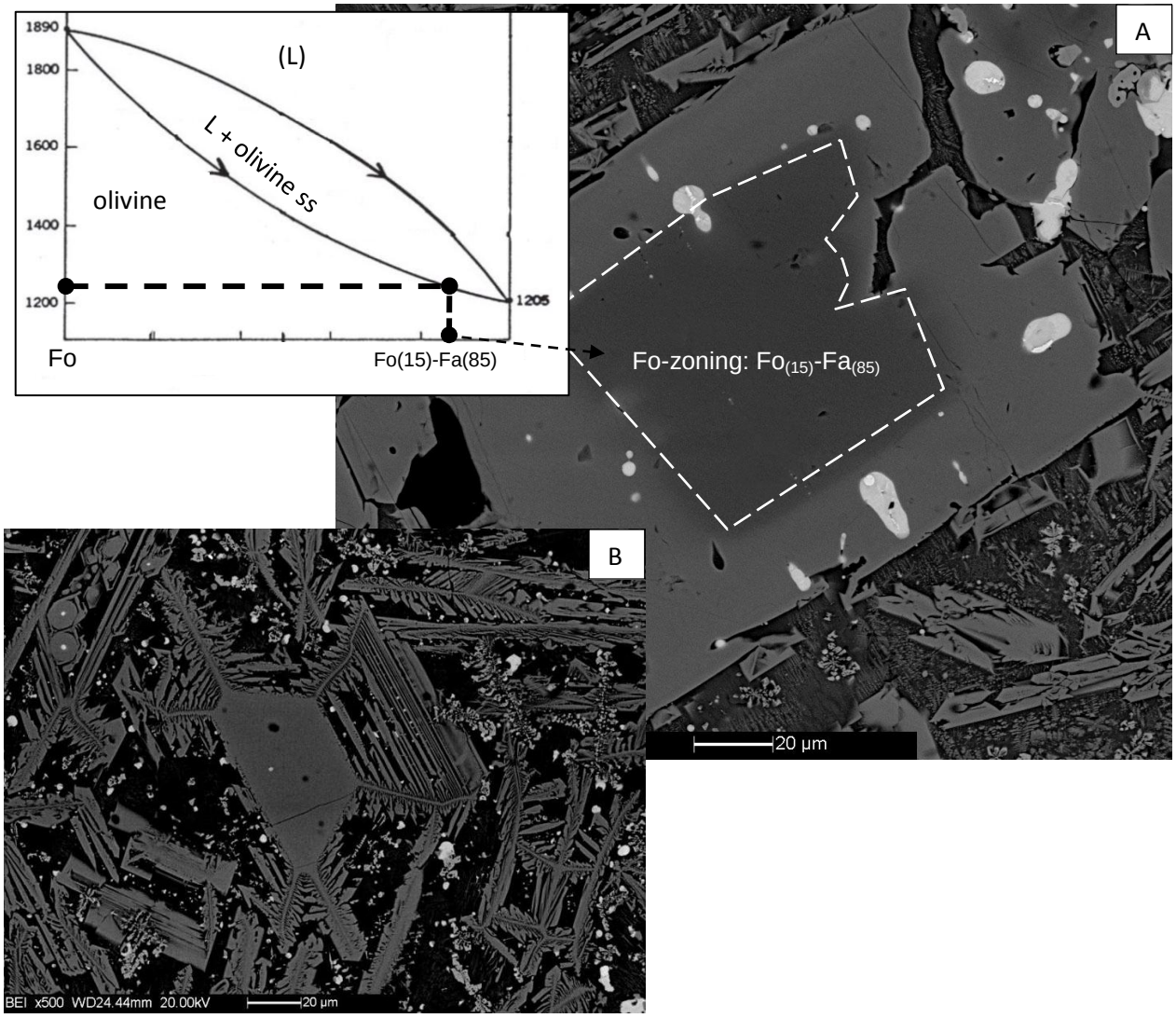

The sulphides observed in the flat slags of Segonzano are larger than the ones observed in the Luserna and Transacqua flat slags.
As shown by the ternary Cu-Fe-S diagram (Fig. 5.23), their composition is mostly Cu_5FeS_4 (bornite) with a wide compositional range ranging from chalcocite to chalcopyrite and pyrrhotite. Moreover, many copper prills were detected.

Fig. 5.21:) BSI micrographs of large Cu-Fe sulphides.

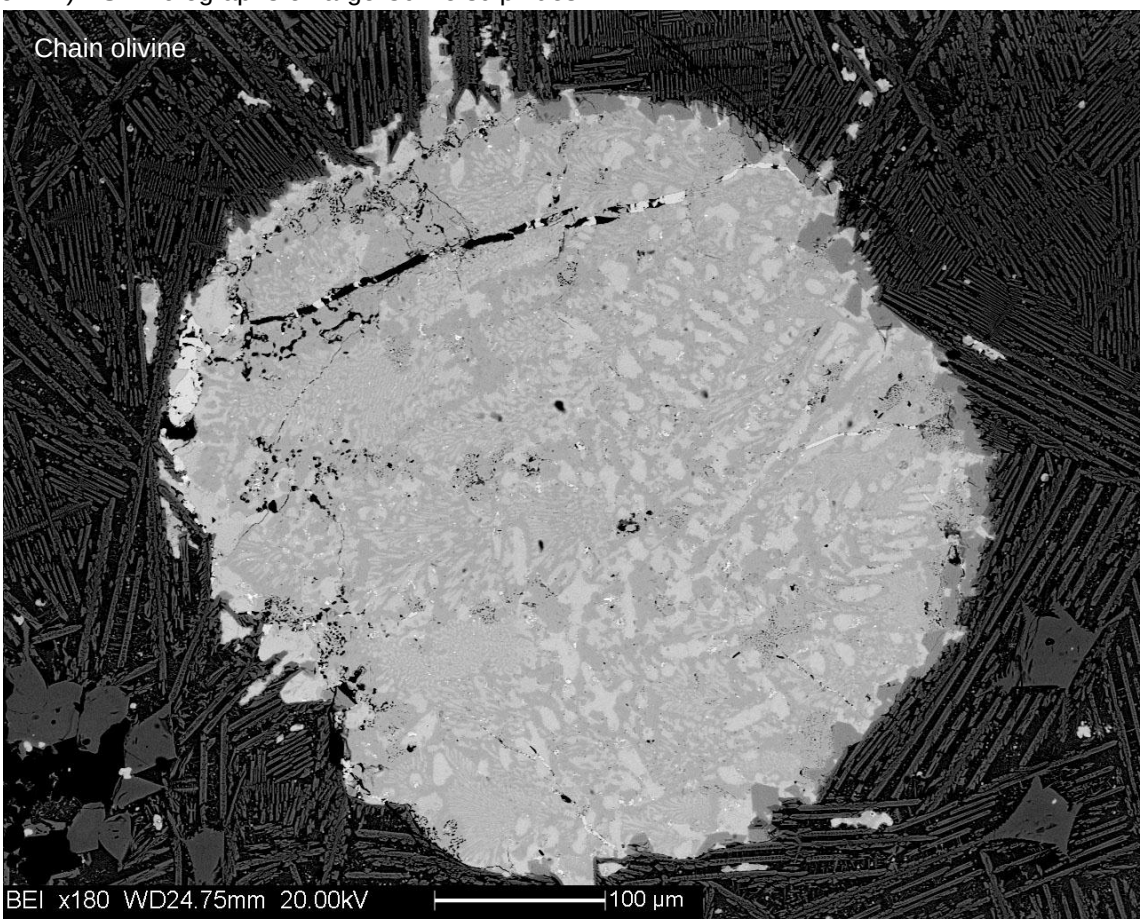

Magnetite, Cu-sulphides (mostly Cu_2S) and copper prills are finely dispersed within the olivine matrix.

Fig. 5.22: Copper prills (Cu), magnetite (Ma) and chalcocite (Ch).

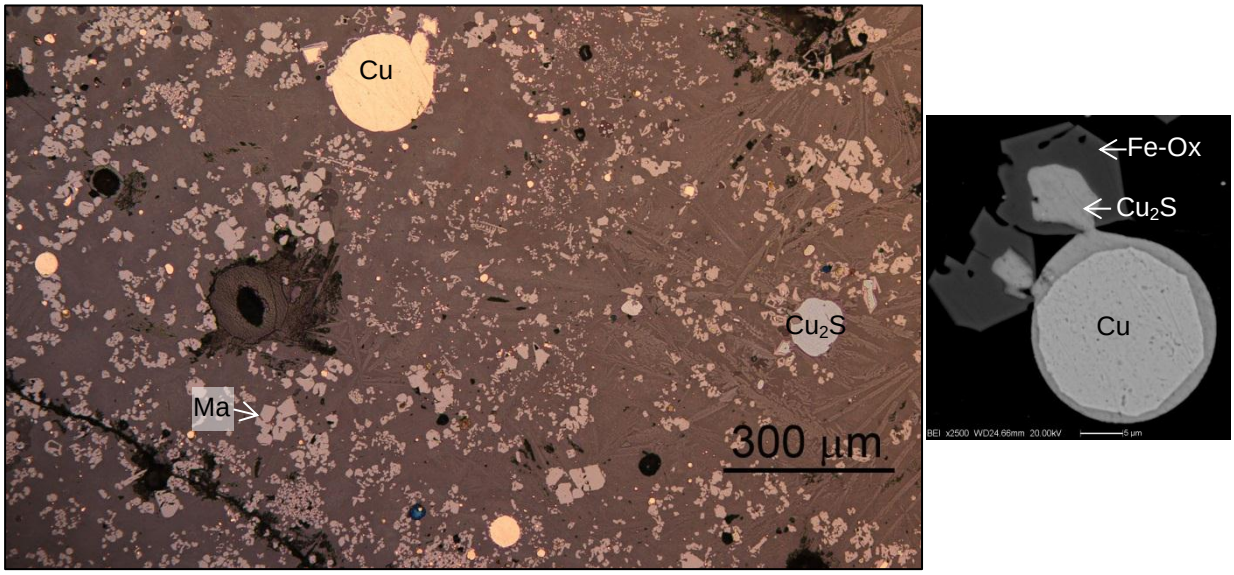

Fig. 5.23: Compositions of the sulphides in the flat slags plotted in the ternary Cu-Fe-S diagram at 700°C.

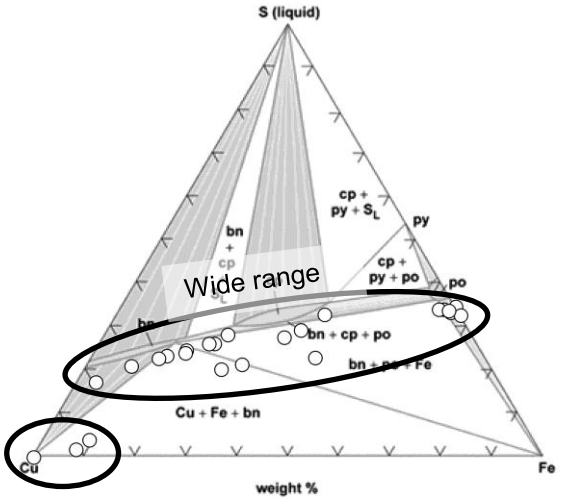

The bulk chemical analyses were performed on the most representative flat slag samples (Tab. 5.16) using the powders prepared for the XRPD analyses.
The data were plotted in the ternary anorthite - FeO (+MgO)- SiO_2 diagram (Fig. 5.24).

Tab. 5.16: XRF chemical bulk compositions of the flat slags of Segonzano.

	Sample	SiO_2	TiO_2	Al_2O_3	Fe_2O_3	MnO	MgO	CaO	Na_2O	K_2O	P_2O_5
FLAT	SEG-P15	31,05	0,11	4	57,13	0,19	0,88	3,24	0,34	1,32	0,19
	SEG-P13	37,94	0,32	9	41,45	0,29	2,82	3,53	0,41	2,33	0,23
	SEG-P14	34,77	0,21	5,8	49,26	0,26	1,6	3,73	0,35	1,83	0,27
	Mean	**34,59**	**0,21**	**6,27**	**49,28**	**0,25**	**1,77**	**3,50**	**0,37**	**1,83**	**0,23**
	SD	3,45	0,11	2,53	7,84	0,05	0,98	0,25	0,04	0,51	0,04

As shown in Figure 5.24, the slags analysed are partially in the field of SiO_2 stability and partly in the fayalite area, showing a different trend compared to the Luserna and Transacqua flat slags trend. This is likely due to their low content of Fe-oxides and their high amount of SiO_2.

Fig. 5.24: Bulk chemical compositions of the flat slags of Segonzano.

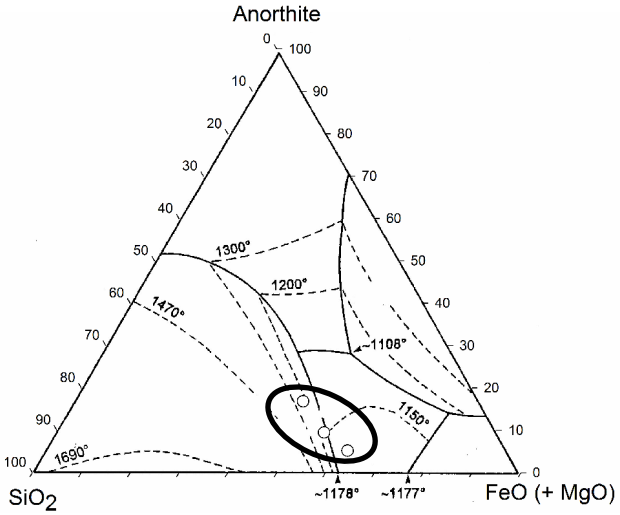

5.4 Discussion and Conclusion

The slags of the Segonzano Peciapian smelting site were produced during high-temperature processes (T≈1300-1380°C), in which the chalcopyrite was used as the charge and the quartz as the flux.
The mineralogical phase analyses and the textural observation of the opaque (Cu-Fe-sulphides, Fe-oxides) and the transparent minerals (olivine, quartz) indicate that the coarse, the massive and the flat slags are the products of different smelting operations.
The quartz-rich coarse type of slags is characterised by a few small Cu-Fe-sulphides partially transformed that may be the by-product of the first smelting process.
The sand of slags found in the site (Fig. 5.2) is probably the product of a kind of beneficiation, during which the large-sized coarse slags were smashed in order to recover the sulphide relict entrapped into the slags. Unfortunately, it has not been possible to obtain a sand sample for the analyses.

The two massive groups of slags (M1 and M2) might have been formed during two different processes. The M1 slags could be related to the smelting of the first matte produced perhaps by adding new quartz. The M2 slags could be the by-product of the smelting of the matte produced during the M1 process formation.
However, more slags are needed in order to verify this hypothesis because their actual quantity is not sufficient to provide a representative statistical sample.

As regards to the flat slags, both the morphological features and the textural analyses entail that these slags were produced during a final refining step of the enriched matte. The flat slags are mainly formed by pure fayalite and the remaining secondary sulphides and copper are entrapped among the fayalite crystal matrix.
In this last step the operating metallurgical chain seems to have reached a high extraction efficiency.

Tab. 5.17: List of the 30 slags of Segonzano Peciapian site.

	Sample Name	Archeo-Type	Density (g/cm^3)	Analytical name
1	17/1	Massive	2,96	SEG-M2
2	17/2	Massive	3,54	SEG-M19
3	18/1	Coarse	2,57	SEG-G9
4	18/2	Fluid	3,73	SEG-F6
5	18/3	Flat	3,46	SEG-P5
6	18/4	Flat	3,69	SEG-P15
7	18/5	Flat	3,42	SEG-P14
8	18/6	Massive	2,93	SEG-M17
9	18/7	Massive	3,22	SEG-M3
10	18/8	Massive	3,19	SEG-M11
11	20/1	Flat	3,39	
12	20/2	Flat	3,33	SEG-P13
13	20/3	Coarse	2,95	SEG-G4
14	Peciapian US 42 /1	Flat	3,48	
15	Peciapian US 42 /2	Coarse	2,53	SEG-G8
16	Peciapian US 42 /4	Massive	2,78	SEG-M21
17	Peciapian US 7 /1	Massive	3,00	SEG-M18
18	Peciapian US 7 /10	Flat	3,38	
19	Peciapian US 7 /11	Massive	3,66	SEG-M12
20	Peciapian US 7 /12	Massive	3,25	SEG-M16
21	Peciapian US 7 /13	Massive	2,68	SEG-M10
22	Peciapian US 7 /14	Flat-Thick	3,21	SEG-PS7
23	Peciapian US 7 /2	Massive	3,08	SEG-M20
24	Peciapian US 7 /3	Flat	3,67	
25	Peciapian US 7 /4	Flat	3,87	
26	Peciapian US 7 /5	Flat	3,37	
27	Peciapian US 7 /6	Flat	3,39	
28	Peciapian US 7 /7	Flat	3,56	
29	Peciapian US 7 /8	Flat	3,41	
30	Peciapian US 7 /9	Flat	3,54	

VI – Technological Process

6.1 Physical proprieties of the slags

Several physical proprieties of the slags, such as their density, their melting point and their viscosity are helpful parameters for reconstructing the smelting process operations. In particular, all these parameters affect the flow behaviour of the slags that provide important information about the process such as: 1) the efficiency of the slag-metal or slag-matte separations, 2) the ability to tap the slags from the furnace and 3) the kinetic of the metal smelting.

The relative density and the melting point have been already mentioned in the previous chapters. The relative densities were measured on the total number of slags provided by the archaeologists using a hydrostatic weighting apparatus.
Additionally, the density could be predicted through models developed in petrology using the bulk chemical compositions of the rocks or (Lange and Carmichael 1987, Johnson and Carmichael 1987, Dingwell and Brearley, 1988, Dingwell et al.1988, Taniguchi, 1989) or, in this case, of the slags.
The first density model was developed by Bottinga and Weill in 1970. The authors found that the molar volume of a silicate melt at a particular pressure and temperature can be approximated by simply adding the partial molar volumes of the constituent liquid oxide components. Refinements of this model have been made using new experimental data and they provided a good accuracy for almost any silicate melts (Lange and Carmichael, 1987). However, it is necessary to bear in mind that, when a model based on rock data sets is used on slags, its application is an approximation.

The slag melting point could be defined as the estimate of the lower limit of the furnace temperature achieved during the formation of the slags.
Regarding the Luserna, Transacqua and Segonzano slags, the melting temperatures were estimated in the chapters III, IV and V through the chemical analyses on the high-temperature zoning of the olivine.

The viscosity of the slags is a new mentioned parameter defined as a measurement of the fluid slag resistance to flow. The viscosity is related to the amount of the mineral phases that compound the slags. In fact, the abundance of minerals such as SiO_2 and Al_2O_3 (viscosity-increasing oxides) increases the slag viscosity (Themelis, 1995). On the contrary, high quantity of FeO, CaO, MgO, MnO (viscosity- reducing oxides) increases the fluidity of the slags (Seki and Oeters, 1984).
As suggested by Bachmann (1982), the viscosity could be calculated as the ratio of the basic or viscosity-reducing oxides sum against the acid or viscosity-increasing oxides sum. This ratio provides an index (K) of viscosity (inversely proportional to the viscosity) that could be used in order to obtain information about the kinetics of the process.

6.1.1 Density

The measured density of the coarse, massive and flat slags of Luserna, Transacqua and Segonzano sites were plotted using the box and whiskers plots and the scatter plots.
The coarse slags of the three sites have the lowest density, while the flat and the massive slags have the highest density values.
Concerning the Luserna and Transacqua sites, the massive slags show the highest density while the massive slags of Segonzano have lower density values.
As discussed in detail in the chapter V, the density behaviour of the massive slags of Segonzano is due to the presence of two different subgroups, one characterised by a higher amount of quartz and the other with a mineralogical composition similar to the massive slags of the Luserna and Transacqua sites.

Tab 6.1: Summary statistics for the density values measured on the slag samples (C: coarse, F: flat, M: massive) of Luserna, Transacqua and Segonzano.

	Type	Count	Average	Median	SD	Min.	Max.	Range	LQ	UQ	IQR
C	LUSERNA	10	2,62	2,64	0,19	2,34	2,89	0,55	2,44	2,74	0,30
	TRANSACQUA	29	2,68	2,66	0,25	2,26	3,42	1,16	2,50	2,77	0,27
	SEGONZANO	3	2,68	2,57	0,23	2,53	2,95	0,42	2,53	2,95	0,42
		Mean	**2,66**	2,62	0,22	2,38	3,09	0,71	2,49	2,82	0,33
F	LUSERNA	61	3,56	3,56	0,09	3,37	3,78	0,41	3,51	3,61	0,10
	TRANSACQUA	48	3,63	3,64	0,18	3,20	3,98	0,78	3,52	3,75	0,22
	SEGONZANO	14	3,50	3,44	0,15	3,33	3,87	0,54	3,39	3,56	0,17
		Mean	**3,56**	3,55	0,14	3,30	3,88	0,58	3,47	3,64	0,16
M	LUSERNA	19	3,68	3,73	0,17	3,32	3,98	0,66	3,60	3,77	0,17
	TRANSACQUA	30	3,72	3,74	0,18	3,28	4,11	0,83	3,64	3,85	0,21
	SEGONZANO	12	3,13	3,14	0,29	2,68	3,66	0,98	2,95	3,24	0,29
		Mean	**3,70**	3,74	0,18	3,30	4,04	0,74	3,62	3,81	0,19

Fig. 6.1: The box and whiskers plots of the density slag typologies of the Luserna, Transacqua and Segonzano sites.

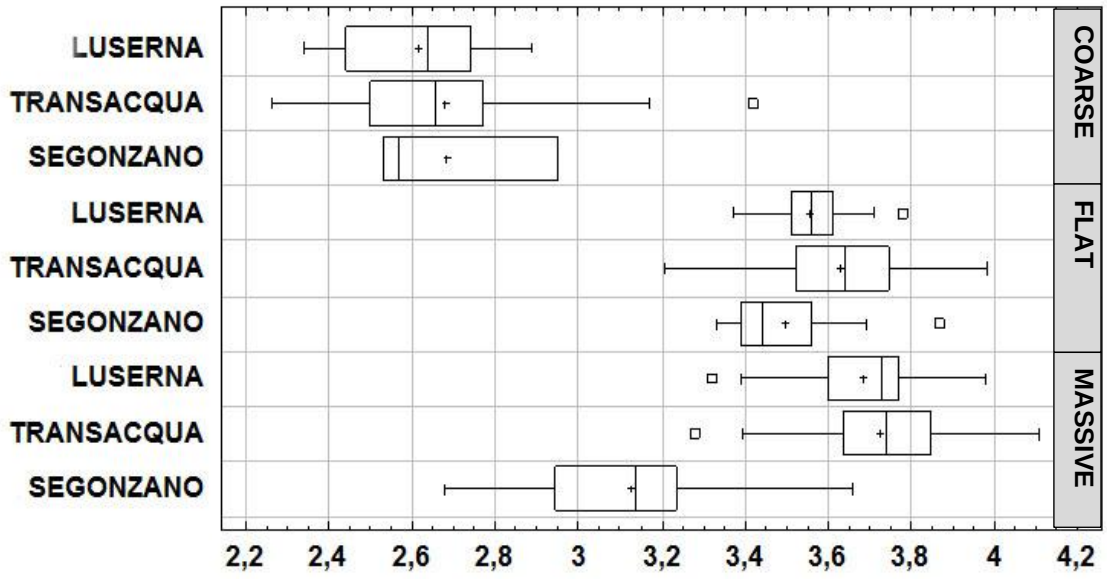

Fig. 6.2: Scatter plots of the coarse, massive and flat slags of Luserna, Transacqua and Segonzano sites.

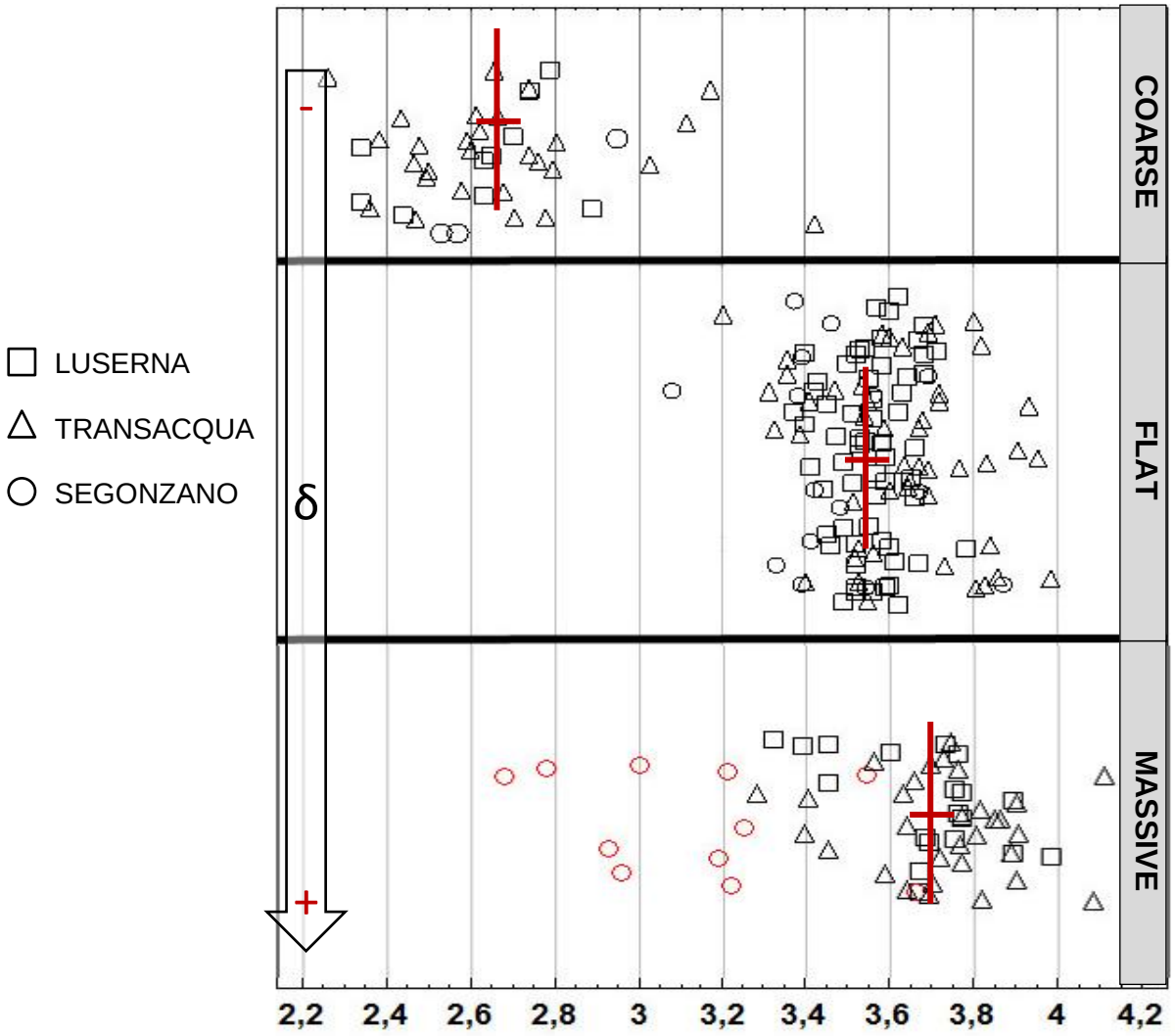

As is well known, the relative density could be affected by the porosity of the material. For this reason, the densities were also calculated using a petrological model based on the bulk chemical composition of the slags at their liquid state by means of the model developed by Lange and Carmichael (1987), which is more accurate in describing the volume and thermal expansion of natural silicate liquids if compared to the first density model of Bottinga and Weill (1970).

As for the liquid state, it is important to observe that the silicate melts are 10-20% less dense than the compositionally equivalent crystalline solids (Best, 2003).

The comparison between the modelled density values and the relative density measured confirmed the slag division in 3 groups (coarse slags with the lowest densities, flat slags with the intermediate-high density values and the Luserna and Transacqua massive slags with the highest densities). It is also indicated a substantial underestimate of the coarse slag densities. As it would be expected, the densities of the massive and the flat slags calculated using the high-temperature model are lower than the ones measured of the solid samples ($\delta \approx 4{,}4$ g/cm^3= density of solid fayalite at T°C=25 as reported by Deer, Howie and Zussmann, 1992; $\delta \approx 3{,}7$ g/cm^3= density of liquid fayalite at 1500°C, Thomas et al. 2012). On the contrary, the modelled densities

of the coarse slags of the three sites and the massive slags of Segonzano are higher than the ones measured by the hydrostatic weighting apparatus.
Thinking about the density as the mass divided by volume, it is evident that the high porosity of the coarse slags of the three sites and of the massive slags of Segonzano increases the total volume of the slags and decreases their measured density.

Tab. 6.2: Comparison between densities. δ: density measured using the hydrostatic weighting apparatus, (δ-10%): density measured (δ) minus 10% of its values; δ modelled: densities calculated using the Petrolog 3 software based on the average of the chemical compositions of each type of slags in the three smelting sites.

SITE	TYPE	δ	δ -10%		δ modelled
Luserna	COARSE	2,62	2,36	≠	2,81
Transacqua		2,68	2,41	≠	2,80
Segonzano		2,68	2,41	≠	2,75
Luserna	FLAT	3,56	3,20	≈	3,17
Transacqua		3,63	3,27	≈	3,35
Segonzano		3,50	3,15	≈	3,10
Luserna	MASSIVE	3,68	3,31	≈	3,32
Transacqua		3,72	3,50	≈	3,52
Segonzano		3,13	2,82	≠	3,18

6.1.2 Melting Temperature

As stated by Kresten (1986) and Freestone (1988), one of the most suitable methods for the estimation of melting temperatures is the calculation of olivine-liquid equilibrium temperatures based upon the partitioning of Mg or Fe between co-existing phases.
In the previous chapters, the working temperatures reached during the smelting were estimated on the basis of the chemical analyses on the olivine zooning, as summarised in Table 6.3.

Tab. 6.3: Temperature of the Fo-zoned core of the olivine observed in the slag types of Luserna, Transacqua and Segonzano.

	LUSERNA	TRANSACQUA	SEGONZANO
COARSE	1240	-	1380
MASSIVE	1260	1280	-
FLAT	-	1280	1240

It can be therefore affirmed that the temperatures achieved during the smelting – that are the minimum operating temperatures achieved in the furnace during the formation of the slags - are approximately 1250°C for Luserna, 1280°C for Transacqua and from 1240°C to 1380°C in the site of Segonzano.

6.1.3 Viscosity

The separation of metal from slag is essentially controlled by the viscosity and the density of the slag. This two parameters are in turn influenced by the temperature and the chemical composition of the slags (Fig 6.3 A and B).

Fig. 6.3: A) The viscosity of a slag as a function of its chemical compositions in terms of the viscosity-increasing oxides (SiO_2, Al_2O_3) and the viscosity-reducing oxides (FeO, MnO, CaO, MgO, Alk_2O), modified after Bachmann (1980).
B) The viscosity as a function of the temperature: the viscosity of the rich-silica slags decreases less by increasing the temperature than the fayalite-rich slags, modified after Bachmann (1980).

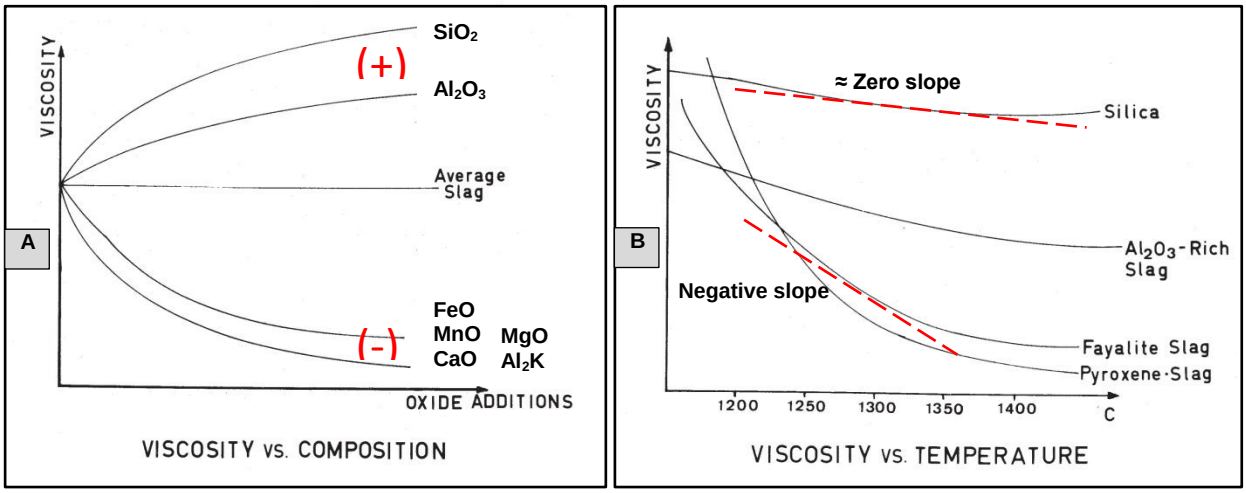

As proposed by Bachamnn (1982), the viscosity of a liquid slag could be expressed as a index (K) calculated through the ratio of the basic oxides sum (CaO, MgO, FeO, MnO, Alk_2O) against the acid oxides sum (SiO_2, Al_2O_3).
This K index was calculated using the viscosity-reducing oxides and the viscosity-increasing oxides obtained by the bulk chemical analyses and converting the sum of the oxides of interest to one hundred weight per cent. Consistently with the range of values gave by Bachmann, the K indices of the Luserna, Segonzano and Transacqua slags vary between 0,48 to 2,18.

Tab. 6.4: Viscosity indices (K) calculated as the mean values (SD: standard deviation) using the bulk chemical composition of the coarse (C), massive (M) and flat (F) slags of Luserna (LU), Transacqua (TR) and Segonzano (SEG). The massive slags of Segonzano have two k-index values, the first (1,24) is referred to the M1 sub-group and the second (1,39) is referred to the M2 sub-group.

		K			
		LU	TR	SEG	
C	MEAN	0,57	0,56	0,48	
	SD	0,1	0,1	0,1	
M	MEAN	1,71	2,18	1,24	1,39
	SD	0,2	0,2	0,2	0,2
F	MEAN	1,39	1,75	1,27	
	SD	0,2	0,2	0,2	

The coarse slags, having the lowest viscosity index, are the most viscous slags. The massive and the flat slags with the highest viscosity indices are the most fluid slags, in

particular the massive of Luserna and Transacqua display the highest viscosity indices. Using the experimental measurements on modern copper slags, Bachmann derived a mathematical relation between temperature, K-index and viscosity (η), as the following:

$$Log\ \eta_{(poise)} = 26{,}46 - 23{,}67\ (T_{(°C)} \times 0{,}001) - 3{,}12\ K + 3{,}84\ (T_{(°C)} \times 0{,}001)^3 + 0{,}59\ K^2 \quad \textbf{(1)}$$

Tab. 6.5: Viscosity expressed in logarithm with base 10 at different temperatures of the coarse (C), massive (M) and flat (F) slags of Luserna (LU), Transacqua (TR) and Segonzano (SEG). The massive slags of Segonzano have two Log η, the first (dark green) is referred to the M1 sub-group and the second (bright-green) is referred to the M2 sub-group.

	Log η (1200°C)				Log η (1300°C)				Log η (1400°C)			
	LU	**TR**	**SEG**		**LU**	**TR**	**SEG**		**LU**	**TR**	**SEG**	
C	3,1	3,1	3,3		2,5	2,6	2,8		2,3	2,3	2,5	
M	1,1	0,7	1,7	1,5	0,5	0,1	1,2	0,9	0,3	0,1	0,9	0,7
F	1,5	1	1,7		0,9	0,5	1,1		0,7	0,2	0,8	

Fig. 6.4: Diagram of viscosity (poise; 10 poise=1 Pascal x second) versus temperature in relation to viscosity coefficients (K). The slag viscosities (poise) of Luserna, Transacqua and Segonzano calculated as the expression (1) were plotted into the diagram. The low-viscous massive slag of Transacqua at 1400°C (log η=0,1) is out of the graph. Reference value in poise: air 10^{-6}, water 10^{-4}, honey 10^{-2}.

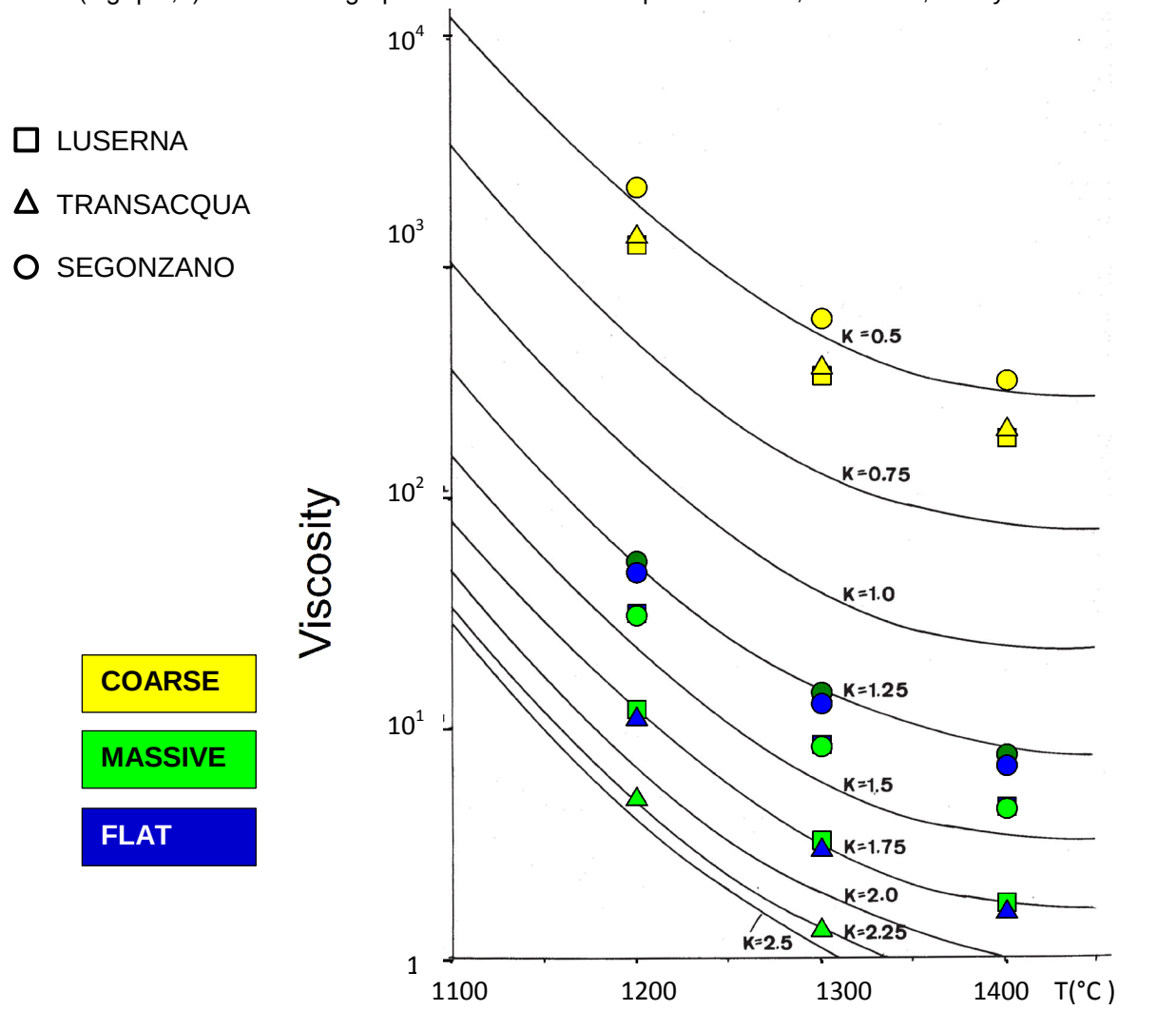

Approximately, two main factors govern the viscosity of the melts: their composition (degree of polymerization) and their temperature (Best, 2004). The silica-rich melts are more polymerised and therefore they are more viscous than the silica-poor melts.
The viscosity of a melt is reduced by increasing the temperature and it consequently loses its structural order and symmetry facilitating therefore ionic mobility.
The Fig. 6.4 illustrates the strong dependence of the melt slags viscosity on the temperature and on the composition. In the temperature range of 1100°C to 1400°C, the viscosity of the melt slags with K-values between 0,75 and 1,75 decreases by one order of magnitude. This is the case of the massive and the flat slags. As the coarse slags have the highest amount of SiO_2 and Al_2O_3 oxides, they have the highest viscosities.

6.2 Mineralogy, Chemistry and Petrography of the slags

In order to verify the presence of different working steps within the whole smelting process, the study of the mineralogical phases and the chemical compositions as well as the petrographic observation of the slags were carried out and fully reported in the previous chapters divided by sites.
In the next paragraphs, the comparison between the results of the Luserna, Transacqua and Segonzano slags is presented.

6.2.1 Mineralogical Phases

The semi-quantitative mineralogical phase evaluations of the three types of slags are almost the same for the three smelting sites. The coarse type has the highest content of quartz and the lowest of olivine. The massive slags of the Luserna and Transacqua sites show a higher amount of olivine and magnetite and the quartz is almost absent. The massive slags of Segonzano are divided into two sub-groups, one rich in quartz and the other almost composed by olivine.
The flat slags of the Luserna, Transacqua and Segonzano sites are composed almost entirely by olivine.

Fig. 6.5: Pie charts of the mineralogical phases of the different types of slags of the three smelting sites.

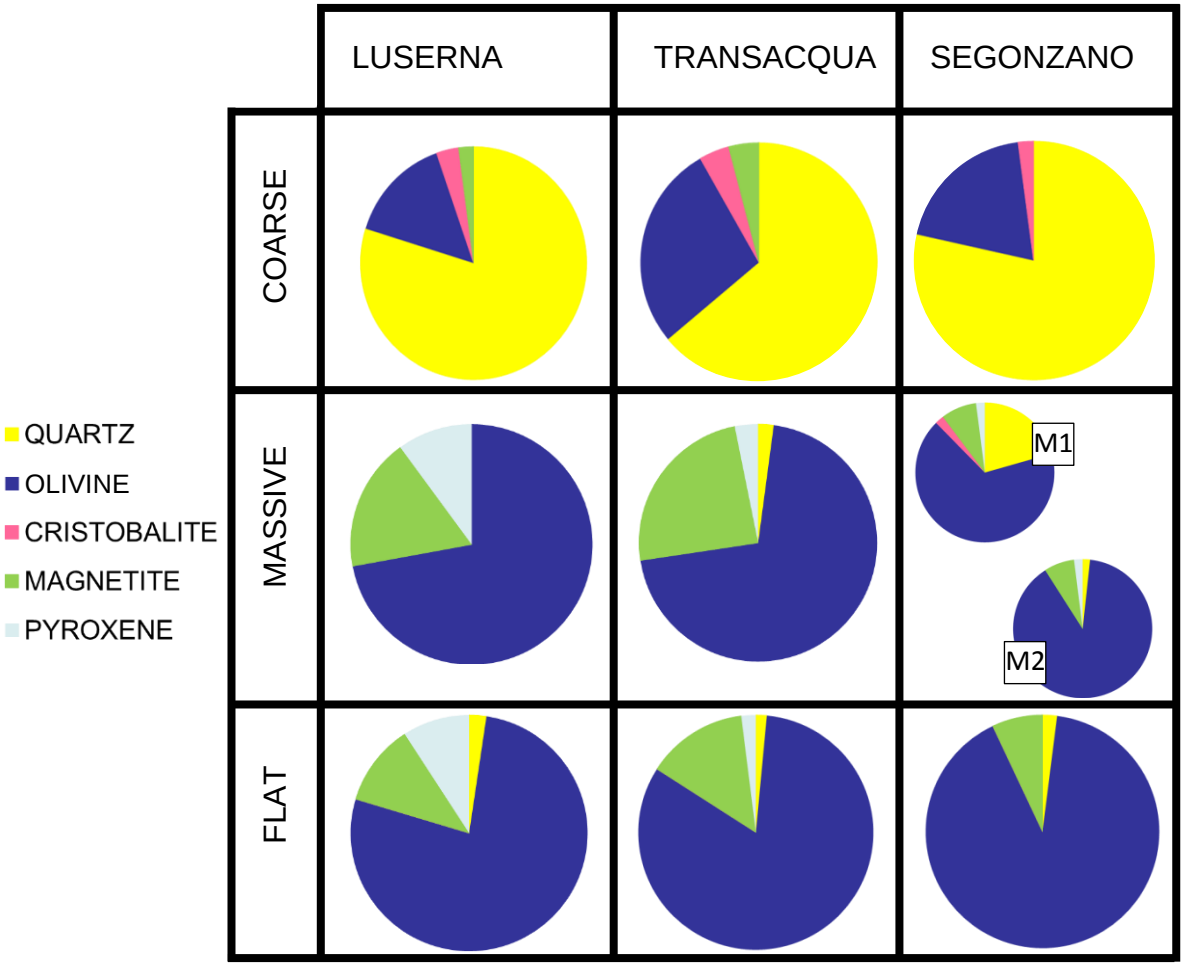

Tab. 6.6: Mean content of the main crystalline phases that characterise the three type of slags. For the massive type the count does not take into account the M1 type of Segonzano.

Slag Types	Quartz	Olivine	Magnetite
COARSE	65	30	3
MASSIVE	5	68	27
FLAT	1,5	83,5	15

6.2.2 Sulphides: Chemical Composition and Petrography

The sulphides observed in the three types of slags of the three sites show different transformation degrees.
As it can be observed in the Fig. 6.6 and 6.8, the coarse slags are characterised by large grain sulphides with an intermediate bornite-chalcopyrite chemical composition.
Two main types of sulphides were observed into the massive slags: 1) sulphides with an intermediate bornite-chalcopyrite composition similar to the ones encountered in the coarse slags but smaller and 2) sulphide with a covellite-chalcocite-like composition. Additionally, several copper prills with different diameters ranging from 10 µm to 250 were observed (Fig. 6.7).
The flat slags are characterised by the smallest sulphides with a chalcopyrite-bornite dominant composition. In the flat slags of Luserna and Segonzano several small Cu-prills were observed.

Fig. 6.6: Examples of sulphides (Cp=chalcopyrite, Po=pyrrhotite, Cv=covellite, Bo=bornite) present into the three slags types at different transformation degrees. (C=coarse slags, M=massive slags, F=flat slags).

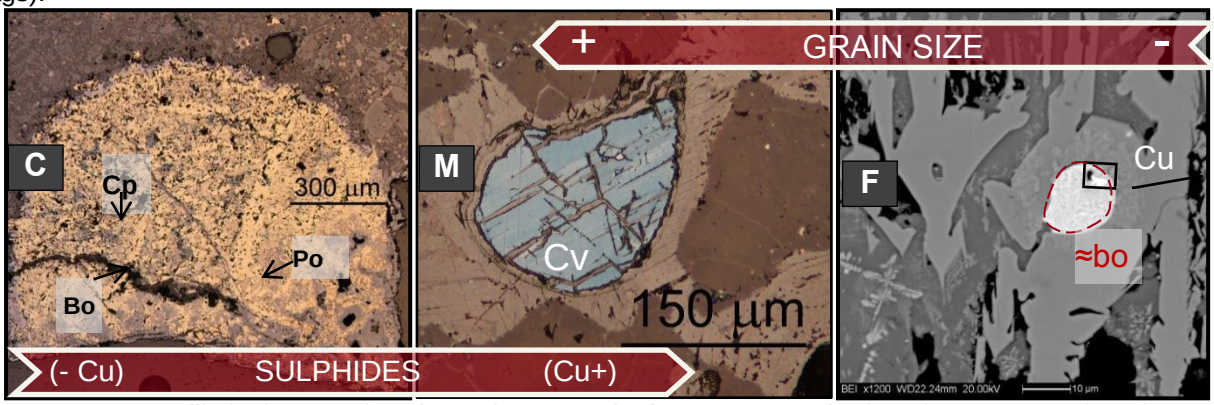

Fig. 6.7: Copper prills in the massive slags of Luserna (LU), Transacqua (TR) and Segonzano (SEG).

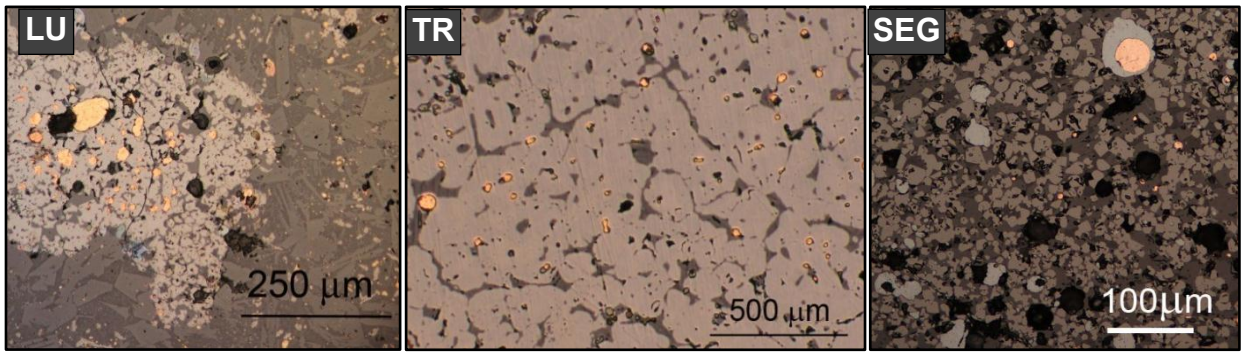

Fig. 6.8: Comparison between the chemical composition of the sulphides observed into the three types of slags (coarse, massive and flat) of the Luserna, Transacqua and Segonzano sites.

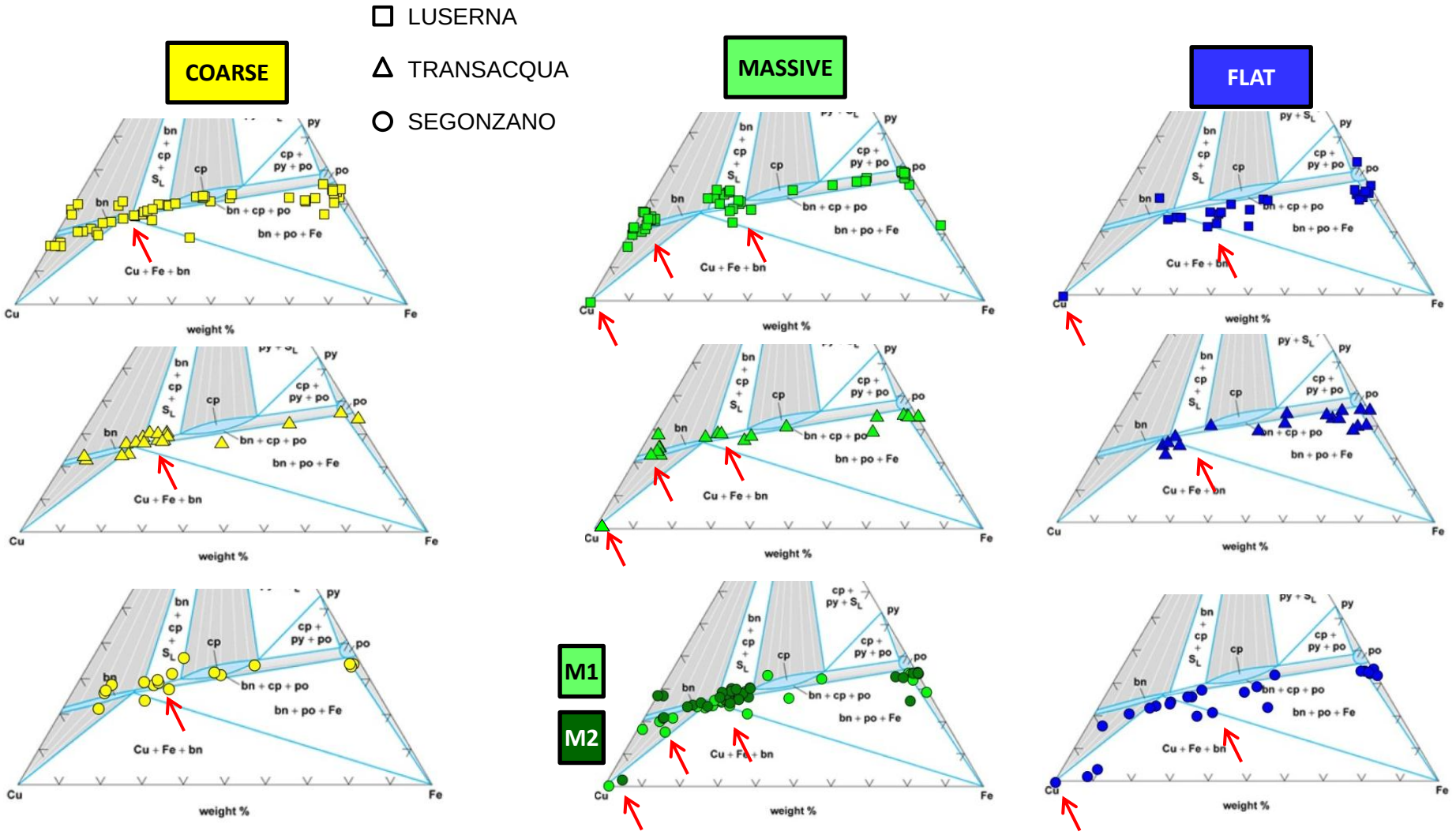

6.2.3 Bulk Chemical Composition

The bulk chemical compositions of the slags were compared using the anorthite- SiO_2-FeO (+MgO) diagram (Fig. 6.9).
The ternary diagram supports the division of the slags in three groups: 1) coarse slags located in the field of stability of SiO_2, 2) massive slags located in the field of stability of the fayalite (except for two Transacqua samples, and part of the massive slags of Segonzano) and 3) flat slags in the field of stability of the fayalite (except for two massive slags of Segonzano and one sample of Transacqua).
The high dispersion of the massive slags is essentially due to the presence of the two sub-groups.

Fig: 6.9: Bulk chemical compositins of the Luserna, Transacqua and Segonzano slags.

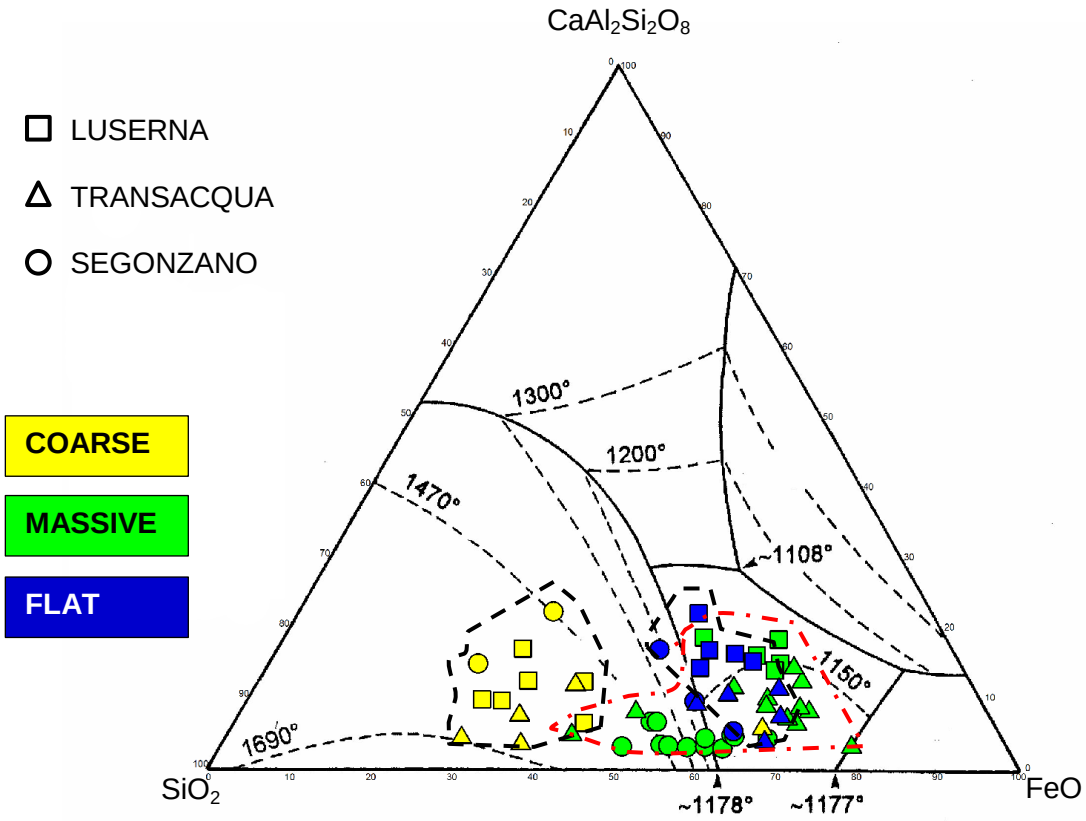

We carried out a comparison between the Luserna, Transacqua and Segonzano slags and the Acqua Fredda slags studied by Metten (2003). In its work, Metten divided the slags in three groups: 1) the *Schlackenkuchen* slags, which correspond to the coarse slags macroscopically and mineralogically, 2) the *Plattenschlacken* slags, which the author divided into two sub-groups called *Homogene Plattenschlacken* and *Heterogene Plattenschlacken*, 3) the *Schlackensand* slags, namely the sand of slags also found in the Segonzano smelting sites (this last type of slags was not analysed in this work because no samples were provided to us by the archaeologists).
Consistently with the bulk chemical analyses of the Luserna, Transacqua and Segonzano coarse slags, the Acqua Fredda Schlackenkuchen slags are mostly in the field of stability of quartz showing a considerably high amount of SiO_2. The same

composition of the Schlackenkuchen slags was observed in the Schlackensand slags, confirming our hypothesis for the production of this type of slags, which was suggested in the Chapter 5 – Segonzano and which says that the sand of slags was produced during a beneficiation of the coarse slags characterised by a high amount of sulphidic charge entrapped into the slags.
The Homogeneous Plattenschlacken type is mainly in the liquidus field of fayalite as the flat slags of Luserna, Transacqua and Segonzano, while the Heterogeneous Plattenschlacken type of slags is partially in the field of stability of quartz and of fayalite.
As Matten well described, this latter sub-type of flat slags is characterised by numerous inclusions of unreacted quartz, similar to the ones observed in the massive M1 of Segonzano.
The massive type not recognised in the work of Matten was likely included into the two sub-groups of the Plattenschlacken slags.

Fig. 6.10: Chemical bulk analyses of the slags of Luserna, Transacqua and Segonzano and the Schlackenkuchen, Plattenschlacken and Schlackensand slags of Acqua Fredda as studied by Metten. The plot was modified after Mettend (2003).

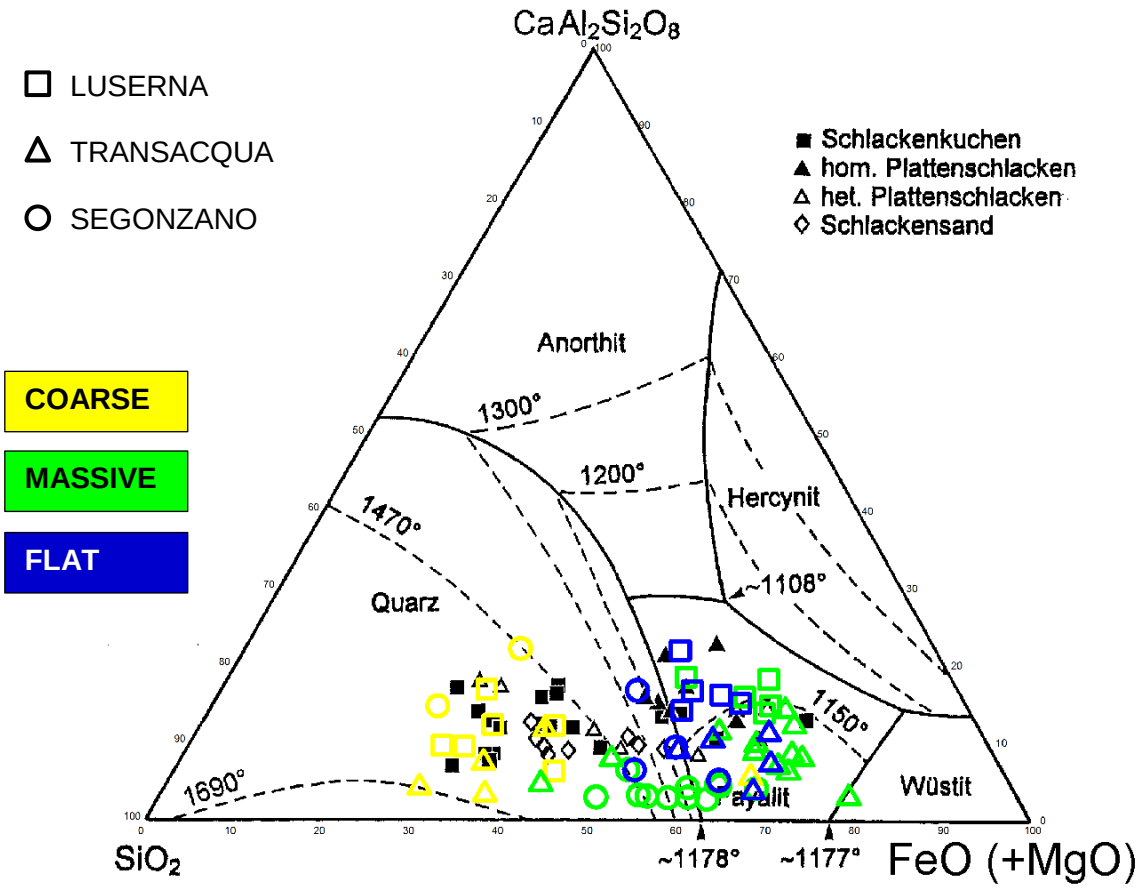

6.3 Interpretation of the Process

6.3.1 Separation rates

As Craddock said (1995), if it was assumed that the smelting took place in a simple shaft furnace, during the high-temperature process four vertical zones of the furnace can be considered: 1) the upper part where ore and flux were charged and heated, 2) the combustion zone in front of the tuyere (when present), 3) the slags "bath" layer and 4) the liquid ingot layer at the bottom of the furnace.
In order to simplify, we can affirm that in the combustion zone two main reactions took place: the transformation of the heated and friable Cu-Fe-sulphide ore through several reactions to metal copper and the formation of slags by reaction of the silica and the metal oxides. Both these two processes are endothermic, i.e. energy-consuming.
Below this zone, the metallic copper or matte aggregated into droplets that sank through the slag forming a liquid ingot.
To be more precise, the slags with a low density and viscosity compared to the matte and the copper underwent an upward force, called positive buoyancy. On the contrary, the copper/matte that are denser than their slags surroundings experienced a downward force called negative buoyancy (Best, 2003).
The movements of copper and matte particles – i.e. the separation rates between copper/matte and slags - are driven by a buoyant force described by the Stoke's Law:

$$V = g\, d^2\, (\Delta \rho)/18\eta \qquad \textbf{(2)}$$

This equation gives the velocity of a sphere (copper or matte prills with diameter = d and density $\rho_{matte/Cu}$) that moves through a viscous fluid (slags with density: ρ_{Slag} and viscosity η) at a specific acceleration of gravity (g). $\Delta \rho$ ($\rho_{matte/Cu}$- ρ_{Slag}) is the contrast in density between the particle (Cu or matte) and the surrounding media (slag).
Considering a mean temperature of 1250°C, the separation rates of the copper/matte and the three types of slags Luserna, Transacqua and Segonzano were calculated and listed in Tab. 6.7.
The types of sulphides involved in the separation processes were chosen on the basis of the chemical sulphide analyses showed in Fig. 6.8: for the coarse slags a mean matte composition of 50% chalcopyrite and 50% bornite was calculated.
For the massive slags a matte composed by 33,3% of bornite, 33,3% of covellite and 33,3% of chalcocite was chosen. Since numerous Cu-prills were observed in the massive slags, the separation rates between the massive type and metallic copper were also calculated.
The flat slags with the lowest amount of sulphides and copper prills were related to a refining process during which mostly raw-copper was produced. Therefore, the separation rates of the flat slags were calculated only considering the metallic copper.

Tab. 6.7: Separation rates in cm/hr. of a droplet of matte (diameter expressed in μm, $10<d_{\mu m}<1000$) composed by 50% of chalcopyrite (Cp) and 50% of bornite (Bo) in the case of the coarse slags, 33,3% of bornite (Bo), 33,3% of covellite (Cv) and 33,3% of chalcocite for the massive slags. The separation rates were calculated also for the metallic copper (diameter expressed in μm, $50<d_{\mu m}<1000$) and the massive and the flat slags of the three sites (LU: Luserna, TR: Transacqua, SEG: Segonzano).

	COARSE - Matte: Cp_{50}-Bo_{50}			MASSIVE - Matte: Bo_{33}-Cv_{33}-Ch_{33}			
d (μm)	LU	TR	SEG	LU	TR	SEG-M1	SEG-M2
1000	2,88	2,67	1,69	319,144	711,29	73,75	122,55
500	0,72	0,67	0,42	79,79	177,82	18,44	30,64
250	0,18	0,16	0,11	19,95	44,46	4,61	7,66
50	0,007	0,007	0,004	0,78	1,78	0,16	0,31
10	0	0	0	0,03	0,071	0,0073	0,01

	MASSIVE -Metallic Cu				FLAT - Metallic Cu		
d (μm)	LU	TR	SEG-M1	SEG-M2	LU	TR	SEG
1000	746,28	1758,46	171,77	290,64	277,52	761,23	191,12
500	186,57	439,62	42,94	72,66	69,38	190,31	47,78
250	46,64	109,9	10,74	18,16	17,35	47,58	11,95
50	1,87	4,4	0,43	0,73	0,69	1,9	0,48
10	0,074	0,18	0,017	0,03	0,03	0,077	0,019

Fig. 6.11: Separation rates plotted in a diameter-prills vs. velocity diagram of the Luserna slags and the matte/copper prills. The numbers indicate the separation rates between: 1) Coarse slags - Matte composed by Cp_{50}-Bo_{50}, 2) Flat slags - Cu, 3) Massive slags – Matte composed by $Bo_{33,3}$-$Cv_{33,3}$-$Ch_{33,3}$, 4) Massive slags-Cu.

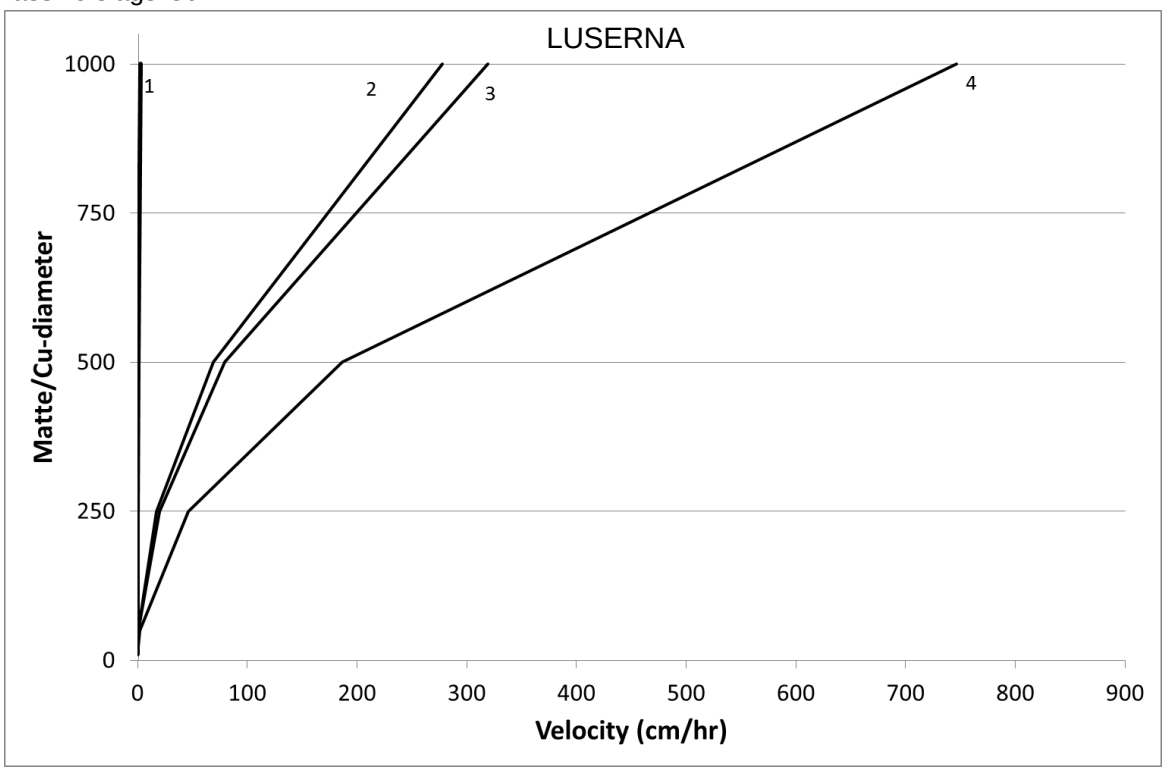

Fig. 6.12: Separation rates plotted in a diameter-prills vs. velocity diagram of the Transacqua slags and the matte/copper prills. The numbers indicate the separation rates between: 1) Coarse slags - Matte composed by Cp_{50}-Bo_{50}, 2) Massive slags – Matte composed by $Bo_{33,3}$-$Cv_{33,3}$-$Ch_{33,3}$, 3) Flat slags - Cu, 4) Massive slags-Cu.

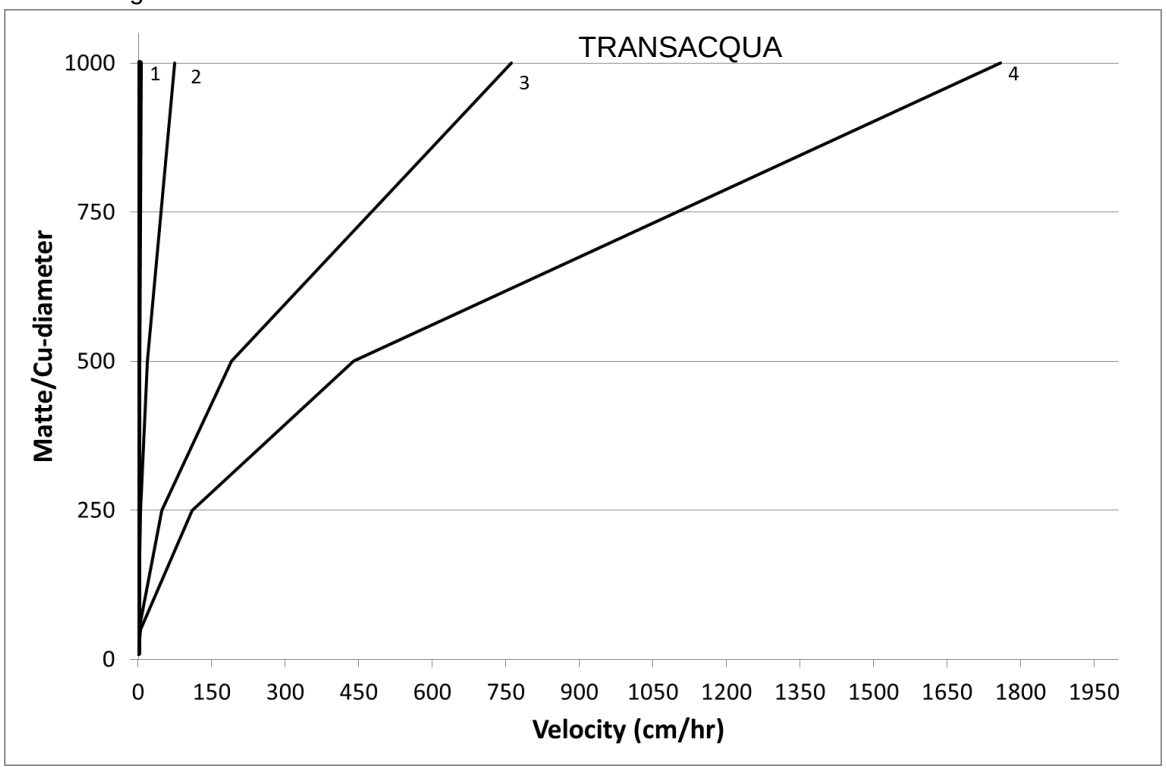

Fig. 6.13: Separation rates plotted in a diameter prills vs. velocity diagram of the Segonzano slags and the matte/copper prills. The numbers indicate the separation rates between: 1) Coarse slags - Matte composed by Cp_{50}-Bo_{50}. 2) M1 slags – Matte composed by $Bo_{33,3}$-$Cv_{33,3}$-$Ch_{33,3}$, 3) M2 slags – Matte composed by $Bo_{33,3}$-$Cv_{33,3}$-$Ch_{33,3}$, 4) M1 slags-Cu, 5)Flat slags - Cu, 6) Massive slags-Cu.

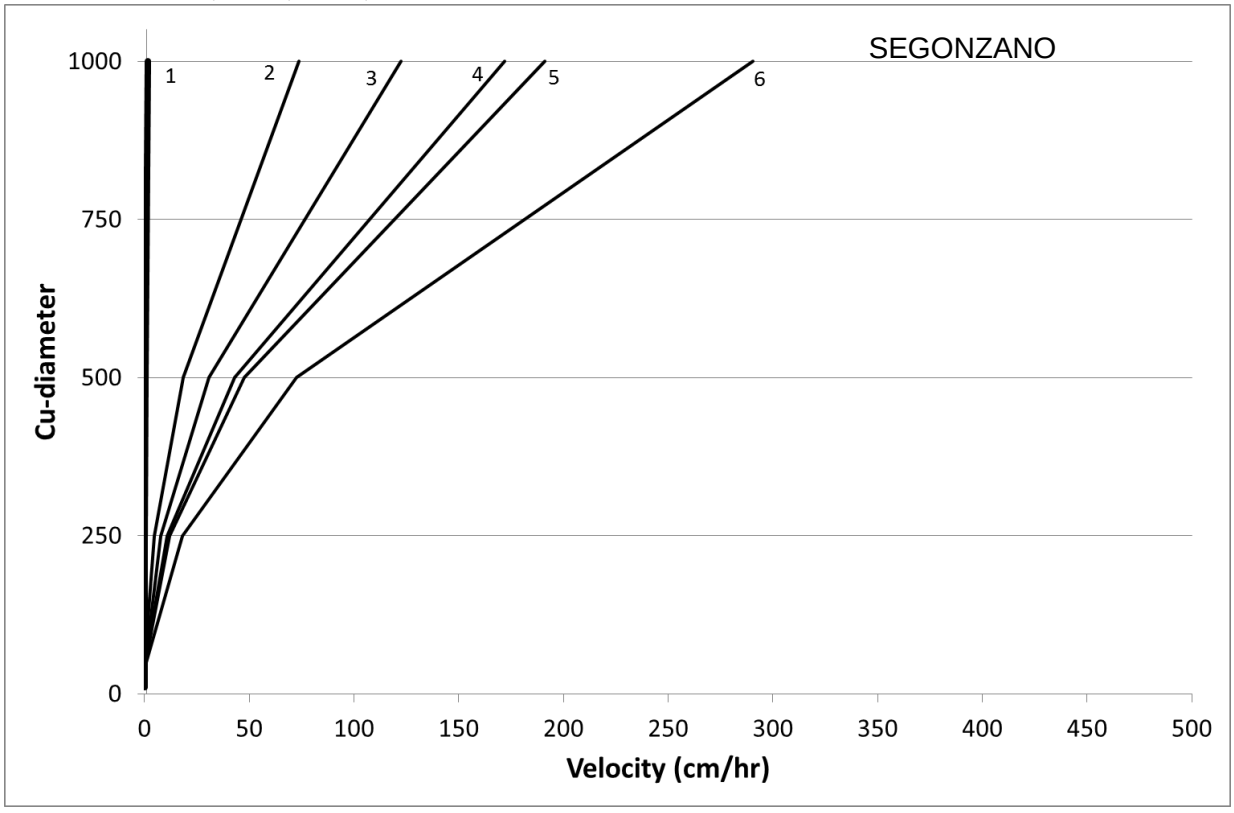

As shown in the plots above (Fig. 6.11-6.13), the slowest separation processes regard the matte and the coarse slags of the three sites. The coarse slags, in fact, have the highest viscosity that hinders both an appreciable separation of the matte and the fluidity of the slags.
The fastest separation processes are between the massive slags and the metallic copper. The low-viscous slags and the high-dense copper have a separation rates that reaches a maximum of ≈1758 cm/hr. (1mm Cu-diameter) in the massive slags of Transacqua and a minimum of ≈172 cm/hr. (1mm Cu-diameter) for the massive M1 of Segonzano. In general, the separation processes of Transacqua are the fastest while those of Segonzano are the slowest.
The second separation process in terms of slow-velocity is the massive-matte separation for the Transacqua and Segonzano slags while in Luserna it regards the separation between the flat slags and the copper prills.
The M1 and M2 types of Segonzano show a different separation velocities between matte and metallic copper with a contrast of Δ ≈118 cm/hr. for the massive-Cu process and Δ≈51 cm/hr. for the massive-matte separation process.
The following plot (Fig. 6.14) compares the fastest separation processes of the massive slags of the different sites and the metallic copper at the different diameters.

Fig. 6.14: Separation rates between massive slags and metallic copper.

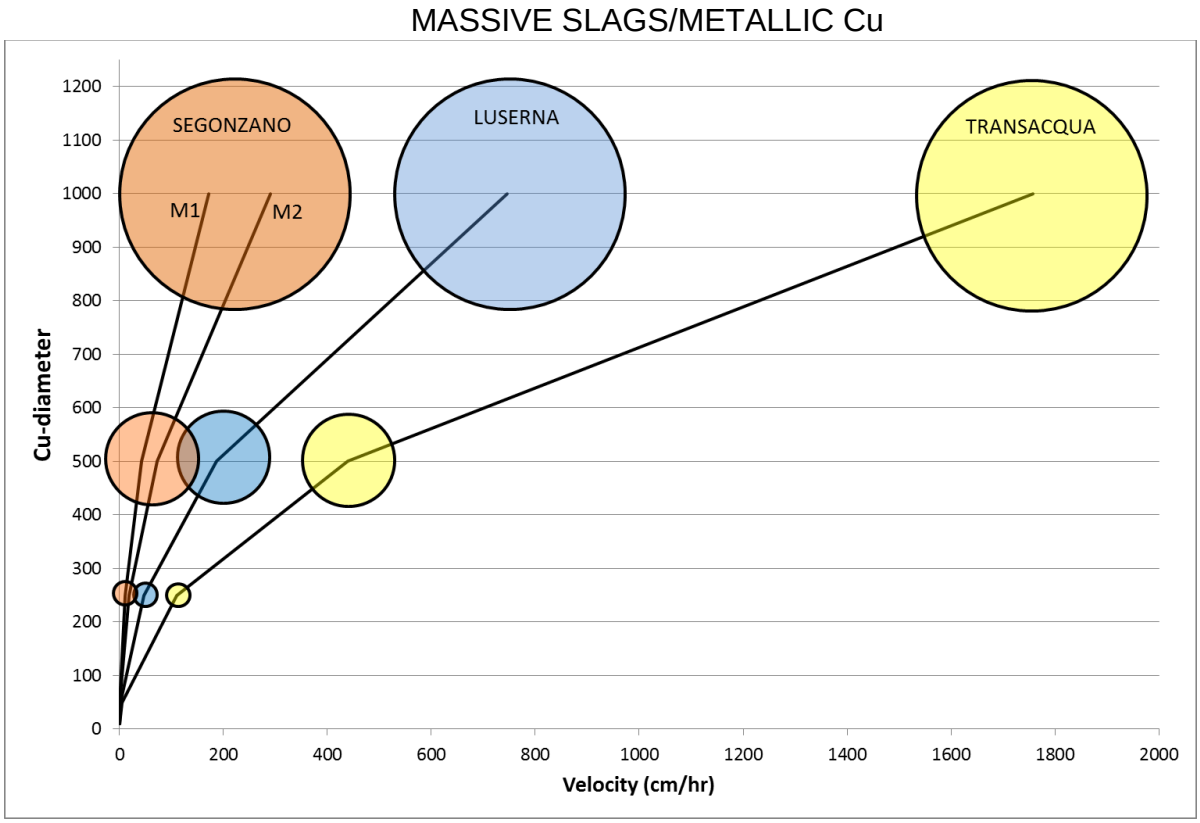

On the basis of the calculated velocity, the temperature (1250°C), the diameters of the metallic copper/matte prills observed in the slags and the thickness of the different types of slags, it is possible to tentatively estimate the duration of the smelting operations.

In the coarse slags (thickness≈ 15cm) the maximum matte diameter encountered is about 1mm, that means that the matte prills with a diameter>1mm were capable of separate through and from the slags indicating a duration of the high-temperature process of at least 4 hours for Luserna and Transacqua and 6 hours for Segonzano. Considering a smaller diameter of matte (500 μm), the hours of the high-temperature required to separate the prills rise to 15 for Luserna and Transacqua and 24 hours for Segonzano.

Fig. 6.15: Duration of the high-temperature operation for the coarse slags of the three sites at different matte diameters (fixed temperature: 1250°C).

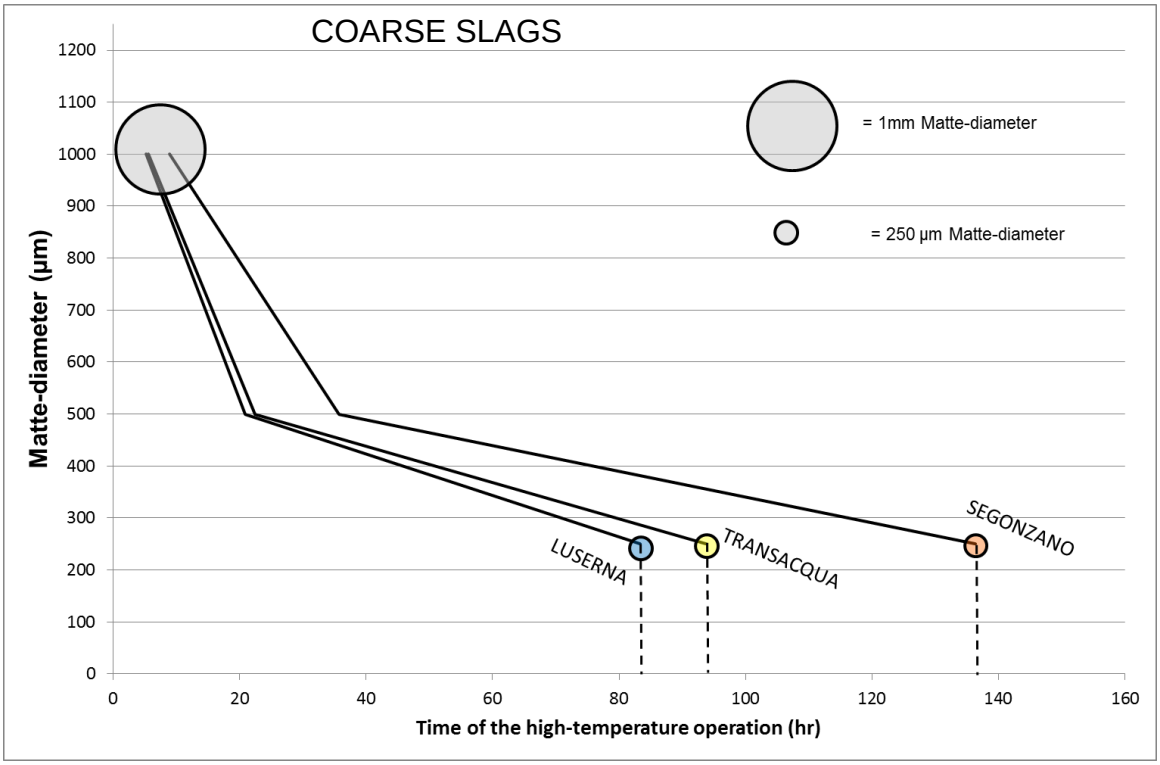

Considering the massive types (thickness≈ 7cm), the mean sulphidic-ore observed has a composition Bo-Cv-Ch-like and a diameter-size between 250μm and 50μm, that indicates high-temperature hours that range from 1 to 9 for Luserna and Transacqua. For Segonzano the time of the high-temperature operation reached 44 and 23 hours for the massive types M1 and the M2, respectively.

The separation process between the massive slags and the metallic copper, considering a mean copper prill diameter of 50μm, might have lasted 4hrs. for Luserna, 2 hrs. for Transacqua and between 16 and 10 for the M1 and M2 slags of Segonzano.

The flat slags (thickness≈1cm) of Luserna is characterised by the presence of the smallest copper prills with a maxim diameter of ≈10μm, while those observed in the Segonzano flat slags are larger (≈250μm). In the flat slags of Transacqua no copper prills were detected.

This is consistent with the separation rates occurred during the smelting (Fig. 6.16), if the Cu-prills present in the flat slags were smaller than 10μm of diameter, it means that the high-temperature process lasted more than 10 hours in Transacqua, more than 30 hours in Luserna and almost 50 hours in Segonzano.

This is the case of Transacqua, where the separation rates are so high to allow the almost total separation between slags and metallic copper with a time of high-temperature activity of approximately 10 hours.
In the Luserna flat slags, the small copper prills observed and the calculated separation rates suggest a time of heat-treatment of more than 20 hours.
In Segonzano, the copper prills are larger (150μm) than the ones in the flat slags of Luserna. This is due to the low separate rates that characterise the smelting product of this site.

Fig. 6.16: Duration of the high-temperature operation for the flat slags of the three sites at different copper diameters (fixed temperature: 1250°C).

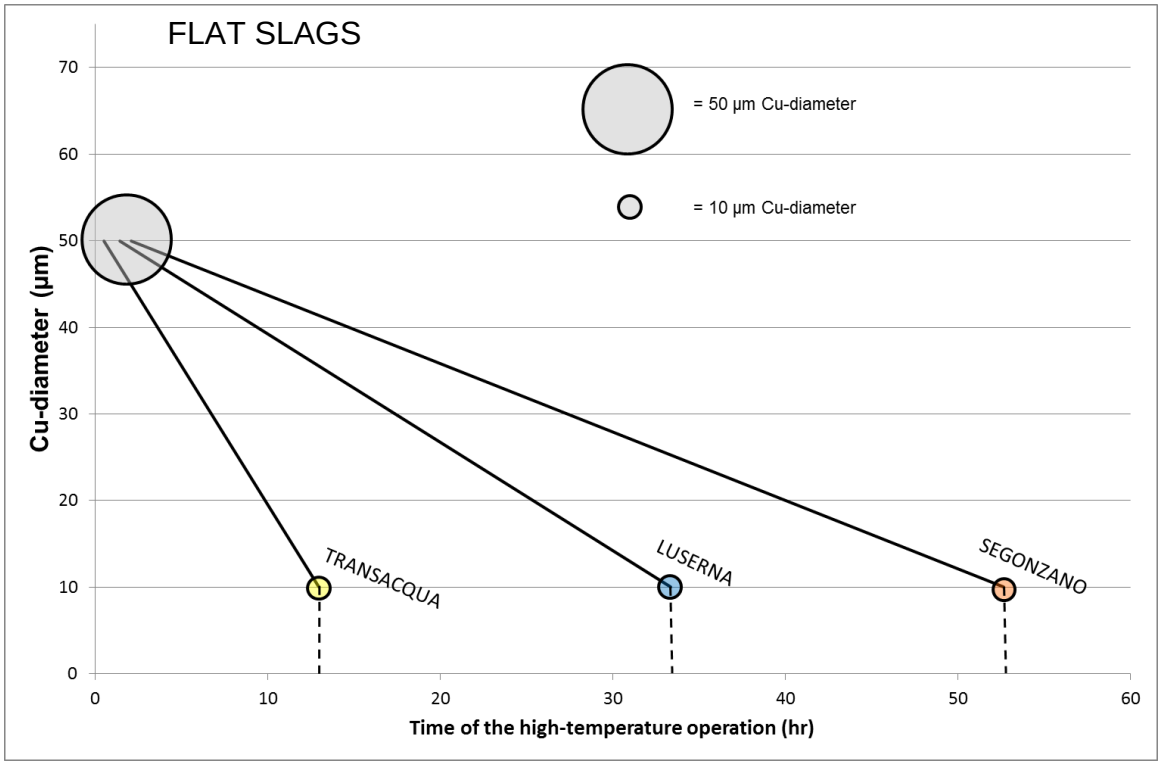

6.3.2 The Smelting Model

Until now, the different types of slags were considered as the products of different smelting operations. However, as pointed out by Craddock (1994), a certain caution is necessary before a multi-stage process is accepted.
On the basis of the literature, the early descriptions of the multi-stage process appeared in the extractive metallurgy texts of the sixteenth century, such as those of Agricola (Hoover and Hoover, 1912), Biringuccio (Smith and Gnudi, 1842) and Ercker (Sisco and Smith, 1951).
Bachmann (1982) gave a full description of the operations of treating the low-grade primary sulphidic ore, by dividing the process in many steps: 1) Beneficiation of the Cu-Fe sulphide ore, 2) Partially roasting (≈800°C) in order to remove the sulphur of the sulphidic ore as sulphur dioxide, 3) Slagging, namely the first smelting operation (T°C>1200°C), in which the roasted ore and the quartz flux were heated in order to remove the iron, 4) Matting as the second smelting operation in which the product of the

slagging stage (the unchanged ore with some copper sulphides) was converted to more enriched Cu-sulphides, 5) Refining of the matte produced to obtain the raw copper. After the first matting, the roasting and the slagging operations could be repeated in order to produce an increasingly Cu-rich matte.

All the evidence accumulated through the analyses of the Luserna, Transacqua and Segonzano slags from the macroscopic to the micrometric scale supports the multi-stages process hypothesis.

As pointed out by Bachmann (1980), several parameters control the smelting operation such as the composition of the charge, the type of furnace and the temperature. Additionally, the viscosity of the slags rules the separation between the matte/copper and the slags resulting in the grade of separation efficiency, in the kinetics of separation and in the slags output (retention liquid slag into the furnace or tapping).

Fig. 6.17: Interdependence of the process parameters, modified after Bachmann (1980).

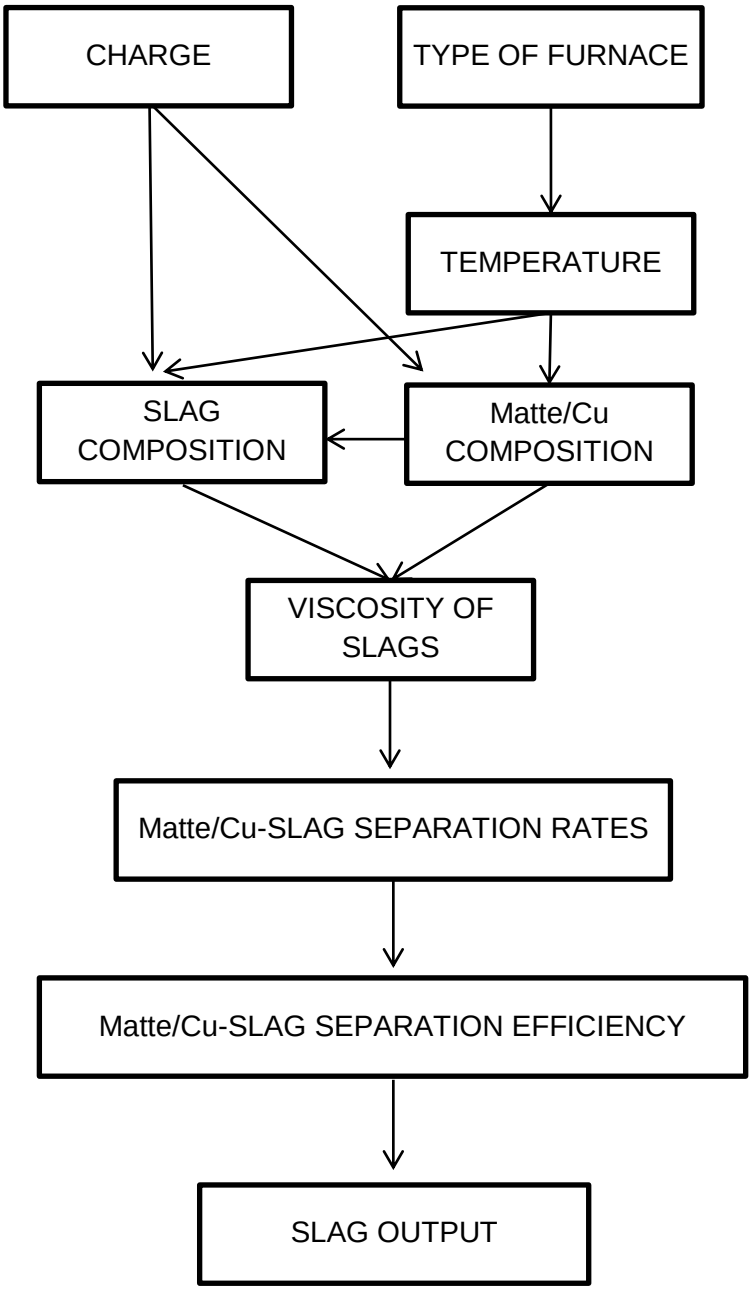

Considering how these parameters vary within the different types of slags, it is possible to outline the working-condition of each high-temperature operations.

Regarding the formation process of the coarse slags of the three sites, it is possible to assume that the sulphidic charge used was chalcopyrite that were heated above 1200°C with quartz in excess, resulting in the formation of a Cp-Bo matte and a quartz-dominant high viscous slags that must have been left cooling into the furnace, because their high-viscosity.

Fig. 6.18: The formation process parameters for the coarse slags.

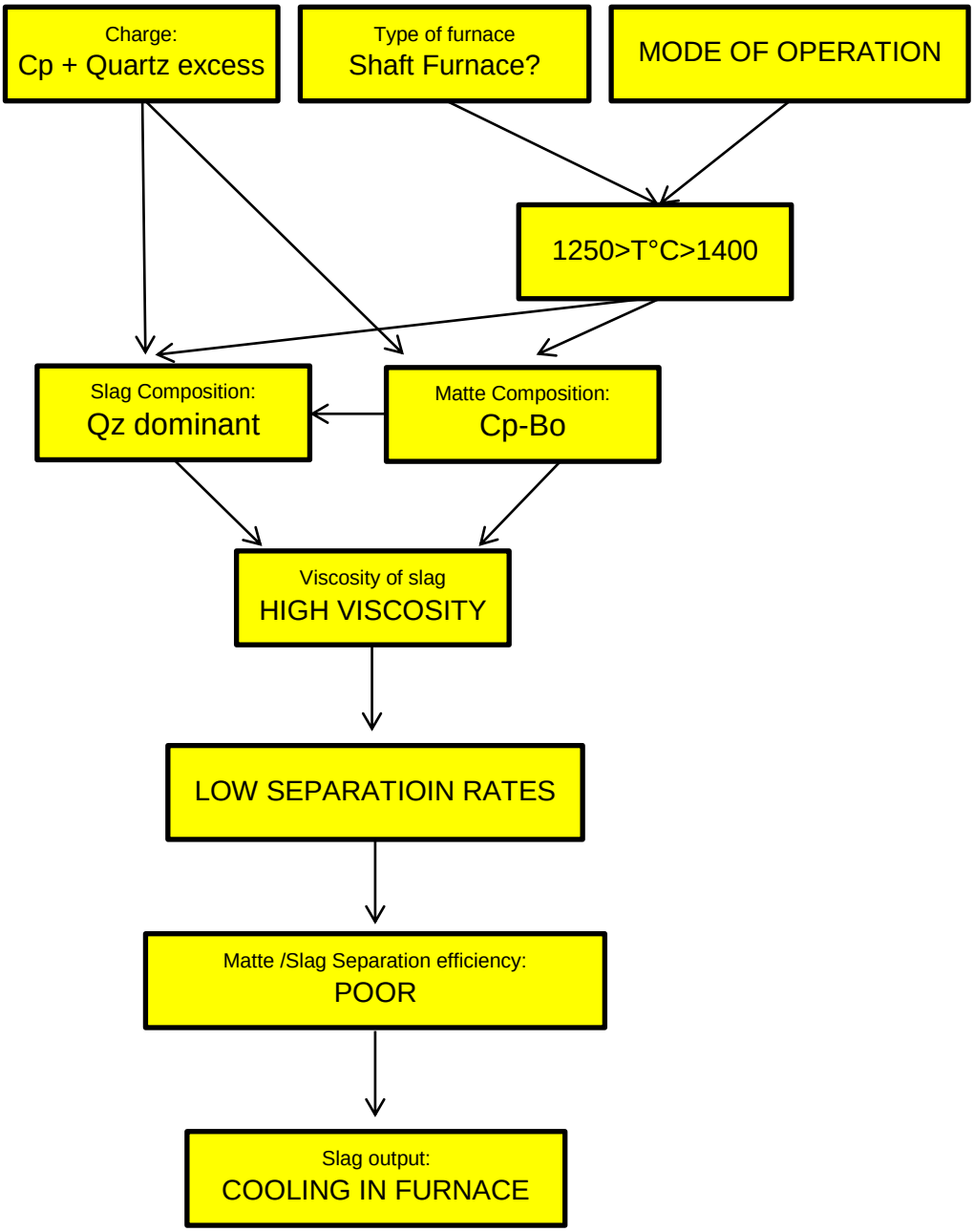

On the basis of these considerations, the only possibility for the formation of the coarse slags is a separate stage operation, which likely corresponds to the slagging process as defined by Bachmann (1982).

Considering the massive slags of Luserna and Transacqua, their bornite-covellite-chalcocite intermediate matte composition suggest an initial Cu-enriched sulphidic charge, similar to the one produced in the coarse slag formation process. The high fluidity of these slags had to result in high separation rates between slags and matte, especially in Transacqua where the smelters were masterfully able to control the fluidity of the slags. In this step, presumably the matting stage, the main product was a Bo-Cv-Ch matte and several copper droplets were produced.
Due to their high fluidity, the massive slags could be tapped rather than let cool in the furnace. However, the macroscopic slag features and the presence of low-cooling rate micro-textures (prismatic olivine) suggest a slow cooling inside the furnace.

Fig. 6.19: The formation process parameters for the massive slags of Luserna and Transacqua.

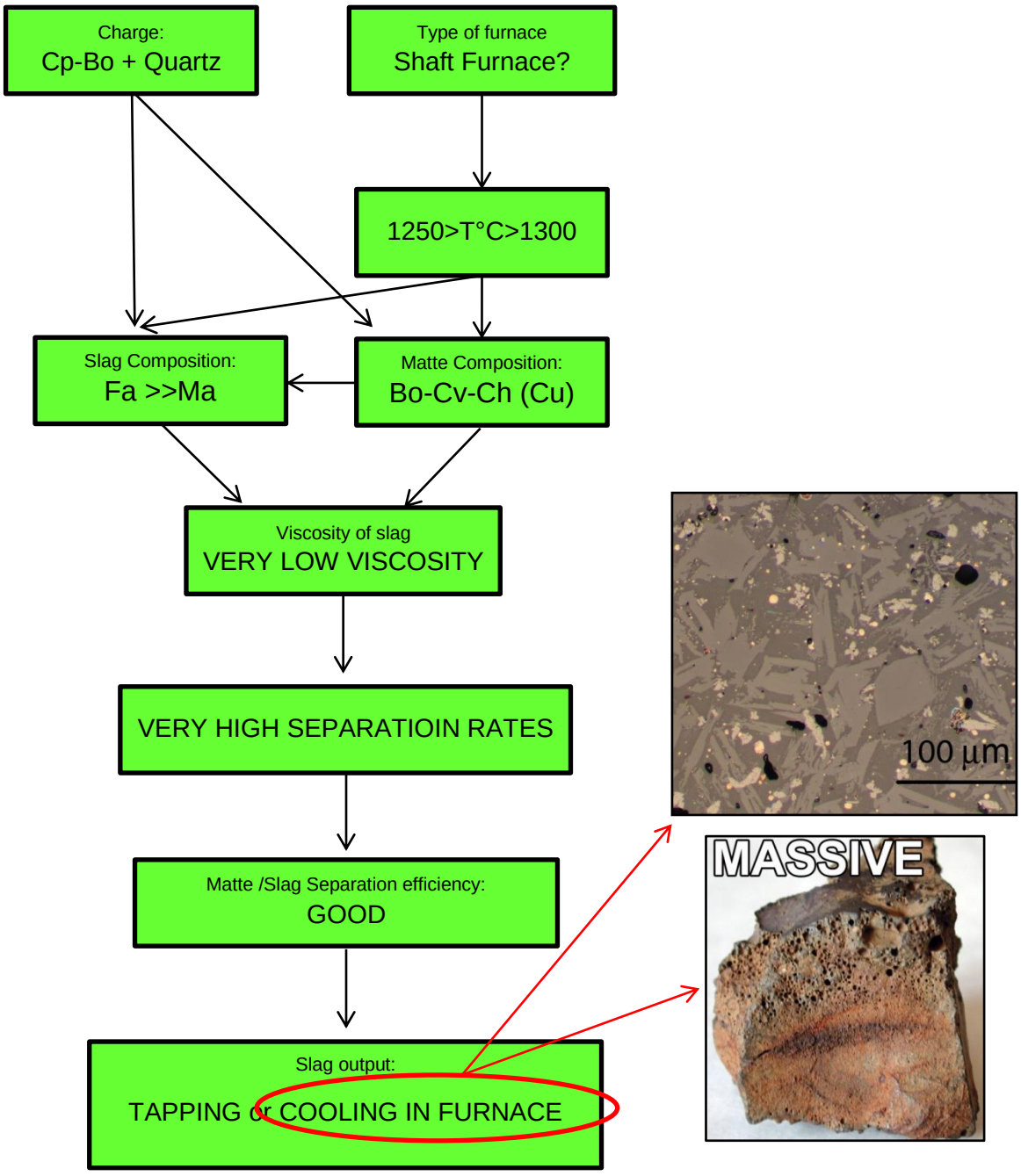

Recalling the low separation matte/Cu-slags efficiency of the smelting operations carried out at Segonzano, the two sub-groups of massive slags (M1 and M2) could be interpreted as a double matting stage, the first stage operating using an excess of quartz (M1 group) and the second stage characterised by the same operating condition of the massive slags of Luserna and Transacqua. However, the actual quantity of M1 and M2 slags (not statistically representative) did not allow to verify this hypothesis.

The flat slags of the three sites have both a completely different entrapped sulphide composition and amount of mineralogical phases with respect to the massive slags. Therefore, the formation processes of these two types of slags are necessarily different. During the flat slags formation process, the used charge was mainly composed by bornite and covellite-chalcocite like the matte produced by the process of the massive slag formation. Fayalitic slags and raw copper were produced by heating the Bo-Cv-Ch charge with quartz. The low viscosity of the slags allowed a good separation between the raw copper and the slags.

Fig. 6.20: The formation process parameters for the flat slags.

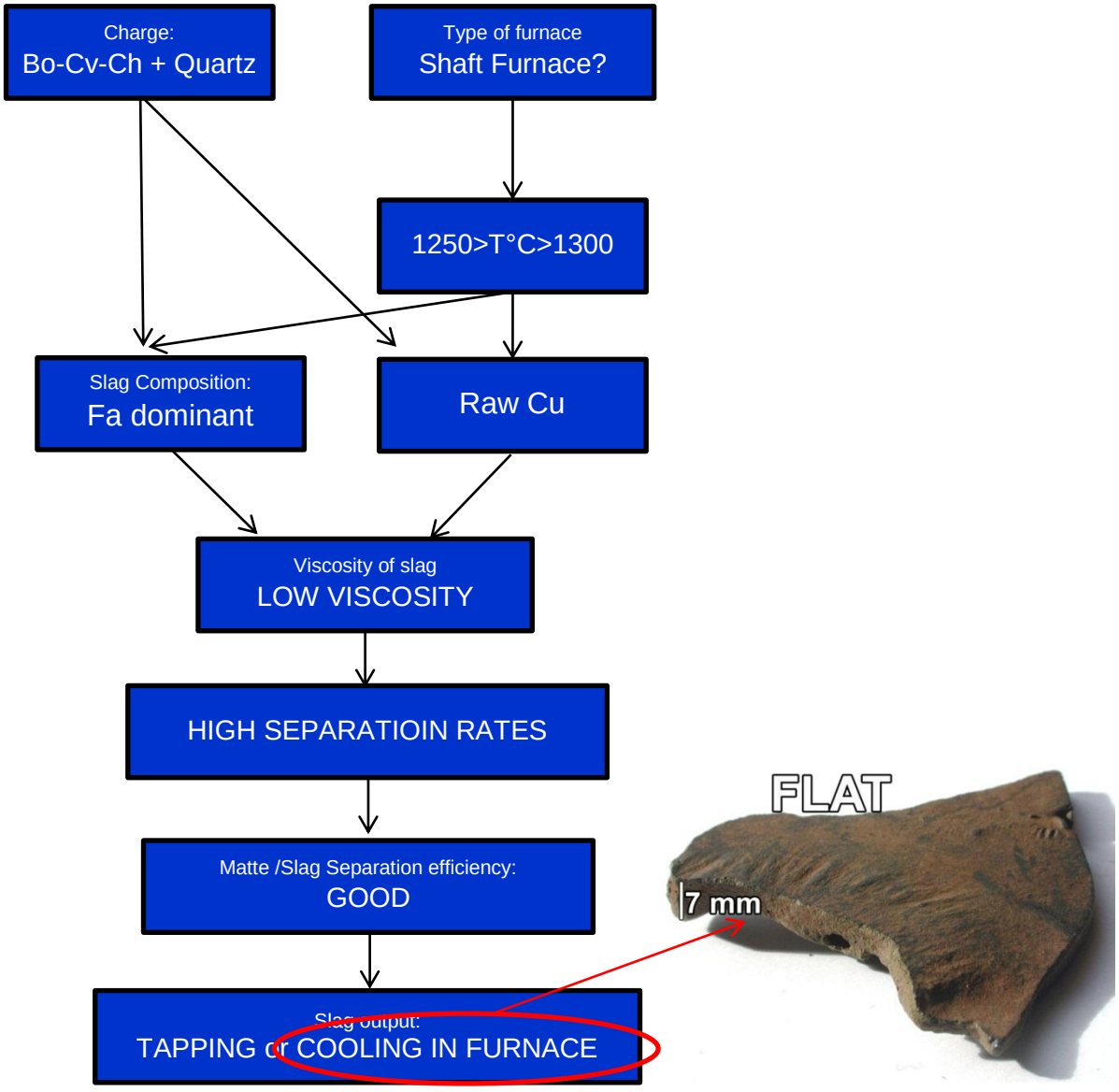

The flat slags could be left cooling inside the furnace or tapped. On the basis of the macroscopic features (smooth sides), it is possible that they formed themselves directly at the surface of the raw molten metal.

To our knowledge, the archaeological remains did not provide specific evidences on the type of furnaces or other information about the smelting process. Therefore, the hypotheses on the multi-stage process carried out at the Luserna, Transacqua and Segonzano smelting sites are entirely based on the analyses of the slags.
It is proposed that the three different slag types are the product of three distinct metallurgical steps:1) the coarse slags are the product of the initial slagging operations, where a Cu-poor matte is produced, mainly of chalcopiritic-bornitic composition, 2) the massive slags are the result of the major matting process, where a Cu-rich matte (bornite-covellite-chalcocite composition) is produced, and 3) the thin flat slags are the product of the final refining process.

Regarding the differences within the smelting sites, in Transacqua the smelters seem to have reached the highest level of extractive skills (highest Matte/Cu-slag separation rates and high grade of extraction efficiency, fluidity of the slags) while in the smelting sites of Segonzano the smelting operations lasted more hours and were more difficult (high-viscous silica-rich slags, poor separation efficiency between Cu and slags specially during the refining process). The high-furnace temperatures reached at the smelting sites of Segonzano (coarse slags≈1380°C) are likely due to the poor ability of the smelters to maintain the slags molten by modifying the relative amount of fuel, ore and flux charged to the furnace.
The smelting operation carried out at Luserna seem to have reached a good Cu-extraction level, with high separation Cu-slags rates and good Cu-extraction efficiency.

VII - Lead Isotope Analyses of the Slags

7.1 Introduction

Today, the isotopes of several elements are used in geology both for dating purposes and to trace the history and mode of formation of rocks and minerals (Faure, 1986).
In the last fifty years, the use of *lead isotopes* has become widespread (Pollard and Heron, 2008), initially because of the potential of the uranium and thorium decay series to provide an estimate of the age of the Earth (see Patterson, 1953), and subsequently because it has been widely used as a technique for dating the placement of metalliferous ore deposits with the *Common lead dating method* (Faure, 1986).
Lead has four naturally occurring isotopes: ^{208}Pb (52.10%), ^{207}Pb (21.11%), ^{206}Pb (25.42) and ^{204}Pb (1.36%), where indicated percentages are the present-day relative abundances in average crustal rocks. The first isotope, ^{204}Pb, is not radiogenic, even though it is very weakly radioactive and decays to stable ^{200}Hg by alpha emission with a long half-life: 1.4x1017 years (Faure, 1986). Because of its very long half-life, ^{204}Pb is treated as a stable reference isotope. The other three isotopes: ^{206}Pb, ^{207}Pb, and ^{208}Pb, are the daughter products of ^{238}U, ^{235}U and ^{232}Th, respectively, and thus are radiogenic and accumulate through time (Faure, 1986). These four isotopes can be combined into several ratios, but only three of them are independent (Villa, 2009). Hence, the two-dimensional representation of the isotopic ratios concern two plots: 1) ^{207}Pb/^{204}Pb as a function of ^{206}Pb/^{204}Pb, and 2) ^{208}Pb/^{204}Pb as a function of ^{206}Pb/^{204}Pb.
Lead occurs in various geological materials as incorporated lead at the time the material formed, and radiogenic lead generated by radioactive decay since that time. The geological materials that incorporate minor amounts of U and Th; and for which the lead isotopic composition will change, become more radiogenic with time. On the contrary, the lead isotopic compositions of the lead-rich sulphides will remain unchanged, having such a low content of uranium and thorium.
Due to their different ages and geological environments, such ore deposits have lead-bearing ores with distinct Pb-isotopic signatures that can enable the ‘‘fingerprinting’’ of anthropogenic lead sources (Lepitre et al., 2003).
The aim of the archaeological studies using the isotopic analysis is to trace the prehistoric artefacts back to their ore source.
In archaeology, the lead isotope analyses were firstly used by Brill and Wampler in 1965. Even though their pioneering work was focused on glasses, the major application of the Common lead dating method in archaeology involves metals. In fact, lead is most commonly associated with copper, iron, silver and zinc sulphide minerals, from which the metal protagonists of the metallurgy history were extracted.
As stressed by Macfarlane (1999), the popularity of this method lies in the presence of measurable lead both in the ores used for the metal production, and in the metal artefacts as well as in the smelting slags. These three types of materials are the overall components of the smelting chaîne opératoire.
Besides, the great availability of published lead isotope data on ore deposits and metal objects, which is mainly due to the systematic analysis of the lead isotope ratios begun

in the 70s (Stos-Gale et al., 2009), ensures that lead isotope analyses are a key tool for the provenance studies of archaeology.
However, it is necessary that this method couples with trace element analysis in order to have a comprehensive metallurgical fingerprint. Although trace elements can be affected by some metallurgical processes (Tylecote et al., 1977, Pernicka, 1999), their investigation may be helpful in the discrimination of the ore source (Artioli et al., 2008).

7.2 Alpine Archaeocopper Project (AAcP)

Respect to the Bronze Age period, different research groups have published data on ores, artefact samples and slags as regards the Mediterranean and Alpine Areas. The Table 7.1 shows the lead isotope analyses so far published, distinguished by country, region and/or area as those in the work of Stos-Gale et al. (2010) with updated references.

Tab 7.1: Lead isotope analyses of the Mediterranean and Alpine Area ores and artefacts of the Bronze Age, modified after Stos-Gale and Gale (2010).

Country	Region / Area	N. published analyses	References
Switzerland	Alps	11	Cattin et al. 2011, Guenette – Beck et al. 2009
Austria	Shwaz, Brixlegg, Innsbruck Region. Styria, Carinthia, Eastern Taueren windonw	93	Höppner et al. 2005, Horner et al. 1997, Koppel et al. 1983a, Schroll et al.2006
Germany, Rep. Czech	Erzerbirge, Bohemia	68	Niederschlag et al. 2003
Italy	North and Alps	155	**Artioli et al. 2009, Nimis et al. 2012**, Curti 1997, Pettke et al. 1996
Italy	Centre	107	Stos-Gale et al. 1995, Lattanzi et al 1992, Dayton et al. 1986
Italy	Sardinia	378	Valera et al. 2005. Stos-Gale et al. 1996, Wagner et al. 1986b, Ludwing et al. 1989, Begamann 2001, Boni et al. 1985, Swainbank et al. 1982
France	Cabrières, Cevennes, Val d'Ayas	181	Baron et al. 2006, Brevart et al. 1982, Le Guen et al. 1991, Prange et al. 2003
Spain	Cantabrico, Catalonia, Linares-La Carolina, Analusia, Castoglia- La Mancia	437	Stos-Gale et al. 1995, Hunt-Ortiz 2003, Santos et al. 2004, Montero Ruiz et al. 2009a&b, Klein et al. 2009, Renzi et al. 2009, Canals et al.1997, Lillo 1992
Turkey	Central Taurus, Black sea	307	Wagner et al. 1985 1986a 1989; Pernicka et al. 1984, Seeliger et al.1985, Yener et al. 1991, Hirao et al. 1995
	Near and Middle East	258	Hauptmann et al. 1992, Stos-Gale and Gale 1980, Stacey et al. 1980
Serbia, Bulgaria, Romania	Balkans	450	Pernicka et al. 1993, Stos-Gale et al. 1998a, Amov 1999, 1993, Gale 2000, Pernicka et al.1997, Bird G. et al. 2010, Marcoux et al. 2002.
Cyprus	Limni, Solea, Larnaca, Kalavasos	455	Gale et al. 1997, Hamelin et al 1988
Greece	Attica, Aegean islands, Thrace, Macedonia	875	Stos-Gale et al. 1996, Wagner et al. 1986b
Portugal	Frieberg, Mannheim, Azambaj	88	Marcoux 1998, Relvas et al. 2001, Velasco et al. 2003

In the last six years, a substantial work of sampling and analysis of the copper mine samples was conducted within the Alpine Archaeocopper project (AAcP, http://www.geoscienze.unipd.it/aacp/welcome.html).
The aims of the AAcP is to define the mineralogical, petrological and geochemical aspects of the ancient copper Italian mines, and to develop a database of elemental and isotopic tracers for provenancing of ancient copper metals and smelting slags. The AAcP is led by Professor Artioli and his group with the collaboration of several academic and non-academic Institutions, such as the Isotopengeologie Institut für Geologie, Universität Bern, in the person of the Professor Igor M. Villa, the Gruppo Archeologico Agordino – ARCA, the Museo di Scienze Naturali dell'Alto Adige, and many others.
The mines taken into consideration are located in different Italian Regions: Veneto, Trentino, Alto Adige, Lombardy, Aosta Valley, Piedmont, Liguria, Emilia Romagna, Tuscany, Sardinia, and also in France: in the Queyras Region. Several copper districts were completely analysed, such as those in the Trentino Region: Valsugana, Val dei Mocheni, Cinque Valli, Vignola, Val Venosta and Val Martello.
Currently, the AAcP database consists of 380 Pb isotopic analyses performed on metallurgical artefacts, ore mine samples, copper smelting slags, and on the products of the metallurgical experiments performed in collaboration with the ARCA group.
So far four works were published using the AAcP database, two of which with the isotopic data: a re-visitation of copper metallogeny in central-eastern Southalpine (Nimis et al., 2012), and the archaeological application on the ancient metals in the Canavero Mountain hoards in the Piedmont (Artioli et al., 2009). The other two papers show only the isotopic ratio plots, containing the conceptual value of the AAcP database (Artioli et al., 2010) and a preliminary application of the database on archaeological slags (Addis et al., 2012).
The analyses of the trace and Rare Earth elements of the database samples, have been partially performed and are still in progress in order to provide a comprehensive geochemistry database.
Considering that there are only a few isotopic works on the Bronze Age in Northern Italy, one should cite the isotopic analysis in the paper of Jung et al. (2011), in which 35 total objects of the Middle and Final Bronze Age were isotopically analysed, 22 from Veneto and Lombardy and 6 from Apulia and Calabria. Unfortunately, it is not possible to compare their data with others, as the isotope ratio data are absent.

7.3 Pb-isotope analyses on the smelting experiment materials

Two seasons of copper smelting experiments were carried out in the summers of 2010 and 2011 in collaboration with ARCA (Gruppo Archeologico Agordino).
The main purpose of the experiments was to explore the effect of different roasting cycles on the process and to produce a highly copper-enriched matte.
Using an artificial air source and carbon coke to feed the combustion, we conducted: a) roasting experiments, b) smelting experiments (starting from chalcopyrite and malachite) and c) matting experiments.
The experiments have shown that there is no complication for smelting copper from a high-grade malachite ore, but only a few experiments provided copper from Cu-Fe-sulphides.
A posteriori, we tried to understand if any change of the Pb-ratios of the Cu-bearing materials during the experiments occurred.
The occurrence of fractionation during the high-temperature non-equilibrium metallurgical process (smelting, refining, casting) has been largely discussed in literature. In several works it was asserted that no isotopic fractionation occurred during the processes (e.g. Gale et al. 2000, Cincotti et al. 2001). In other works, the possibility of the Pb-isotopic composition to change signal during the metallurgical process, due to the evaporated loss of lead (Pollard and Heron 2008), was taken into consideration.
More recently, the experiments carried out by Cui and Wu (2011) showed that the change in the lead isotope ratios due to the fractionation usually does not exceed the instrumental error. This confirm that the fractionation cannot influence the results of the provenance study.

After the experiments were carried out, we decided to measure the lead isotope ratios on the chalcopyrite as the Cu-bearing starting material (Cp) and on the copper (Cu) as the final products of the smelting.

Tab 7.2: Lead isotope ratios of the chalcopyrite (Cp) and copper (Cu). “Product- Starting” is the difference of the Pb-ratio values of Cu and Cp.

SAMPLE		$^{206}Pb/^{204}Pb$	±2SE	$^{207}Pb/^{204}Pb$	±2SE	$^{208}Pb/^{204}Pb$	±2SE
STARTING MATERIAL	**Cp**	18,857	0,002	15,657	0,002	38,775	0,007
PRODUCT MATERIAL	**Cu**	18,858	0,002	15,659	0,002	38,783	0,006
Product – Starting =		0.001		0.002		0.008	

The lack of information concerning the loss of lead during the experiments does not allow us to assert that no fractionation occurred.
However, the low variability of the Pb-ratios measured between the starting and the product materials (comparable with the instrumental error) indicates that no considerable change occurred on the Cu-bearing materials during the experimental smelting processes.

7.4 Pb-isotope analyses on the different slag components

Along with the instrumental fractioning of the lead during the analyses (Chapter 2 – Paragraph 2.6) and the high-temperature treatments, there is one more issue related to the metallurgical process and to the kind of material, how the flux and fuel can influence the isotopic signal of the product materials.
We developed a sampling strategy to apply to the archaeological slags in order to directly investigate their isotopic contamination, which, if present, it is most likely caused by the lead signal of the flux.
The idea was to perform isotopic analyses on the different parts of the same slags: on the chalcopyrite relicts, on the restitic quartz and on the reacted sulphides (as the matte). The analyses were also performed on the bulk of the slags.

Fig: 7.1:Cross-section of a coarse archaeological slag. The starting materials (chalcopyrite: Cp and quartz: Qz) were marked as circles, the product materials (matte: M) and the bulk were marked as squares.

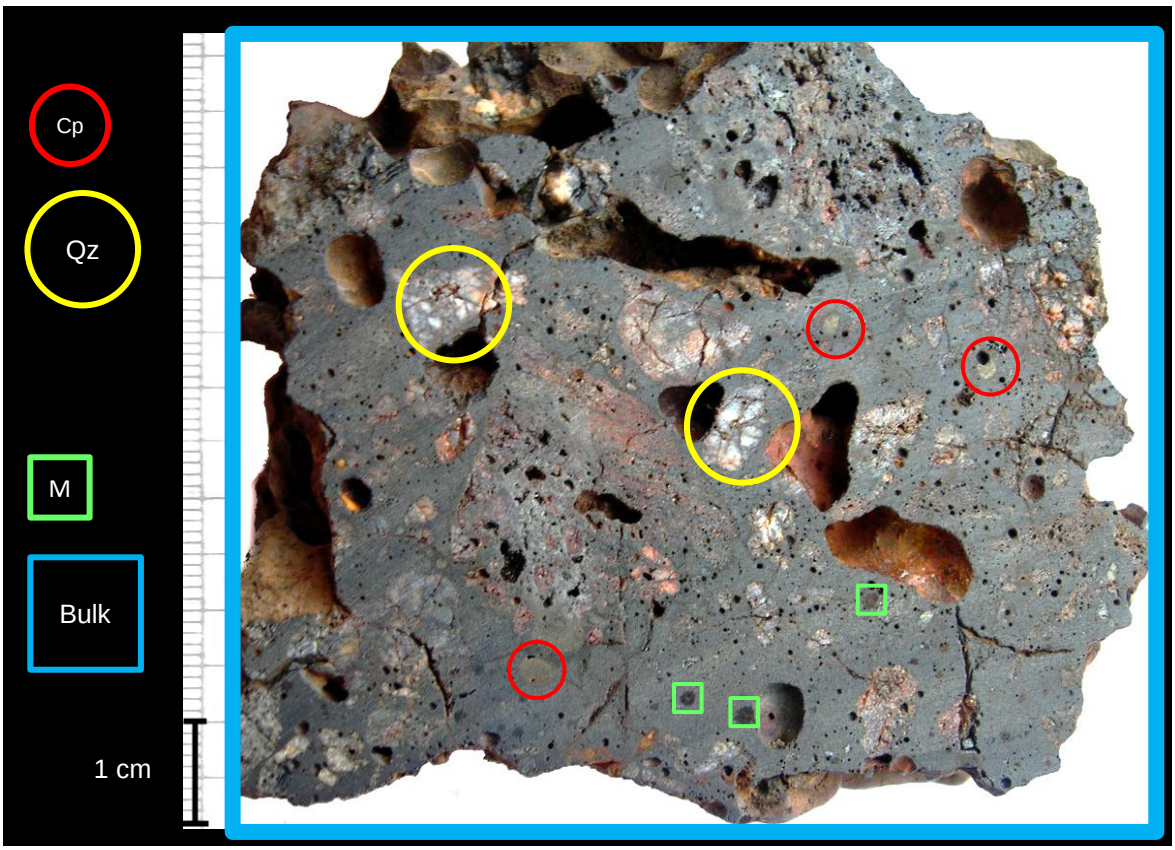

It is assumed that the signal of the chalcopyrite relict corresponds to the signal of the sulphides used as a charge during the prehistoric smelting.
Several coarse slags were sectioned and micro-sampled using the Micro-Drill device under the stereomicroscope. The powders obtained were weighted and analysed by XRPD. Then the same powder samples were analysed at the MC-ICP-MS instrument.
The isotope ratios displayed in the next four plots came from two coarse slags of the Luserna site, called LU-G58 (see Fig. 7.3 pink-coloured square) and LU-G59 (see Fig. 7.3 green-coloured square).

Fig.7.2: Lead isotope ratios of quartz (Qz), bulk, chalcopyrite (Cp) and matte (M) of the LU-G58 and LU-G59 slags. The analytical uncertainties for the samples are smaller than the size of the symbol.

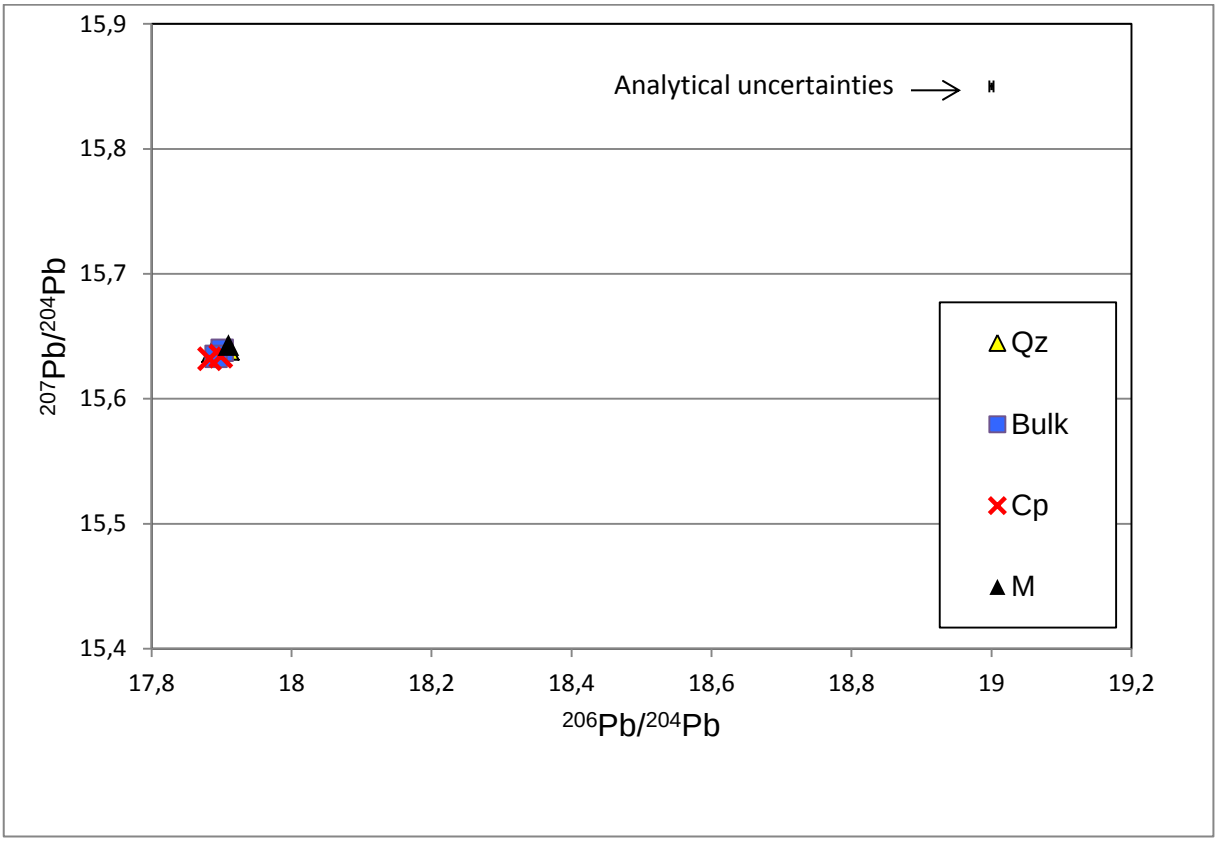

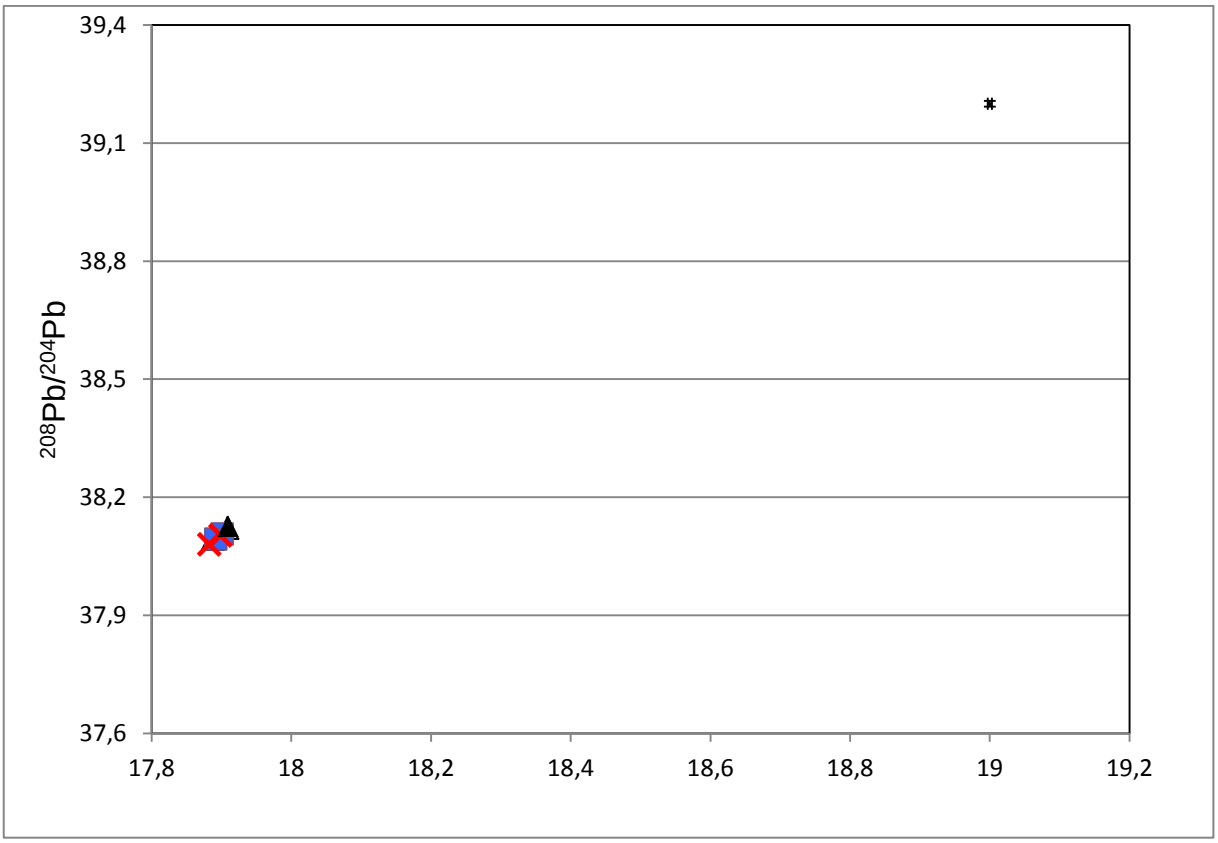

Fig.7.3: Enlargement area of Fig. 7.2. LU-G58 data are in the pink-coloured square and LU-G59 are in the green-coloured square. The analytical uncertainties are represented by the cross symbols.

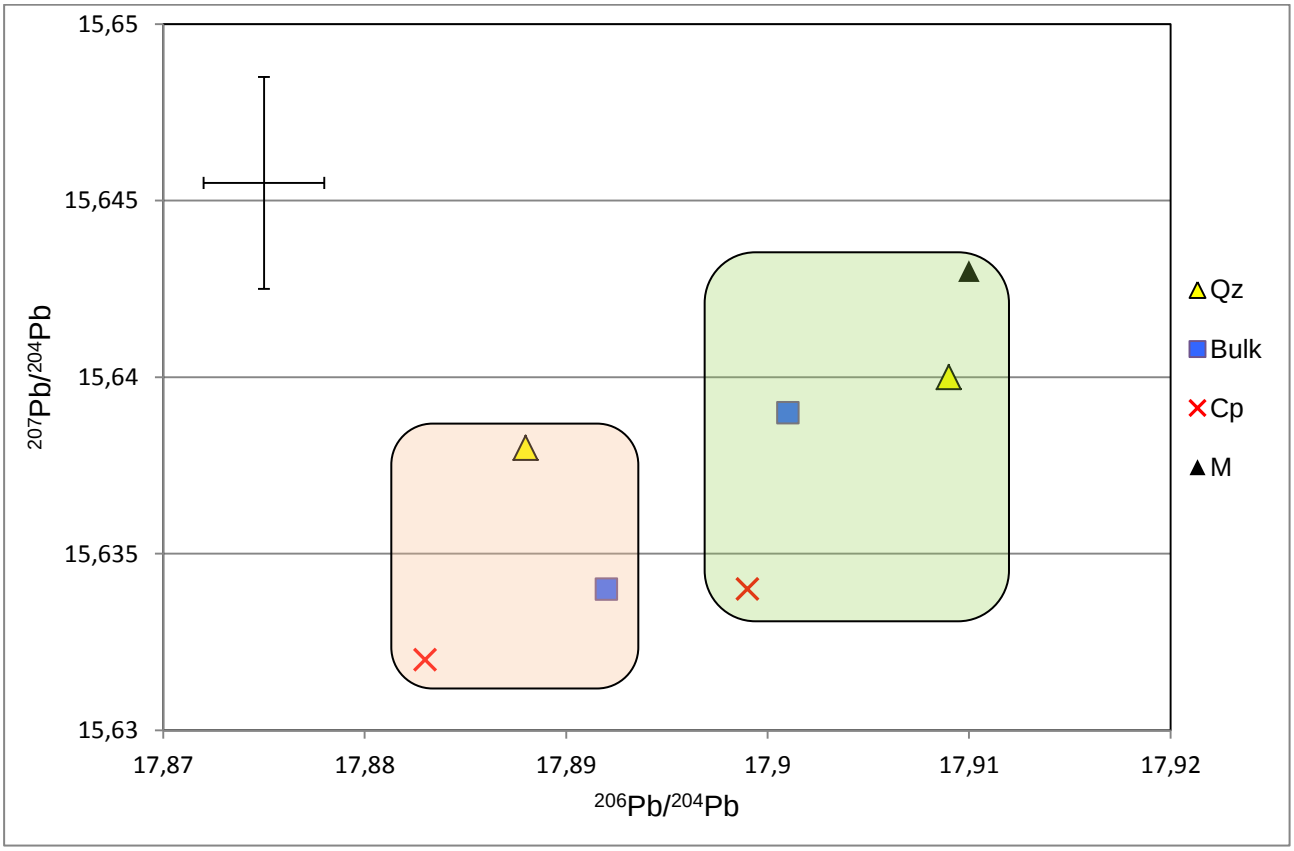

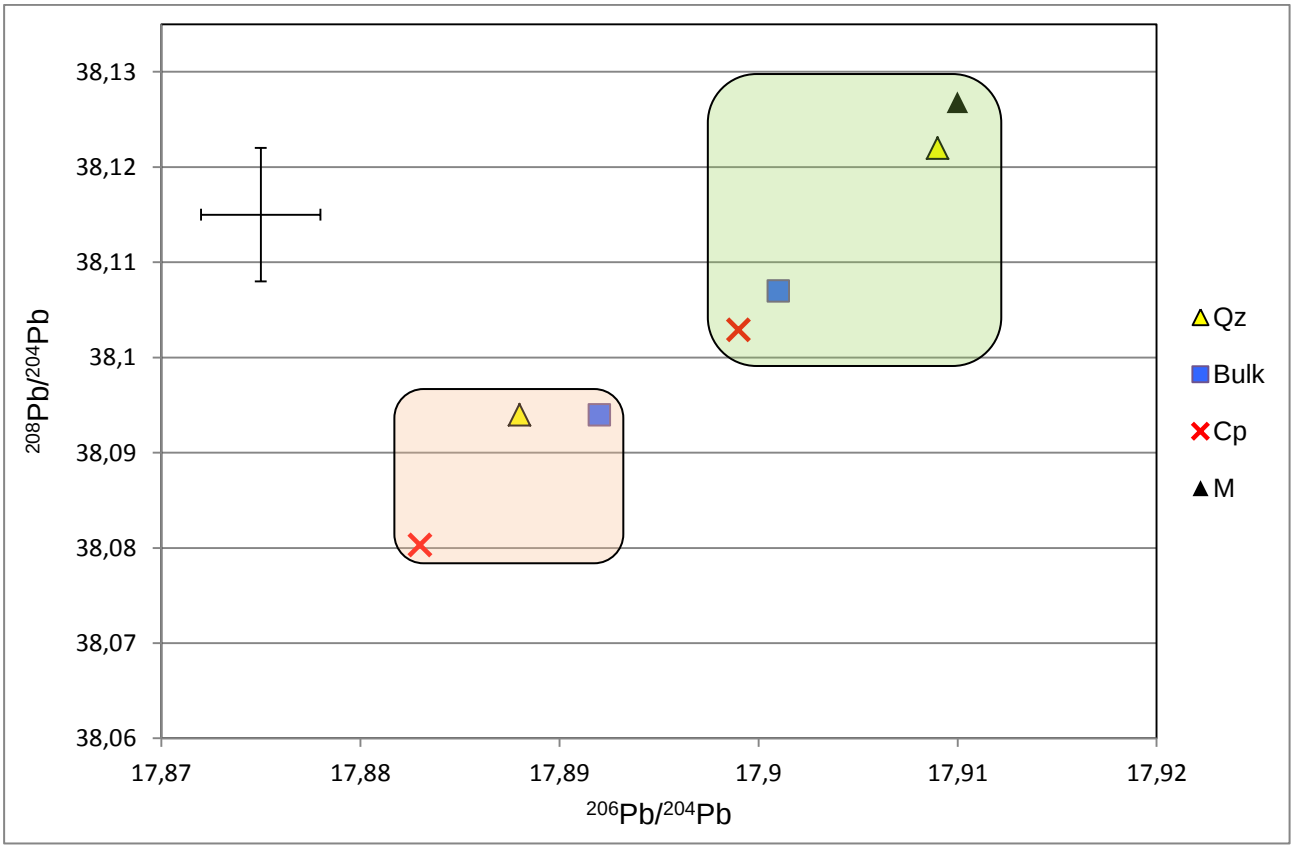

Tab. 7.3: Lead isotopes analyses on different components of two coarse slags, LU-G58 and LU-G59.

		$^{206}Pb/^{204}Pb$	2SE	$^{207}Pb/^{204}Pb$	2SE	$^{208}Pb/^{204}Pb$	2SE
LU-G58	**Cp**	17,883	0,004	15,632	0,003	38,080	0,008
	Qz	17,888	0,001	15,638	0,001	38,094	0,005
	Bulk	17,892	0,002	15,634	0,002	38,094	0,005
LU-G59	**Cp**	17,899	0,004	15,634	0,003	38,103	0,008
	Qz	17,909	0,002	15,640	0,002	38,122	0,005
	Bulk	17,901	0,002	15,639	0,002	38,107	0,004
	M	17,910	0,002	15,643	0,002	38,127	0,005

The different components of the slags and the bulk isotopically overlap. Magnifying the interested area of the two plots (fig. 7.3), an increase in the isotopic ratios of Qz, M and Bulk occurred starting from the lowest ratios of Cp. The differences between these isotopic values are likely due to a tiny fractionation process, for which a simultaneous increase of the $^{206}Pb/^{204}Pb$, $^{207}Pb/^{206}Pb$ and $^{208}Pb/^{204}Pb$ ratios occurred.
However, the whole differences of the Pb-ratio values within the individual slags are very close to the range of the 2SE values, which means they are not significant.
The two enlarged plots also show a chalcopyrite-like isotopic composition of the quartz. Therefore, as Stos-Gale et al. asserted (1998), two hypotheses may be valid: 1) the quartz-flux used for the smelting contained lead of the same isotopic composition of the sulphide ore. 2) The amount of lead introduced by the quartz (and the charcoal) is negligible in comparison with the amount of lead contained in the sulphide ore. This does not imply any change from the isotopic signal of the sulphide ore to the final product (matte) as well as to the bulk composition.
Hence, the slag bulk can be safely used for the isotopic provenance analysis, as they show almost the same isotopic composition of the chalcopyrite relicts.
The following results of the lead isotope analysis performed on the slags of the Transacqua and Segonzano sites always refer to the slag bulk.

7.5 Geographical context of Luserna, Transacqua and Segonzano

The smelting site of Luserna, Transacqua and Segonzano are located in the Trentino province.

Fig. 7.4: Map of the Luserna, Transacqua and Segonzano smelting sites and the Trentino province.

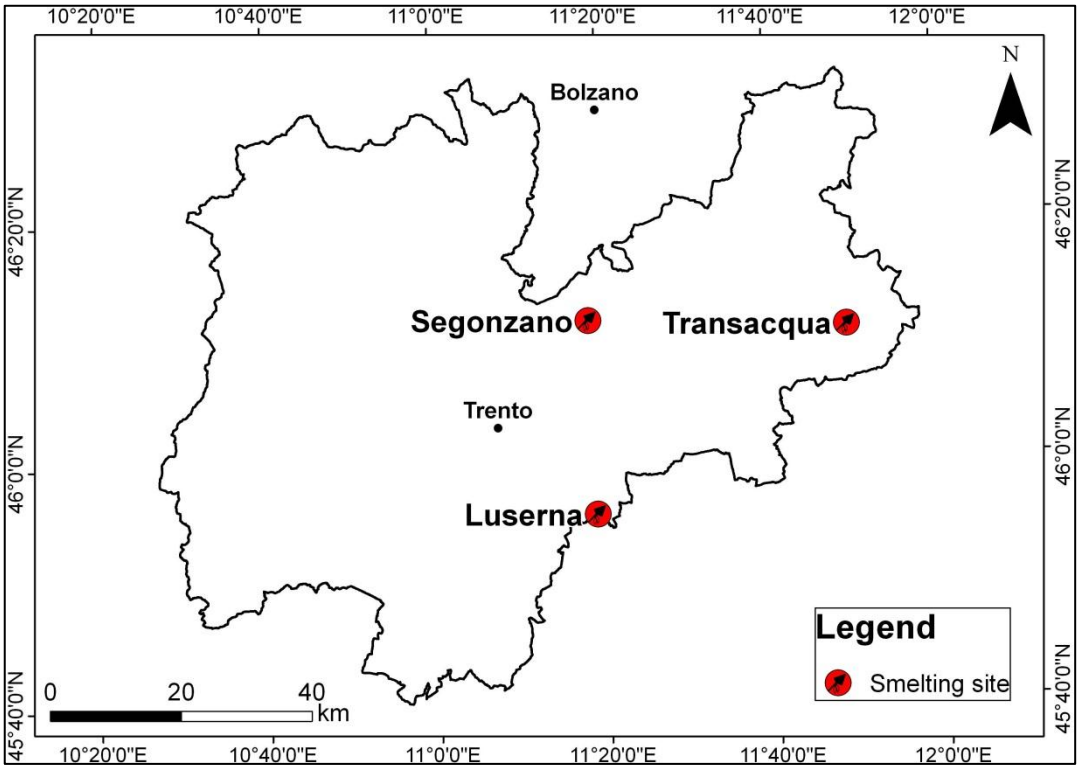

The smelting site of Luserna is located about 25 km southeast of Trento in the Lavarone-Vezzena plateau, which has the highest smelting site density of the Trentino province (Preuschen, 1973; Pearce and De Guio, 1999, Cierny, 2008).
As shown in the fig. 7.5, the site is close of several mines exploited in the Prehistory and located in the Valsugana Area, such as Calceranica and Vetriolo mines.

The smelting site of Transacqua (1080 m a.s.l.) is located in the Fiera di Primiero Area, North of Valsugana, near to the border between the province of Trentino ad Veneto.
Several mines studied by the AAcP were studied near the Transcaqua smelting site such as Valle Imperina, Valbona, Pattine.

The smelting sites situated near the village of Segonzano in the Peciapian Area is located about 20 km northeast of Trento at 1350 m a.s.l..

Fig. 7.5: Map of the Luserna, Transacqua and Segonzano sites and several mines studied by the AAcP on the Digital Elevation Model (DEM) using the World Terrain Base developed by ESRI (2009, http://www.esri.com).

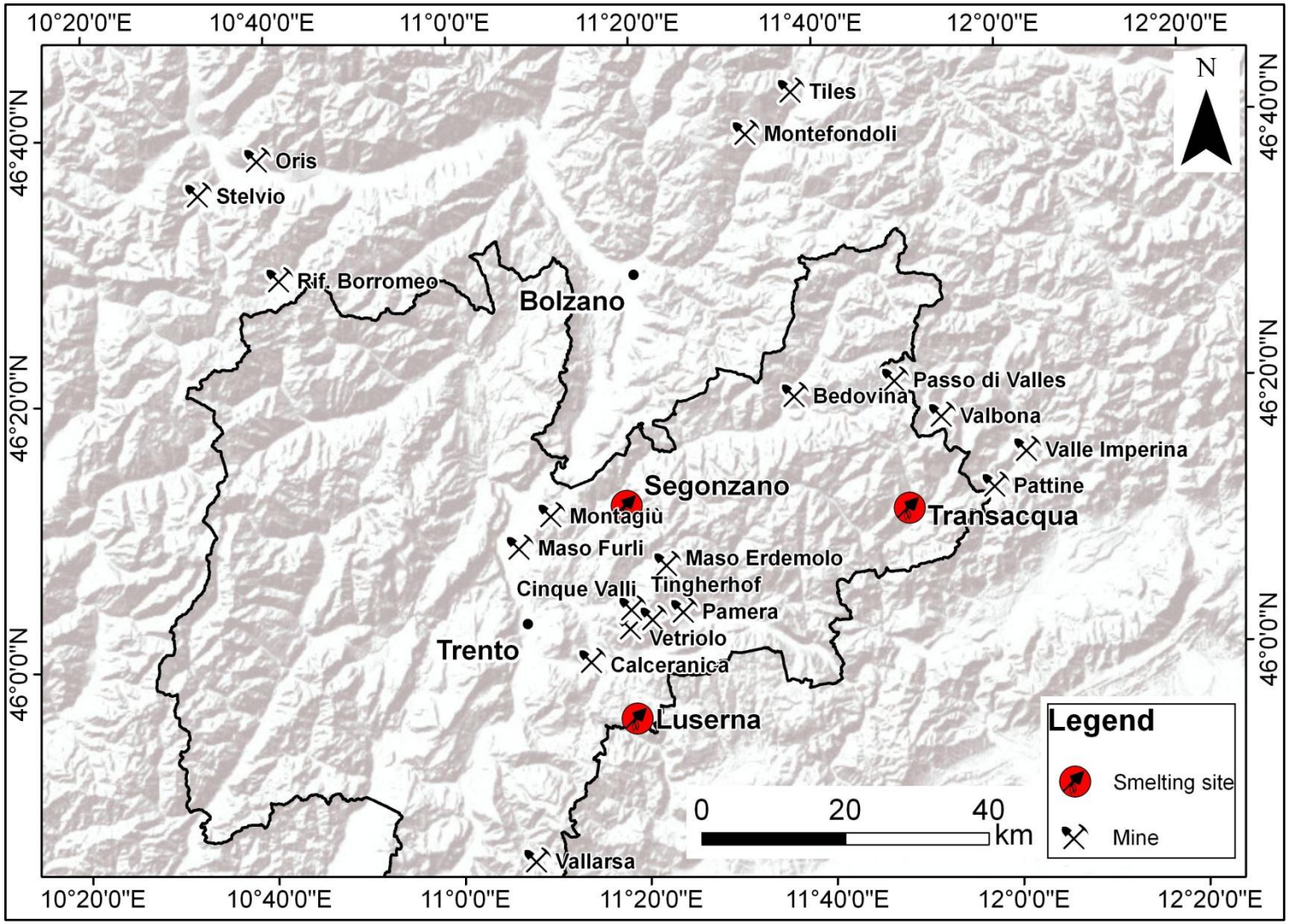

7.6 Results

A number of 16 slags of the Luserna site (32 total measurements performed on the bulk and on different parts of the slags: chalcopyrite, matte, quartz and copper prills) were analysed by means of MC-ICP-MS as well as 7 slags from the Segonzano site and 9 Transacqua slag samples. Lead isotope analyses performed on these slags are listed in the Table 7.4 and plotted in the Figure 7.6.

Tab. 7.4: Samples analysed and Pb isotope values divided by sites. For the Segonzano, the Transacqua and partially the Luserna slags (in the cases where it is not specified), the measurements were performed on the bulk.
Cp: chalcopyrite, M:matte, Qz: quartz, Cu: copper prills, He: hematite.
2SE is analytical uncertainties calculated as twice the individual in-run precision on the samples.

	SIGLA	TYPE	$^{206}Pb/^{204}Pb$	2SE	$^{207}Pb/^{204}Pb$	2SE	$^{208}Pb/^{204}Pb$	2SE
LUSERNA	LU-G56	C	18,047	0,002	15,655	0,003	38,276	0,008
	LU-G56 Cp		18,059	0,002	15,658	0,002	38,302	0,007
	LU-G56 M		18,039	0,003	15,644	0,002	38,259	0,006
	LU-G56 Qz		17,970	0,001	15,647	0,002	38,191	0,005
	LU-G56 Qz>90		17,938	0,002	15,644	0,002	38,157	0,005
	LU-GM 57	C	18,003	0,002	15,654	0,002	38,242	0,007
	LU-GM57 M		18,114	0,003	15,655	0,003	38,342	0,007
	LU-GM57 Cp		17,989	0,003	15,648	0,002	38,217	0,006
	LU-GM 57 Cu		17,954	0,002	15,640	0,002	38,161	0,006
	LU-GM 57 Qz>90		17,920	0,002	15,641	0,002	38,134	0,004
	LU-GM 57 Qz		17,984	0,002	15,652	0,002	38,215	0,005
	LU-G 58	C	17,892	0,002	15,634	0,002	38,094	0,005
	LU-G58 Cp		17,883	0,004	15,632	0,003	38,080	0,008
	LU-G58 Qz<90		17,884	0,002	15,637	0,002	38,085	0,004
	LU-G58 Qz>90		17,888	0,001	15,638	0,001	38,094	0,005
	LU-G 59	C	17,901	0,002	15,639	0,002	38,107	0,004
	LU-G59 Cp		17,899	0,004	15,634	0,003	38,103	0,008
	LU-G59 M		17,910	0,002	15,643	0,002	38,127	0,005
	LU-G59 He		17,904	0,002	15,639	0,002	38,112	0,004
	LU-G59 Qz>90		17,909	0,000	15,640	0,002	38,122	0,005
	LU-G69	C	18,047	0,002	15,655	0,002	38,276	0,005
	LU-G 70	C	18,043	0,002	15,651	0,002	38,273	0,005
	LU-G71	C	18,012	0,003	15,650	0,003	38,237	0,010
	LU-M4	M	17,967	0,002	15,645	0,002	38,186	0,006
	LU-PS 45	M	18,029	0,002	15,649	0,002	38,249	0,004
	LU-M47	M	17,958	0,002	15,645	0,002	38,179	0,006
	LU-PS65	M	17,967	0,002	15,643	0,002	38,180	0,006
	LU-P6	F	18,047	0,002	15,649	0,003	38,266	0,009
	LU-P9	F	18,048	0,002	15,651	0,003	38,273	0,008
	LU-PR34	F	18,126	0,001	15,653	0,001	38,348	0,004
	LU-P61	F	18,139	0,001	15,652	0,001	38,358	0,004
	LU-P68	F	18,006	0,002	15,649	0,002	38,228	0,005

	SIGLA	TYPE	$^{206}Pb/^{204}Pb$	2SE	$^{207}Pb/^{204}Pb$	2SE	$^{208}Pb/^{204}Pb$	2SE
SEGONZANO	SEG-G4	C	18,004	0,002	15,643	0,002	38,220	0,004
	SEG-G9	C	18,225	0,001	15,663	0,001	38,448	0,002
	SEG-M2	M	18,236	0,003	15,666	0,003	38,474	0,007
	SEG-M10	M	18,211	0,002	15,662	0,002	38,441	0,005
	SEG-P5	F	18,186	0,002	15,659	0,002	38,417	0,006
	SEG-P13	F	18,190	0,002	15,662	0,002	38,424	0,006
	SEG-P14	F	18,093	0,002	15,651	0,002	38,307	0,005
TRANSACQUA	TR-G1	C	18,317	0,002	15,685	0,002	38,628	0,008
	TR-G3	C	18,284	0,001	15,674	0,001	38,573	0,004
	TR-G8	C	18,356	0,003	15,671	0,003	38,625	0,007
	TR-G9	C	18,317	0,002	15,684	0,002	38,624	0,009
	TR-M2	M	18,275	0,002	15,670	0,002	38,549	0,004
	TR-M11	M	18,266	0,002	15,674	0,002	38,553	0,005
	TR-PS17	M	18,257	0,003	15,666	0,003	38,522	0,007
	TR-P14	F	18,291	0,001	15,670	0,001	38,566	0,003
	TR-PS18	F	18,375	0,002	15,674	0,002	38,651	0,006

As it is shown by the plots of the lead isotope ratios (Fig. 7.6a-b), the slags of the three sites are clustered in three different groups.

Fig. 7.6a: Pb-isotope plots of the slags of the Luserna, Segonzano and Transacqua sites. The analytical uncertainties for the samples are smaller than the size of the symbol.

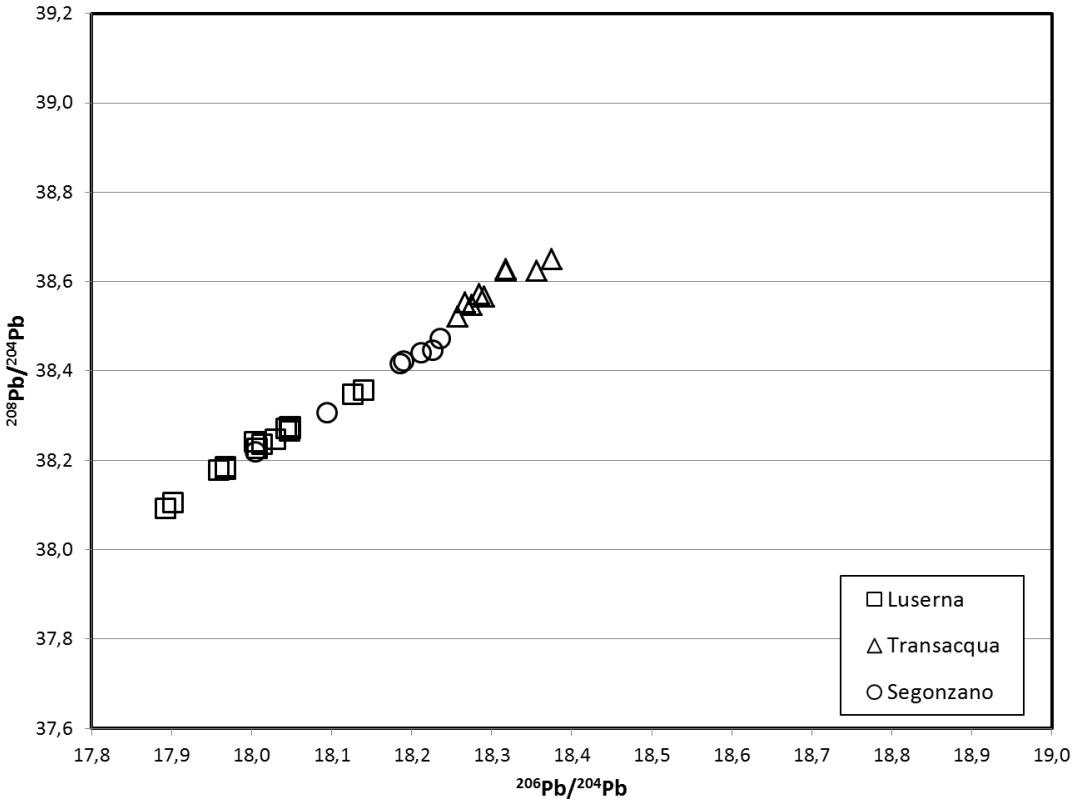

Fig. 7.6b: Pb-isotope plots of the slags of the Luserna, Segonzano and Transacqua sites. The analytical uncertainties for the samples are smaller than the size of the symbol.

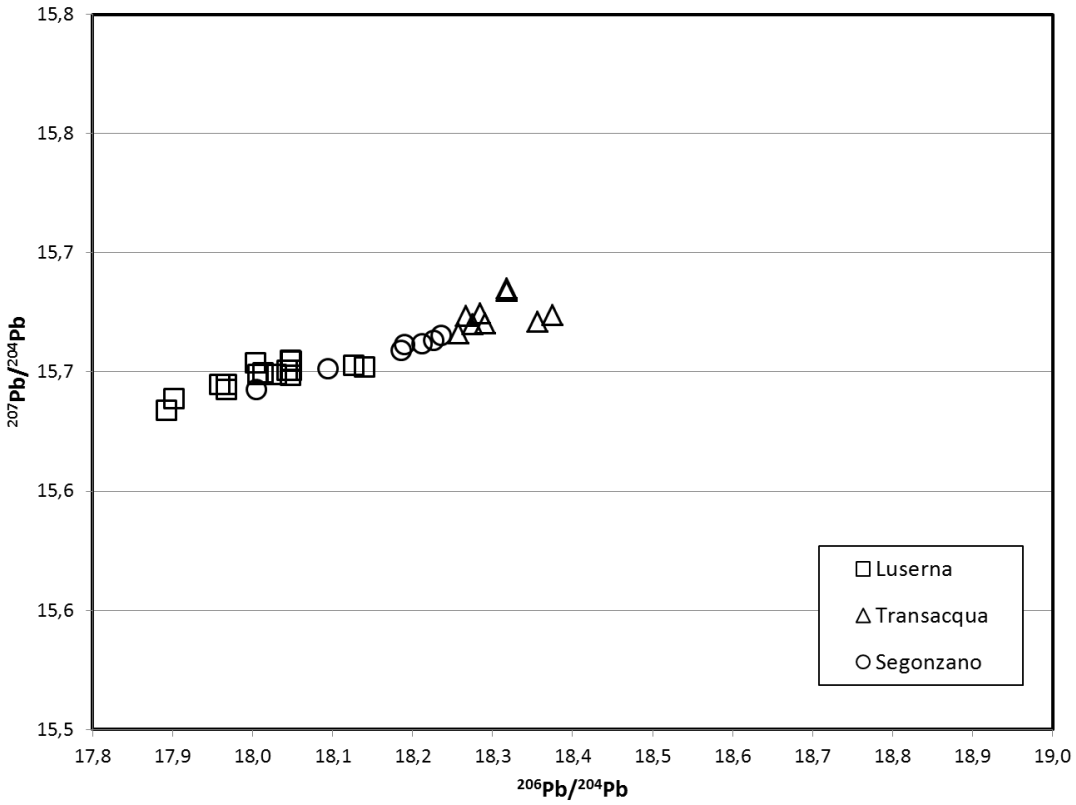

Archaeologically, the evidences of the ancient metallurgical activity in the Trentino Area have been distinguished into two different areas and periods (Perini, 1988). In the central Trentino at the valley sites located in Valdagine and Alta Valsugana, there are evidences of the most ancient metallurgy dated from the Chalcolithic Period to the Early Bronze Age. Romagnano Loc, Vela Valbusa, Acquaviva di Besenello and Montesei di Serso are the most important sites where these early metallurgical activities took place.
The second types of evidences occurred in the Eastern Trentino during the Final and the Late Bronze Age. These sites are located between 1000 and 2000 metres above the sea level, close to water, characterized by a high amount of slags. The Luserna (Lavarone-Vezzena plateau), Segonzano (Val di Cembra) and Transacqua (Primiero Area) sites belong to this type of metallurgical sites.
On the basis of these remarks, the comparison of the slags with the Alpine Archaeocopper Project database has taken into account the deposits of the Central-Eastern Southalpine Area located in Trentino and Veneto Regions (Pb-isotope data in the Tab. 7.6), as studied by Nimis et al. (2012). They have identified five main isotopic groups of deposits, which are listed from the least radiogenic to the most radiogenic: 1) the pre-Variscan stratiform deposits, 2) the post-Variscan, Early Permian vein and breccia-pipe and the Triassic fluorite-dominated vein deposits 3) the deposits in Upper Permian-Lower Triassic sediments, 4) the deposits associated with Triassic magmatic rocks and 5) the deposit related to tectono-metamorphic mobilization (Pattine mine).

Fig.7.7: Lead isotope data for deposits of the central-eastern Southalpine, modified after Nimis et al. (2012). The analytical uncertainties for the samples are smaller than the size of the symbol.

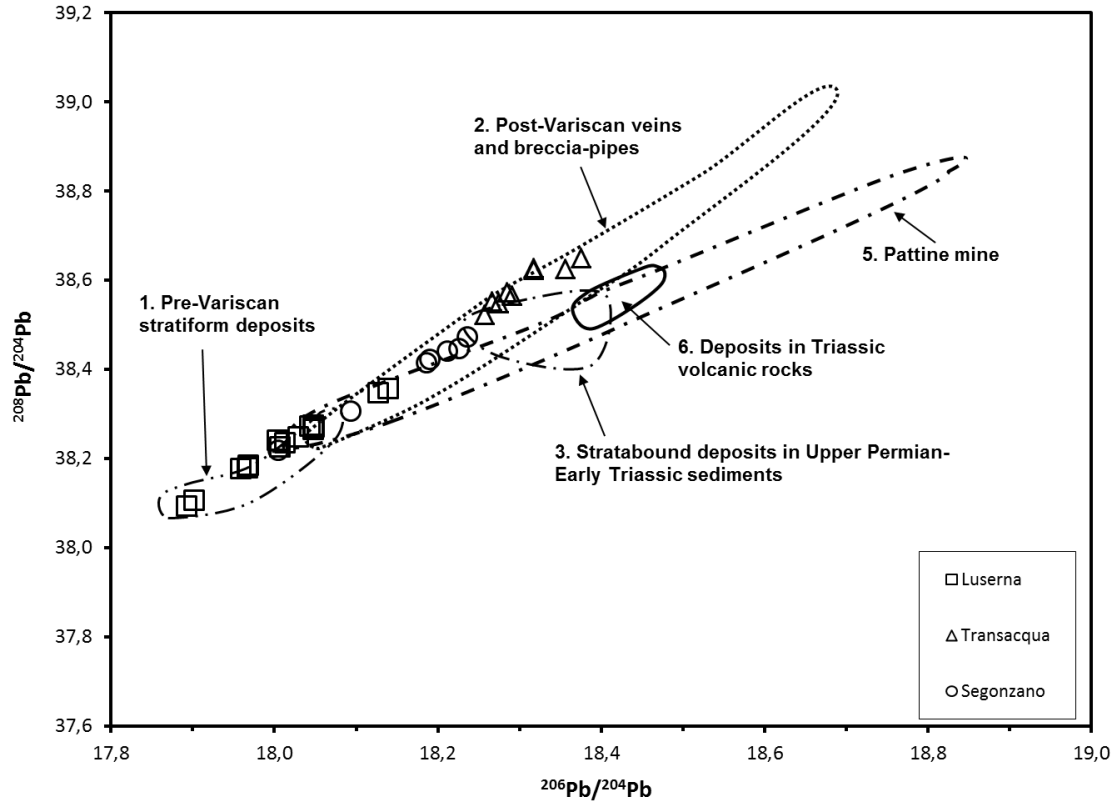

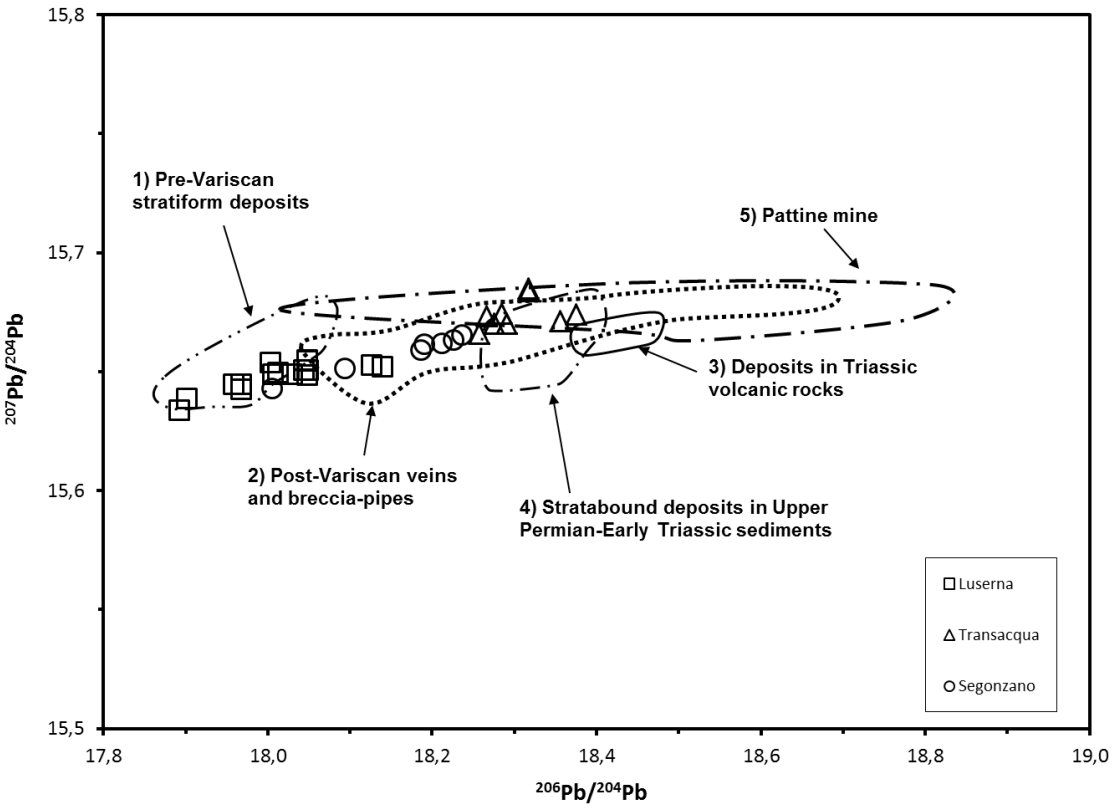

KDE Representation

An useful representation of the data is given by the kernel density estimation (KDE), a non-parametric smoothing method as an alternative to the confidence ellipsoids.
The kernel density estimates (KDEs) can be also thought as an alternative to the histogram (Baxter et al., 1997). The KDE typically provide a smoother representation of the data than the one given by the histogram, simplifying the presentation and the comparison of several data sets in a single figure.
As said by Baxter and Beardah (1997), given *n* points (X_1, X_2, . . . , X_n) situated on a line a KDE can be obtained by placing a ‘‘bump’’ at each point and then summing each bump up. The shape of the bump is defined by a mathematical function called the kernel K(x). The spread of the bump is determined by a band-width (h) that is analogous to the width of the intervals of a histogram.
As pointed out by (Beardah et Baxter, 1995), the choice of one kernel function rather than another (una piuttosto che un’altra) makes little difference to the appearance of the KDE.

Fig. 7.8: Construction of a bivariate kernel density estimate: A) kernel mass being centred about each observation. B) Contour diagram of the resulting kernel estimate (Wand and Jones, 1995).

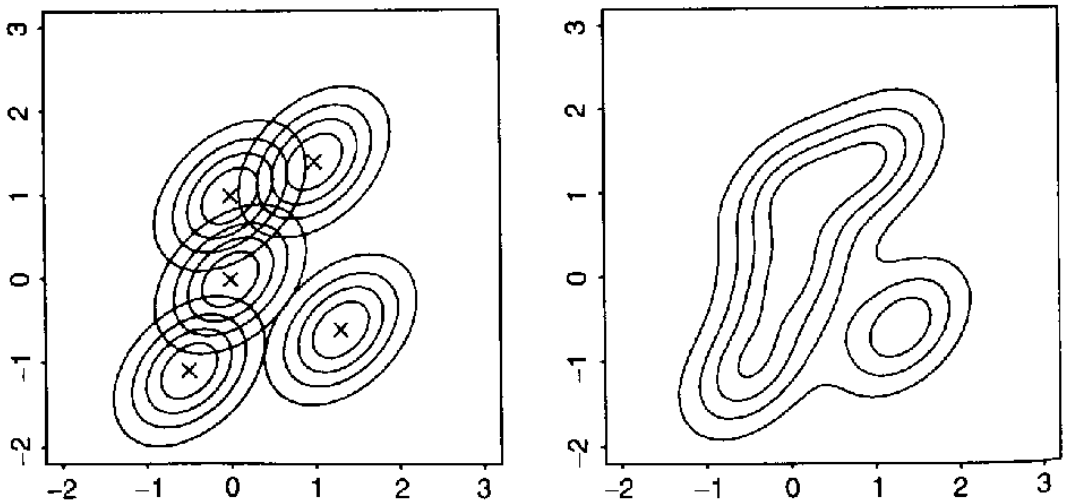

On the contrary, the smoothing parameter (h) choice is critical and many methods have been developed in order to choose the (h) to maximize the closeness between the KDE and the real density.
If (h) it is too large, we “oversmooth” by erasing details; if (h) it is too small we “undersmooth” by filtering out spurious detail.
Some simplistic methods of automatically choosing (h) are based on the assumption of normality. If this assumption is not valid the results were “oversmoothed”.
For the bivariate KDE two smoothing parameters (h_1) and (h_2) are needed in order to control the smoothing in two orthogonal directions.
If (h_1=h_2) the “bumps” of the kernel function are spherically symmetric (circular contours), on the contrary if (h_1≠h_2) the “bumps” have elliptical contours.
Regarding the lead isotope data analyses, the papers of Baxter et al. (2000) and Scaife (1998) showed that the use of KDEs requires quite large sample sizes (N>20).

For small sample sizes (say N<20) non-parametric KDEs may also be difficult to interpret.

The KDEs presented in this work were obtained using routines written by Lee (2009) for the MATLAB package.
We used MATLAB because it is important to have the facility to interactively vary the smoothing parameters. In fact, as said by Beardah and Baxter (1995), the boundary between “oversmoothing” and “undersmoothing” is quite big and the visual inspection of KDE obtained using various values of (h) should quickly lead to a satisfactory value of the smoothing parameters.
In practice, we started using the automatical (h_1) and (h_2) calculations with the method proposed by Sheather and Jones (1991). Then we reduced these values and we try to find the best KDE representation, as suggested by Beardah and Baxter (1995).

7.6.1 Lead Isotope Analyses of the Slags of Luserna

The Luserna slags have the least radiogenic compositions, with $^{206}Pb/^{204}Pb$ ratio values in the range 17.89 - 18.14. The $^{207}Pb/^{204}Pb$ ratios exhibits a variation ranging from 15.63 to 15.65, and the $^{208}Pb/^{204}Pb$ ratios are in the range 38.09 - 38.35.
As it is shown in Fig. 7.8, the isotopic signature of Luserna slags is similar to the one in the pre-Variscan stratiform deposits.
Using this KDE representation, it is observed that the isotope values of the Luserna slags are characterized by a main concentration of values (Fig. 7.9).

Fig. 7.9: Bivariate contour plot based on a two-dimensional kernel density estimate for the Luserna lead isotope ratios $^{207}Pb/^{204}Pb$ vs $^{206}Pb/^{204}Pb$.

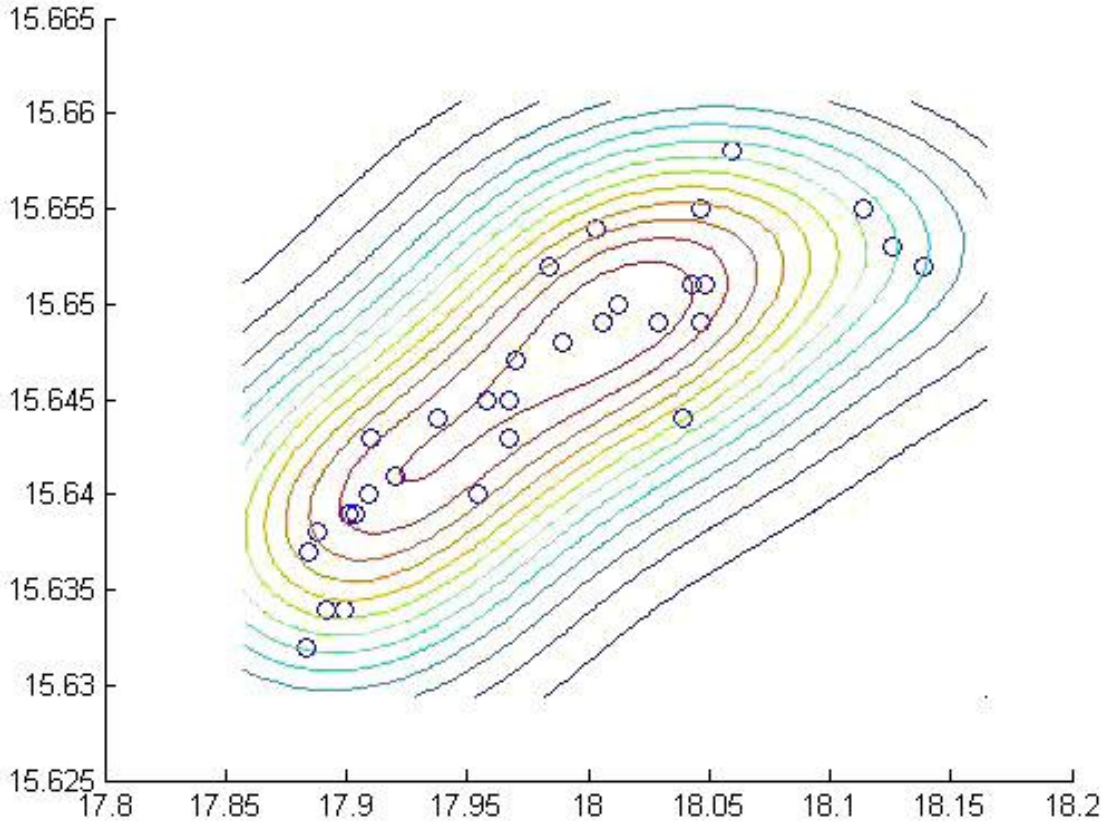

The isotopic composition of these slags partly overlap those of the least radiogenic post-Variscan samples. The next two isotopic-plots (Fig. 7.12) show the comparison between the samples of Luserna, the pre-Variscan deposits and the post-Variscan mines geographically close to the smelting site of Luserna, as shown by the map in figure 7.10

Fig. 7.10: Map of the Luserna smelting site and the mines studied by the AAcP project on the DEM of Trentino (pixel sizes=25x25 metres).

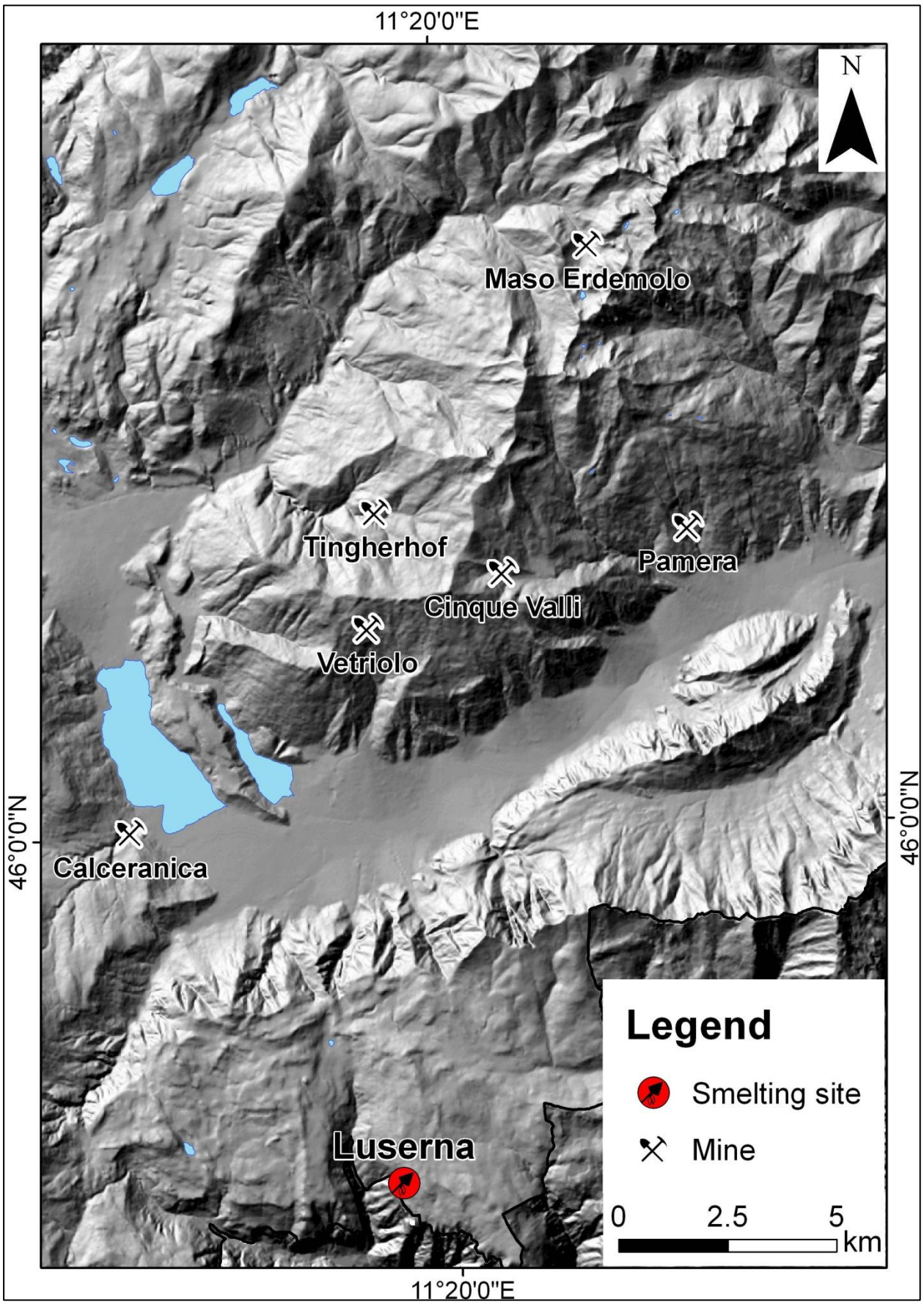

Fig. 7.11: Lead isotope data for the Luserna slags and several significant mines of Trentino and Veneto provinces. The analytical uncertainties for the samples are smaller than the size of the symbol.

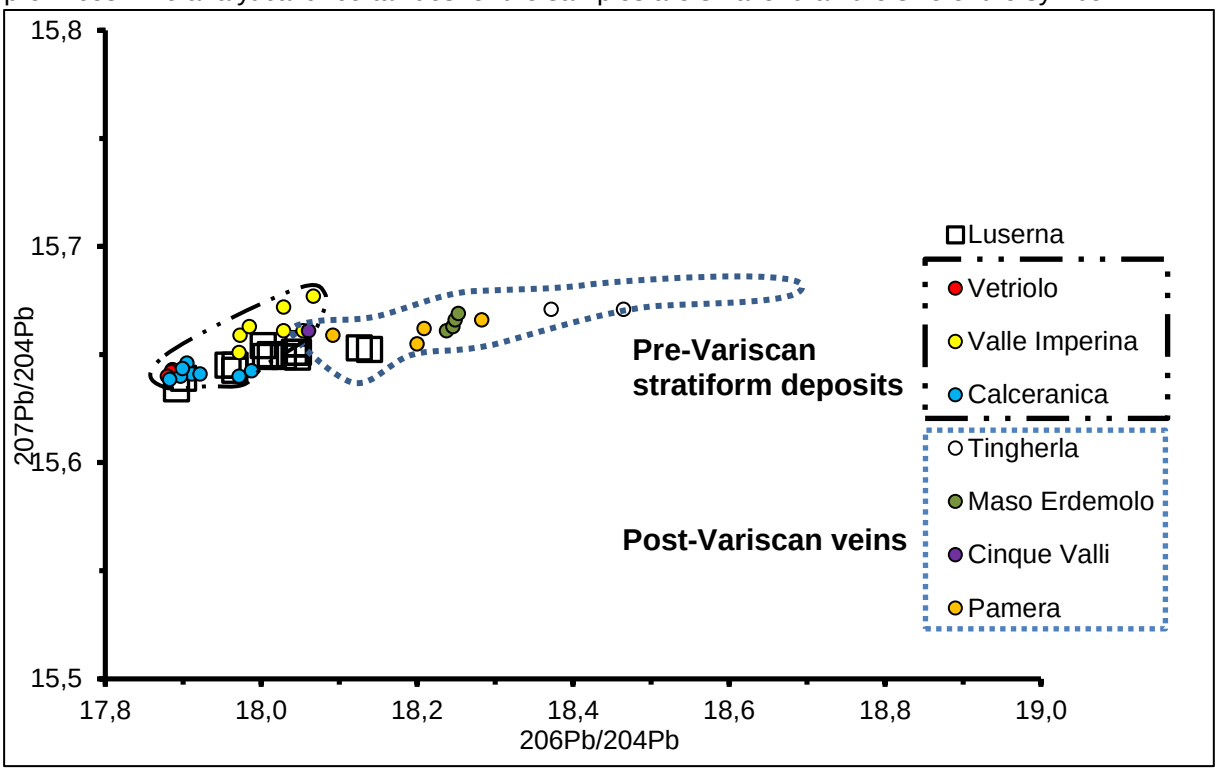

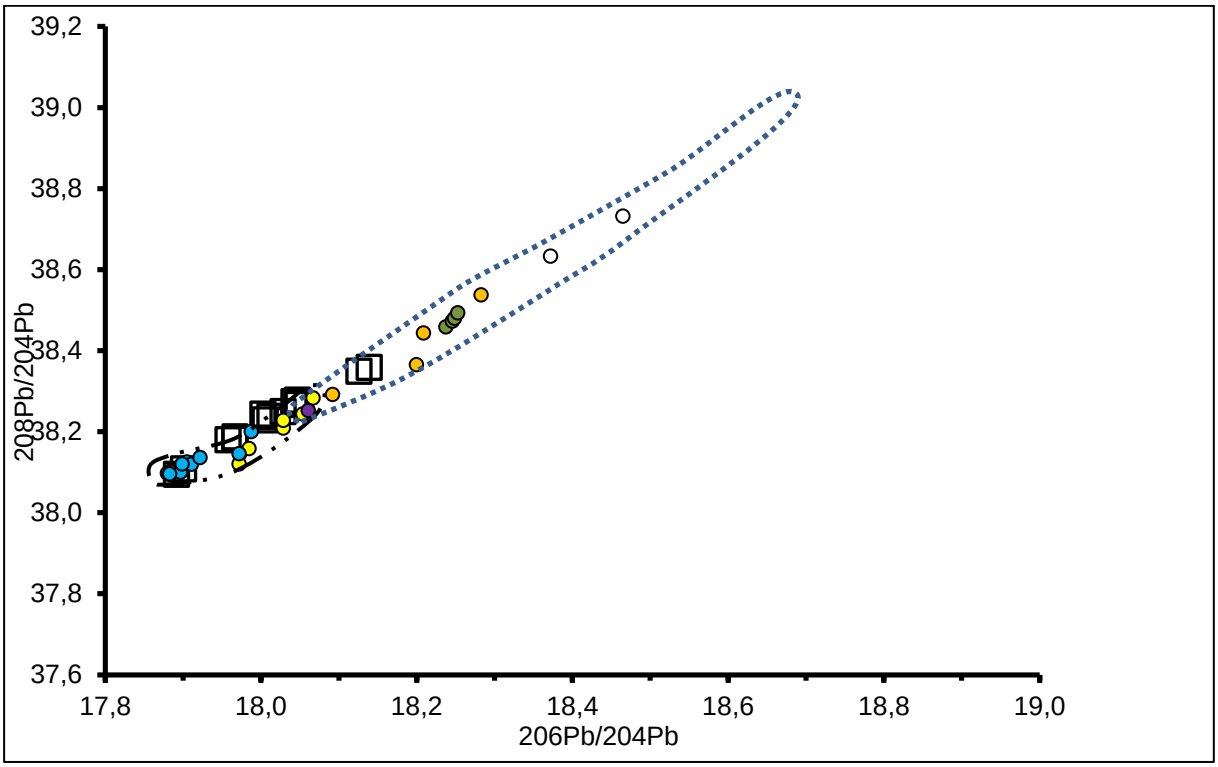

The cloud of the lead isotope points regarding the Luserna slags mainly matches with the field of the pre-Variscan stratiform deposits, composed by the mines of Calceranica, Vetriolo and Valle Imperina.

In the next plot, the KDE representation of the cloud concerning the Luserna isotope data has been coupled with the scattering plot of the pre-Variscan deposits.
It can be observed that the Calceranica and Vetriolo mines match well with the field of the main concentration of Luserna slags identified by using the KDEs representation.

Fig. 7.12. The Luserna slags plotted in the $^{207}Pb/^{204}Pb$ vs $^{206}Pb/^{204}Pb$ contour plots are coupled with the scattering plot of the Pb-isotopic values of the Calceranica, Vetriolo and Valle Imperina mines.

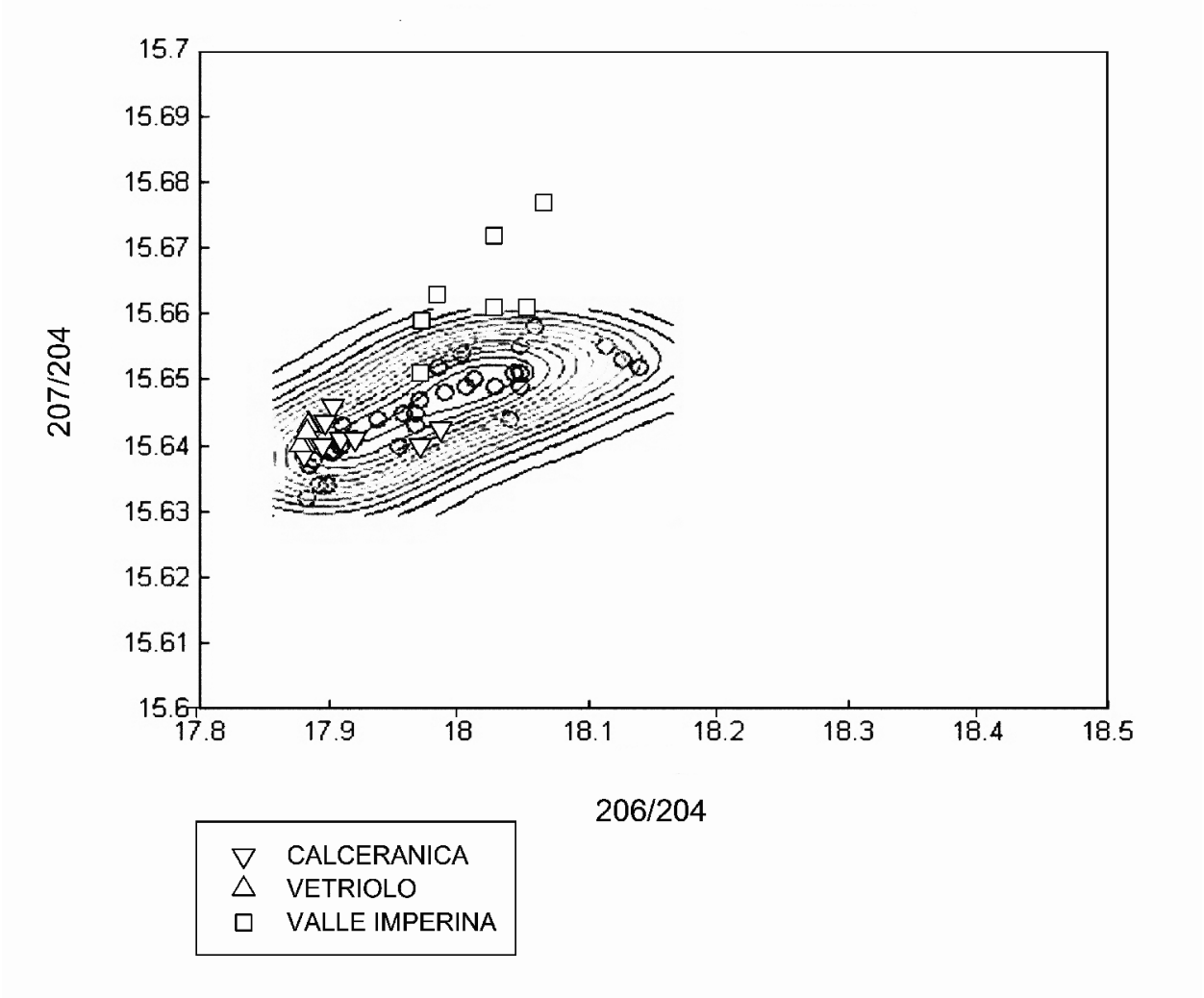

7.6.2 Lead Isotope Analyses of the Slags of Transacqua

The most radiogenic group of slags is formed by the Transacqua samples, with $^{206}Pb/^{204}Pb$ ranging from 18.26 to 18.37. The $^{207}Pb/^{204}Pb$ ratios and $^{208}Pb/^{204}Pb$ range from 15.67-15.69 and 38.52 -38.65 respectively.
From the metallogeny point of view, these slags are distributed partially in the Pb-isotopic ranges of the post-Variscan veins deposits (group 2, Fig. 7.5) and partly in the range of the stratabound deposits in Upper Permian Early Triassic sediments (group 3, Fig. 7.5).
This last group is formed by one deposit studied by the AAcP (Maso Furli, 2 measured samples) and the deposits published by Koppel and Schroll (1985).
In the next plots we considered the Pb-isotope data of the Maso Furli mine as two sample points and the mines studied by Koppel and Schroll as the field named *deposits in Upper Permian-Lower Triassic sediments*.
The *post-Variscan veins deposits* is formed by three different radiogenic subgroups. The least radiogenic of them corresponds to sulphide-rich deposits in the metamorphic basement and in the lower-intermediate units of the Permian volcanic sequence, as written by Nimis et al. (2012). The mines that form this subgroup are Cinque Valli, Pamera, Maso Erdemolo, Quadrate, Terlano and Montefondoli. Specifically, the comparison with this subgroup only considered the Maso Erdemolo and Montefondoli mines, because their lead composition is similar to the slags of Transacqua.
From the geographical point of view, the comparison with the AAcP database has taken into account several mines close to the Transacqua site located in the Veneto Region, such as Pattine and Valle Imperina mines.

Fig. 7.13: Map of the Transacqua and Segonzano sites and several mines studied by the AAcP on DEM.

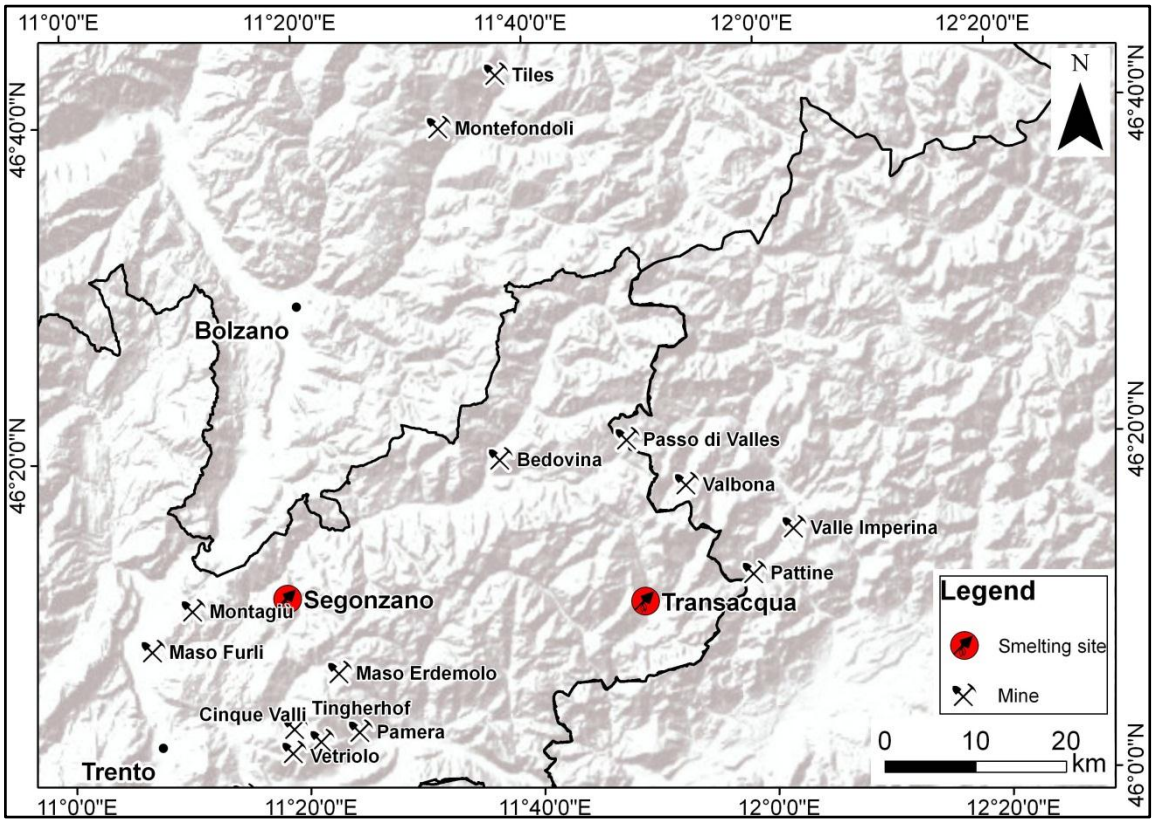

Fig. 7.14: Lead isotope data of Transacqua slags and several significant mines in the Trentino e Veneto Regions. The analytical uncertainties for the samples are smaller than the size of the symbol.

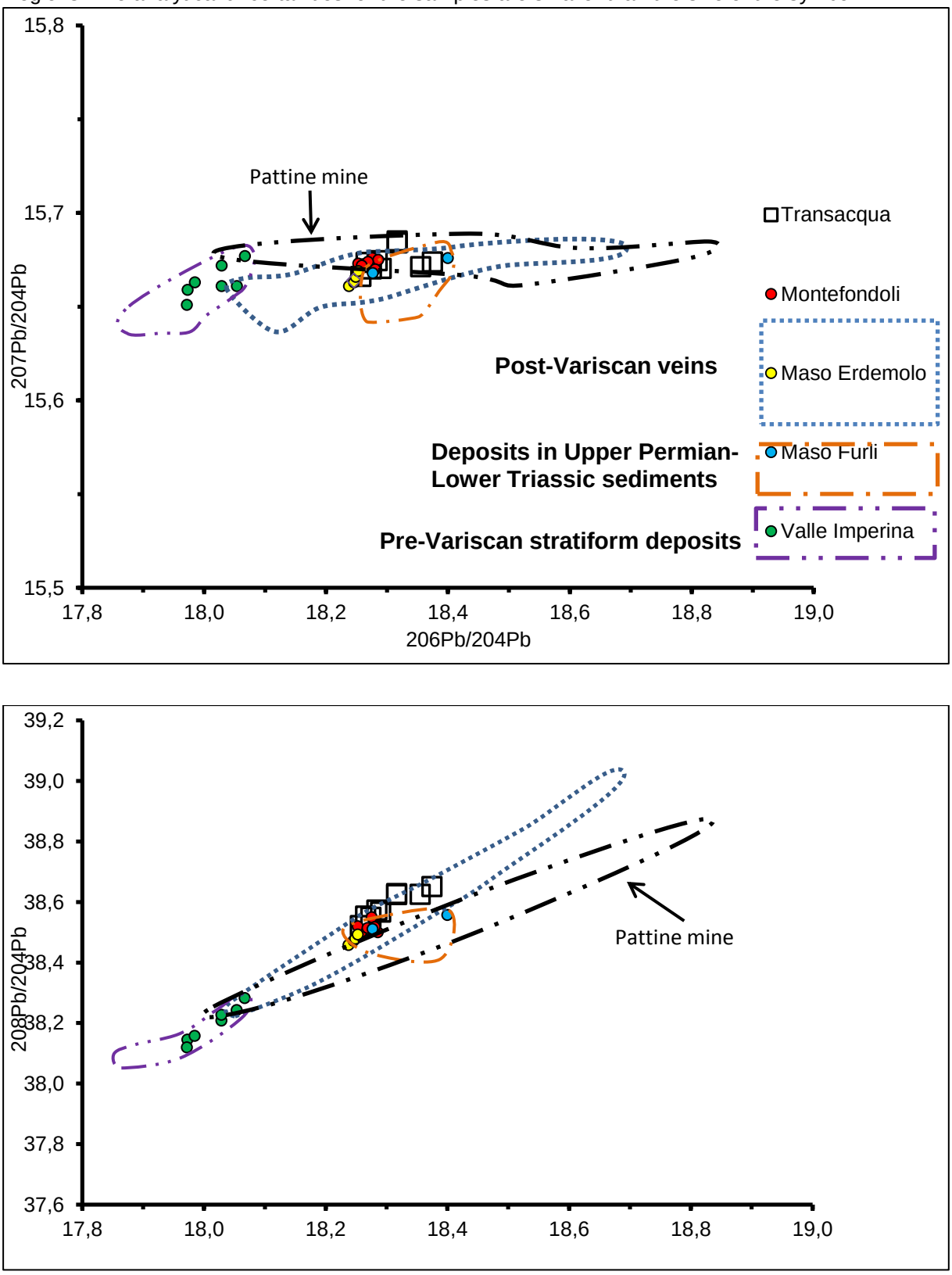

The two-dimensional kernel density estimation diagram shows a partially overlap between the main concentration of the Transacqua slag Pb-points and the cloud of the mine of Montefondoli (100 km North, Alto-Adige province).

Fig. 7.15: The Transacqua slags plotted in the $^{207}Pb/^{204}Pb$ vs $^{206}Pb/^{204}Pb$ contour plot coupled with the scattering plot of the Pb-isotopic values of the Montefondoli and Maso Erdemolo mines.

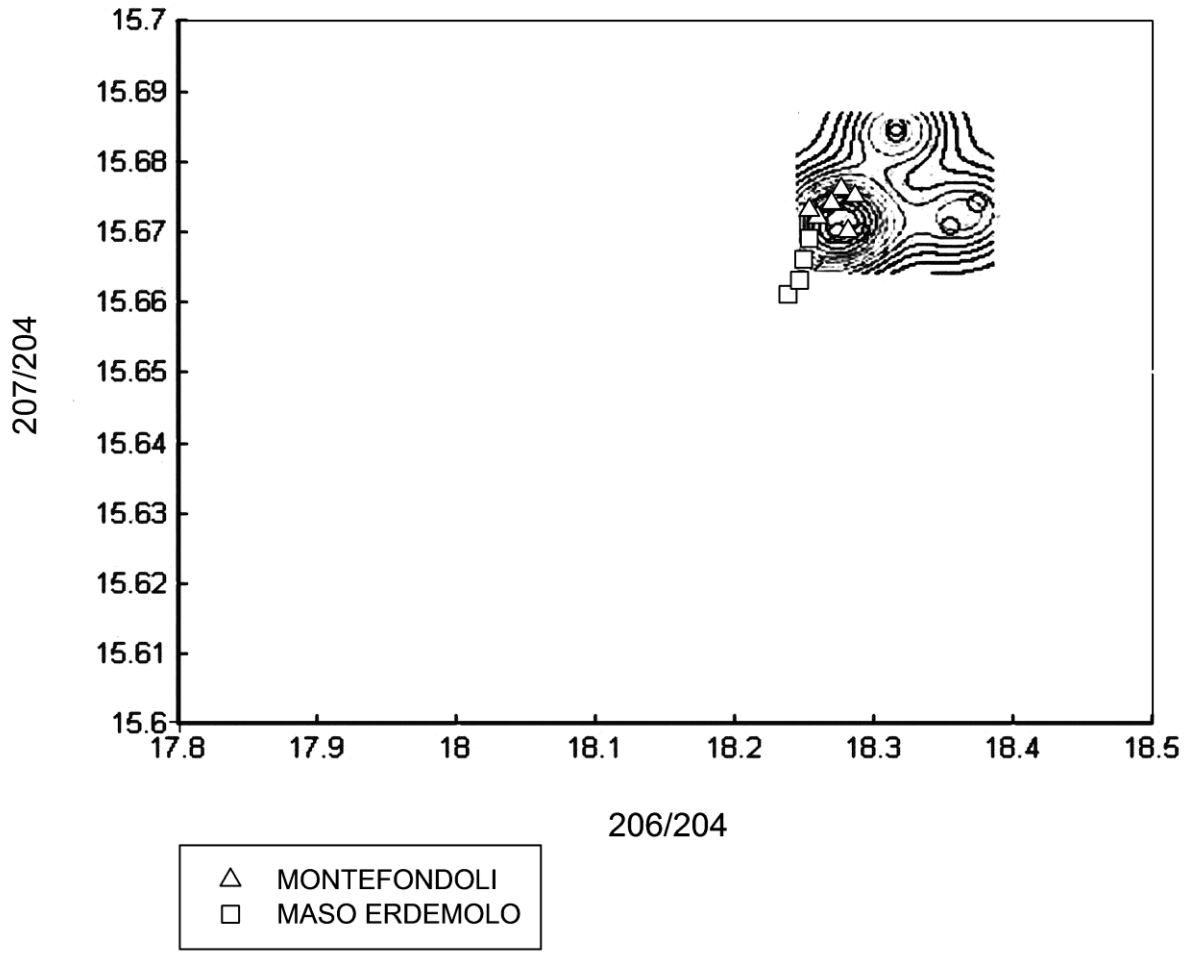

7.6.3 Lead Isotope Analyses of the Slags of Segonzano

The intermediate radiogenic group of the Segonzano slags is characterized by $^{206}Pb/^{204}Pb$ values in the range 18.19 – 18.24, by $^{207}Pb/^{204}Pb$ values ranging from 15.66 to 15.67 and by $^{208}Pb/^{204}Pb$ ratios between 38.42 and 38.47. Two slags of Segonzano called SEG-P14 and SEG-G4 are in the Luserna slag Pb-range. It has to be noticed that the $^{206}Pb/^{204}Pb$ ratios of SEG-G4 have the highest instrumental error, for that reason the interpretation of this measurement could be misleading.
The slags of Segonzano, like those of Transacqua, have lead ratios that are consistent with the first sub-group of the post-Variscan mines (Maso Erdemolo, Cinque Valli, Pamera mines).
Geographically, the Segonzano archaeological site is close to the Maso Furli mine, which belongs to the stratabound deposits in Upper Permian-Early Triassic sediments.

Fig.7.16: Map of the Segonzano and Luserna smelting sites and the mines studied by the AAcP project on the DEM of Trentino (pixel sizes=25x25 metres).

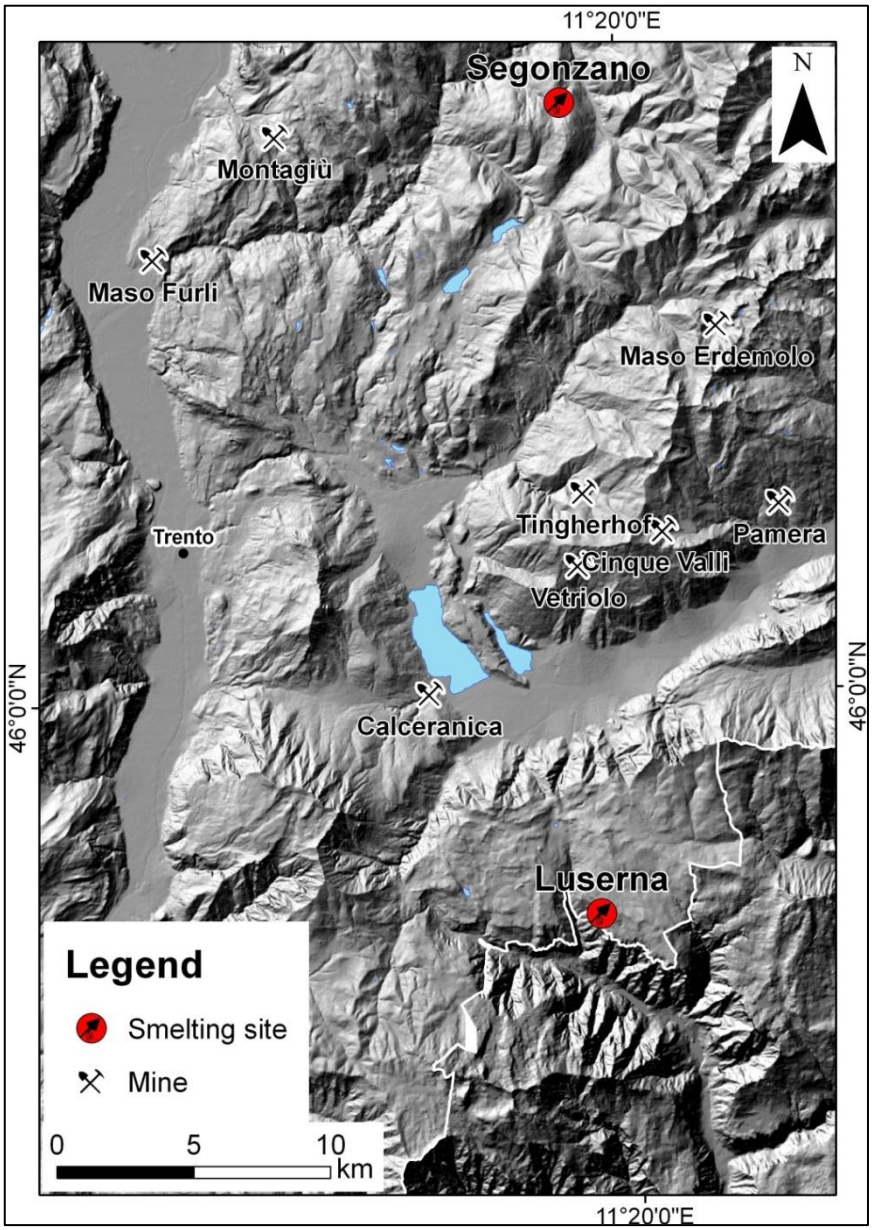

A close look to Fig. 7.17 reveals the isotopic correspondence between the Pamera, Maso Erdemolo and partially with Cinque Valli mines and the slags of Segonzano.

Fig. 7.17: Lead isotope data of the Segonzano slags and several significant mines of the Veneto Region. The analytical uncertainties for the samples are smaller than the size of the symbol.

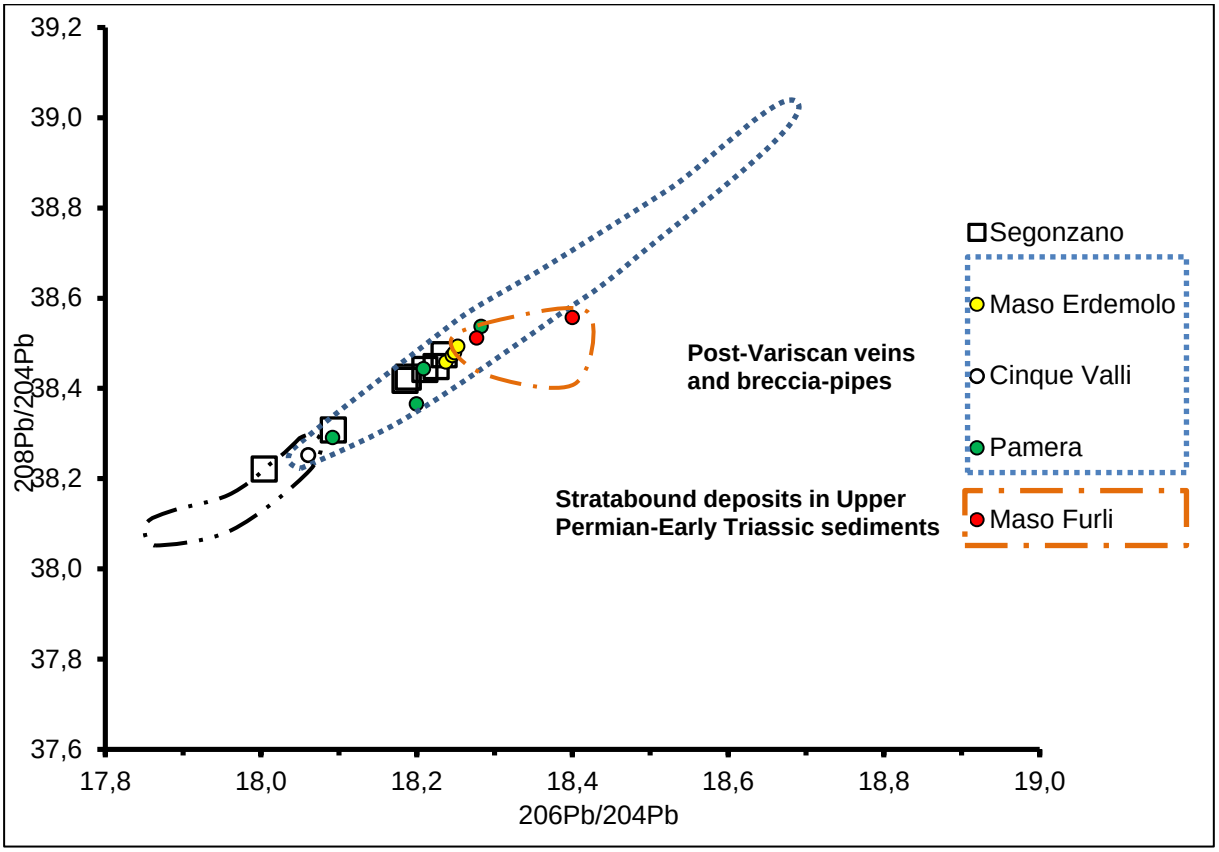

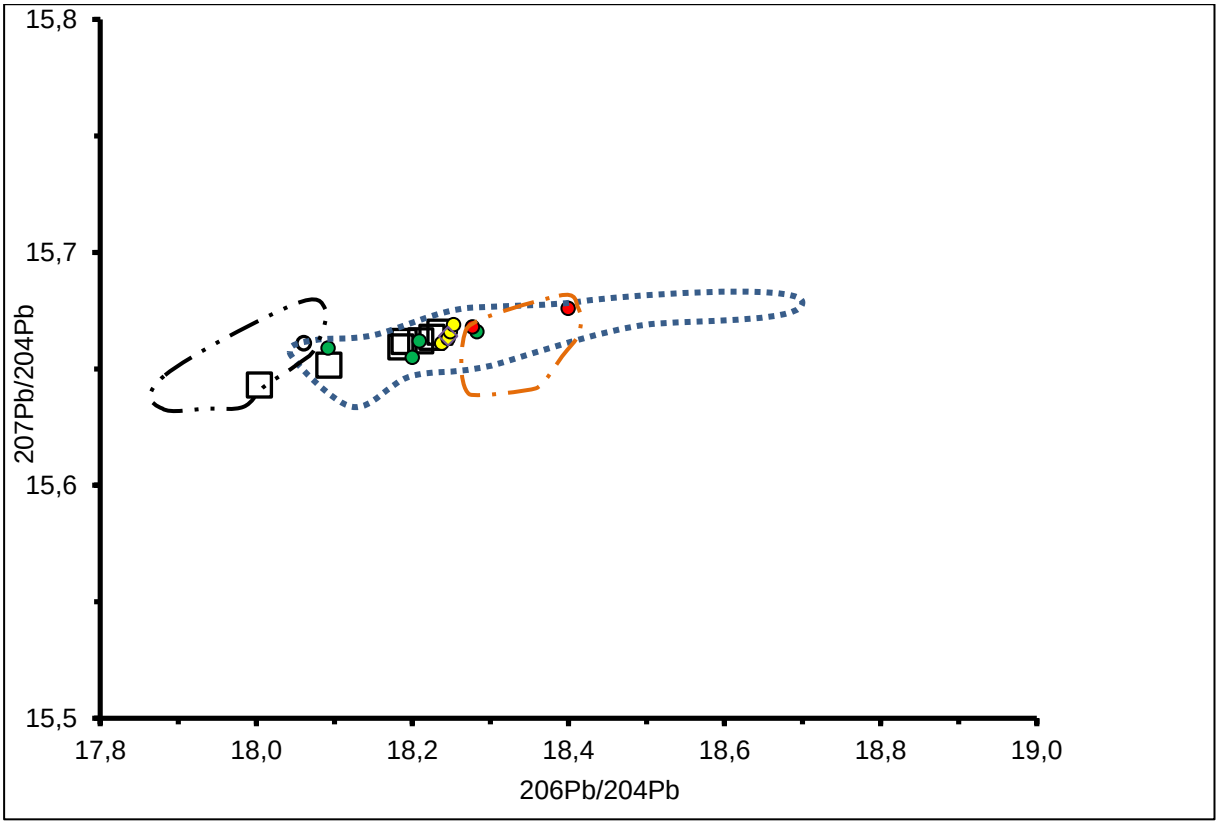

More in detail, the isotopic data of the Pamera and Maso Erdemolo mines reveals a good Pb-isotopic correspondence with the central density area of the contour plot of the Segonzano slags.

Fig. 7.18: The Segonzano slags plotted in the $^{207}Pb/^{204}Pb$ vs $^{206}Pb/^{204}Pb$ contour plot coupled with the scattering plot of the Pb-isotopic values of the Pamera and Maso Erdemolo mines.

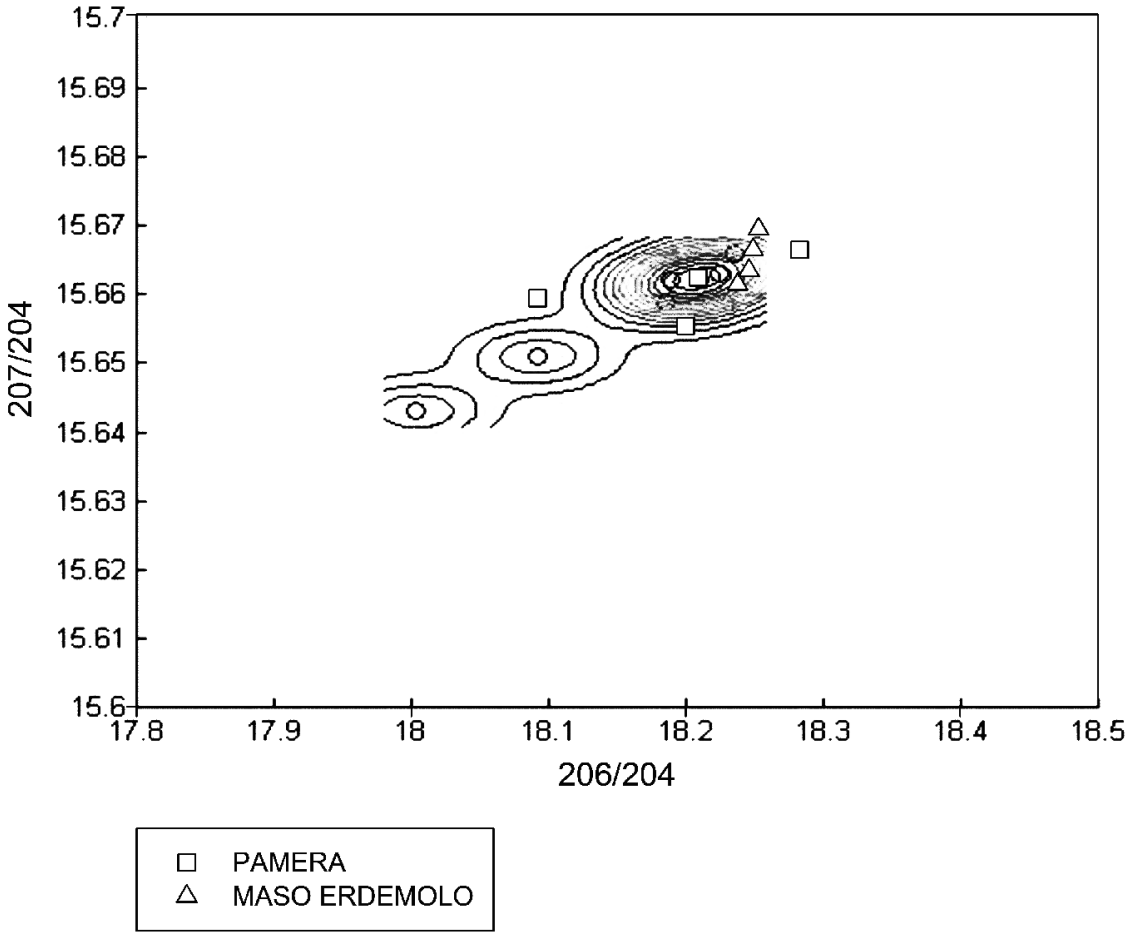

7.7 Discussion and Conclusion

Isotopically, the charge used in the Luserna smelting site likely came from one of the three pre-Variscan deposits: Calceranica, Vetriolo and Valle Imperina.
In fact the other compared mines, such as Tingherla, Maso Erdemolo (Val dei Mocheni) and Pamera, have a completely different isotopic signal. Contrary to those affirmed by Preuschen (1973), the unique data of the Cinque Valli mine should not be taken into account because no evidence of copper sulphide outcrops were found (Barillari et al., 1966). Due to its large distance from Luserna, it was also excluded the Valle Imperina mine. The other two pre-Variscan mines: Calceranica and Vetriolo are both located in the Valsugana, near the smelting site, and were possibly exploited in the Prehistory, as declared by Preuschen (1973).
Geographically, it is more likely that the mine source was Calceranica because of its lower altitude (500 m), than the Vetriolo mine, which is situated at a height of 1650 metres (Fig. 7.20). Regarding the ore source, it is likely that the Luserna site was supplied from only one mining area during the whole metallurgical activity.
As for the Transacqua site (Primiero Area, North of Valsugana), the mines of Valle Imperina and Pattine both located in the Val del Mis are geographically close to the site (Fig. 7.20) but have a different isotopic compositions. The mine of Maso Erdemolo, situated in Val dei Mocheni, is close to the Transacqua site but does not has a comparable isotopic signature. The Montefondoli mine (Valle Isarco, Province of Bolzano) is the only mine studied by the AAcP that has a comparable isotopic signature to the Transacqua slags but it is located at about 100 km to the North of the site, therefore cannot be the ore-source mine.
There are several mines around both the Val dei Mocheni and the Primiero Area, such as Pralongo, Castelpietra and Col Santo (Preuschen, 1973; Pearce,2007) that have not been analysed by the AAcP yet. Further analytical investigations are needed in order to verify the ore source for the smelting site of Transacqua
The source of the Segonzano smelting site is compatible with the Valsugana mine of Pamera (Pacheri, altitude 980 m) and the Val dei Mocheni mine of Maso Erdemolo. These two mines were both exploited in the Prehistory (Preuschen, 1973).
Other mines geographically close to the site, such as Furli di Lavis, do not match well with the isotopic field of the Segonzano slags. The Cinque Valli mine, as said above, has not been considered because unlikely was exploited in the Prehistory.
Other mines geographically close, such as Furli di Lavis, do not match well with the isotopic field of the Segonzano slags. However, it cannot be excluded that other exploited mines in the Valsugana or in the Val dei Mocheni supplied the Segonzano site. For this reason supplementary isotopic data from the other mines exploited in the Bronze Age will be required.
In conclusion, the large sample size of the Luserna slags and of the pre–Varisican deposits allowed to locate the source of the ore smelted with a certain precision.
However, the results are not always clear. In fact there are still provenance doubts for the Transacqua and Segonzano sites, which are characterized by small sample sizes.
These doubts will be likely solved by improving the isotopic data and using the trace element analysis, which is currently in progress.

Fig. 7.19: The three smelting sites and several mines studied by the AAcP with the relative distances in kilometres (coloured concentric circles), .

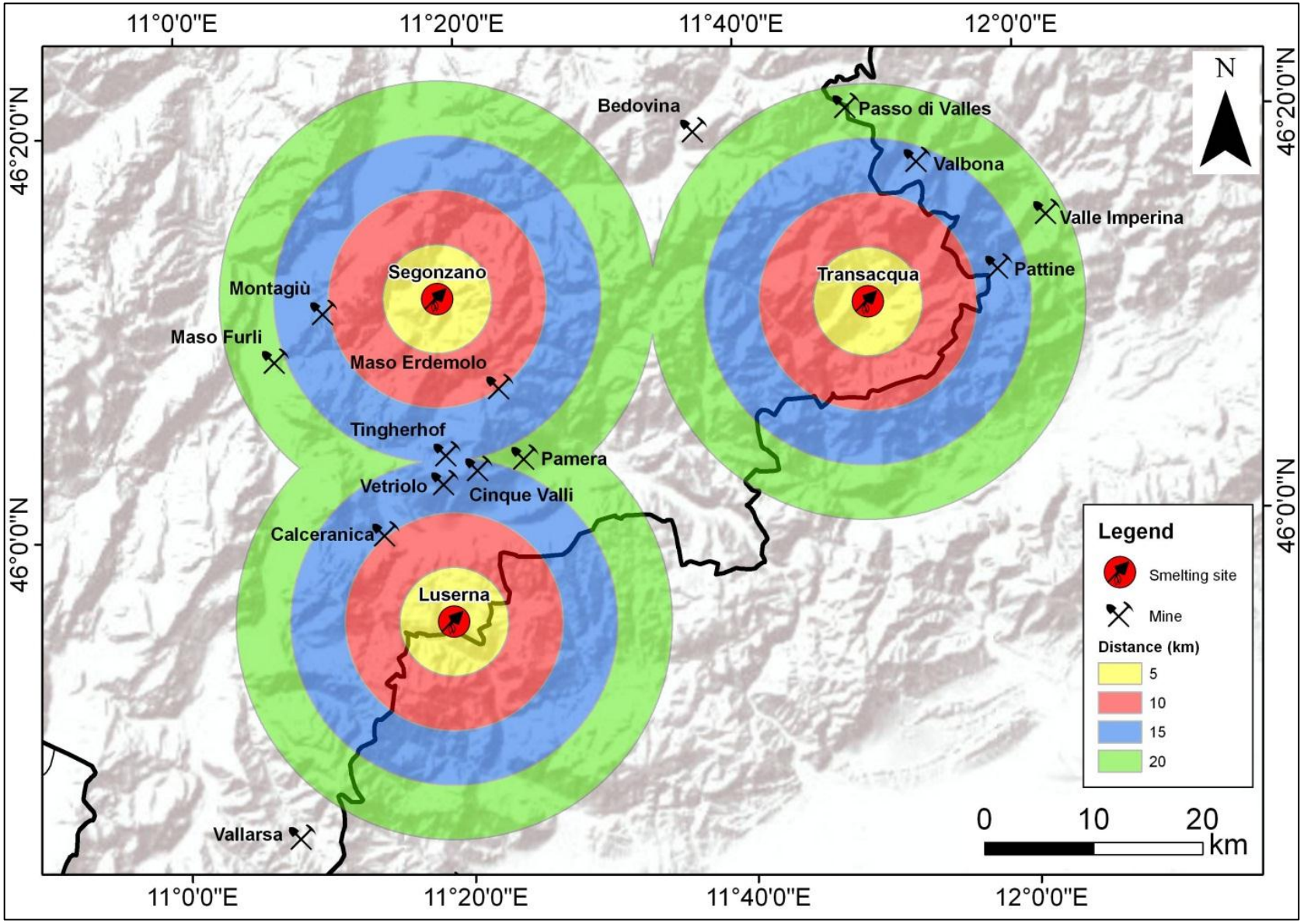

Tab. 7.5: List of the deposits studied by the AAcP with the isotopic lead ratios, as in the work of Nimis et al. (2012), and new data from the Calceranica mine.

DEPOSIT	SAMPLE	REGION	AREA	DEPOSIT TYPE	$^{206}Pb/^{204}Pb$	2SE	$^{207}Pb/^{204}Pb$	2SE	$^{208}Pb/^{204}Pb$	2SE
CALCERANICA	**CALC-1**	TRENTINO	Valsugana	STRATIFORM MASSIVE SULPHIDE (PRE-VARISICAN)	17,905	0,002	15,646	0,002	38,125	0,005
	CALC-2	TRENTINO	Valsugana	STRATIFORM MASSIVE SULPHIDE (PRE-VARISICAN)	17,911	0,002	15,641	0,002	38,119	0,006
	CALC-3	TRENTINO	Valsugana	STRATIFORM MASSIVE SULPHIDE (PRE-VARISICAN)	17,922	0,002	15,641	0,002	38,136	0,008
	CALC-4	TRENTINO	Valsugana	STRATIFORM MASSIVE SULPHIDE (PRE-VARISICAN)	17,972	0,002	15,640	0,002	38,145	0,006
	M1200	TRENTINO	Valsugana	STRATIFORM MASSIVE SULPHIDE (PRE-VARISICAN)	17,897	0,002	15,640	0,001	38,099	0,004
	CAL 5	TRENTINO	Valsugana	STRATIFORM MASSIVE SULPHIDE (PRE-VARISICAN)	17,9879	0,002	15,6425	0,0021	38,1999	0,0056
	CALC 6	TRENTINO	Valsugana	STRATIFORM MASSIVE SULPHIDE (PRE-VARISICAN)	17,8829	0,002	15,6385	0,0022	38,0950	0,0062
	CALC7	TRENTINO	Valsugana	STRATIFORM MASSIVE SULPHIDE (PRE-VARISICAN)	17,8991	0,002	15,6435	0,0022	38,1199	0,0071
VETIOLO	**VET-0**	TRENTINO	Valsugana	STRATIFORM MASSIVE SULPHIDE (PRE-VARISICAN)	17,883	0,001	15,640	0,002	38,094	0,004
	VET-2p	TRENTINO	Valsugana	STRATIFORM MASSIVE SULPHIDE (PRE-VARISICAN)	17,880	0,001	15,640	0,001	38,097	0,004
	VET2sp	TRENTINO	Valsugana	STRATIFORM MASSIVE SULPHIDE (PRE-VARISICAN)	17,887	0,002	15,643	0,002	38,100	0,006
	VET-p3c	TRENTINO	Valsugana	STRATIFORM MASSIVE SULPHIDE (PRE-VARISICAN)	17,886	0,002	15,643	0,002	38,106	0,006
	VET-p3s	TRENTINO	Valsugana	STRATIFORM MASSIVE SULPHIDE (PRE-VARISICAN)	17,885	0,002	15,642	0,002	38,101	0,006

DEPOSIT	SAMPLE	REGION	AREA	DEPOSIT TYPE	$^{206}Pb/^{204}Pb$	2SE	$^{207}Pb/^{204}Pb$	2SE	$^{208}Pb/^{204}Pb$	2SE
VALLE IMPERINA	**VI03p1**	VENETO	Agordino	STRATIFORM MASSIVE SULPHIDE (PRE-VARISICAN)	17,985	0,002	15,663	0,002	38,158	0,006
	VI04p1	VENETO	Agordino	STRATIFORM MASSIVE SULPHIDE (PRE-VARISICAN)	17,973	0,002	15,659	0,002	38,145	0,006
	VI-05	VENETO	Agordino	STRATIFORM MASSIVE SULPHIDE (PRE-VARISICAN)	18,029	0,003	15,672	0,003	38,227	0,007
	VI-06	VENETO	Agordino	STRATIFORM MASSIVE SULPHIDE (PRE-VARISICAN)	18,029	0,004	15,661	0,004	38,208	0,008
	VI-07	VENETO	Agordino	STRATIFORM MASSIVE SULPHIDE (PRE-VARISICAN)	17,972	0,002	15,651	0,002	38,120	0,007
	VI-08	VENETO	Agordino	STRATIFORM MASSIVE SULPHIDE (PRE-VARISICAN)	18,054	0,002	15,661	0,002	38,243	0,007
	VI-09	VENETO	Agordino	STRATIFORM MASSIVE SULPHIDE (PRE-VARISICAN)	18,067	0,002	15,677	0,002	38,283	0,005
PAMERA	**P28**	TRENTINO	Valsugana	BRECCIA PIPE	18,200	0,003	15,655	0,006	38,365	0,006
	P3	TRENTINO	Valsugana	BRECCIA PIPE	18,283	0,002	15,666	0,002	38,537	0,006
	PA6	TRENTINO	Valsugana	BRECCIA PIPE	18,209	0,004	15,662	0,004	38,443	0,011
	PAM-1	TRENTINO	Valsugana	BRECCIA PIPE	18,092	0,002	15,659	0,002	38,291	0,006
CINQUE VALLI	**5VA 1p**	TRENTINO	Valsugana	SULPHIDE-RICH VEIN SYSTEM	18,061	0,003	15,661	0,003	38,252	0,008
MONTEFONDOLI	**CD-a-11**	ALTO ADIGE	Valle Isarco	SULPHIDE-RICH VEIN SYSTEM	18,259	0,002	15,672	0,002	38,501	0,005
	MFO_Ap1	ALTO ADIGE	Valle Isarco, Chiusa	SULPHIDE-RICH VEIN SYSTEM	18,253	0,002	15,673	0,002	38,520	0,005
	MFO_Ap2	ALTO ADIGE	Valle Isarco, Chiusa	SULPHIDE-RICH VEIN SYSTEM	18,276	0,003	15,676	0,003	38,550	0,008
	MFO_Ap3	ALTO ADIGE	Valle Isarco, Chiusa	SULPHIDE-RICH VEIN SYSTEM	18,286	0,002	15,675	0,003	38,500	0,008
	MFO-KW	ALTO ADIGE	Valle Isarco, Chiusa	SULPHIDE-RICH VEIN SYSTEM	18,281	0,001	15,670	0,001	38,518	0,002
	MFO-MU	ALTO ADIGE	Valle Isarco, Chiusa	SULPHIDE-RICH VEIN SYSTEM	18,269	0,002	15,674	0,002	38,514	0,006

DEPOSIT	SAMPLE	REGION	AREA	DEPOSIT TYPE	$^{206}Pb/^{204}Pb$	2SE	$^{207}Pb/^{204}Pb$	2SE	$^{208}Pb/^{204}Pb$	2SE
MASO ERDEMOLO	**GRUA_Cp1**	TRENTINO	Val dei Mocheni	SULPHIDE-RICH VEIN STOCWORK	18,238	0,002	15,661	0,002	38,458	0,006
	GRUA_Ddxp1	TRENTINO	Val dei Mocheni	SULPHIDE-RICH VEIN STOCWORK	18,246	0,002	15,663	0,002	38,472	0,004
	GRUA_Dsxp1	TRENTINO	Val dei Mocheni	SULPHIDE-RICH VEIN STOCWORK	18,249	0,001	15,666	0,002	38,479	0,004
	GRUA_Ep1	TRENTINO	Val dei Mocheni	SULPHIDE-RICH VEIN STOCWORK	18,253	0,001	15,669	0,002	38,493	0,004
MONTAGIU'	**MOND-1**	TRENTINO	Val d'Adige	SULPHIDE-RICH VEIN	18,405	0,001	15,677	0,002	38,672	0,006
	MOND-2	TRENTINO	Val d'Adige	SULPHIDE-RICH VEIN	18,417	0,003	15,676	0,004	38,682	0,008
	MOND-3	TRENTINO	Val d'Adige	SULPHIDE-RICH VEIN	18,405	0,002	15,677	0,003	38,676	0,008
TINGHERHOF	**TING-1**	TRENTINO	Valsugana	FLUORITE-RICH VEIN	18,372	0,002	15,671	0,002	38,633	0,006
	TING-2	TRENTINO	Valsugana	FLUORITE-RICH VEIN	18,465	0,002	15,671	0,002	38,738	0,006
VALLARSA SASSO NEGRO	**VAL-2**	TRENTINO	Vallarsa	FLUORITE-RICH VEIN	18,825		15,703		38,867	
	VAL-p1	TRENTINO	Vallarsa	FLUORITE-RICH VEIN	19,886		15,758		39,361	
	VAL-p3	TRENTINO	Vallarsa	FLUORITE-RICH VEIN	18,756		15,690		38,629	
PATTINE	**PA-02i**	VENETO	Agordino	REMOBILIZATION VEINS	18,800	0,002	15,681	0,002	38,840	0,004
	PA05i	VENETO	Agordino	REMOBILIZATION VEINS	18,419	0,008	15,681	0,008	38,545	0,010
	PA-09i	VENETO	Agordino	REMOBILIZATION VEINS	18,496	0,002	15,674	0,002	38,615	0,004
	PAT_P1	VENETO	Agordino	REMOBILIZATION VEINS	18,500	0,004	15,667	0,003	38,587	0,008
	PAT_P2	VENETO	Agordino	REMOBILIZATION VEINS	18,522	0,003	15,669	0,004	38,606	0,010
	PAT_P3	VENETO	Agordino	REMOBILIZATION VEINS	18,329	0,003	15,681	0,003	38,485	0,008
	PAT-BOR	VENETO	Agordino	REMOBILIZATION VEINS	18,038	0,002	15,676	0,002	38,248	0,010

DEPOSIT	SAMPLE	REGION	AREA	DEPOSIT TYPE	$^{206}Pb/^{204}Pb$	2SE	$^{207}Pb/^{204}Pb$	2SE	$^{208}Pb/^{204}Pb$	2SE
MASO FURLI	**LAV-1**	TRENTINO	Val d'Adige	CARBONATE-HOSTED STRATABOUND	18,400	0,002	15,676	0,002	38,557	0,007
	LAV-2	TRENTINO	Val d'Adige	CARBONATE-HOSTED STRATABOUND	18,277	0,002	15,668	0,002	38,511	0,006

VIII – General Conclusion

The results of the physical, mineralogical and petrographic analyses on the Luserna, Transacqua and Segonzano slags lead to exclude the presence of one single metallurgical step of copper extraction in LBA eastern Alpine smelting process.
The different proportions of the unreacted minerals versus the newly formed phases and the abundance of metallic copper into the three different groups, indicate a smelting process performed in three standardised steps, two of smelting and one of refining, related to different levels of matte enrichment, copper reduction and separation efficiency.
This interpretation partially diverge to the models proposed so far, in which only two smelting steps are assumed, the first related to the production of the cake/coarse slags and the second associated with the presence of the Plattenschlake/flat slags.
In this frame, the new typological group of slags referred as massive plays an important role to the understanding of the process.
Further analysis of the slags excavated from other Alpine smelting Bronze Age sites are needed to confirm the widespread presence of this typological group of slags during the LBA.
The charge used for the smelting in Luserna, Transacqua and Segonzano was essentially chalcopyrite.
The mine source for the Luserna slags came from two possible sources, Calceranica and Vetriolo mines.
Further analytical investigation are needed to identify the mines that supplied the smelting sites of Transacqua and Segonzano, that likely were situated in the Valsugana and Val dei Mocheni areas, respectively.

Acknowledgments

I thank the Soprintendenza per i Beni Librari Archivistici e Archeologici della Provincia Autonoma di Trento, especially in the persons of Dr. Franco Nicolis and Dr. Paolo Bellintani for allowing us to study the site's materials. I am grateful Elena Silvestri for collaboring in the selection of the samples and in the early measurements of the density.

I would also like to thank the following people from the Department of Geoscience of Padua University for helping us during the analysis: Mr Stefano Castelli, Dr. Federico Zorzi, Mr Leonardo Tauro, Dr. Daria Pasqual, Dr. Luca Peruzzo, Dr. Aurelio Giaretta, P.I. Sandra Boesso, Emanuela, Danieletto, Dr. Carlo Vinante, Dr. Giancarlo Cavazzini and Dr. Elena Masiero.

Finally, I thank the Cassa di Risparmio di Padova e Rovigo for the financial support.

IX - BIBLIOGRAPHY

Addis A., Angelini I., Artioli, G. 2012. Final Bronze Age copper slags from Luserna (Trentino, Italy). Atti VII Congresso Nazionale di Archeometria. Conference Proceeding on CD.

Amov, B., B. Kolkovski, R. Dimitrov. 1993. Hydrothermal ore mineralisation in the Rhodope metallogenetic zone on the basis of the isotopic composition of lead in galena, Annuaire de l'Universte de Sofia „St. Kliment Ochridski", Faculte de Geologie et Geographie, Livre 1-Geologie, Tome 85, 73-98, and references quoted therein.

Amov B. G. 1999.Lead isotope data for ore deposits from Bulgaria and the possibility for their use in archaeometry. Berliner Beitrage zur Archaometrie, 16, 5-19.

Anguilano L., Angelini I., Artioli G., Moroni M., Baumgarten B., Oberrauch H., 2002. Smelting slags from Copper and Bronze Age archaeological sites in Trentino and Alto Adige. Proceedings for the II Congresso Nazionale di Archeometria (A.i.A.r), ed. by D'Amico C., 29 January – 1 February 2002, Bologna, 627-638.

Artioli, G., Angelini, I., Giunti, I., Omenetto, P., Villa, I.M. 2009. La provenienza del metallo degli oggetti di Monte Cavanero: considerazioni basate sugli isotopi del Pb e sulla geochimica delle mineralizzazioni cuprifere limitrofe. In: Venturino Gambari, M. (Ed.), Il ripostiglio del Monte Cavanero di Chiusa di Pesio (Cuneo). LineLab.Edizioni, Alessandria, pp. 167e178.

Artioli G., Baumgarten B.,Marelli M., Giussani B., Recchia S., Nimis P., Giunti I., Angelini I., Omenetto P. 2008. Chemical and isotopic tracers in alpine copper deposits: geochemical links between mines and metal. Geo Alp. 5:139-148.

Artioli G., Giunti I., Angelini I., Gruppo ARCA, Giussani B., Marelli M., Recchia S., Nimis P., Omenetto P., Villa I.M. 2010. Legami geochimici tra miniere scorie e metallo: verso un modello per determinare la provenienza e la diffusione del rame preistorico. FRAMMENTI n.2: Conoscere e tutelare la natura Bellunese. Provincia di Belluno Editore.

Bachmann H. G. 1982. The identification of slag from archaeological sites. Occasional Pubblication No.6. Published by the Institute of Archaeology, 31-34 Gordon Square, London, WC1H 0PY.

Barillari A., Jobstraibizer P.G., Omenetto P. 1966. Il giacimento a piombo, zinco e rame di Cinque Valli in Valsugana (Trentino). Symposium internazionale sui giacimenti minerari delle Alpi. Trento – Mendola, 11-19 settembre 1966.

Baron, S., Carignan, J., Laurent, S., Ploquin, A. 2006. Medieval lead making on Mont-Lozere Massif (Cevennes-France): Tracing ore sources using Pb isotopes. Applied Geochemistry 21, 241-252.

Baron S., Tamas C.G., Cauuet B., Munoz M. 2011. Lead isotope analyses of gold-silver ores from Rosia Montana (Romania): a first step of a metal provenance study of Roman mining activity in Alburnus Maior (Roman Dacia). Journal of Archaeological Science, 38(5), 1090-1100.

Barton P.B., Skinner B.J. 1967. Sulfide mineral stabilities. In: Geochemistry of Hydrothermal Ore Deposits. Barnes H.L. (ed.) New York: Holt, Rinehart and Winston, pp. 236-333.

Baxter M. J., Beardah C. C., Westwood S. 2000. Sample Size and Related Issues in the Analysis of Lead Isotope Data. Journal of Archaeological Science (2000) 27, 973–980.

Baxter M. J., Cool H.E.M. 2010. Detecting modes in low-dimensional archaeological data. Journal of Archaeological Science 37, pp. 2379-2385.

Begemann F., Schmitt-Strecker S., Pernicka E., Lo Schiavo F. 2001. Chemical composition and lead isotope of copper and bronze from Nuragic Sardinia. European Journal of archaeology, 4, 43-85.

Belshaw N. S., Freedman P. A., O'Nions R. K., Frank M., and Guo Y. 1998. A new variable dispersion double-focussing plasma mass spectrometer with performance illustrated for Pb isotopes. Int. J. Mass Spec. Ion. Proc. 181, 51–58.

Bellintani P., Mottes E., Nicolis F., Silvestri E., Stefan L., Bassetti M., Degasperi N., Cappellozza N. 2009. New Evidence of Archaeometallurgical Activities During the Bronze Age in Trentino. Proceedings for the 1st Mining in European History-Conference of the SFB-HIMAT, 12.–15. November 2009, Innsbruck.

Bird G., Brewer P.A., Macklin M.G., Nikolova M., Kotsev T., Mollov M., Swain C. 2010. Quantifying sediment-associated metal dispersal using Pb isotopes: Application of binary and multivariate mixing models at the catchment-scale. Environmental pollution 158, 2158-2169.

Boni M., Koeppel V. 1985. Ore-lead isotope pattern from the Inglesiente-Sulcis Area (SW Sardinia) and the problem of remobilization of metals. Mineralium Deposita 20, 185-193.

Brevart, O.; Dupre, B.; Allegre, C.J. 1982. Metallogenic provinces and the remobilisation process studies by lead isotopes; lead-zinc ore deposits from the southern Massif Central, France. Economic Geology 77/3: 564-575.

Brill R.H., Wampler J.M. 1965. Isotope studies of ancient lead. American Journal of Archaeology 69:165–166.

Brill R.H., Wampler J.M. 1967. Isotope studies of ancient lead. American Journal of Archaeology 71:63–77.

Burger E., Bourgarit D., Rostain P., Corazza L., Artioli G. 2007. The mystery of Plattenschlacke in protohistoric copper smelting: early evidence at the early bronze age site of Saint Veran, French Alps. Proceedings for the II International Conference Archaeometallurgy in Europe, Aquileia, 17-21 June 2007, pre-conference on cd.

Campbell F.C. 2012 Phase Diagrams. Understanding the basics. ASM International. pp. 463.

Canals A., Cardellach E. 1997. Ore lead and sulphur isotope pattern from the low-temperature veins of the Catalonian Coastal Ranges (NE Spain). Mineralium Deposita, 32: 243-249.

Carancini G.L., Peroni R. 1997. La koinè metallurgica. Catalogo Mostra: Le terramare. La più antica civiltà padana. M. Barbabò Brea, A. Cardarelli, M. Cremaschi, Modena, Foro Boario 15-1 giugno. Milano 1997. Pp. 595-601.

Carancini G.L., Peroni R. 1999. L'Età del Bronzo in Italia: per una cronologia della produzione metallurgica. Quaderni di Protostoria 2, 1999. Pp. 1-85.

Cattin F., Guénette-Beck B., Curdy P., Meisser N., Ansermet S., Hofmann B., Kündig R., Hubert V., Wörle M., Hametner K., Günther D., Wichser A., Ulrich A., Villa I.M, Besse M. 2011. Provenance of Early Bronze Age metal artefacts in Western Switzerland using elemental and lead isotopic compositions and their possible relation with copper minerals of the nearby Valais. Journal of Archaeological Science 38 (2011) 1221e1233.

Cattin F., Guénette-Beck B., Besse M., Serneels V. 2009. Lead isotopes and archaeometallurgy. Archaeological and Anthropological Sciences 1:137–148.

Cattoi E., D'Amico C., Fabbris S. 1995. Studio petroarcheometrico di scorie di fusione della fine dell'Età del Bronzo e confronti con scorie dell'Età del Rame/Bronzo Antico in Trentino. Preistoria Alpina v. 31 (1995), 125-145

Cierny J. 2008. Prähistorische Kupferproduktion in den südlichen Alpen: Region Trentino Orientale. Der Anschnitt, Beiheft ; 22. Bergbau-Museum, 248 pages.

Cierny J., Marzatico F., Perini R., Weisgerber G. 2004. La riduzione del rame in località di Acqua Fredda al Passo del Redebus (Trentino) nell'età del Bronzo Recente e Finale.

Alpenkpfer, Rame delle Alpi. Der Anschnitt , Benihefl 17. Bergbau-Museum. Pp. 125-154.

Cui, J., Wu, X. 2011. An experimental investigation on lead isotopic fractionation during metallurgical processes. Archaeometry 53, 1 (2011) 205–214.

Curti E. 1987. Lead and oxygen isotope evidence for the origin of the monte rosa gold lode deposits (western alps, Itali): a comparison with archean lode deposits. Economic geology, 82, 2115-2140.

Dayton J.E., Dayton A. 1986. Uses and limitations of lead isotopes in archaeology. Proceedings of the 24th International Archaeometry Symposium, eds. J.S. Olin & M.J. Blackman. Smithsonian Institution Press, Washington D.C. pp. 13-41.

De Guio A. 1994. L'altopiano di Asiago dal Bronzo Medio all'inizio dell'Età del Ferro. In: Storia dell'Altopiano dei Sette Comuni. Territorio e Istituzioni. pp. 157-178.

Donaldson C.H., 1976. An experimental investigation of olivine morphology. Contrib. Mineral. Petrol., 57, 187-213.

Duncan D. B. 1955. Multiple Range and Multiple F Test. Biometrics Vol. 11, No. 1, Mar. 1995. pp 1-42.

Faure, G. 1986. Principles of Isotope Geology. John Wiley, New York (2nd edn.).

Gale, N.H.; Stos-Gale, Z.A.; Maliotis, G.; Annetts, N. 1997a. Lead isotope data from the Isotrace Laboratory, Oxford: Archaeometry data base 4, ores from Cyprus. Archaeometry 39 (1): 237-246.

Gale, N.H.; Stos-Gale, Z.A.;Fasnacht, W. 1997b. Movable finds: metal and metalworking in Alambra, a Middle Bronze Age site in Cyprus". In J.E. Coleman, J.A. Barlow, M.K. Mogelonsky and K.W. Schaar (eds.): Investigations by Cornell University 1974-1985. 129-41 and 371-438.

Gale N.H., Stos-Gale Z.A., Radouncheva A., Ivanov I.,Lilov P., Todorov T., Panayotov I. 2000. Early metallurgy in Bulgaria. In: Annuary of department archaeology, volume 4–5. New Bulgarian University, Institute of Archaeology with Museum, Bulgarian Academy of Sciences, Sofia, pp 102–168.

Gale, N. H., and Stos-Gale, Z. A. 2000. Lead isotope analyses applied to provenance studies, in Modern analytical methods in art and archaeology. eds. E. Ciliberto and G. Spoto, 503–84, Chemical Analyses Series 155, JohnWiley & Sons, Inc., New York.

Giunti I. 2011. Geochemical and isotopic tracers in copper deposits and ancient artifacts: a database for provenance. Ph.D. dissertation. University of Padua, Department of Geoscience. 1-208.

Guenette-Beck B., Meisser N., Curdy P. 2009. New insights into the ancient silver production of the Wallis area, Switzerland. Archaeol. Anthropol Sci, 1, 215-229.

Hamelin, B., Dupre B., Brevart O., Allegre C.J. 1988 Metallogenesis at Paleo-spreading centers: lead isotopes in sulfides, rocks and sediments from the Troodos ophiolite (Cyprus) Chemical Geology 68: 229-238.

Hauptmann, A.; Begemann, F.; Heitkemper, R.; Pernicka, E.; Schmitt-Strecker, S. 1992. Earlycopper produced in Feinan, Wadi Araba, Jordan:the composition of ores and copper. Archeomaterials 6 (1): 1-33.

Herdits H. 2003. Bronze Age smelting site in the Mitterberg mining area in Austria. In Mining and metal production – Through the Ages ed. by Craddock P., Lang J., The British Museum press, London 2003, 69-75.

Hirao, Y.; Enomoto, J.; Tachikawa, H. 1995. Lead isotope ratios of copper, zinc and lead minerals in Turkey in relation to the provenance study of artefacts. In H.I.H. Prince Takahito Mikasa (ed.): Essays on Ancient Anatolia and its surrounding civilisations. Harrassovitz Verlag, Wiesbaden. 89-114.

Hirata, T., 1996. Lead isotopic analysis of NIST standard reference materials using multiple collector-inductively coupled plasma mass spectrometry coupled with modified external correction method for mass discrimination effect. The Analyst 121, 1407e1411.

Höppner B., Bartelheim M., Huijsmans M., Krauss R., Martinek K., Pernicka E., Schwab R. 2005. Prehistoric copper production in the Inn Valley (Austria), and the earliest copper in central Europe. Archaeometry 47(2):293–315.

Horner J., Neubauer F., Paar W.H., Hansmann W., Koeppel V., Robl K. 1997. Structure, mineralogy, and Pb isotopic composition of the As-Au-Ag deposit Rotgulden, Eastern Alps (Austria): signicance for formation of epigenetic ore deposits within metamorphic domes.Mineralium Deposita, 32: 555-568.

Horwitz, E.P., Chiarizia, R., Dietz, M.L. (1992): A novel strontiumselective extraction chromatographic resin. Solvent Extr. Ion Exch., 10, 313–336.

Hunt-Ortiz, M.A. 2003. Prehistoric Mining and Metallurgy in South-West Iberian Peninsula. BAR International Series 1188.

Ineson P.R. 1989. Introduction to practical ore microscopy. Longman Scientific & Technical (Harlow, Essex, England and New York) 181 pages.

Jung R., Mehofer M., and Pernicka E. 2011. Metal Exchange in Italy from the Middle to the Final Bronze Age (14th–11th Century B.C.E.). Metallurgy: Understanding How Learning WhY. Studies in Honor of James D. Muhly edited by Philip P. Betancourt and Susan C. Ferrence. Prehistory Monographs 29, 231-248. INSTAP Academic Press.

Klein, S.; Domergue, C.; Lahaye, Y.; Brey, G.P.; Von LKaenel, H.-M. 2009. The lead and copper isotopic composition of copper ores from the Sierra Morena (Spain). Journal of Iberian Geology 35 (1): 59-68.

Koppel V., Schroll E. 1983a. Lead isotopes of paleozoic, stratabound to stratiform galena bearing sulfide deposits of eastern alps (Austria): implications for their geotectonic setting: Schweiz. Mineral. Petrogr. Mitt. v. 63, p. 347-360.

Koppel V., Schroll E. 1985. Herkunft des Pb der triassichen Pb-Zn-Vererzungen in den Ost- und Su¨dalpen. Arch. Lagersta¨ttenforschung Geol. Bund., 6, 215–222.

Lattanzi P., Hansmann W., Koeppel V., Costagliola P. 1992. Source of metals in Metamorphic Ore-forming Processes in the Apuane Alps (NW Tuscany, Italy): constraints by Pb-isotope Data. Mineralogy and petrology, 45, 217-229.

Le Guen, M.; Orgeval, J.-J. and Lancelot, J. 1991. Lead isotope behaviour in a polyphased Pb-Zn ore deposit: Les Malines (Cevennes, France). Mineral Deposits 26: 180-188.

Lepitre M.E., Allen D.M. 2003. Differentiating sources of dissolved lead in mine waters using lead isotope techniques, Sullivan Mine, British Columbia. Water Resources Research, Vol. 39, No. 1.

Lillo J. 1992. Vein type base metal ores in linares la carolina (Spain): ore lead isotopic constrains. European Journal of Mineralogy, 4, 337-343.

Ludwig K.R., Vollmer R., Turi B., Simmons K.R., Perna G. 1989. Isotopic constraints on the genesis of base-metal ores in southern and central Sardinia. European journal of mineralogy, 1, 657-666.

Marcoux E. 1998. Lead isotope systematics of the giant massive sulphide deposits in the Iberian Pyrite Belt. Mineralium Deposita, 33: 45 – 58.

Marcoux E., Grancea L., Lupulescu M., Milési J. 2002. Lead isotope signatures of epithermal and porphyry-type ore deposits from the Romanian Carpathian Mountains. Mineralium Deposita. Volume 37, Number 2, 173-184.

Macfarlane, A. 1999. The lead isotope method for tracing the sources of metal in archaeological artifacts: strengths, weaknesses and applications in the Western

Hemisphere, in Metals in antiquity. eds. S. M. M. Young, A. M. Pollard, P. Budd and R. A. Ixe. Pp: 310–16, Bar International Series 792, Archaeopress, Oxford.

Metten B., 2003. Beitrag zur spätbronzezeitlichen Kupfermetallurgie im Trentino (Südalpen) im Vergleich mit anderen prähistorischen Kupferschlacken aus dem Apenraum. METALLA (Bochum) 2003, 10 (1/2), 1-122.

McGill, R. A., Budd, P., Scaife, B., Lythgoe, P., Pollard, A. M., Haggerty, R., and Young, S. M. M., 1999, The investigation and archaeological applications of anthropogenic heavy metal isotope fractionation, in Metals in Antiquity. eds. S. M. M. Young, A. M. Pollard, P. Budd and R. Ixer. Pp: 258–61, Bar International Series 792, Archaeopress, Oxford.

Montero-Ruiz, I.; Castanyer, P.; Gener, M.; Hunt, M.; Mata, J.M.; Pons, H.; Rovira-Llorens, S.; Rovira- Hortala, C.; Renzi, M.; Santos-Retolaza, M.; Santos-Zalduegui, J.F. 2009a: Lead and silver metallurgy in Emporion (L'Escala, Girona, Spain). Proceedings of the 2nd International Conference on Archeometallurgy in Europe, Aquileia, Italy 2007. Cd-Rom proceedings.

Montero-Ruiz, I.; Gener, M.; Renzi, M.; Hunt, M.; Rovira, S.; Santos-Zalduegui, J.F. 2009b. Provenance of elad in first Iron Age sites in Southern Catalonia (Spain)". Proceedings ISA 2006. Eds. J.F. Moreau, R. Auger, J. Chabot and A. Herzog. Quebec. 391-398.

Morton G., Wingrove J. 1969. Constitution of bloomery slag. Part I: Roman. Journal of the Iron and Steel Institute 207: 1556–64.

Morton G., Wingrove J. 1972. Constitution of bloomery slag. Part II: Medieval. Journal of the Iron and Steel Institute 210: 478–88.

Nicolis F., Bellintani P., Artioli G., Cappellozza N. 2007. Archaeological excavation at Pletz von Mozze, Luserna, Trentino, Italy. A case of study for assessment of Late Bronze Age metallurgical activities. 2nd International Conference Archaeometallurgy in Europe 2007, 17-21 June, 2007. Aquileia Italy

Niederschlag E., Pernicka E., Seifert Th., Bartelheim M. 2003. The determination of lead isotopes ratios by multiple collector ICP-MS: a case of study of early bronze age artefacts and their possible relation with ore deposits of the Erzgebirge. Archaeometry 45, 1, 61 -100.

Nimis P., Omenetto P., Giunti I., Artioli G., Angelini I. Lead isotope systematics in hydrothermal sulphide deposits from the central-eastern Southalpine (northern Italy). Eur. J. Mineral. 2012, 24, 23-37.

Patterson, C.C., 1953. The isotopic composition of meteoritic, basaltic and oceanic leads, and the age of the Earth. Proceedings of the Conference on Nuclear Processes in Geologic Settings, Williams Bay, Wisconsin, September 21-23, 1953. pp. 36-40.

Pearce M.J. 2007. Bright Blades and Red Metal: Essays on north Italian prehistoric metalwork London: Accordia Research Institute.

Pearce M.J., De Guio A. 1999. Between the mountains and the plain: an integrated metals production and circulation system in later Bronze Age north-eastern Italy In: Prehistoric alpine environment, society and economy. Papers of the international colloquium PAESE 1997 in Zurich. 289-293

Perini R. 1988. Evidence of metallurgical activity in Trentino from Chalcolitich Times to the end of the Bronze Age. Atti del colloquio internazionale di Archeometallurgia: Archeometallurgia Ricerche e Prospettive. Bologna – Dozza Imolese. 18-21 ottobre 1988. Pp 53-59.

Pernicka E.; Begamen F.; Schmitt-Streckers S.; Torodova H.; Kuleff I. 1997. Prehistoric copper in Bulgaria, Eurasia Antiqua, Zeitschrift fur archaologie Eurasiens, Deutcsches Archaologischens Institut 3, 41-180.

Pernicka, E.; Begemann, F.; Schmitt-Strecker, S.; Wagner, G.A. 1993. Eneolithic and Early Bronze Age copper artefacts from the Balkans and their relation to Serbian copper ores. Praehistorisches Zeitschrift 68 (1): 1-54.

Pernicka, E.; Seeliger, T.C.; Wagner, G.A.; Begemann, F.; Schmitt-Strecker, S.; Eibner, C.; Õztunali, Õ.; Baranyi, I. 1984. Archäometallurgische Untersuchungen in Nordwestanatolien, Jahrbuch des Römisch-Germanischen Zentralmuseums 31: 533-99.

Pernicka E.,1999. Trace element fingerprinting of ancient copper: a guide to technology of provenance?. Young SMM, Pollard AM, Budd P, Ixter RA (eds). Metals in antiquity. BAR International Series 792. Hadrian Books, Oxford, pp 163-171.

Pettke T., Frei R. 1996. Isotope systematics in vein gold from brusson, Val d'Ayas (NW Italy). 1. Pb/Pb evidence for a piemonte metaophiolote Au source. Chemical Geology, 127, 111-124.

Pollard, A.M., Herdon, C. 2008. Archaeological Chemestry. RSC Publishing, Cambridge, UK, 437pp.

Prange M., Ambert P., Strahm C. 2003. Geochemical and lead isotopic caracterisation of copper ores and metal objects from Cabrières (Hérault, Languedoc, France). Archaeometallurgy in Europe, proceedings, vol. 2, Milan, p. 283-292.

Preuschen E. 1973. Estrazione mineraria dell'Età del Bronzo nel Trentino. Preistoria Alpina – Rendiconti. Vol. 9, pagg 113-150.

Ramdohr P. 1969. The ore minerals and their intergrowths. Pergamon Press, 1969 - Nature - 1174 pages.

Rehkämper, M., Halliday, A.N., 1998. Accuracy and long-term reproducibility of lead isotopic measurements by MC-ICP-MS using an external method for correction of mass discrimination. Int. J. Mass Spec. 181, 123e133.

Rehkämper, M., Mezger, K., 2000. Investigation of matrix effects for Pb isotope ratio measurements by multiple collector ICP-MS: verification and application of optimized analytical protocols. J. Anal. Spectrom. 15, 1451e1460.

Rehren T., Pernicka E. 2008. Coins, artefacts and isotopes -Archaeometallurgy and Archaeometry. Archaeometry 50 (2):232–248.

Renzi, M.; Montero-Ruiz, I.; Bode, M. 2009. Non-ferrous metallurgy from the Phoenician site of La Fonteta (Alicante, Spain) a study of provenance. Journal of Archaeological Science 36: 2584-2596.

Relvas J., Tassinari C., Munha J., Barriga F. 2001. Multiple sources for ore-forming fluids in the Neves Corvo VHMS deposit of the Iberian Pyrite Belt (Portugal): strontium, neodymium and lead isotope evidence. Mineralium Deposita, 36, 416-427.

Russell R.D., Farquhar R.M. 1960 Lead isotopes in geology. Interscience Publisher. 243 p. New York.

Seeliger, T.C.; Pernicka, E.; Wagner, G.A.; Begemann, F.; Schmitt-Strecker, S.F.; Eibner, C.; Öztunali, Ö.; Baranyi, I. 1985. Archaeometallurgische Untersuchungen in Nord- und Ostanatolien. Jahrbuch des Romisch-Germanischen Zentralmuseums Mainz 32: 597-659.

Schroll E., Koppel V., Cerny I. 2006. Pb and Sr isotope and geochemical data from the Pb-Zn deposit Bleiberg (Austria): constraints on the age of mineralization. Mineralogy and Petrology, 86, 129-156.

STATGRAPHICS® Centurion XVI User Manual, 2009. StatPoint Technologies, Inc. pp. 294. www.STATGRAPHICS.com

Stos-Gale, Z. 1991. Isotopic Analyses of Ores, Slags and Artefacts: The Contribution of Archaeometallurgy. Archeologia delle Attività Estrattive e Metallurgiche. V Ciclo di Lezioni sulla Ricerca Applicata in Archeologia. Certosa di Pontignano (SI) – Campiglia Marittima (LI), 9 -21 settembre 1991. Edizioni all'Insegna del Giglio.

Stos-Gale, Z.A., Gale N.H. 2009. Metal provenancing using isotopes and the Oxford archaeological lead isotope database (OXALID). Archaeological and Anthropological Sciences 1:195–213.

Stos-Gale, Z.A., Gale N.H. 2012. Bronze Age metal artefacts found on Cyprus - metal from Anatolia and the Western Mediterranean. Trabajos de Prehistoria 67, N.º 2, julio-diciembre 2010, pp. 389-403.

Stos-Gale, Z.A.; Gale, N.H. 1980. Sources of galena, lead and silver in Predynastic Egypt. Actes du XXeme Symposium International d'Archeometrie. Revue d'Archeometrie 5/III: 285-295.

Stos-Gale, Z.A.; Gale, N.H. and Annetts, N. 1996. Lead isotope analyses of ores from the Aegean. Archaeometry 38 (2): 381-390.

Stos-Gale, Z.A.; Gale, N.H.; Houghton, J.; Speakman, R. 1995. Lead isotope analyses of ores from the Western Mediterranean. Archaeometry 37 (2): 407-415.

Stos-Gale, Z.A.; Gale, N.H.; Annetts, N.; Todorov, T.; Lilov, P.; Raduncheva, A.; Panayotov, I. 1998a. Lead isotope data from the Isotrace Laboratory, Oxford: Archaeometry Database 5, Ores from Bulgaria. Archaeometry 40 (1): 217-226.

Stos-Gale, S.; Maliotis, G.; Gale, N.H. 1998b. A preliminary survey of the Cypriot slag heaps and their contribution to the reconstruction of copper production on Cyprus. In T. Rehren, A. Hauptmann and J. Muhly (eds.): Metallurgica Antiqua, in Honour of Hans-Gert Bachmann and Robert Maddin. Deutches Bergbau Museum, Bochum. 235-262.

Sugaki A., Shima H., Kitakaze A., Harada H. 1975. Bull. Soc. Econ. Geol., 70 [4] 806-823 (1975).

Swainbank I.G., Shepherd T.J., Caboi R., Massoli-Novelli R. 1982. Lead isotopic composition of some galena ores from Sardinia. Periodico di mineralogia, 51, 275-286.

Tylecote, R.F. 1987. The early history of metallurgy in Europe. Longman, London and New York. 391 pp.

Tylecote R.F., Ghaznavi H.A., Boydell P.J. 1977. Partitioning of trace elements betweem the ores, fluxes, slags and metal during the smelting of copper. Journal of Archaeological Science 1997, 4, 305-333.

Valera PG, Valera RG, Rivoldini A (2005) Sardinian ore deposits and metals in the Bronze Age. In: Lo Schiavo F, Giumlia-Mair A, Sanna U, Valera RG (eds) Archaeometallurgy in Sardinia: from the origins to the beginning of the Early Iron Age. Monographies Instrumentum 30, Monta-gnac, pp 43–87.

Velasco F., Herrero J.M., Yusta I., Alonso J.A., Seebol , Leach D. 2003.Geology and Geochemistry of the Reosin Zinc-Lead Deposit, Basque-Cantabrian basin, Northern Spain. Economic geology, 98, 1371-1396.

Vernon R.H. 2006. A Practical Guide to Rock Microstructure. Cambridge University Press, 606 pages.

Villa, I.M., 2009. Lead isotopic measurements in archeological objects. Archaeol. Anthropol. Sci. 1, 149-153.

Wagner, G.A.; Begemann, F.; Eibner, C.; Lutz, J.; Oztunali, O.; Pernicka, E.; Schmitt-Strecker, S.F. 1989. Archäometallurgische Untersuchungen an Rohstoffquellen des frühen Kupfers Ostanatoliens. Jahrbuch des Römisch-Germanischen Zentralmuseums Mainz 36: 637-686.

Wagner, G.A.; Pernicka, E.; Seeliger, T.; Lorentz. I.B.; Begemann, F.; Schmitt-Strecker, S.F.; Eibner, C.; Oztunali, O. 1986a. Geochemische und isotopische Characteristika früher Rohstoffquellen fur Kupfer, Blei, Silber und Gold in der Turkei". Jahrbuch des Römisch-Germanischen Zentralmuseums Mainz 33: 723-752.

Wagner, G.A.; Pernicka, E.; Seeliger, T.C.; Oztunali, O.; Baranyi, I.; Begemann, F. and Schmitt-Strecker, S. 1985. Geologische Unterschungen zur frûhen Metallurgie in NW-Anatolien". Bulletin of the Mineral Research and Exploration Institute of Turkey. 101/102: 45-81.

Wagner, G.A.; Pernicka, E.; Vavelidis, M.; Baranyi, I.; Bassiakos, Y. 1986b. Archaeometallurgische Untersuchungen auf Chalkidiki". Der Anschnitt 38 Heft 5-6. 166-186.

Weisgerber G., Willies L. 2000. The use of fire in prehistoric and ancient mining-firesetting
In: Paléorient. 2001, Vol. 26 N°2. pp. 131-149.

Wessa P. (2012), Bivariate Kernel Density Estimation (v1.0.9) in Free Statistics Software (v1.1.23-r7), Office for Research Development and Education, URL http://www.wessa.net/Ian.Holliday/rwasp_bidensity.wasp/

White, W.M., Albarède, F., Télouk, P., 2000. High-precision analysis of Pb isotopic ratios using multi-collector ICP-MS. Chem. Geol. 167, 257e270

Yener, K.A.; Sayre, E.V.; Özbal, H.; Joel, E.C.; Barnes, I.L.; Brill, R.H. 1991. Stable lead isotope studies of Central Taurus ore sources and related artefacts from Eastern Mediterranean Chalcolithic and Bronze Age sites. Journal of Archaeological Science 18(5): 541-577.

Yund A.R., Kullerud G. 1966. Thermal stability of assemblages in the Cu-Fe-S system. Journal of Petrology 7:454-488.

Appendix

Tab. A: Chemical composition of the sulphides of the Luserna, Transacqua and Segonzano sites obtained by means of EDS point analyses.

		SAMPLE	POINT N.	S	Fe	Cu
LUSERNA	**COARSE**	LU-G58	14	33,5	65,1	1,4
			19	33	64,6	2,4
			23	30,7	34,3	35
			26	31,8	53,8	14,4
			31	31,7	60,5	7,8
			45	21,9	6,2	71,9
			47	20,8	10,6	68,6
			48	26,9	65,2	7,9
		LU-M60	5	20,7	2,6	76,7
			6	16,3	1,3	82,4
			7	19,8	0,7	79,5
			8	23,9	4,4	71,7
			9	21,7	0	78,3
			11	38,1	59,9	2
			12	38,2	60,3	1,5
			13	38,2	60,2	1,6
			17	32,2	18,6	49,2
			18	31,6	18,1	50,3
			19	37,8	60,9	1,3
		LU-M50	2	21,5	3,1	75,4
			4	24,5	4,1	71,4
			7	23,8	2,6	73,6
			9	22	0	78
			10	22	0	78
			18	26,6	0	73,4
			22	25,2	2,8	72
			23	26,4	0,8	72,8
			24	26,4	0,5	73,1
		LU-M47	1	28,8	23,3	47,9
			2	34,4	44,1	21,5
			3	27,2	27,1	45,7
			4	34,5	63,5	2
			5	30,6	16,1	53,3
			6	38,4	59,6	2
			7	24,2	3,2	72,6
			8	36,5	51,7	11,8
			9	32,9	34,8	32,3
			10	35,6	51,9	12,5
			11	29,5	23,3	47,2
			12	29,9	22,5	47,6
			13	27,4	22,4	50,2

			14	35,4	49,7	14,9
			16	24,3	3,2	72,5
			17	22,7	2,9	74,4
			18	24,5	2,4	73,1
			23	28,9	18,3	52,8
			24	38	60,5	1,5
			25	30,5	14,5	55
			26	36,4	61,3	2,3
		LU-PS68	4	34,7	45	20,3
			8	32,3	31,4	36,3
			9	29,4	16,8	53,8
			10	31,6	17,4	51
			13	24,6	27	48,4
			15	30	15,7	54,3
			16	32	33,2	34,8
			17	24,3	20,7	55
			18	29,2	24,9	45,9
			26	33,5	40,2	26,3
			29	30,1	24,4	45,5
			30	33,9	35,6	30,5
			34	33,1	46,4	20,5
		LU-M4	4	33	15,5	51,5
			5	32,3	18,9	48,8
			6	32,8	18,9	48,3
			7	37,6	61	1,4
			8	38	60,5	1,5
			13	26,8	21,9	51,3
			15	22,6	77,4	0
			16	23,4	24,3	52,3
			20	32,1	66,2	1,7
		LU-P9	2	27,7	10,6	61,7
			3	26,6	12	61,4
			4	7,2	11,9	80,9
			120	22,4	21,2	56,4
			121	27,1	23,7	49,2
			122	21,7	12	66,3
			123	32,5	24,6	42,9
			127	26,9	30,7	42,4
			132	24,4	19,4	56,2
			133	21,4	12,2	66,4
			138	20,4	12,5	67,1

	TYPE	Sample	Point n	Fe	S	Cu
SEGONZANO	COARSE	SEG-G4	1	40,15	33,73	26,12
			3	63,81	34,09	2,09
			4	33,34	31,02	35,64

			15	31,41	31,75	36,84
			16	18,54	28,24	53,22
			25	7,78	25,96	66,26
			26	19,35	28,91	51,73
		SEG-G8	1	18,77	29,62	51,6
			2	8,36	28,31	63,33
			9	18,54	23,88	57,58
			10	63,62	33,41	2,97
			11	5,2	3,42	91,39
			16	62,93	34,14	2,93
			17	8,53	21,62	69,85
			18	22,79	27,1	50,11
			19	21,41	31,36	47,23
			21	15,81	29,05	55,13
			22	7,79	26,96	66,25
			23	1,56	0,26	98,18
			24	22,03	35,81	42,16
	MASSIVE	SEG-M11	2	20,84	28,86	50,3
			3	62,66	34,78	2,56
			4	64,07	34,62	1,31
			7	22,5	29,18	48,32
			8	63,73	34,74	1,54
			9	18,94	27,57	53,49
			10	21,16	28,54	50,3
			11	40,67	33,04	26,29
		SEG-M18	1	64,91	32,68	2,41
			2	26,39	22,42	51,19
			4	64,96	35,04	0
			5	15,72	26,52	57,76
			6	12,08	24,6	63,32
			7	20,51	24,83	54,66
			9	65,07	34,93	0
			10	7,37	21,15	71,47
			13	70,34	28,97	0,69
			14	34,97	27,16	37,86
			15	25,91	34,09	39,99
		SEG-M20	1	65,14	34,86	0
			2	4,44	20,1	75,46
			3	16,02	24,9	59,07
			6	4,79	21,12	74,1
			7	14,32	24,28	61,4
			8	17,8	26	56,2
			9	0,82	0,54	98,64
			10	1,11	17,71	81,18
			14	7,48	16,9	75,62
			15	63,39	34,44	2,17
			16	17,47	26,43	56,1

		SEG-M12	2	59,84	33,68	6,48
			3	19,87	25,94	54,19
			4	24,17	27,51	48,32
			6	65,36	34,64	0
			8	18,34	26,72	54,94
			9	1,49	27,91	70,59
			13	22,06	28,62	49,33
			14	63,95	34,72	1,32
		SEG-M16	1	65,4	34,6	0
			4	10,69	25,08	64,24
			6	18,82	27,67	53,51
			7	12,5	25,77	61,73
			10	9,53	24,58	65,89
			11	21,94	26,77	51,29
			13	0	27,93	72,07
			16	4,95	21,3	73,75
			17	20,18	25,7	54,12
			20 BIS	18,39	30,07	51,54
			21	17,9	28,37	53,74
		SEG-M17	3	18,66	29,35	51,99
			4	23,14	30,3	46,56
			6	16,49	28,96	54,55
			7	19,72	29,88	50,4
			8	16,65	27,39	55,96
			9	23,28	30,15	46,57
			11	65,2	34,8	0
			14	3,47	2,37	94,15
			15	14,8	24,69	60,5
			16	61,98	33,43	4,59
			25	67,38	26,31	6,31
	FLAT	SEG-P13	1	14,64	23,07	62,3
			4	63,73	33,63	2,65
			8	30,35	21,09	48,56
			9	40,9	32,45	26,65
			10	24,18	27,88	47,94
			13	0	0	100
			14	22,6	25,83	51,58
			17	65,4	32,91	1,7
			18	0	0	100
			19	65,75	34,25	0
			20	7,45	1,74	90,81
			22	17,86	24,3	57,84
			27	67,71	32,29	0
			28	17,96	23,7	58,34
			30	9	3,9	87,1
			31	0	0	100
			33	13,34	22,45	64,21

			34	62,76	33,62	3,62
		SEG-P14	4	0	0	100
			5	3,7	17,04	79,25
		SEG-P15	1	64,85	33,32	1,83
			3	21,53	25,81	52,67
			4	8,85	20,71	70,45
			6	0	0	100
			15	43,96	22,64	33,4
			17	26,84	19,97	53,18
			21	38,02	28,9	33,07
			25	35,57	27,26	37,16

	TYPE	sample	n	FeK	S K	CuK
TRANSACQUA	COARSE	TR G3	7	14,59	23,8	61,61
			8	35,78	27,05	37,17
			10	5,06	22,06	72,89
			11	21,1	27,98	50,92
			15	4,03	23,16	72,82
			16	19,66	28,06	52,29
			17	60,37	36,27	3,36
		TR G7	3	20,69	30,32	48,98
			4	15,54	28,89	55,57
			9	13,14	23,34	63,52
			10	20,77	29,88	49,35
			11	49,39	32,99	17,62
			14	16,52	30,27	53,21
			15	18,65	30,03	51,32
		TR G8	5	12,42	26,97	60,61
			6	21,42	29,17	49,4
			10	14,64	27,32	58,04
			11	16,66	27,23	56,11
			12	20,88	27,67	51,45
			14	65,5	34,5	0
	MASSIVE	TR M2	2	17,2	28,71	54,08
			3	63,43	33,8	2,77
			5	4,43	24,46	71,11
			6	18,21	28,59	53,19
			7	4,22	24,43	71,35
			8	62,38	34,11	3,51
			11	25,09	26,62	48,28
			12	5,71	22,24	72,06
			16	2,07	28,35	69,58
		TR M12	5	66,47	33,53	0
			8	26,22	27,9	45,87
			9	55,76	33,58	10,66
		TR M20	1	66,33	33,67	0
			3	4,25	23,37	72,38

			4	14,63	27,55	57,81
			7	56,9	29,11	13,99
			9	3,25	22,27	74,48
			10	33,88	30,66	35,45
			12	63,85	33,64	2,51
	FLAT	TR P4	2	57,99	34,6	7,41
			3	56,67	32,21	11,12
			5	43,87	33,66	22,47
			11	64,52	29,79	5,69
			12	63,9	28,6	7,51
			14	66,69	30,1	3,21
			20	58,47	32,12	9,41
		TR P15	1	54,58	33,29	12,13
			3	20,4	23,85	55,75
			6	38,97	28,4	32,63
		TR P16	17	15,88	23,85	60,27
			20	44,84	30,68	24,47
			21	18,05	21,08	60,87
			23	65,28	34,72	0
			24	16,89	24,74	58,37
		TR P18	2	25,63	29,95	44,42
			6	17,83	26,65	55,51
			8	62,71	34,9	2,38